

~~CONFIDENTIAL~~

Copy 10

N71-75443
NASA-TMX-57072

U.S. AIR FORCE - U.S. NAVY
NATIONAL AERONAUTICS AND
SPACE ADMINISTRATION

RESEARCH-AIRPLANE-COMMITTEE REPORT
ON CONFERENCE ON THE
PROGRESS OF THE X-15 PROJECT

A COMPILATION OF THE PAPERS PRESENTED

NASA FLIGHT RESEARCH CENTER
Edwards Air Force Base,
California

November 20-21, 1961

~~NASA FILE COPY~~

~~Restricted/~~

This material contains information affecting the national defense of the United States within the meaning of the espionage laws, Title 18, U.S.C., Secs. 793 and 794, the transmission or revelation of which in any manner to an unauthorized person is prohibited by law.

Return to
NASA HQ. LIBRARY (KSS-10)
WASHINGTON, D.C. 20546 STOP 85
HQ. LIBRARY (KSS-10)

Restriction/Classification Cancelled

~~CONFIDENTIAL~~
Restricted/
Classification
Cancelled

Restriction/Classification Cancelled

N71-75443

U.S. AIR FORCE - U.S. NAVY
NATIONAL AERONAUTICS AND SPACE ADMINISTRATION

RESEARCH-AIRPLANE-COMMITTEE REPORT ON CONFERENCE
ON THE PROGRESS OF THE X-15 PROJECT

A Compilation of the Papers Presented

NASA Flight Research Center
Edwards Air Force Base, California

ORIGINAL PAGE IS
OF POOR QUALITY

November 20-21, 1961

TABLE OF CONTENTS

INTRODUCTION vii
LIST OF CONFEREES ix

TECHNICAL PAPERS PRESENTED

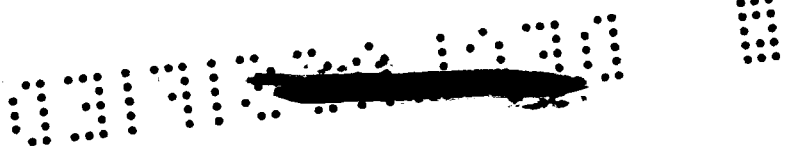
November 20, 1961

Session Chairman: De E. Beeler (NASA Flight Research Center)

1. STATUS OF X-15 RESEARCH PROGRAM (L) by De E. Beeler and Thomas A. Toll (NASA Flight Research Center) 1
2. PRELIMINARY RESULTS OF AERODYNAMIC HEATING STUDIES ON THE X-15 (L) by Richard D. Banner, Albert E. Kuhl, and Robert D. Quinn (NASA Flight Research Center) 11
3. STRUCTURAL HEATING EXPERIENCES OF THE X-15 (L) by Eldon E. Kordes, Robert D. Reed (NASA Flight Research Center), and Alpha L. Dawdy (North American Aviation, Inc.) 29
4. STRUCTURAL DYNAMIC EXPERIENCES OF THE X-15 (L) by Gareth H. Jordan, Norman J. McLeod (NASA Flight Research Center), and Lawrence D. Guy (NASA Langley Research Center) 47

Session Chairman: Edwin W. Johnston (North American Aviation, Inc.)

5. LANDING LOADS AND DYNAMICS OF THE X-15 AIRPLANE (L) by James M. McKay and Eldon E. Kordes (NASA Flight Research Center) 61
6. AERODYNAMIC FORCES ON COMPONENTS OF THE X-15 (L) by Earl R. Keener and Chris Pembo (NASA Flight Research Center) 73
7. A COMPARISON OF FULL-SCALE X-15 LIFT AND DRAG CHARACTERISTICS WITH WIND-TUNNEL RESULTS AND THEORY (L) by Edward J. Hopkins (NASA Ames Research Center), David E. Fetterman, Jr. (NASA Langley Research Center), and Edwin J. Saltzman (NASA Flight Research Center) 83



8. STABILITY AND CONTROL DERIVATIVE CHARACTERISTICS OF THE X-15 (✓). by Harold J. Walker and Chester H. Wolowicz (NASA Flight Research Center) 99

9. RÉSUMÉ OF X-15 HANDLING QUALITIES (✓) by Robert M. White (Air Force Flight Test Center), Glenn H. Robinson, and Gene J. Matranga (NASA Flight Research Center) 113

10. LATERAL DIRECTIONAL CONTROL CHARACTERISTICS (✓) by Forrest S. Petersen, Herman A. Rediess, and Joseph Weil (NASA Flight Research Center) 131

11. X-15 MISSION PLANNING AND OPERATIONAL PROCEDURES (✓) . . . by Robert G. Hoey (Air Force Flight Test Center) and Richard E. Day (NASA Flight Research Center) 155

November 21, 1961

Session Chairman: Lt. Col. Edwin F. Pezda (Aeronautical Systems Division, U.S. Air Force)

12. X-15 STABILITY AUGMENTATION SYSTEM. (✓) by Lawrence W. Taylor, Jr. (NASA Flight Research Center) and George B. Merrick (North American Aviation, Inc.) 171

13. DEVELOPMENT OF X-15 SELF-ADAPTIVE FLIGHT-CONTROL SYSTEM (✓). by Robert P. Johannes (Aeronautical Systems Division, U.S. Air Force), Neil A. Armstrong (NASA Flight Research Center), and Thomas C. Hays (Aeronautical Systems Division, U.S. Air Force) 183

14. FLIGHT CHARACTERISTICS OF X-15 HYPERSONIC FLOW-DIRECTION SENSOR (✓). by William D. Mace (NASA Langley Research Center) and Jon L. Ball (NASA Flight Research Center) 195

15. FLIGHT EXPERIENCE WITH X-15 INERTIAL DATA SYSTEM (✓) . . . by Jay V. Christensen (NASA Ames Research Center) and John A. Dodgen (NASA Langley Research Center) 203

16. XLR99 ENGINE OPERATING EXPERIENCE (✓). by Richard G. Leiby (Air Force Flight Test Center), Donald R. Bellman, and Norman E. DeMar (NASA Flight Research Center) 215



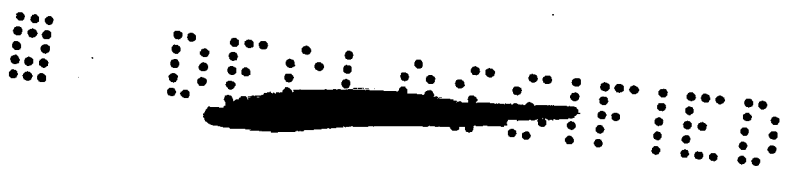


- 17. DEVELOPMENT OF IMPROVED CERAMIC COATINGS TO INCREASE THE LIFE OF XLR99 THRUST CHAMBER (U) . by Lawrence N. Hjelm (Aeronautical Systems Division, U.S. Air Force) and Bernard R. Bornhorst (Air Force Flight Test Center) 227
- 18. BIOASTRONAUTICS SUPPORT OF THE X-15 PROGRAM (U) by Burt Rowen, Ralph N. Richardson (Air Force Flight Test Center), and Garrison P. Layton, Jr. (NASA Flight Research Center) 255
- 19. X-15 PROPULSION SUBSYSTEM COMPONENT DEVELOPMENT (U) by Robert L. Wiswell, Phillip Olekszyk (Air Force Flight Test Center), and John W. Gibb (North American Aviation, Inc.) 265

Session Chairman: John V. Becker (NASA Langley Research Center)

- 20. OPERATIONAL RELIABILITY EXPERIENCE WITH THE X-15 AIRCRAFT (U) . by James E. Love and John A. Palmer (NASA Flight Research Center) 277
- 21. X-15 PILOT-IN-THE-LOOP AND REDUNDANCY EVALUATION (U) . . . by Robert G. Nagel (Air Force Flight Test Center) 289
- 22. A PILOT'S IMPRESSION OF THE X-15 PROGRAM (U) by Joseph A. Walker (NASA Flight Research Center) 303
- 23. X-15 EXPERIENCE FROM THE DESIGNER'S VIEWPOINT (U) . . . by L. P. Greene and R. L. Benner (North American Aviation, Inc.) 313
- 24. FUTURE PLANS FOR THE X-15 (U) by Paul F. Bikle (NASA Flight Research Center) and Edwin F. Pezda (Aeronautical Systems Division, U.S. Air Force) 329





INTRODUCTION

This document is a compilation of the papers presented at the Conference on the Progress of the X-15 Project held at the NASA Flight Research Center, Edwards Air Force Base, California, November 20-21, 1961. This conference was held by the Research Airplane Committee of the U.S. Air Force, the U.S. Navy, and the National Aeronautics and Space Administration to report on the technical status of this research airplane. The papers were presented by members of the staffs of North American Aviation, Inc.; Aeronautical Systems Division, U.S. Air Force; Air Force Flight Test Center; and National Aeronautics and Space Administration.

Preceding page blank

CONFIDENTIAL

LIST OF CONFEREES

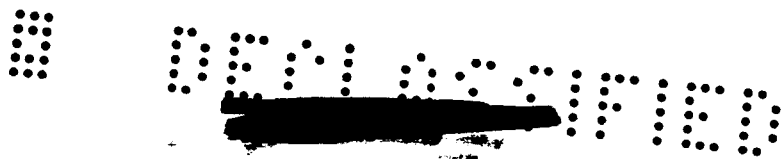
The following were registered at the Conference on the Progress of the X-15 Project, NASA Flight Research Center, Edwards Air Force Base, California, November 20-21, 1961.

ABBOTT, Ira H.	NASA Headquarters
ALBERI, Americo	Republic Aviation Corporation
ALLWARDT, Victor L.	General Dynamics/Astronautics
ANDERSON, Lt. Col. C. E., Jr.	Air Force Flight Test Center
ANDERSON, J. W.	General Dynamics/Convair
ANDERSON, Capt. Loren A.	U.S. Air Force Academy
ANDERTON, Capt. F. R., Jr.	Air Force Flight Test Center
APPLETON, Dave T.	Westinghouse Electric Corporation
ARMSTRONG, Neil A.	NASA Flight Research Center
ARNDT, Capt. Ralph W.	U.S. Naval Postgraduate School
ARNOLD, William B.	Thiokol Chemical Corporation
ATCHISON, James R.	Aeronautical Systems Division, Wright-Patterson Air Force Base
ATTIAS, John J.	Space Technology Laboratories
AVERY, Dr. W. H.	NASA Res. Advisory Comm. on Chemical Energy Systems
AYDELOTTE, John	The Boeing Company
BADDER, Robert M.	Aeronautical Systems Division, Wright-Patterson Air Force Base
BAKER, Joel R.	The Boeing Company
BALL, Jon L.	NASA Flight Research Center
BANNER, Richard D.	NASA Flight Research Center
BARTER, John W.	Douglas Aircraft Company
BARTH, Jack E.	USN Rep., Douglas Aircraft Company
BAXTER, John F.	The Martin Company
BECKER, John V.	NASA Langley Research Center
BEELER, De E.	NASA Flight Research Center
BEILMAN, John L.	Cornell Aeronautical Laboratory
BEKEY, George A.	Space Technology Laboratories
BELL, Alfred J.	Johns Hopkins University
BELL, L. W.	Air Force Flight Test Center
BELLMAN, Donald R.	NASA Flight Research Center
BENNER, Roland L.	North American Aviation, Inc.
BERGERON, Roland P.	Aeronutronic Div., Ford Motor Co.
BERKOW, Murray	Republic Aviation Corporation
BERMAN, S. D.	AFIFS-B, Norton Air Force Base
BERRY, D. T.	Air Force Flight Test Center
BIKLE, Paul F.	NASA Flight Research Center
BILLET, Frank	The Marquardt Corporation
BLAND, W. M.	NASA Manned Spacecraft Center
BLOOM, Harold L.	General Electric Company

CONFIDENTIAL

BONSER, Thomas H.	Aeronautical Systems Division, Wright-Patterson Air Force Base
BORMAN, Maj. Frank	Air Force Flight Test Center
BORNHORST, Lt. B. R.	Air Force Flight Test Center
BOSEE, Capt. Roland A., USN	Naval Air Center, Philadelphia
BOWEN, Lt. Ray M.	Air Force Institute of Technology
BOWRY, Lt. Col. D. W.	Air Force Flight Test Center
BOYD, John W.	NASA Ames Research Center
BRADFORD, Robert P.	Thiokol Chemical Corporation
BRADSHAW, Harold R.	Bureau of Naval Weapons
BRANCH, Brig. Gen. I. L.	Air Force Flight Test Center
BRANDT, J. C.	Air Force Flight Test Center
BRATT, Maj. Harry R.	Air Force Flight Test Center
BRIDGE, Charles S.	Litton Systems, Inc.
BROWN, Col. E. W.	Weapons System Evaluation Group
BROWN, Harvey H.	NASA Headquarters
BROWNELL, Lt. Col. G. S.	AFSC Liaison Office, NASA Ames Research Center
BRUNOW, Charles L.	Chance Vought Corporation
BUCHANAN, Maj. R. S.	Air Force Flight Test Center
BULLER, R. L.	Aerojet General Corporation
BURNOR, Lt. Col. R. H.	Headquarters, Air Defense Command
BUSSING, Paul R.	The Boeing Company
CAMPBELL, Roy A.	North American Aviation, Inc.
CARDER, Alden B.	Douglas Aircraft Company
CARLSON, Dale K.	General Dynamics/Pomona
CARLSON, Lt. Col. D. D.	Arnold Engineering Development Center
CARNRIGHT, Maj. R. G.	Aeronautical Systems Division, Wright-Patterson Air Force Base
CHAMPE, George W.	Protection, Inc.
CHRISINGER, Maj. J. E.	U.S. Air Force Academy
CHRISTENSEN, H. H.	General Electric Company
CHRISTENSEN, Jay V.	NASA Ames Research Center
CLARK, Capt. Hugh D.	Aeronautical Systems Division, Wright-Patterson Air Force Base
CLARK, O. J.	Air Force Flight Test Center
CODE, Dr. Arthur D.	Washburn Observatory
COHN, Benedict	The Boeing Company
COKELEY, Edmond R.	North American Aviation, Inc.
COLEMAN, Richard L.	Naval Ordnance Test Station, China Lake, Calif.
COLLIGAN, Col. R. L., Jr.	NASA Res. Advisory Comm. on Aircraft Operating Problems
COLLINS, B. J.	A C Spark Plug
CONLON, J. W.	NASA Manned Spacecraft Center
COOK, William H.	NASA Res. Advisory Comm. on Aircraft Operating Problems

CONFIDENTIAL



COONEY, T. V.
COOPER, Maj. Gen. Marcus F.
COULTER, Col. John M.

COUR-PALAIS, B. G.
COWGILL, Edward L.
CROSSFIELD, A. Scott
CURLANDER, John C.

DAHLEN, Valentine

DANIS, Frank
DAWDY, Alpha L.
DAY, Richard E.
DEAN, Jack
DeMAR, Norman E.
DEMETRIADES, Dr. Anthony
DEMLER, Maj. Gen. M. C.
DENTEL, Keith Eugene
DICKENSON, Warren T.

DOCKEN, Richard G.

DODGEN, John A.
DOELL, James F.
DONATELLI, Philip A.
DONLAN, Charles J.
DOYLE, G. B.
DRAKE, D. E.
DRAKE, H. M.
DRYDEN, Hugh L.
DUGGER, Gordon L.
DUNN, George R.
DUNN, Orville R.

EASON, William M.
EASTMAN, Maj. Burns R.
EDWARDS, Capt. F. G., USN

EKERN, Capt. Harold O.

ERB, Capt. Richard I.

ERICKSON, John W.
EVANS, A. J.

NASA Flight Research Center
Headquarters, Air Force Systems Command
Aeronautical Systems Division,
Wright-Patterson Air Force Base
NASA Manned Spacecraft Center
The Boeing Company
North American Aviation, Inc.
The Martin Company

Aeronautical Systems Division,
Wright-Patterson Air Force Base
Thiokol Chemical Corporation
North American Aviation, Inc.
NASA Flight Research Center
Rocketdyne
NASA Flight Research Center
California Institute of Technology
Director of Advanced Technology, USAF
Bureau of Naval Weapons
NASA Res. Advisory Comm. on Aircraft
Operating Problems
Aeronautical Systems Division,
Wright-Patterson Air Force Base
NASA Langley Research Center
North American Aviation, Inc.
Thiokol Chemical Corporation
NASA Langley Research Center
Ryan Aerospace
Douglas Aircraft Company
NASA Flight Research Center
NASA Headquarters
Johns Hopkins University
General Dynamics/Astronautics
NASA Res. Advisory Comm. on Aircraft
Aerodynamics

General Dynamics/Fort Worth
Air Force Flight Test Center
Naval Air Test Center, Patuxent
River, Md.

Aeronautical Systems Division,
Wright-Patterson Air Force Base
Aeronautical Systems Division,
Wright-Patterson Air Force Base
General Dynamics/Astronautics
NASA Headquarters



FARISH, Dr. Preston

NASA George C. Marshall Space Flight
Center

FARR, Alton E.

Douglas Aircraft Company

FEDZIUK, Henry A.

NASA Langley Research Center

FEHR, Robert W.

Hughes Aircraft Company

FELTZ, C. H.

North American Aviation, Inc.

FETTERMAN, David E. Jr.

NASA Langley Research Center

FETTY, Maj. Randall L.

Air Force Flight Test Center

FIELD, Robert E.

North American Aviation, Inc.

FILBIN, Richard F.

Raytheon Company

FILES, Lt. Col. Roger B.

Headquarters, Air Defense Command

FINCH, Thomas W.

NASA Flight Research Center

FISCHEL, Jack

NASA Flight Research Center

FIUL, Abraham

Space Technology Laboratories

FLEMING, John R.

Protection, Inc.

FLEMING, William A.

NASA Headquarters

FOELSCH, George F.

General Dynamics/Convair

FOSTER, Norman B.

David Clark Company

FRANKLIN, M. R.

NASA Manned Spacecraft Center

FRENCH, R. H., Jr.

The Martin Company

FULGHAM, Capt. Dan D.

Air Force Flight Test Center

FULLER, Richard G.

Lockheed Aircraft Corporation

GALLANES, Harry

North American Aviation, Inc.

GARWOOD, J. S.

Sperry Gyroscope Company

GIBB, John W.

North American Aviation, Inc.

GILDEA, D. J.

North American Aviation, Inc.

GILLOOLY, R. P.

McDonnell Aircraft Corporation

GILMORE, Arthur W.

NASA Res. Advisory Comm. on Aircraft
Aerodynamics

GILRUTH, R. R.

NASA Manned Spacecraft Center

GLENN, John E.

Norair Div., Northrop Corporation

GODSEY, Vernon E.

The Boeing Company

GOLDING, N. J., Jr.

McDonnell Aircraft Corporation

GORAN, R. C.

McDonnell Aircraft Corporation

GORANSON, R. Fabian

NASA Headquarters

GREEN, Norris H.

North American Aviation, Inc.

GREENE, L. P.

NASA Res. Advisory Comm. on Aircraft
Aerodynamics

GREER, Lt. Col. Edwin H.

Headquarters, Air Defense Command

GREGER, Lt. Col. Jack J.

Air Force Flight Test Center

GREGORY, Col. John L.

Tactical Air Command, Langley AFB

GUTH, Ralph E.

Aeronautical Systems Division,

Wright-Patterson Air Force Base

HAHN, Edward J.

The Boeing Company

HAINLINE, B. C.

The Boeing Company

HALDEMAN, George W.
HALL, Bertrand M.
HAMMACK, J. B.
HARDY, H. D.
HARER, R. J.
HARRIMAN, T. J.
HARVEY, Q. C., Jr.
HAUGER, Harry H., Jr.
HAYS, T. C.
HEALD, E. R.
HEIMERDINGER, A. G.
HENDERSON, Col. A. M.
HENNRICH, 2d Lt. Carl W.
HENRY, Sq. Ldr. J. G., RCAF

HERMANN, Robert A.

HICKS, R. D.
HILDEBRAND, Robert B.

HJEIM, 1st Lt. L. N.

HOEHNE, Vernon O.
HOEY, Robert G.
HOGE, H. J.

HOLCOMB, Don C.
HOLLEMAN, E. C.
HOLLENBERG, Harold O.
HOLM, Robert J.
HOLMES, Vet V.
HOLMES, Walter T.
HOPE, J. I.

HOPKINS, Edward J.
HOPSON, George D.
HORST, Carl O.

HOUTZ, John Edwin

HOWELL, Clarence S., Jr.

IRWIN, K. S.
IVERSON, James R.

JABLECKI, Col. Leon S.
JACKSON, B. G.

Civil Aeronautics Board
Douglas Aircraft Company
NASA Manned Spacecraft Center
Bureau of Naval Weapons
Air Force Flight Test Center
Giannini Controls Corporation
North American Aviation, Inc.
Douglas Aircraft Company
Minneapolis-Honeywell Regulator Co.
Douglas Aircraft Company
Douglas Aircraft Company
David Clark Company
U.S. Air Force Academy
Aeronautical Systems Division,
Wright-Patterson Air Force Base
Aeronautical Systems Division,
Wright-Patterson Air Force Base
Air Force Flight Test Center
NASA Res. Advisory Comm. on Missile
and Space Vehicle Aerodynamics
Aeronautical Systems Division,
Wright-Patterson Air Force Base
Battelle Memorial Institute
Air Force Flight Test Center
NASA Res. Advisory Comm. on Aircraft
Structures
Space Technology Laboratories
NASA Manned Spacecraft Center
Bureau of Naval Weapons
Litton Systems, Inc.
Douglas Aircraft Company
North American Aviation, Inc.
NASA Res. Advisory Comm. on Aircraft
Aerodynamics
NASA Ames Research Center
General Dynamics/Convair
Aeronautical Systems Division,
Wright-Patterson Air Force Base
Aeronautical Systems Division,
Wright-Patterson Air Force Base
The Boeing Company

Air Force Flight Test Center
Ryan Electronics

Arnold Engineering Development Center
NASA Manned Spacecraft Center

JENKINS, Maj. John I.
JOHANNES, Lt. Robert P.

Air Force Missile Development Center
Aeronautical Systems Division,
Wright-Patterson Air Force Base
Air Force Flight Test Center
Westinghouse Electric Corporation
Rocketdyne
North American Aviation, Inc.
NASA Flight Research Center
Air Force Flight Test Center

JOHNSON, Capt. D. C.
JOHNSON, Melvin
JOHNSON, Wayne R.
JOHNSTON, Edwin W.
JORDAN, Gareth H.
JOYCE, 2d Lt. W. T.

NASA Flight Research Center
Air Force Institute of Technology
Grumman Aircraft Engineering Corp.
Lockheed Aircraft Corporation
Naval Air Test Center, Patuxent
River, Md.

KEENER, Earl R.
KEISTER, Paul H.
KELLY, Thomas J.
KERRIS, W. E.
KING, Lt. Comdr. R. R., USN

Pacific Telephone and Telegraph
The Boeing Company
Air Force Flight Test Center
Thiokol Chemical Corporation
NASA Flight Test Center
North American Aviation, Inc.
NASA Flight Research Center
NASA Res. Advisory Comm. on Missile
and Space Vehicle Structures

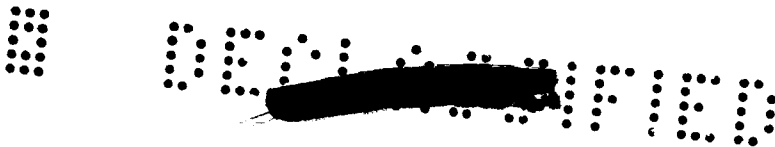
KLEMPENBERG, Henry H.
KLOPFENSTEIN, H. W.
KNIGHT, Capt. W. J.
KOCH, Harry A.
KORDES, Eldon E.
KRAMER, Oliver R.
KUHLE, Albert E.
KULLAS, A. J.

Pacific Telephone and Telegraph
Princeton University
General Dynamics/Convair
Lockheed Aircraft Corporation
Bureau of Naval Weapons
NASA Flight Research Center
Weapons Systems Evaluation Group
The Boeing Company
Air Force Flight Test Center
The Boeing Company
Minneapolis-Honeywell Regulator Co.
General Dynamics/Fort Worth
Aeronautical Systems Division,
Wright-Patterson Air Force Base

LAMBERT, John L.
LAMERS, Lt. John P., USN
LANFLISI, Raymond R.
LANGE, R. H.
LA ROE, Capt. E. T.
LAYTON, Garrison P., Jr.
LEATHERBURY, C. H.
LEE, Alan H.
LEIBY, Capt. Richard G.
LEWIS, Delbert S.
LINDAHL, John Henry
LINDSTROM, Frederick A.
LIU, Tung-Sheng

The Boeing Company
Douglas Aircraft Company
NASA Flight Research Center
Republic Aviation Corporation
Air Force Flight Test Center
Nortronics Div., Northrop Corp.
Douglas Aircraft Company

LOESCH, R. L., Jr.
LONDELIOUS, J. C.
LOVE, James E.
LU, Hoshen R.
LUDWIG, John H.
LUKESH, John S.
LUNDRY, Jerry L.



MABRY, G. C.
MACE, William D.
Mac HALEC, Joseph M.
MAGGIN, Bernard
MAGRUDER, W. M.
MAHOFF, A. A.
MANGINI, Raymond L.
MANGURIAN, George N.

MARTIN, James E.
MARTIN, J. A.
MARTIN, Maj. Reese S.
MATRANGA, Gene J.
McCARTER, William B.
McCULLEY, Capt. James A.

McDIVITT, Capt. James A.
McEACHERN, Maj. L. J.
McELMURRY, Maj. T. U.
McGOWEN, Gilbert L.
McGUIRE, William M.
McINTIRE, Col. H. J.
McLEOD, Norman J.
MEEKS, Howard D.

MEIER, Joseph W.
MELLEN, David L.
MERRITT, Maj. Jack, Jr.
MESSING, W. E.
MESSINGER, Bernard L.
MEYFARTH, Lt. Philip F.
MILLER, Chester W.
MILLS, George R.
MISSELHORN, John E.
MIX, Comdr. L. R.

MONAGHAN, Reginald J.
MONTGOMERY, James F.
MOSES, Harry C.
MULL, L. S.

MULLINS, Denver W.

MUMFORD, Nickolas V. S
MURRAY, Arthur
MURRAY, Joe H.

Douglas Aircraft Company
NASA Langley Research Center
Minneapolis-Honeywell Regulator Co.
NASA Headquarters
Douglas Aircraft Company
Douglas Aircraft Company
Naval Missile Center, Point Mugu, Calif.
NASA Res. Advisory Comm. on Aircraft
Structures
Chance Vought Corporation
NASA Flight Research Center
Headquarters, U.S. Air Force
NASA Flight Research Center
Defence Research Board
Aeronautical Systems Division,
Wright-Patterson Air Force Base
Air Force Flight Test Center
Air Force Flight Test Center
Air Force Flight Test Center
Texas Instruments, Inc.
Minneapolis-Honeywell Regulator Co.
Air Force Flight Test Center
NASA Flight Research Center
Aeronautical Systems Division,
Wright-Patterson Air Force Base
Aerojet-General Corporation
Minneapolis-Honeywell Regulator Co.
Air Force Special Weapons Center
NASA Flight Research Center
Lockheed Aircraft Corporation
Air Force Institute of Technology
McDonnell Aircraft Corporation
Nortronics Div., Northrop Corporation
Aerojet-General Corporation
Navy Liaison Office, Air Force Flight
Test Center
British Embassy
Naval Missile Center, Point Mugu, Calif.
Westinghouse Electric Corporation
NASA Res. Advisory Comm. on Aircraft
Structures
Aeronautical Systems Division,
Wright-Patterson Air Force Base
Chance Vought Corporation
The Boeing Company
General Dynamics/Convair

NAGEL, Robert G.
NAUMANN, Erwin A.
NELSON, Alfred, M.
NELSON, Lewis A.
NEUBECK, Capt. F. G.
NORTH, Warren J.
NYLAND, Frederic S.

Air Force Flight Test Center
The Bendix Corporation
NASA Headquarters
Norair Div., Northrop Corporation
Air Force Flight Test Center
NASA Headquarters
The RAND Corporation

O'HARA Frank
OLASON, M. L.
OLEKSZYK, Lt. Phillip
OSTLING, Roy V.

British Embassy
The Boeing Company
Air Force Flight Test Center
The Boeing Company

PALMER, Lt. John A.
PALMER, J. M., Jr.
PAPPAS, Costas E.
PARTRIDGE, Hilary G.
PASSMAN, Richard A.
PATTERSON, Maj. G. K.
PEMBO, Chris
PEPPING, Raymond A.

NASA Flight Research Center
Douglas Aircraft Company
Republic Aviation Corporation
The Sierracin Corporation
General Electric Company
Air Force Flight Test Center
NASA Flight Research Center
NASA Res. Advisory Comm. on Missile
and Space Vehicle Aerodynamics

PERKINS, C. L.
PETERSEN, Comdr. Forrest S.
PETERSON, William R.
PEZDA, Col. E. F.

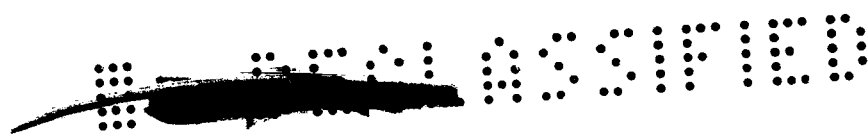
The Boeing Company
NASA Flight Research Center
Minneapolis-Honeywell Regulator Co.
Aeronautical Systems Division,
Wright-Patterson Air Force Base
Aeronautical Systems Division,
Wright-Patterson Air Force Base

POPE, Alan Y.
PORTER, R. F.
POSTLE, Robert S., Jr.
POWELL, David G.
POWERS, Sidney A.
PRESTON, G. Merritt
PROUDFOOT, Robert C.

Sandia Corporation
Air Force Flight Test Center
Bell Aerosystems Company
Stanley Aviation Corporation
Norair Div., Northrop Corporation
NASA Manned Spacecraft Center
Aeronautical Systems Division,
Wright-Patterson Air Force Base

RAHN, Robert O.
REDIESS, Herman A.
REED, Robert D.
REISERT, Donald
RICH, B. R.
RICHARDSON, Maj. R. N.
RICHTER, Donald M.
RITTER, Robert A.
ROBERTS, Lt. Col. Ray O.

Douglas Aircraft Company
NASA Flight Research Center
NASA Flight Research Center
NASA Flight Research Center
Lockheed Aircraft Corporation
Air Force Flight Test Center
North American Aviation, Inc.
Naval Air Material Center
Air Force Missile Development Center



ROBERTS, Wilbur E.
 ROBINSON, Glenn H.
 ROBINSON, Russell E.
 RORER, Everett E.

ROSS, Franklin J.

ROSS, William S.
 ROTELLI, R. L.
 ROUZIE, R. L.
 ROWAN, Lt. Col. Burt
 RUBIN, Bernard

RUGIENIUS, Flt. Lt. A. V.
 RUHL, L. F.

SALTZMAN, Edwin J.
 SANDERS, T. H.
 SANDERSON, K. C.
 SANGSTER, William A.
 SAROKON, Daniel
 SCHETZER, Julius D.
 SCHOFIELD, B. L.
 SCHUCK, O. H.

SCHUELER, Clarence J.
 SCHUERCH, Dr. Hans U.

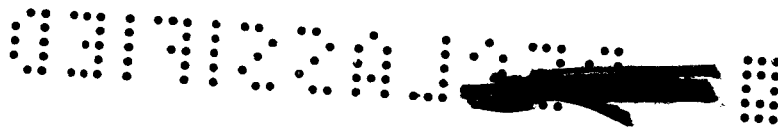
SCHWARTZ, Maj. David C.
 SCHWEIKHARD, W. G.
 SCOLES, Richard J.
 SCOVILLE, Lt. Col. C. L.
 SEAMAN, Robert W.
 SEARCY, William E.
 SEATON, Capt. R. F.
 SEIELSTAD, Harold E., Jr.
 SELVO, James E.
 SHANTZ, Irving

SHEVELL, Richard S.
 SIERADZKI, Henry J.
 SIRY, Joseph W.
 SJOBERG, S. A.
 SMITH, A. M. O.
 SMITH, D. R.
 SMITH, Col. Harold V.
 SMITH, Capt. Richard E.

Hughes Aircraft Company
 NASA Flight Research Center
 General Electric Company
 Aeronautical Systems Division,
 Wright-Patterson Air Force Base
 Office of the Secretary of the
 Air Force, R & D
 McDonnell Aircraft Corporation
 The Boeing Company
 The Boeing Company
 Air Force Flight Test Center
 Aeronautical Systems Division,
 Wright-Patterson Air Force Base
 Defence Research Board
 Douglas Aircraft Company

NASA Flight Research Center
 The Boeing Company
 NASA Flight Research Center
 General Electric Company
 General Dynamics/Astronautics
 Space Technology Laboratories
 Air Force Flight Test Center
 NASA Res. Advisory Comm. on Control,
 Guidance, and Navigation
 Arnold Engineering Development Center
 NASA Res. Advisory Comm. on Missile
 and Space Vehicle Structures
 Air Force Systems Command, Edwards AFB
 Air Force Flight Test Center
 General Electric Company
 Air Force Systems Command, Andrews AFB
 Thiokol Chemical Corporation
 Rocketdyne
 Air Force Flight Test Center
 Radioplane Div., Northrop Corp.
 North American Aviation, Inc.
 Naval Ordnance Laboratory, Silver
 Spring, Md.
 Douglas Aircraft Company
 Rohr Aircraft Corporation
 NASA Goddard Space Flight Center
 NASA Manned Spacecraft Center
 USN Rep., Douglas Aircraft Co.
 Air Force Flight Test Center
 Air Force Flight Test Center
 Air Force Flight Test Center





SONNABEND, David
SOULÉ, Hartley A.
SMELT, Ronald

SPEAKER, Robert F.
SPIELBERG, Irvin N.
STACEY, Richard A.
STACK, John
STALONY-DOBZANSKI, J. A.
STANLEY, Robert M.
STARR, Sterling V.
STEELE, Frederick I.
STEEN, Lt. Col. C. H.
STEIN, Samuel
STETSON, Capt. John R.
STOLIKER, F. N.
STORY, Martin W.
SULLINS, Robert T., Jr.
SUNLIN, William M.
SWENSON, Floyd A.
SYLVESTER, M. A.

TAYLOR, Lawrence W., Jr.
TAYLOR, R. E.
TAYLOR, Robert M.
TEBBEN, Capt. G. D.
TEEGARDEN, D. L.
TERESHKOW, Henry
THERIAULT, Paul W.
THOMPSON, Floyd L.
THOREN, Rudolph L.
TIZIO, Vincent J.
TOLL, Thomas A.
TRUSZYNSKI, Gerald M.
TSCHIRGI, Joseph M.
TURNER, William N.

URBANIK, John G.

VENSEL, J. R.
VIDEAN, E. N.
VOGELEY, Arthur W.

WAGNER, ALC W. R.
WALCOTT, John K.
WALKER, Harold J.

Philco Corporation
NASA Langley Research Center
NASA Res. Advisory Comm. on Missile
and Space Vehicle Aerodynamics
Bureau of Naval Weapons
Space Technology Laboratories
North American Aviation, Inc.
NASA Headquarters
A C Spark Plug
Stanley Aviation Corporation
General Dynamics/Convair
McDonnell Aircraft Corporation
Headquarters, USAF
NASA Lewis Research Center
Air Force Flight Test Center
Air Force Flight Test Center
Lear, Inc.
General Dynamics/Astronautics
Ryan Electronics
The Boeing Company
Ballistic Research Laboratories,
Aberdeen Proving Ground

NASA Flight Research Center
Air Force Flight Test Center
David Taylor Model Basin, Navy Dept.
Air Force Flight Test Center
Air Force Flight Test Center
AVCO Corporation
Lockheed Aircraft Corporation
NASA Langley Research Center
Lockheed Aircraft Corporation
Republic Aviation Corporation
NASA Flight Research Center
NASA Headquarters
Douglas Aircraft Company
Hughes Aircraft Company

Republic Aviation Corporation

NASA Flight Research Center
NASA Flight Research Center
NASA Langley Research Center

Air Force Flight Test Center
Westinghouse Electric Corporation
NASA Flight Research Center

WALKER, Joseph A.	NASA Flight Research Center
WAREING, Maj. J. T.	Headquarters, USAF
WATSON, R. E.	The Boeing Company
WATSON, Robert M.	Grumman Aircraft Engineering Corp.
WEIL, Joseph	NASA Flight Research Center
WEISENBERG, I. J	Space Technology Laboratories
WESSELHOFF, Robert E.	Ryan Aeronautical Company
WHEELHOUSE, Lt. Col. H. L.	Tactical Air Command, Langley AFB
WHITAKER, Prof. H. P.	M.I.T. Div. of Sponsored Research
WHITE, Maj. Robert M.	Air Force Flight Test Center
WHITTEN, James B.	NASA Langley Research Center
WILEY, Capt. Daniel R.	Aeronautical Systems Division, Edwards, Calif.
WILLIAMS, G. H.	Norair Div., Northrop Corp.
WILLIAMS, J. J.	NASA Manned Spacecraft Center
WILLIAMS, W. C.	NASA Manned Spacecraft Center
WILLIAMS, Maj. Wayland W.	Headquarters, Strategic Air Command
WISWELL, Robert L.	Air Force Flight Test Center
WOLOWICZ, Chester H.	NASA Flight Research Center
WOOD, Drury W., Jr.	Douglas Aircraft Company
WOOD, Maj. James W.	Air Force Flight Test Center
WOOD, R. F.	Air Force Flight Test Center
WOODLING, Carroll H.	NASA Langley Research Center
WORLEY, George F.	Douglas Aircraft Company
YOLER, Yusuf A.	The Boeing Company
YORKE, Duane	Grumman Aircraft Engineering Corp.
YOUNGQUIST, J. R.	NASA Res. Advisory Comm. on Chemical Energy Systems
ZALESKI, Lt. Charles D.	Air Force Flight Test Center



1. STATUS OF X-15 RESEARCH PROGRAM (L)

By De E. Beeler and Thomas A. Toll

NASA Flight Research Center

~~XXXXXXXXXXXX~~ N71-75444

It was recognized early in planning for the X-15 project that a very important benefit would be derived from accelerating and focusing the research required to support manned flight in the hypersonic speed ranges within and outside the earth's atmosphere. It has been evident from the previous two X-15 conferences that there has been much research generated within both the government and industry during the development of the X-15. Equally important was the development of a flight research program designed to assess the various problem areas in relation to each other, thereby allowing them to be viewed in their proper perspective. The program also was expected to uncover certain problem areas that had been overlooked. It is in these latter areas that the greatest progress has been made since the last X-15 conference.

The purpose of this conference is to present some of the most pertinent information obtained in the conduct of the flight program and to give some indication of the immediate and future plans for completing the project.

The purpose of this paper is to discuss briefly the events and progress of the project since the last conference to give the project status at the present time, and to orient generally the various papers to be given during these two days.

It may be recalled that at the time of the 1958 Conference, construction of the first X-15 aircraft was nearing completion and preparations were being made for delivery of the airplane to the Flight Test Division of North American Aviation, Inc. The final airplane configuration discussed at the conference and on display at North American after the conference is shown in figures 1 and 2. Some features worth noting are the wing leading-edge sweep angle of 25° , side tunnels running lengthwise of the fuselage for housing plumbing and control cables, a horizontal tail that provided both pitch and roll control, and vertical tail surfaces which are nearly symmetrical about the fuselage. A portion of the lower vertical surface was to be jettisoned before each landing and recovered by parachute. It also was stated at the 1958 Conference that delays in the development of the X-15 engine would require that the first flights be accomplished with an interim rocket engine, having less than $1/3$ the thrust expected from the X-15 rocket engine. The landing weight was stated to have increased to approximately 15,000 pounds and the corresponding launch weight would be approximately 33,000 pounds.

~~XXXXXXXXXXXX~~

The external configuration of the X-15, as it has been flown in the program, generally speaking, is similar to that shown here. The flight program has included some specific external-configuration variations, however, which are pertinent to the papers to be presented at this conference. These configuration variations are shown in figure 3.

The interim engine used initially in the program was a combination of two of the engines designed for the X-1 airplane, which had a total of eight rocket cylinders, produced a total thrust of approximately 16,000 pounds, and used alcohol and water as fuel. The upper right portion of the figure shows the installation of the X-15 ammonia-burning engine, which produces approximately 57,000 pounds thrust at an altitude of 45,000 feet and is throttleable to 28,000 pounds. All flights except one have been flown with the lower rudder on, except, of course, for landing. One flight to a Mach number of 4.3 and to an altitude of 78,000 feet has been made with the lower rudder off. As the program progressed to the higher temperature conditions, the familiar nose boom with attitude sensing vanes and static- and total-pressure sensors was replaced with a nitrogen-cooled, null-seeking ball, which provided airplane attitude to the pilot and to the recording equipment.

The mode of operation for the X-15 flight program was described at the 1958 Conference and is illustrated in figure 4. Two B-52 airplanes had been converted for launching the X-15 aircraft from a location between the fuselage and inboard engine nacelles of the right wing of the B-52 bombers. This arrangement has worked extremely well, and some aspects of the operation will be discussed in subsequent papers.

The research flights were planned to be conducted along the instrumented range extending approximately 420 nautical miles northeast of Edwards, Calif., to Wendover, Utah. Only two of the three instrumented stations along the range, Edwards and Beatty, have been required in the program completed to date. Later flights, at altitudes above 250,000 feet with corresponding higher speeds, will require the use of the Ely station and a greater length of the range.

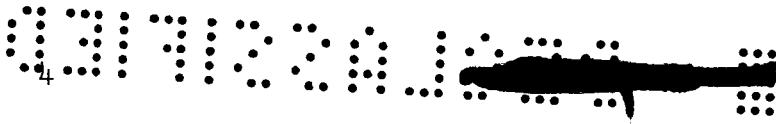
The flight progress, relative to the overall X-15 project, is shown in figure 5. As may be recalled, the X-15 project was initiated with conceptual studies made by the NACA and discussions between the NACA and the military services during the period from 1952 to 1954. The design and construction of the three airplanes occurred during the period from 1956 to 1959, with additional construction periods required to make repair as a result of two accidents. One period of two months followed damage to an aircraft during a landing, which will be discussed at this conference. An additional construction period is indicated for rebuilding and modification of the third aircraft after an explosion during a ground run of the X-15 rocket engine, which will also be discussed at this conference.

A total of 45 flights have been made in the 29 months since the first X-15 flight. Of this total, 30 flights, one of which was a glide flight, have been made with the interim engine in the period from June 1959 to February 1961. The remaining 15 flights were made with the X-15 rocket engine during the past year. To complete the project progress, the dates of the conference reports by the Research Airplane Committee to Industry are shown as mid 1956, 1958, and the present date.

The conduct of the X-15 flight program to date possibly can best be described simply as a series of progressive steps to higher speed and higher altitudes, with some deviations from this approach made to investigate higher structural heating rates and stability and control at high angles of attack. The program therefore has effectively focused and directed the desired research efforts in areas such as aerodynamic heating, structural integrity, hypersonic stability and control, and flight control systems, and at the same time has provided the program support required to insure a reasonable level of flight safety.

Figure 6 presents a summary of the flight program progress for each of the three airplanes, including the events that affected the program progress. During the last half of 1959, the contractor flew the number 1 airplane for two flights - one glide and one powered. The contractor also flew the number 2 airplane from September 1959 until approximately mid 1960. All eleven of the contractor flights were with the interim engine for the purpose of evaluating the airplane and the various propulsion and flight control systems. During this period, the number 2 airplane was damaged during an emergency landing after a fire developed in the engine compartment during flight. The government received the number 1 airplane with the interim engine and performed the first flight in March 1960. Airplane 1 was tested from this date until February 1961, during which time the maximum speed and altitude for the interim engine was achieved. Six pilots of the Air Force, Navy, and NASA participated in this phase of the program. The number 2 airplane was the first to be converted to the X-15 engine and was flown by the contractor for three flights during November and December of 1960 to demonstrate engine throttling and engine restart capability.

The government flew the X-15 with the XLR99 engine first in March of 1961 and continued the research program that had been started with the number 1 airplane. After engine conversion, the number 1 airplane was returned to the government and was flown again in August. Both the number 1 and number 2 airplanes have been used interchangeably since that time in support of the flight program. The number 3 airplane has not as yet been flown but has now been prepared for initiation of its flight program. This airplane suffered major damage in May 1960, during a ground run of the XLR99 rocket engine and has been rebuilt and modified to accommodate an advanced control system which will be discussed during this conference.



A summary of the predicted and accomplished performance is presented in figure 7. The solid curves show the design envelopes of altitude and velocity predicted for the LR11 and XLR99 engines. The shaded area shows what has been accomplished to date. A maximum altitude of 217,000 feet has been achieved, and in the recent speed flight a velocity of 6,005 feet per second was reached.

The sources of the information being derived from the X-15 program which forms the basis for the papers to be presented are summarized as follows:

X-15 airplane	Instrumentation Postflight inspection
X-15 pilot	Biomedical data Pilot commentary
Launch airplane (B-52)	Instrumentation Crew commentary
Chase aircraft	Pilot comments Photography
Ground equipment	Tracking Photography Telemetry

It should be emphasized that valuable research data are derived from many sources in addition to the basic instrumentation carried on board the airplane. The manner in which these various sources contribute will become more obvious as the conference progresses; however, for a program of this nature, it is not possible to provide specific instrumentation to take care of all eventualities. Therefore, much of our understanding of the results of the program comes from such sources as postflight inspection, comments by the pilots of the X-15 and chase airplanes, and from photography.

Next, the research areas that form the basis for the program objectives are itemized:

RESEARCH AREAS

- Aerodynamic and structural heating
- Hypersonic stability and control
- Control at low dynamic pressure
- Piloting problems
- Landing
- Aeromedical studies
- Simulation
- Flight control systems



[REDACTED]

From the time the program was first conceived, the first four items listed have been recognized as being of primary importance. The program has been very productive in these areas, in that answers are being obtained which, for the most part, could not have been obtained by other means.

Considerable information on aerodynamic heating and its effect on the aircraft structure already has been obtained, and it is expected that the program can continue to be productive in this area for some time to come. Problems of stability and control at hypersonic speeds had been anticipated at the 1958 Conference. The present vertical-tail configuration was arrived at as the best compromise with respect to the various areas of concern. At present some assessment is possible of the relation of the airplane geometry to its handling qualities. Experience to date with control at low dynamic pressures still is rather limited; however, it is expected that flights planned for the near future should be very productive in this area. The problems of piloting have, of course, received considerable attention and will be dealt with in four papers. It seems appropriate to remark at this time, however, that the pilot has appeared to be the most trouble-free component of the entire X-15 system.

The usefulness of the X-15 in providing information on the last four items - landing problems, aeromedical studies, simulation, and control systems - was not fully anticipated originally, but has become obvious as the potential of the aircraft was considered in greater detail. Papers will be presented to cover the results obtained to date in all of the research areas listed above.

In the process of performing any research program, valuable information frequently is obtained as a result of problems that had not been anticipated. Some of the more significant items of this category are as follows:

- Panel flutter
- Structural deformation
- Landing loads
- Structural effects on stability augmentation system
- Engine-nozzle erosion
- Aerodynamic noise (B-52)

Panel flutter had not been expected, but was detected early in the program. Although the basic structure of the airplane has been proven sound, some local structural deformations have occurred. Flight experience has revealed interesting phenomena relative to the development of loads in the landing gear on ground contact. A problem resulted from unexpected coupling of structural response with the action of the

[REDACTED]

stability augmentation system. Engine-nozzle

erosion resulted in some reduction in engine life and has inspired some very interesting studies of the causes. With regard to the condition of the X-15 coupled to the B-52, some concern was expressed at the 1958 Conference of the possibility of a problem resulting from the effect of B-52 engine noise on the X-15 structure. Although this problem did not materialize, effects of pressure fluctuations in the B-52 wing cutout provided to accommodate the X-15 vertical tail did bring about a requirement for a structural change to both the upper and lower X-15 vertical-tail surfaces. All of these problems will be described in detail along with the solutions that have been applied in the various papers to be presented.

These remarks have briefly indicated the status of the X-15 flight research program. Those papers that follow, in view of time allocated in this conference and due to recency of some of the data, represent only a brief summary of the large amount of detailed data that have been collected to date from the X-15 flight program. The detailed data are being analyzed as rapidly as possible for publication and for discussion as required with individual specialists having interest in the X-15 results.

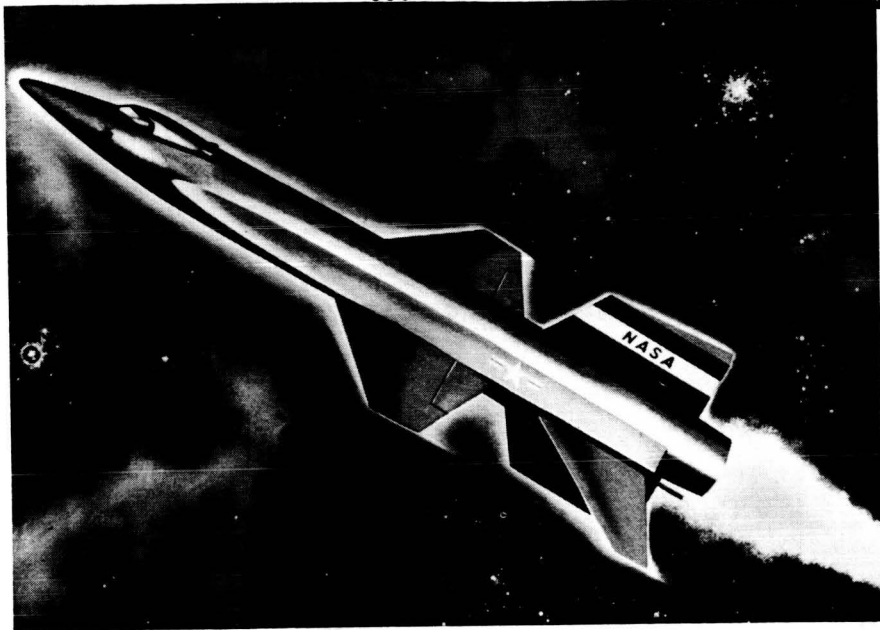
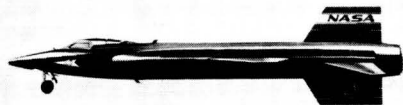
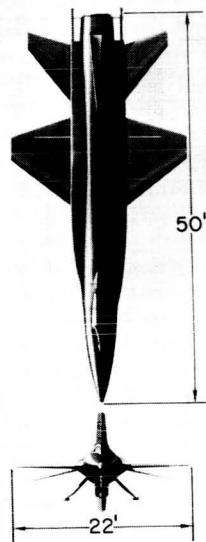


Figure 1

X-15 RESEARCH AIRPLANE



DESIGN MAXIMUM VELOCITY 6,000 FT/SEC

DESIGN ALTITUDE - 250,000 FT

STRUCTURAL TEMPERATURE TO REACH
1,200 DEGREES FAHRENHEIT

AIRCRAFT WEIGHT, LB
 LAUNCH 33,000
 LANDING 14,700

POWER PLANT-ROCKET
THROTTLEABLE 28,500 TO 57,000 LB

Figure 2

X-15 AIRPLANE CONFIGURATIONS

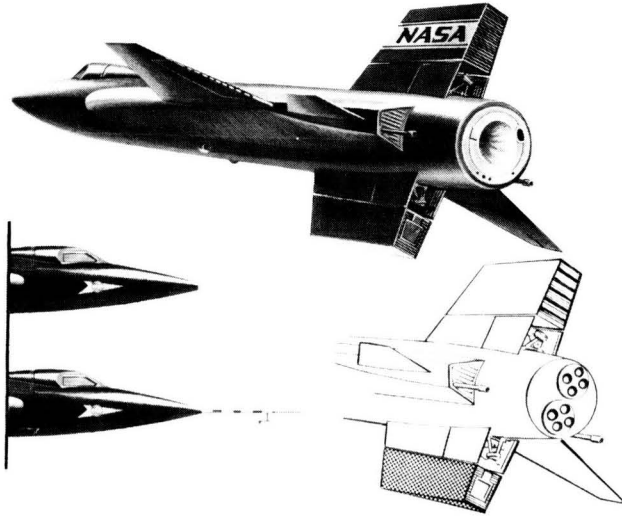


Figure 3

X-15 RESEARCH MISSION

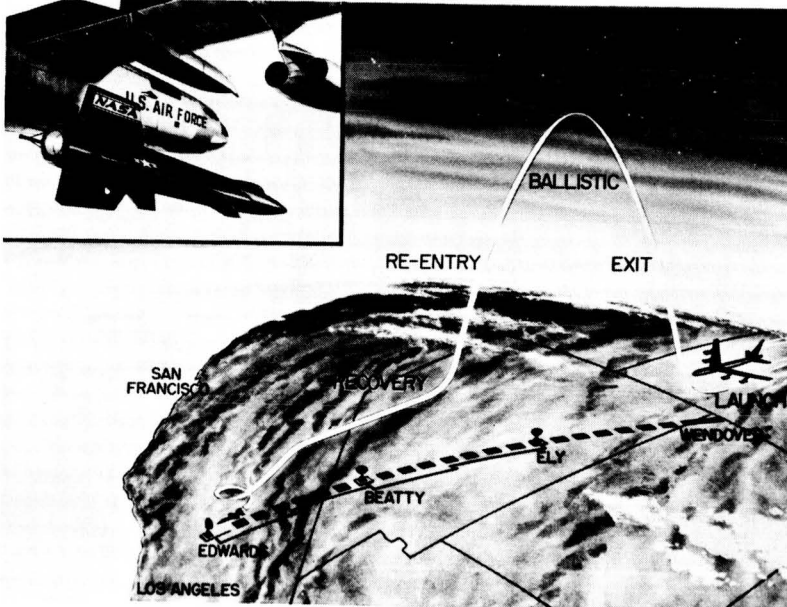


Figure 4

X-15 PROJECT PROGRESS

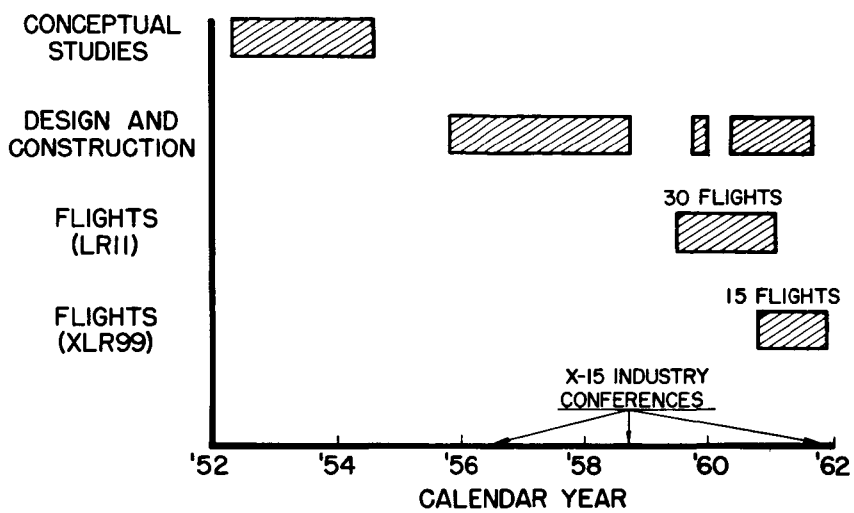


Figure 5

X-15 FLIGHT PROGRESS

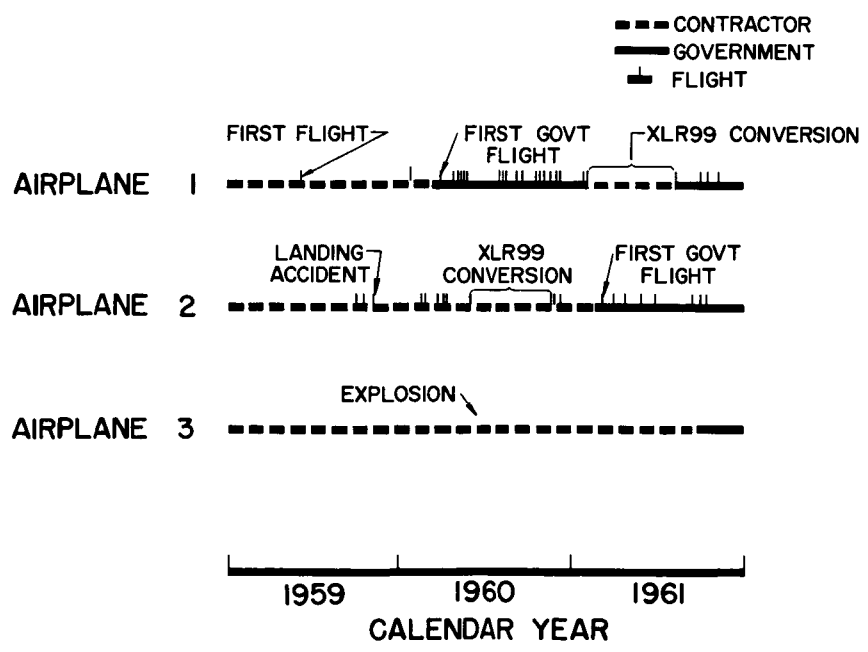


Figure 6

03710201030 8

X-15 PERFORMANCE ENVELOPE

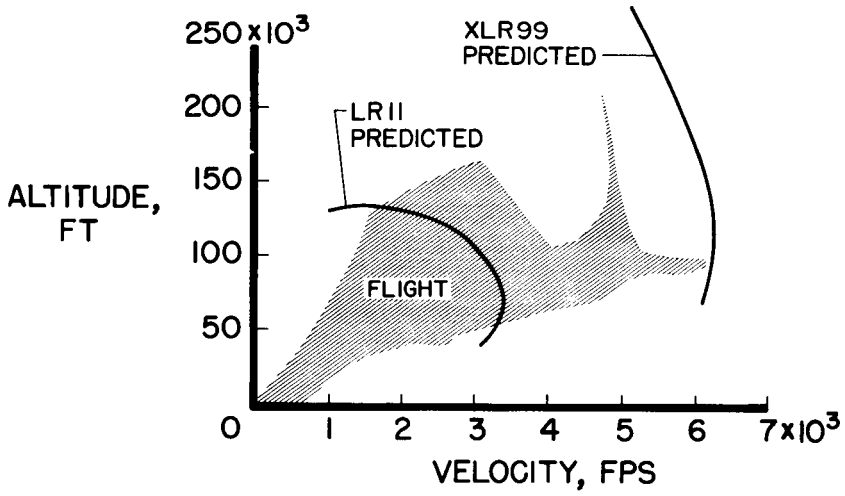


Figure 7

2. PRELIMINARY RESULTS OF AERODYNAMIC HEATING STUDIES ON THE X-15 AIRPLANE

By Richard D. Banner, Albert E. Kuhl, and Robert D. Quinn

NASA Flight Research Center

N71-75445 SUMMARY

The results of the preliminary flight heat-transfer studies on the X-15 airplane are presented, together with a discussion of the manner in which the data have been obtained, a comparison of measured and calculated turbulent heat-transfer coefficients, a correlation of the model test results and the flight results for turbulent heat transfer, some information on boundary-layer transition, and a comparison of measured and calculated skin temperatures at several locations on the airplane.

INTRODUCTION

One of the primary purposes of the X-15 program is the measurement and analysis of the aerodynamic heating of the airplane in actual flight. In the course of expanding the performance and altitude capabilities of the airplane, a considerable amount of heating data in the form of measured temperature has been obtained. These data, together with simplified calculations, have been used to define a safe operational environment for the airplane. For certain flight conditions the temperature data have been used to obtain heat-transfer coefficients and have been compared with the results of model tests and prediction methods.

In view of the discrepancies between the various turbulent heat-transfer methods, designers attempt to choose a conservative approach. The heat-transfer data obtained in the X-15 model tests, together with flight-test data of the airplane, provide a means of assessing the adequacy of current aerodynamic heat-transfer design procedures.

SYMBOLS

c_p specific heat, $\frac{\text{Btu}}{\text{lb} \cdot ^\circ\text{F}}$

h heat-transfer coefficient, $\frac{\text{Btu}}{\text{ft}^2 \cdot ^\circ\text{F} \cdot \text{sec}}$

H altitude, ft

Mach number

Prandtl number

N_{St} Stanton number, $\frac{h}{\rho_l V_l c_p}$

$N_{St,i}$ incompressible Stanton number (by Blasius theory, $\frac{0.0296}{(N_{Pr})^{2/3} (R_l)^{1/5}}$; reduced experimental data, $N_{St} \left[\frac{(T^*)_{aw}}{T_l} \right]^{.65}$)

p pressure

$p_{t,A}$ attached-shock total pressure

$p_{t,N}$ total pressure behind normal shock

$p_{t,\infty}$ free-stream total pressure

R Reynolds number, $\frac{\rho V x}{\mu}$

T temperature, °F or °R

T^* reference temperature, $T^* = T_l + 0.5(T_w - T_l) + 0.22(T_R - T_l)$

$(T^*)_{aw}$ adiabatic-wall reference temperature, $(T^*)_{aw} = T_l + 0.72(T_R - T_l)$

T_R boundary-layer recovery temperature, $T_R = T_l \left(1 + \frac{\gamma - 1}{2} \eta M_l^2 \right)$

V velocity, ft/sec

x length, ft

x_w length from wing leading edge, ft

x_f length from fuselage nose, ft

- α angle of attack, deg
- γ ratio of specific heats
- δ_{SB} speed-brake deflection
- η recovery factor ($\sqrt{N_{Pr}}$ for laminar flow, $\sqrt[3]{N_{Pr}}$ for turbulent flow)
- μ coefficient of viscosity, lb/ft-sec
- ρ density, lb/cu ft

Subscripts:

- l local
- W wall or skin
- ∞ free stream

INSTRUMENTATION

The number and location of surface thermocouples and static pressure orifices for the X-15 flight tests are shown in figure 1. There are 293 surface thermocouples on the airplane. The thermocouples are 30-gage chromel-alumel wires, spot-welded to the inside surface of the skin. There are 136 surface pressure orifices. The static pressure taps are 5/16-inch outside-diameter tubing installed flush with the outside surface of the skin. Both the thermocouple wires and the tubes are connected to onboard recording instruments in the fuselage of the aircraft.

The instrumentation is primarily located on the right-hand side of the airplane; however, there are corresponding measurements on the left-hand side of the forward fuselage and the midspan station of the vertical tail. No instrumentation is located in the vicinity of the liquid-oxygen and fuel tanks, which are integral tanks. The instrumentation on the wing is primarily located at three spanwise stations, both top and bottom. On the top and bottom of the horizontal tail, only thermocouples have been installed.

Although temperature data have been obtained at most of the locations shown in figure 1 during all of the flights accomplished to date,



relatively few have met the requirements for accurate reduction of heat-transfer data by the transient-skin-temperature procedure. Transient analysis requires high skin heating rates and low skin temperatures, while relatively constant flight conditions are maintained.

TEST CONDITIONS

Two types of flights which are of interest in the aerodynamic heating study are shown in figure 2. The maximum speed for both flights was near 5,000 feet per second. The flight shown on the left of figure 2 attained a relatively low altitude near 100,000 feet. Heat-transfer-coefficient data were obtained from the skin heating rates during a period of time (shown by the shaded strip) when velocity, altitude, and angle of attack were relatively constant and when the skin temperature was increasing at a rapid rate. The flight shown on the right of figure 2 is typical of many high altitude flights during which the velocity, altitude, and angle of attack are changing quite rapidly, and for this reason heat-transfer-coefficient data are not reduced. However, the heat transfer during high-altitude flights can sometimes be inferred from comparisons of calculated and measured skin temperatures.

Flight heat-transfer data have been obtained at Mach numbers near $M_{\infty} = 3, 4, \text{ and } 5$. During the design of the X-15, heat-transfer tests were conducted on a 1/15-scale model of the X-15, and turbulent heat-transfer data were obtained at Mach numbers of $M_{\infty} = 3, 4.65, \text{ and } 7$. Both the model test conditions and the present flight-test conditions are shown in figure 3 in terms of the parameters which affect heat transfer. Also shown is the variation in the heat-transfer parameters that is obtained from the X-15 design speed and altitude flight missions. (The Reynolds numbers and wall (or skin) temperatures have been based upon a location 1 foot behind the wing leading edge.)

As is frequently the case, the X-15 design flight conditions were outside the range of the wind-tunnel test conditions, and it was necessary to extrapolate the turbulent heat-transfer data on the model, obtained at relatively low Reynolds numbers and heating rates, to the Reynolds numbers and heating rates of the flight conditions.

METHODS

The difficulty in extrapolating turbulent heat-transfer data, as well as in predicting the actual level, is illustrated in figure 4. At the lower Mach number, Eckert's reference-temperature method (ref. 1)

and the theory of Van Driest (ref. 2) tend to agree better than at the higher Mach number. At both Mach numbers, however, the reference-temperature method indicates a lower level at the adiabatic-wall condition and a greater increase in heat transfer with increased heating (lower values of T_w/T_R) than does the theory of Van Driest.

Some recent results of a study by Winkler (ref. 3) indicate about the same level of heat transfer as the reference-temperature method at the adiabatic-wall condition but show a decrease with increasing rate of heat transfer, which is the opposite behavior to that predicted by the other theories and empirical methods. Winkler interprets the results as confirmation of data previously obtained (ref. 4). The data of reference 4 were generally discounted by Sommer and Short in their development of the T' method (ref. 5).

One of the primary difficulties in the analysis of turbulent heat-transfer data is the determination of the conditions to be used in the flat-plate equations based on the flow properties at the boundary-layer edge. In this regard, the X-15 data, presented herein, have been based upon the assumption that the flow properties at the boundary-layer edge (behind leading-edge regions) can be calculated by conventional attached-shock methods (ref. 6). The adequacy of this assumption is discussed in the next section.

DISCUSSION OF RESULTS

Surface Pressures and Heat Transfer

Surface-pressure and heat-transfer-coefficient data have been obtained during low angles of attack for Mach numbers near 3, 4, and 5, and at altitudes of less than 100,000 feet. For the most part, the flow has been turbulent. The surface pressures and heat transfer which have been measured on the lower wing surface about midsemispan and on the lower fuselage center line at a Mach number of about 4 and at an angle of attack of about 4° are shown in figure 5. In the upper part of the figure measured pressures are compared with calculated pressures and in the lower part of the figure measured heat-transfer data are compared with calculations. For the wing, the surface pressures are closely estimated by assuming an attached shock and expanded flow over the wing. Similarly, good agreement is shown for the lower fuselage center line, where a tangent-cone approximation has been used to calculate the local pressure levels. Calculation of the turbulent heat transfer is not quite so straightforward, however, since, in addition to the local static-pressure level, some idea of the local total pressure is required. The estimation of a local total pressure is somewhat involved, since an

understanding of the entropy change along a streamline is required. In lieu of this information, the total-pressure level can be bracketed between the free-stream total pressure and the total pressure that would exist behind a specified number of shocks. When the limiting local-flow conditions have thus been established and a choice of a turbulent heat-transfer method has been made, local heat-transfer coefficients can be calculated.

The calculations shown in figure 5 as the upper and lower boundaries of the shaded areas represent the heat-transfer coefficients that would be calculated when Eckert's reference-temperature method is used, together with the measured static pressures and the assumption of the free-stream total pressure and the total pressure behind a normal shock. The assumption of free-stream total pressure overestimates the measured levels of turbulent heat transfer by 50 to 60 percent. The assumption of a total-pressure level equal to that behind a normal shock overestimates the measured data by 15 to 25 percent.

Shown by the solid line in figure 5 are calculated heat-transfer coefficients which have been obtained by assuming the calculated static pressure, the total pressure that is calculated behind the attached shock, and neglecting the effect of heating rate on the heat-transfer coefficient. This approach overestimates the measured data by 10 to 20 percent. Neglecting the effect of heating rate in the calculation of the heat-transfer coefficient is accomplished by substituting the boundary-layer recovery temperature for the skin temperature in the equation used to calculate the reference temperature. The result is interpreted as an adiabatic-wall reference temperature and accounts only for the effects of compressibility on the heat transfer. The attached-shock total pressure was used, since it is believed that it is a better approximation than either the free-stream or the normal-shock total pressure. Whether this approach can be generalized depends largely on subsequent measurements of the actual total-pressure levels in flight over a range of skin heating rates. The simplicity afforded by this approach and the favorable agreement that has been obtained has resulted in the choice of this method for computing the local levels of turbulent heat transfer.

This approach has also been chosen to illustrate the correlation between flight-test data and the model data which were obtained at different Reynolds numbers and heating rates. The correlation is shown in figure 6. Flight data, obtained at Mach numbers of 3, 4, and 5, and model data, obtained at a Mach number of 3, have been reduced by the adiabatic-wall reference-temperature method to the incompressible value of the dimensionless heat-transfer coefficient, the Stanton number, divided by the local Reynolds number to the 0.8 power and are shown plotted against the local Reynolds number. In this manner, the flat-plate theory now corresponds to the solid lines shown and the data obtained at various Mach numbers and local Reynolds numbers can be

shown for comparison. For the lower wing surface, both the flight data and the model data are correlated fairly well over the Reynolds number range of the tests. For the forward fuselage, the dashed line represents a 15-percent increase over the flat-plate theory to allow for conical flow. Most of the flight data correlate fairly well over the Reynolds number range, and the use of a conical transformation results in slightly conservative estimates. The model data, which were obtained at Mach 3 and an angle of attack of zero on the side of the fuselage, seem to agree favorably. The bottom fuselage data on the model, however, are from 50 to 100 percent higher than the remainder of the data. This result is thought to be caused by roughness effects, since sand-grain roughness was applied on both sides of the model bottom center line in order to trip the boundary layer and assure turbulent flow at angles of attack.

At a conference on the X-15 in July 1958, Martin R. Kinsler at North American Aviation, Inc., used the model data to determine empirical factors that would correct flat-plate heat-transfer coefficients to those computed from the model data. These same factors were incorporated in computed programs to correct heat-transfer coefficients computed for the full-scale airplane flying assigned missions. It is interesting to note that if the theory is adjusted to fit the model bottom center-line data and the results are extrapolated to the flight Reynolds number range, a considerable overestimate of the flight heat transfer is obtained.

Boundary-Layer Transition

A particular area of interest in the flight results is boundary-layer transition. At present, two methods are used to detect laminar and turbulent areas on the airplane in flight. The first, of course, is the thermocouple data reduced to heat-transfer coefficients, which show a much higher level of heat transfer in a turbulent boundary layer than in a laminar boundary layer. The second is in the use of temperature-sensitive paints which are applied to large surface areas of the airplane prior to a flight.

How these methods are used and an illustration of the type of transition that has been detected on the X-15 is shown in figure 7. In the upper right is a postflight photograph of the lower surface of the X-15 wing, which had been coated with temperature-sensitive paint prior to flight. This wing is opposite the heavily instrumented wing. The line on the photograph shows the corresponding location of the midsemi-span thermocouple row. The postflight temperature-paint patterns indicated high-temperature, wedge-shaped areas originating at leading-edge expansion joints and extending a considerable distance rearward. The

surface discontinuities of the expansion joints, which are rather severe, apparently produce turbulent flow during the entire flight and lead to higher temperatures in the wedge-shaped areas.


The measured heat-transfer data seem to substantiate this analysis, an example of which is shown in the lower left-hand side of figure 7. Two independent sets of data are shown for a Mach number of about 4 and an angle of attack of about 4° . The data shown by the round symbols are for the normal leading edge of the wing with expansion joints. The data shown by the square symbols were obtained with the boundary layer artificially tripped at the leading edge immediately ahead of the thermocouple station. The data that were obtained with the normal leading edge show an abrupt increase in the heat transfer from a laminar level to a turbulent level at a distance of about 1.2 feet from the leading edge. This distance corresponds approximately to the point where the lateral spread of turbulence originating at the leading-edge joint would cross the thermocouple station. From this point rearward the turbulent level of heat transfer is about the same as that for the all-turbulent case, and both sets of data appear to be fairly well predicted by the turbulent method discussed previously.

Since these data were obtained, small shields (fig. 8) have been used to cover the leading-edge expansion joint and thus to reduce the severity of the surface discontinuity. Recent tests with the shields installed still show the wedge-shaped patterns in the temperature paints, although it is believed that the length of time during a flight that the turbulent wedges exist has been reduced. It should be pointed out that the light areas shown in the photograph of the wing (fig. 7) do not necessarily imply laminar flow, but rather that these areas were at least not all turbulent during the flight.

Boundary-layer transition, which may be produced by such discontinuities in the surface of a high-speed vehicle, would be extremely difficult to predict. As yet, for the X-15, there has not been established parametric correlation which would allow the prediction of the transition location on the wing a priori. Under these circumstances, it would seem that conservative estimates of transition should still be required.

Skin Temperatures

In order to compare measured skin temperatures with predicted values, based on the turbulent heat-transfer correlation presented earlier, and to illustrate how boundary-layer transition during flight affects the resulting skin temperature, figure 9 shows measured and calculated temperatures for a point on the wing during both the low-



and high-altitude flights. This location is on the lower surface of the wing, about midsemispan, and is 1.4 feet from the leading edge. For the low-altitude flight, the measured data indicate all-turbulent flow at this point, since a fairly high skin heating rate and maximum temperature were experienced. The calculated turbulent skin temperature agrees quite well during the high heating period but slightly overestimates the measured value near its peak and during a period of cooling just following the peak temperature. A close look at the trajectory (fig. 2) indicates a fairly high angle of attack during this period, and the differences seen in the measured and calculated temperatures may be due to the inability to predict the local flow conditions properly during this period of time.

For the high-altitude flight, this point on the wing appears to be experiencing some laminar flow. An all-turbulent calculation results in a higher temperature than was measured during the exit phase of the trajectory, greater cooling during the ballistic portion, and an overestimate of the maximum temperature that was experienced during the reentry. The assumption of laminar flow during the latter part of the exit phase and the ballistic portion of the trajectory results in better agreement between the measured and calculated data. This location on the wing is felt to be affected by the adjacent turbulent wedge, which originates at the leading edge and was previously discussed. Exactly what causes this location to go laminar at the higher altitudes is not known, but it may be that the turbulent wedge either vanishes or that its lateral spread is delayed.

It appears that when the boundary layer is known to be either laminar or turbulent, the skin temperature can be predicted with reasonable accuracy. This statement seems to apply regarding other areas of the airplane also. Flow on the fuselage, for example, seems to be turbulent over the entire length, at least for the relatively low angles of attack that have been experienced to date. In discussing the fuselage temperatures, it will be of interest to look first at typical temperature measurements that have been obtained near the stagnation region of the fuselage, which is the area of the high-speed flow-direction sensor. These data are shown in figure 10.

The sensor is 6.5 inches in diameter, spherically shaped, and heat-sink constructed. An orifice is located at the stagnation point and measures the stagnation pressure. Four other orifices are located about 40° from the stagnation point in the vertical and horizontal planes and measure differential pressures. A servo system nulls the sensor in the free-stream direction.

Thermocouples have been installed on the inside surface of the sensor at various angular positions. Measured data which were obtained

during the high-altitude flight at locations 20° and 80° from the stagnation point are shown by the symbols. It is noted that the measured temperatures at the 20° location are 200° to 250° higher than at the 80° location. In order to calculate the inside surface temperatures, a spherical segment of the sensor was divided into small lumps and the conduction and convective heat-transfer problem was simulated in a digital computer. Newtonian pressures with isentropic expansion and Lees' laminar theory were used to obtain the aerodynamic heating input and the resulting calculated temperatures are shown by the solid lines. Good agreement is shown for the calculated and measured values at the 20° location, but the measured values at the 80° location are considerably higher than the calculations. Significant differences are noted between the measured and calculated heating rates at the 80° location during the early part of the exit phase and during the reentry and suggest that the high heating at the 80° location is associated with high Reynolds numbers. There are several possible reasons why heating at the 80° location is higher than would be expected. First, there may be turbulence induced by the upstream pressure orifice at this location; secondly, the close proximity of the lip on the assembly may create either a stagnant region or separated flow; or, the cause may be a combination of these phenomena. Some early wind-tunnel tests obtained at the Langley Research Center of a similar configuration had shown quite high heating could be expected on the assembly lip itself, but the results that are presently being experienced in flight were not evident in the tunnel tests. The higher heating in this region has not caused any alarm, nor is it expected to, since cooling has been provided for the assembly in the event it is required.

The surface discontinuity presented by the assembly lip certainly seems sufficient to trip the boundary layer to turbulent flow, if it is not already turbulent, since most of the heat-transfer and skin-temperature data that have been obtained on the fuselage have been at the turbulent level. Evidence of this is presented in figure 11, where measured skin temperatures are compared with calculated values for the low-altitude flight. In addition, similar comparisons are made for the lower speed brake, which also seems to be in an all-turbulent area.

On the the forward-fuselage lower center line, the measured temperature data are shown for a point 11 feet behind the nose. The solid line represents calculated values based on tangent-cone static and total pressures and the adiabatic-wall reference temperature. The calculated temperatures agree fairly well with the measured data, although slightly high near and just following the peak temperature, where higher angles of attack were experienced during the flight.

The speed brake provides another interesting area for comparisons to be made, since the use of such a high drag device is intended to reduce the overall heating of the airplane during reentry flight, as well as to provide increased directional stability. The measured skin temperature is shown in figure 11 for a point near the rear of the speed brake. For the flight shown, the speed brake was deflected 35° at a time 80 seconds, which was just prior to burnout. Model data indicated that with the speed brake deflected, the heat transfer could be closely estimated if the flow length was chosen from the hinge line. The calculation labeled x_1 is based on this assumption and is seen to overestimate the maximum measured temperature about 100° . For comparison, temperatures have been calculated based on the flow length from the leading edge and the values labeled x_2 are seen to estimate the measured values more closely. The ratio of these two lengths would indicate a 25-percent reduction in the level of heat transfer when the distance from the leading edge is used. As a matter of interest, a calculation is shown for the case of the speed brake undeflected, which when compared with the measured data, indicates a 500° temperature rise on the speed brake due to its use during the flight.

CONCLUDING REMARKS

Heat-transfer data have been obtained on the X-15 in flight to speeds near free-stream Mach numbers of 3, 4, and 5, and at relatively low angles of attack. Turbulent heat-transfer methods are reviewed and compared with the X-15 flight data. The level of heat transfer predicted by the reference-temperature method, which accounts for the effect of heating rate, is from 15 to 60 percent higher than the measured data, depending upon the assumed total-pressure level. Closer agreement with the measured data was obtained when the effect of heating rate was neglected and attached-shock total-pressure levels were used. Some evidence of the manner in which boundary-layer transition takes place on the airplane in flight has been shown and the results suggest the advisability of continuing to use conservative estimates for the transition location.



REFERENCES

1. Eckert, Ernst R. G.: Survey on Heat Transfer at High Speeds. WADC Tech. Rep. 54-70 (Contract No. AF 33(616)-2214, RDO No. 474-143), Wright Air Dev. Center, U.S. Air Force, Apr. 1954.
2. Van Driest, E. R.: The Problem of Aerodynamic Heating. Aero. Eng. Rev., vol. 15, no. 10, Oct. 1956, pp. 26-41.
3. Winkler, Eva M.: Investigation of Flat Plate Hypersonic Turbulent Boundary Layers With Heat Transfer. [Preprint] 856-59, American Rocket Soc., June 1959.
4. Lobb, R. K., Winkler, Eva M., and Persh, Jerome: NOL Hypersonic Tunnel No. 4 Results VII: Experimental Investigation of Turbulent Boundary Layers in Hypersonic Flow. NAVORD Rep. 3880, U.S. Naval Ord. Lab. (White Oak, Md.), Mar. 1, 1955.
5. Sommer, Simon C., and Short, Barbara J.: Free-Flight Measurements of Turbulent-Boundary-Layer Skin Friction in the Presence of Severe Aerodynamic Heating at Mach Numbers From 2.8 to 7.0. NACA TN 3391, 1955.
6. Ames Research Staff: Equations, Tables, and Charts for Compressible Flow. NACA Rep. 1135, 1953. (Supersedes NACA TN 1428.)

X-15 AIRPLANE SURFACE INSTRUMENTATION

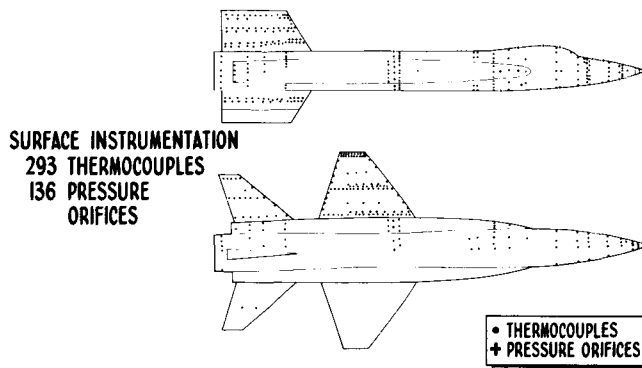


Figure 1

TYPICAL HEATING FLIGHTS

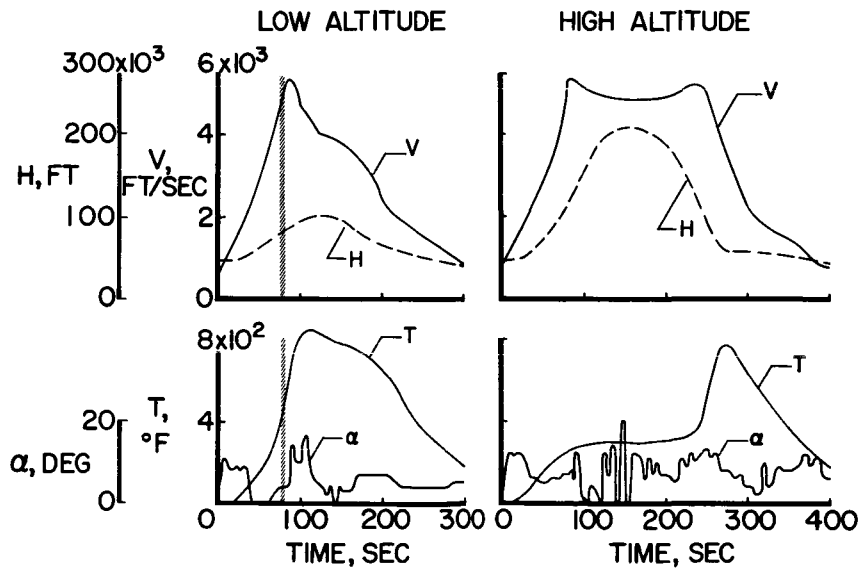


Figure 2





HEAT-TRANSFER TEST CONDITIONS

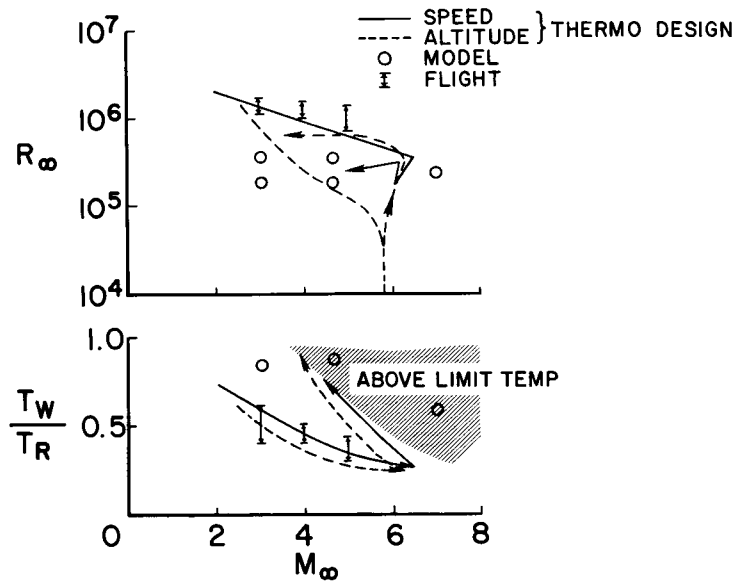


Figure 3

TURBULENT HEAT-TRANSFER METHODS

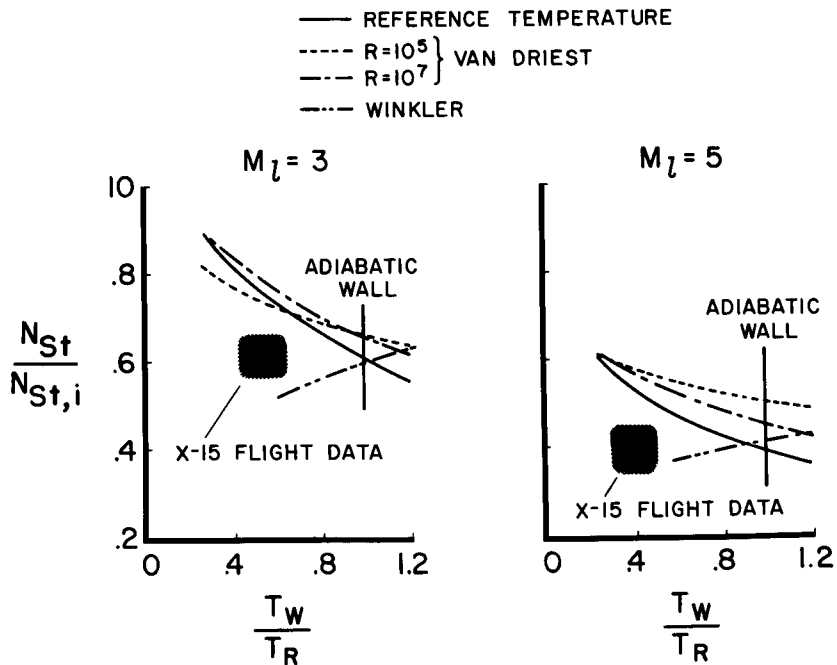


Figure 4



SURFACE PRESSURES AND HEAT TRANSFER

$M_{\infty} \approx 4, \alpha \approx 4^\circ$

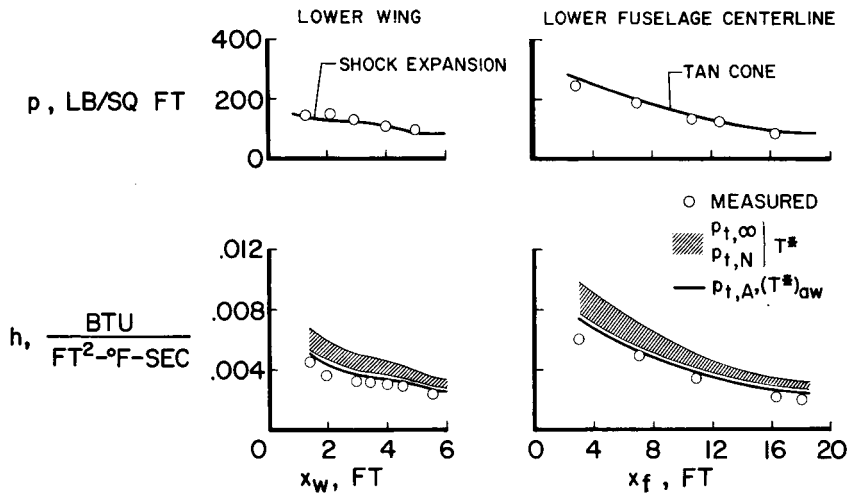


Figure 5

REYNOLDS NUMBER CORRELATION

ADIABATIC REFERENCE TEMPERATURE

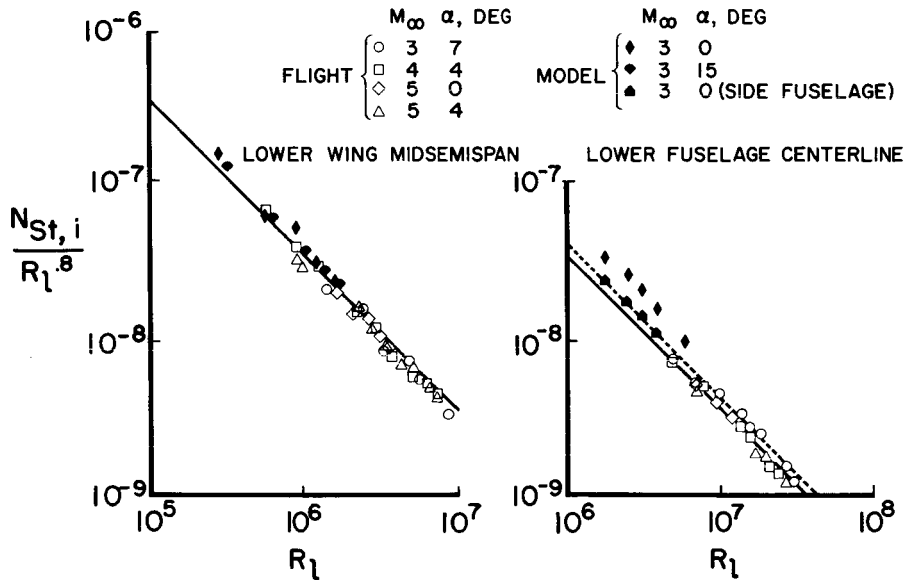
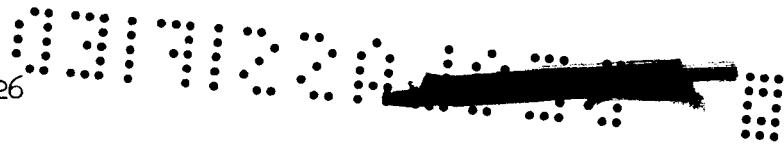


Figure 6



WING BOUNDARY-LAYER TRANSITION

$M_\infty \approx 4, \alpha \approx 4^\circ$

- NORMAL LEADING EDGE
(ADJACENT "WEDGE" EFFECT)
- TRIPPED AT LEADING EDGE
(ALL TURBULENT)
- CALCULATED

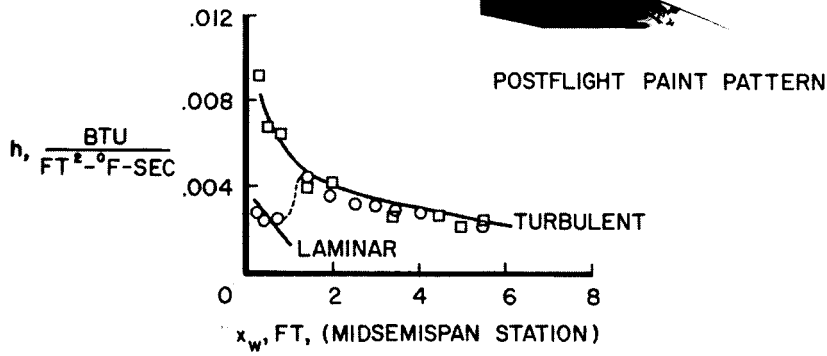
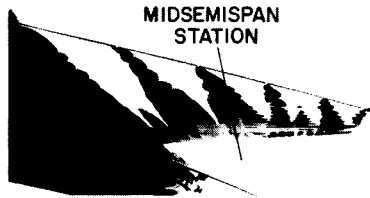


Figure 7

WING LEADING-EDGE EXPANSION JOINTS

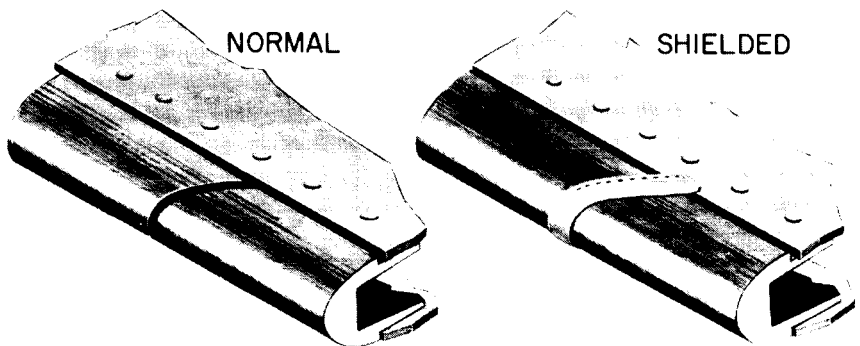


Figure 8



WING SKIN TEMPERATURES

$x_w = 1.4$ FT, LOWER MIDSEMISPAN

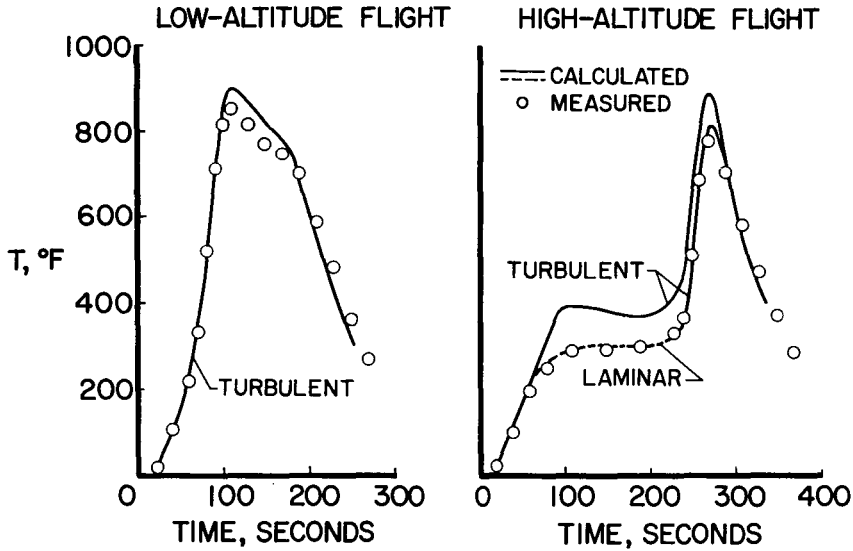


Figure 9

FLOW-DIRECTION-SENSOR TEMPERATURES HIGH-ALTITUDE FLIGHT

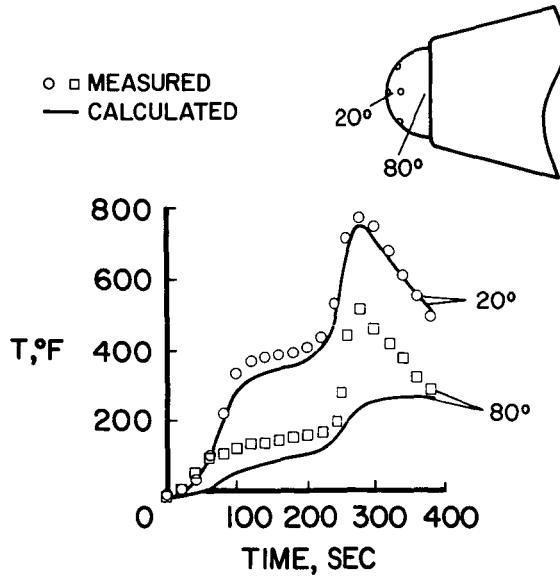


Figure 10



SKIN TEMPERATURES IN TURBULENT AREAS LOW-ALTITUDE FLIGHT

○ MEASURED
— CALCULATED

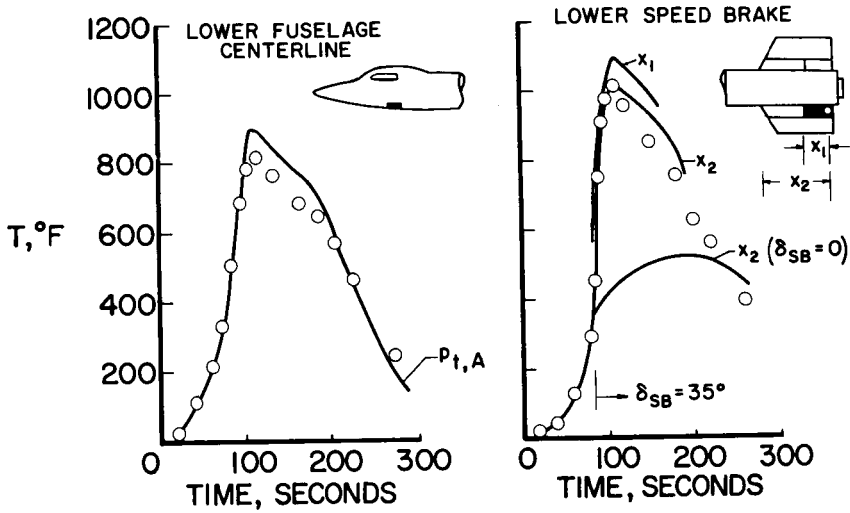


Figure 11



3. STRUCTURAL HEATING EXPERIENCES OF THE X-15 (U)

By Eldon E. Kordes, Robert D. Reed
NASA Flight Research Center

and Alpha L. Dawdy
North American Aviation, Inc.

N71-75446

3

The expected structural temperatures and their effect on the development and design of the X-15 airplane structure have been described in previous conferences, and Banner, Kuhl, and Quinn (paper no. 2) have discussed in detail the many factors affecting the heat input to the structure. The purpose of the present paper is to show the magnitude of structural temperatures measured during the flight program and to describe structural problems that have developed due to structural heating.

The entire airplane is designed as a hot structure and is basically monocoque or semimonocoque as indicated in figures 1 and 2. The external surface is Inconel X, and titanium is used extensively for the internal structure. The forward fuselage section contains the double-walled pressure compartments for the pilot and instruments. The center fuselage section is formed by the oxidizer tank ahead of the wing and the fuel tank with frames for supporting the wing. The rearward fuselage structure supports the empennage, main landing gear, and engine. The wing is of multispar construction of taper-milled Inconel X skin with titanium substructure. The horizontal and vertical tails are two-cell box structures with stabilizing ribs. The wing, horizontal tail, and vertical tail have segmented leading-edge heat sinks of Inconel X. A tunnel along each side of the fuselage for housing control cables, hydraulic lines, and instrument wiring is formed by removable panels. Throughout the structure, extensive use has been made of corrugations and beading to minimize thermal stress.

The thermocouple instrumentation on the X-15 was shown by Banner, Kuhl, and Quinn (paper no. 2). Many areas of the X-15 airplane do not contain thermocouples and in the areas where thermocouples are available, the spacing and location do not permit detection of local hot spots and severe gradients that may develop. A method that has been successful in obtaining qualitative measurements of maximum temperature distribution in conjunction with thermocouple measurements is the use of temperature-sensitive paints.

As is well known, the X-15 flight program has proceeded toward the design speed and altitude mission in small increments. For example, the speed increments have been accomplished by flying along a

trajectory similar to the mission trajectory and programming engine shutdown to give the desired Mach number. For all speed flights the peak Mach number occurs at engine shutdown. Recovery portions of each flight have been used to obtain stability data and evaluate handling qualities; and hence the recovery was different for each flight. The differences in the flight profiles make it almost impossible to obtain systematic research data on structural heating; therefore, this paper will present only examples of temperature levels and distribution experienced during this program. From consideration of structural safety, the present program has pointed out structural problems while they are still minor.

First to be discussed are the maximum structural temperature level and the distribution measured on the fuselage and the wing. The maximum skin temperature distribution measured on the flight to maximum speed is presented in figure 3. These temperatures occurred during the recovery portion of the flight several minutes after engine shutdown and, because of the maneuvers performed, cannot be attributed entirely to peak Mach number. The sketches on the left for the forward fuselage and on the right for wing midsemispan show the thermocouple locations by the solid points and the measured temperatures by the open symbols. The solid curves, included for reference, are for the calculated maximum temperature distribution for a design speed mission. The dip in the curves near the 5 percent fuselage station is attributable to the thicker skin in this region, and the rise is caused by the insulation in the cockpit area, which blocks internal radiation. The low temperatures near the 40 percent station are caused by the lox tank. On the wing, the higher temperatures near the trailing edge are a result of the thinner skin. Effects of the heat sink of the internal structure are not shown since internal temperature measurements are not adequate. These data are the temperatures measured on a speed flight to a Mach number of 6.04 and are representative of the levels reached during the X-15 program. It should be mentioned that on all speed flights above a Mach number of 4, the maximum temperatures followed the same trends.

The large gap between measured temperatures and the temperatures predicted for design can be attributed to values of heat transfer used in the design calculations and differences in the flight profiles. With a flight profile chosen to minimize heating effects, the high-speed flights have been accomplished without extreme structural temperatures.

The maximum temperatures measured at various points on the X-15 during the flight program are summarized in figure 4. Maximum temperatures are shown for the canopy frame, ball nose, lower fuselage, side fairings, lower wing skin, wing leading edge, lower ventral, lower speed brake, and horizontal tail. These maximum temperatures did not

all occur on the same flight; however, they serve to illustrate the highest temperature levels that the structure has experienced up to this time, with the exception of local hot spots which are discussed subsequently.

The temperatures presented thus far do not show variation during the flight or the gradient through the structure. In order to illustrate these quantities, typical temperature histories for the front spar of the wing at the midsemispan are presented in figure 5. These temperatures were measured on a flight to a maximum Mach number M_{MAX} of 5.28.

The sketch gives the thermocouple location on the lower skin, the lower spar cap, the web, and the upper skin. The number by each thermocouple is used to identify the curve. Time is measured from launch from the B-52 after a "cold soak" at an altitude of 45,000 feet, and the time of peak Mach number is given for reference. On this flight the lower skin temperature shown by the solid curve increased at 6.25° per second during powered flight, and the maximum temperature occurred about 150 seconds after peak Mach number. This time corresponds to the time of maximum temperature difference between the lower skin and the spar web of about 570° F. From the standpoint of thermal stresses in the structure, the temperature gradient, together with the temperature level, defines the most severe condition on each flight. The measured data give the temperature levels but, with the limited number of thermocouples on the spar, the complete thermal gradient cannot be determined from flight measurements and must be obtained from analysis. Calculated gradients are compared with flight data for the time of maximum gradient in figure 6. The temperature is shown as a function of the wing thickness measured from the lower surface. The solid curve was obtained from calculations, and the points are from the flight measurements at the numbered points shown on the sketch. For these calculations, the heat transfer to the external skin was determined first on the basis of the time history for the skin temperatures by the method described in the previous paper by Banner, Kuhl, and Quinn. This heat input was used to compute the thermal gradient through the spar and included 4 inches of each cover sheet. The spar cross section was divided into 30 elements for the calculations. Good agreement is seen to exist between calculated and measured temperatures at the four thermocouple locations shown on the sketch. This thermal gradient has been used to calculate the thermal stresses in this isolated spar element. The stress calculations have neglected the interaction with the adjacent structure and are used primarily to monitor the changes in the thermal-stress level for various flight conditions. Thermal stresses calculated for the gradient shown are presented in figure 7. The curves on the right indicate the variation of normal stress through the spar and the curves on the lower left show the variation of the normal

stress in the lower skin. Included for reference are the thermal stresses calculated for a design speed mission. The stress levels for the Mach 5.28 flight at 225 seconds are seen to be well below the stresses predicted for this design condition, except in the lower skin at the spar cap where the compressive stress is higher for the Mach 5.28 flight.

Some of the areas of the X-15 where structural problems have developed on the fuselage and wing as a result of heating or thermal stresses are shown in figure 8. They include the side fairings, nose-gear compartment, canopy seal, canopy glass, and wing leading edge. The first temperature problem occurred on the side-fairing panels along the lox tank before the X-15 was first flown. Pronounced elastic buckles appeared in the panels as a result of tank contraction when the tank was filled for the first time. The buckling was relieved by adding a 1/8-inch expansion joint to the tunnel fairing near the wing leading edge.

After the flight on March 7, 1961, in which a Mach number of 4.43 was reached, several permanent buckles were formed in the outer sheet of the fairing between the corrugations near the edge of a panel. Since these fairing panels are required to carry local air loads only, these buckles did not seriously affect the structural integrity. The maximum temperatures measured on the side fairing during this flight are shown in figure 9 for two fuselage stations in the area of the lox tank. The insert is a photograph of a typical buckle in the fairing panel. This buckle occurred near the wing leading edge on the left side of the airplane. The scales help show the extent of the buckle; the depth of the buckle is about 1/4 inch. At station 202, just forward of the tank, the temperature was 590° F on the lower fairing and at station 335, just behind the lox tank, the temperature was 480° F. No measurements were available on the lox tank. The temperatures shown occurred after engine shutdown, which, on this flight, left about 20 percent of the fuel still in the tanks. The cold tank, about -260° F for liquid oxygen, together with the high skin temperatures on the fairings resulted in large gradients, and hence the buckles. The important results found were that these thermal gradients between the lox tank and the fairings were actually higher than calculated for the original design. The design was based on complete fuel burnout before the maximum skin temperatures were encountered. As a result of this experience, four expansion joints were installed in the fairing forward of the wing to give a total expansion capacity of slightly over 1 inch. To date, this modification has prevented additional permanent buckles in the fairing for similar flights to higher temperatures.

The surface irregularities produced by the buckles were expected to cause local hot spots on high-speed flights. As a check on this

effect, the buckle areas were painted with temperature-sensitive paint for the flight to a Mach number of 4.6. The results showed that the maximum temperature in the buckle area was essentially the same as in other areas on the panel, and there was no evidence of local hot spots.

Another heating problem that has developed on the X-15 is due to airflow into the interior of the structure. This flow has caused unexpected high temperatures around the speed-brake actuators, and loss of instrumentation wires at the roots of the wing and tail surfaces. On the forward fuselage, the seal of the canopy has been damaged because of a slight raising of the front edge by cabin pressure, which allowed hot air to flow against the seal. This problem has been solved by attaching a shingle-type strip to the fuselage just ahead of the canopy joint to prevent airflow under the edge of the canopy. A similar problem has developed in the nose-gear compartment. The small gap at the rear end of the nose-gear door was sufficiently large to allow the airstream to enter the compartment and strike the bulkhead between the nose-gear compartment and the cockpit. This stream caused a local hot spot. Aluminum tubing, for the pressure-measuring system, is attached to this bulkhead in the nose-gear compartment, and during a flight to Mach 5.2, portions of this tubing melted away. This damage is shown in figure 10. Shown are the aluminum tubing with the damaged area and the titanium bulkhead between the nose gear and pilot compartment. The bulkhead was heated to about 530° F, which was sufficiently high to scorch the paint on the bulkhead in the pilot's compartment so that smoke was caused in the cockpit. Since this flight, an Inconel compression seal has been added to the rear end of the nose-gear door and additional protection has been provided by placing a baffle plate across the compartment just behind the door opening.

The windshield glass originally installed on the X-15 was soda-lime tempered plate glass. This choice was based on a predicted maximum temperature of 740° F. Data obtained on early flights indicated that outer-face temperatures near 1,000° F could be expected with a differential temperature between faces of 750° F. It was apparent that soda-lime glass would not withstand these temperatures and that alumino-silicate glass should be a satisfactory replacement. The alumino-silicate glass has higher strength and better thermal properties which reduce the expected temperature and gradients to about 70 percent of those predicted for soda-lime glass. The alumino-silicate glass withstood thermal tests to temperatures which were about 1.5 times the expected flight values. Subsequently, the alumino-silicate glass was installed in all three X-15 airplanes; however, one of the soda-lime windshields was inadvertently installed at a later date and it fractured during recovery from an altitude flight to 217,000 feet. On a speed flight to a Mach number of 6.04, one of the alumino-silicate glass panels also fractured. In both cases the glass fragments remained in place during the remainder of the flight and photographs of the fractured panels are shown in

figures 11 and 12. Figure 11 shows the soda-lime glass and figure 12 is the alumino-silicate glass. The fracture pattern in figure 11 is not typical of tempered glass, but the one in figure 12 is typical. In both cases, the retainer frame buckled near the center of the upper edge of the glass and created a local hot spot at this point. Failure of both glass panels started adjacent to this buckle. Subsequent to the last failure, the retainer has been changed from Inconel X that was 0.050 inch thick to titanium that is 0.10 inch thick in order to eliminate buckling.

Structural problems have developed on the wing leading edge because of thermal gradients and local hot spots not detected by the thermocouples. In order to study the overall temperature levels on the wing structure, the temperature-sensitive paint mentioned earlier has been used. Paint has been applied to the surface of the wing and tail before a flight, and the color changes and patterns examined after the flight to determine gross skin temperature. Figure 13 is a photograph showing the paint patterns on the bottom wing surface. Figure 13 is from one of the early flights. This figure shows the wing lower surface, the fuselage with frost on the liquid oxygen tank, the wing leading edge, and the wing tip. The "fence" on top of the wing is actually the tip of the vertical stabilizer. The light areas on the wing surface reached maximum temperatures between 250° F and 400° F. The dark areas represent temperatures above 400° F. The heat sink of the internal structure is clearly seen. Note the wedge-shaped dark areas of high temperature that start at four points on the leading edge and extend back over the wing. These areas start at the expansion joints in the leading edge heat sink. On the first flight above Mach 5 these areas of local heating were much more pronounced. The temperature distributions in the vicinity of these slots, on a flight to Mach 5.3, are shown in figure 14. These data were obtained from the paint pattern since no thermocouples were located in this region; however, the paint colors obtained were correlated with thermocouple data at other points on the wing. This figure shows a segment of the wing leading edge, the expansion joint, and a section of the lower skin. The expansion joints are slots about 0.080 inch wide cut in the heat sink. The average leading-edge temperature was 830° F and just outboard of the slot on the leading edge is a small area with temperatures above 1,000° F. An area between 970° F and 1,000° F extends rearward on the skin about 8 inches, and the average skin temperature away from the slot is below 800° F. On this flight, permanent interrivet buckles were formed directly behind the three outboard slots of the leading edge. The type of buckle and the location are illustrated by the upper sketch in figure 15. This sketch shows a portion of the leading-edge heat sink, the expansion slot, the external skin with the buckle, and the fastener location. Note that the fastener spacing directly behind the slot is wider than the spacing along the solid portion of the leading edge. Subsequent analysis of the leading-edge structure has indicated that several factors contributed to the

permanent buckling of the skin. One factor is the thermal stresses in the skin caused by the high gradients around the local hot spot. Another factor is the wide fastener spacing through the leading edge at the slot. A third reason for the buckles is the fact that the original segmentation of the leading-edge heat sink did not adequately relieve the thermal-induced compression loads. The skins at the slots acted as a splice plate for the heat-sink bar and thus were buckled in compression. In order to minimize this buckling problem, three design changes have been made. Two of the changes are shown in the lower sketch. An 0.008-inch-thick Inconel tab welded along one edge was installed over each slot to prevent tripping the boundary layer, and thus to minimize the local hot spots, as was explained in the previous paper by Banner, Kuhl, and Quinn. A fastener was added at the slot to decrease the fastener spacing and to increase the skin buckling allowable. In order to reduce the load that the skin splice must carry at each slot, the third change was to add expansion slots with cover tabs in three of the outboard segments of the leading edge. No additional damage has occurred at the original slots; however, the original slots had a shear tie to prevent relative displacement of the leading-edge segments, whereas shear ties at the new slots could not be provided without costly rework at the structure. A structural analysis showed that sufficient shear stiffness was present in the leading edge to meet the design requirements without shear ties, but relative displacement of the leading-edge segments was expected at the new slots. The extent of this relative displacement during the last speed flight is shown in figure 16. This photograph shows the leading-edge segments and the cover tab at one slot. Examination of the deformed cover tab and the wing skins indicates the magnitude of this displacement, which was over 1/8 inch at this slot. Several modifications to the leading-edge structure which are under consideration include the addition of shear ties at the new slots.

Overall temperature on the wing upper surface obtained during the speed flight to a Mach number of 5.30 is shown by the isotherms in figure 17. These isotherms were obtained from the color patterns of the temperature-sensitive paint. The term "isotherm" is used in a broad sense, since all color changes do not occur at exactly the same time. It can be seen that the region near the wing root is less than 380° F and along the leading edge several regions are above 750° F. Small areas of high temperature directly behind the expansion joints are still present, even with the cover tabs, but the affected area is much smaller and does not extend forward to the leading edge. Similar applications of the temperature-sensitive paint have been used on other areas of the X-15 to obtain qualitative measurements of the temperatures. These areas include the cockpit canopy, horizontal and vertical tail, speed brakes, fuselage nose area, and protuberances such as probes, antennas, and vent lines.



In conclusion, maximum temperatures measured on the X-15 show that speeds in excess of a Mach number of 6 have been accomplished without extreme structural temperatures. Comparison of calculated and measured internal temperatures has shown that satisfactory thermal gradients through the structure can be calculated from known heat input to the exposed surfaces. In general, the hot structure concept used for the primary structure of the X-15 airplane has proven quite satisfactory. However, structural problems have developed during the flight program as a result of local hot spots and discontinuities in the structural elements. Many of these problems pertain to the X-15 only; however, thermal problems with windshield glass, airflow through openings in the external structure, and structural discontinuities are expected to appear on all hypersonic vehicles until adequate design information is available in these problem areas.

X-15 STRUCTURE

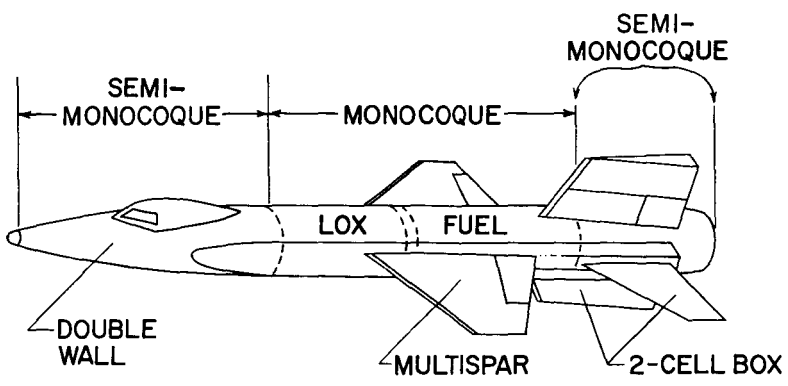


Figure 1

STRUCTURAL DETAILS

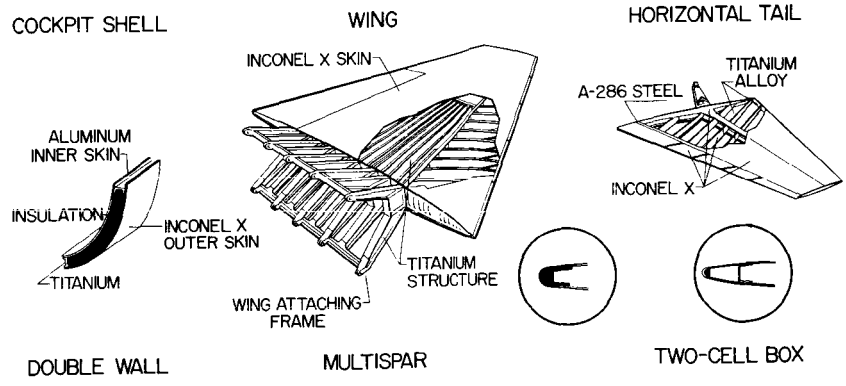


Figure 2



MAXIMUM SKIN TEMPERATURES

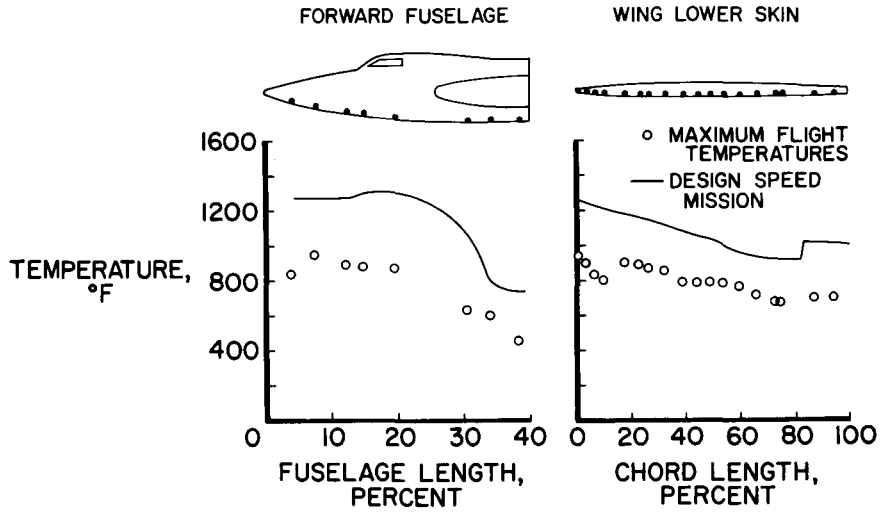


Figure 3

SUMMARY OF MAXIMUM TEMPERATURES

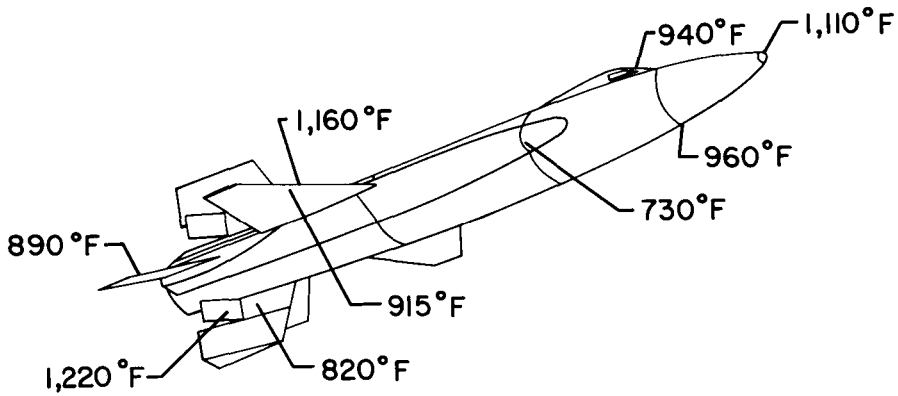


Figure 4

**WING-SPAR TEMPERATURES DURING
FLIGHT TO $M_{MAX} = 5.28$
FRONT SPAR MIDSEMISPAN**

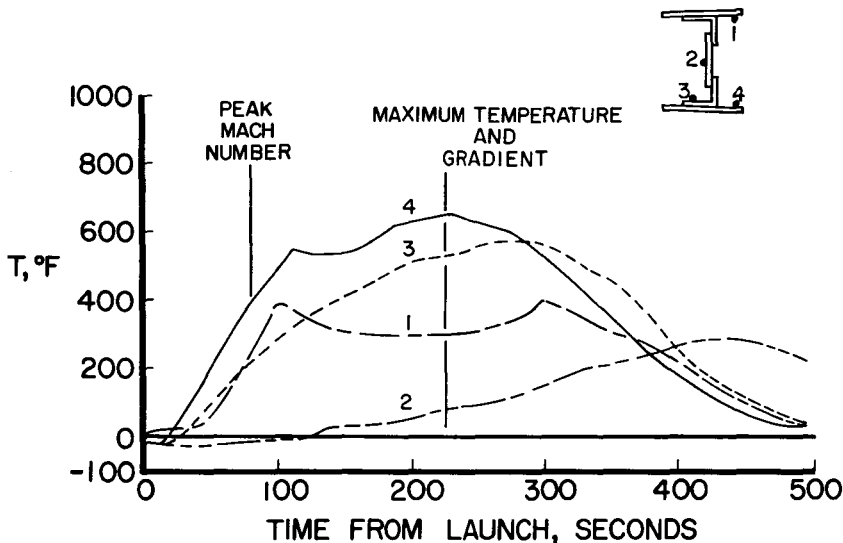


Figure 5

**CALCULATED SPAR TEMPERATURES AT
TIME = 225 SECONDS
FLIGHT TO $M_{MAX} = 5.28$**

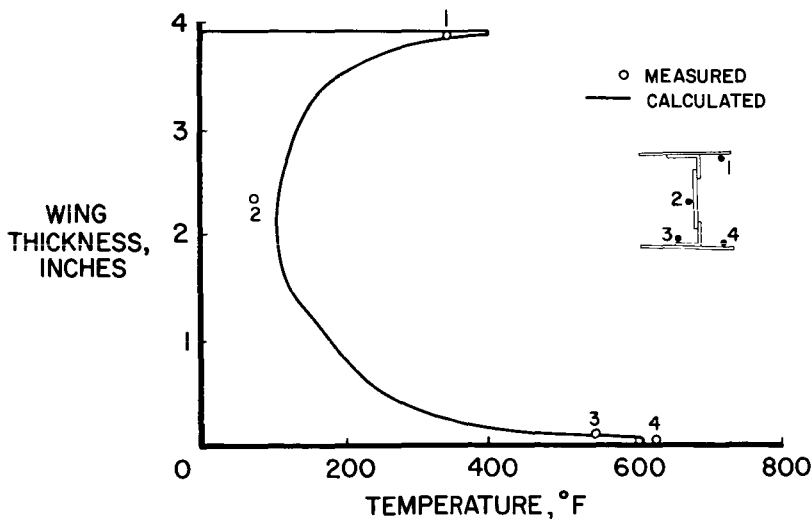


Figure 6

MAXIMUM THERMAL STRESS FRONT SPAR MIDSEMISPAN

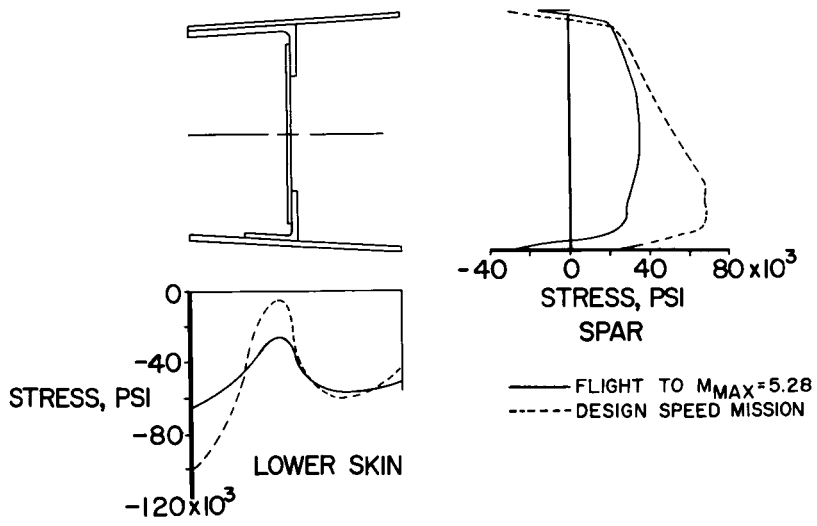


Figure 7

THERMAL PROBLEM AREAS

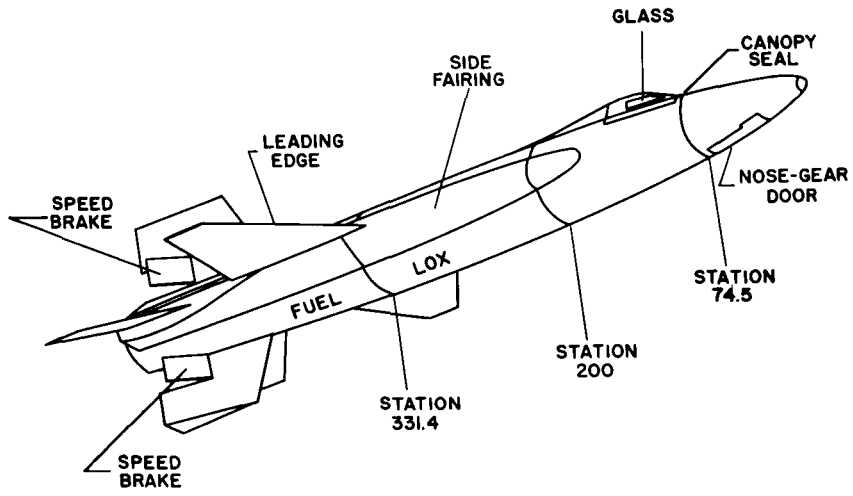


Figure 8

MAXIMUM SIDE-FAIRING TEMPERATURES DURING FLIGHT TO $M_{MAX} = 4.43$

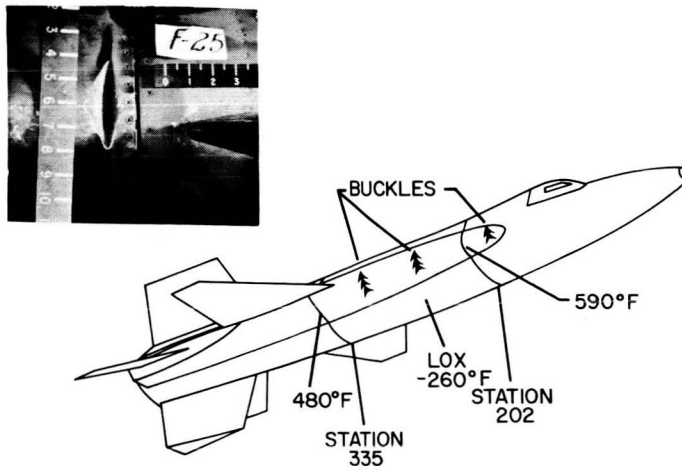


Figure 9

HEAT DAMAGE TO ALUMINUM TUBING



Figure 10

037020 J 17 00

DAMAGED WINDSHIELD GLASS FOLLOWING
FLIGHT TO 217,000 FEET ALTITUDE

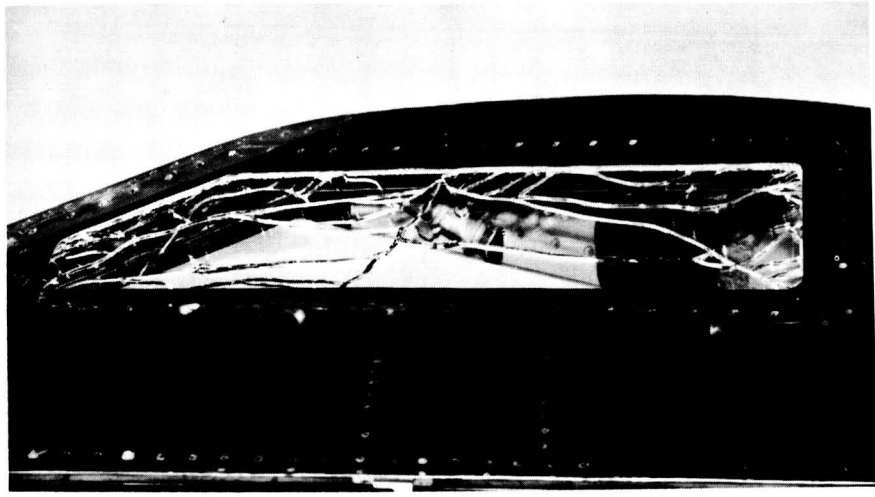


Figure 11

DAMAGED WINDSHIELD GLASS FOLLOWING
FLIGHT TO $M_{MAX} = 6.04$

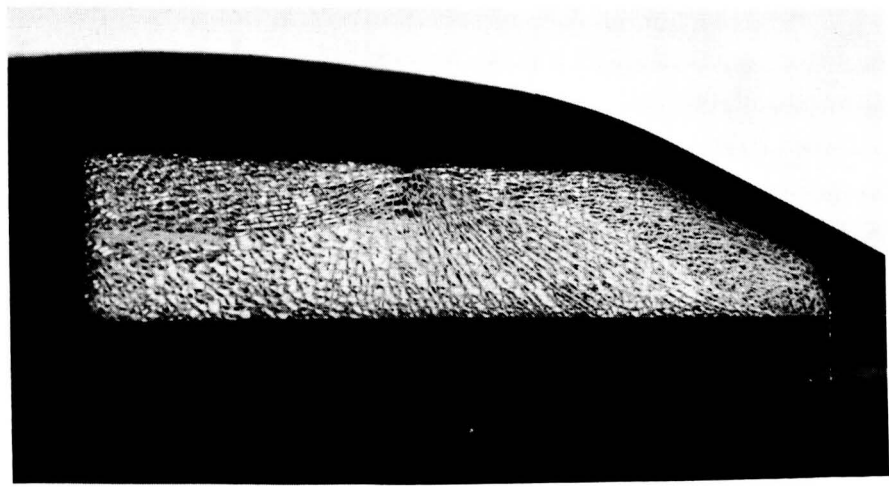


Figure 12

[REDACTED]

TEMPERATURE-SENSITIVE-PAINT PATTERNS ON X-15 WING

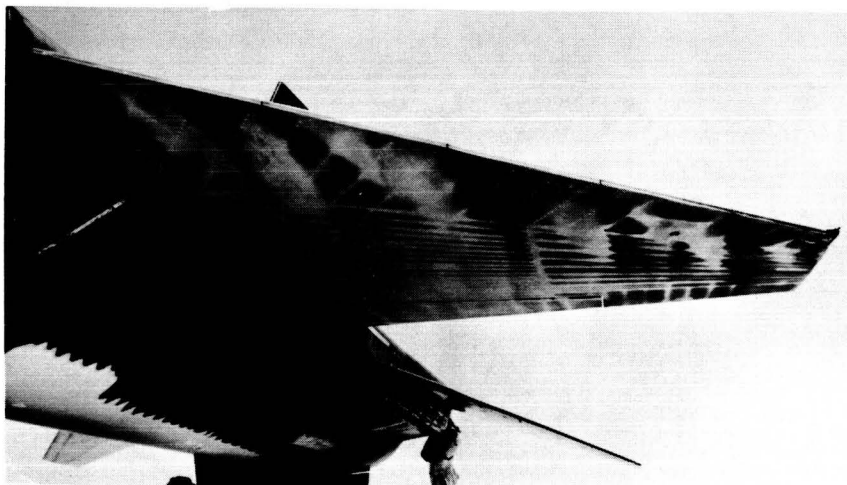


Figure 13

TEMPERATURE DISTRIBUTION AFT OF LEADING-EDGE EXPANSION SLOT

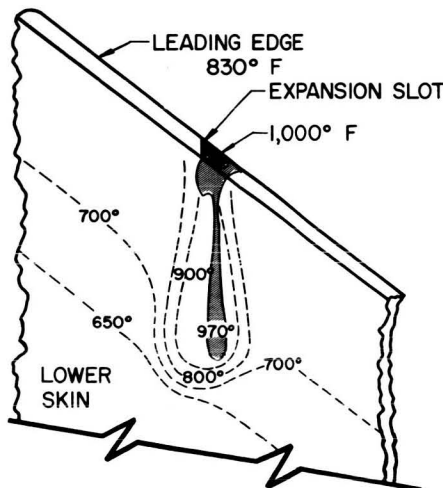


Figure 14



WING SKIN BUCKLE FOLLOWING FLIGHT TO $M_{MAX} = 5.28$

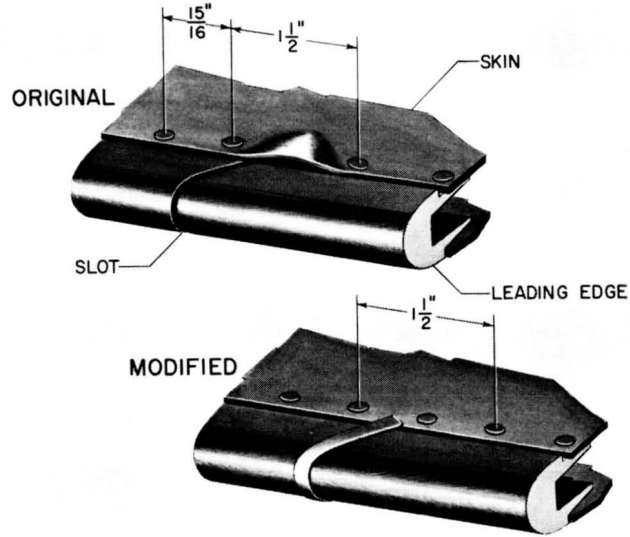


Figure 15

LEADING-EDGE DISPLACEMENT AT NEW EXPANSION SLOTS DURING FLIGHT TO $M_{MAX} = 6.04$

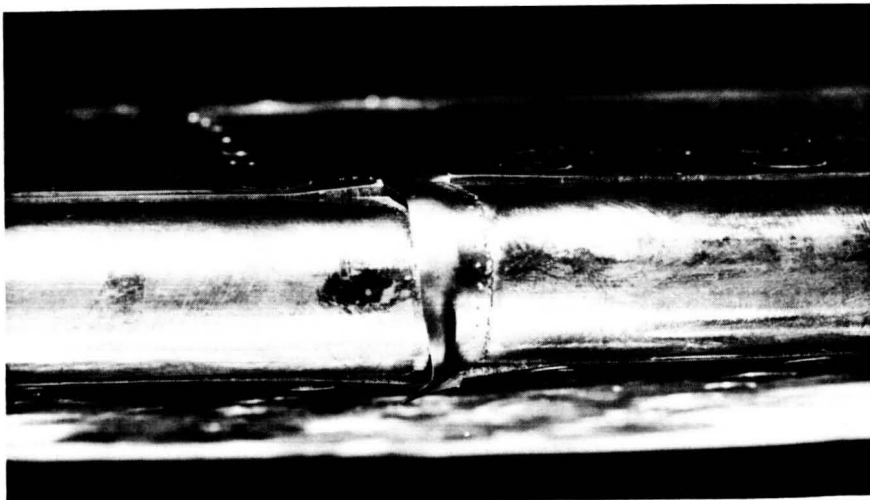


Figure 16

WING ISOTHERMS FOLLOWING FLIGHT TO $M_{MAX}=5.30$

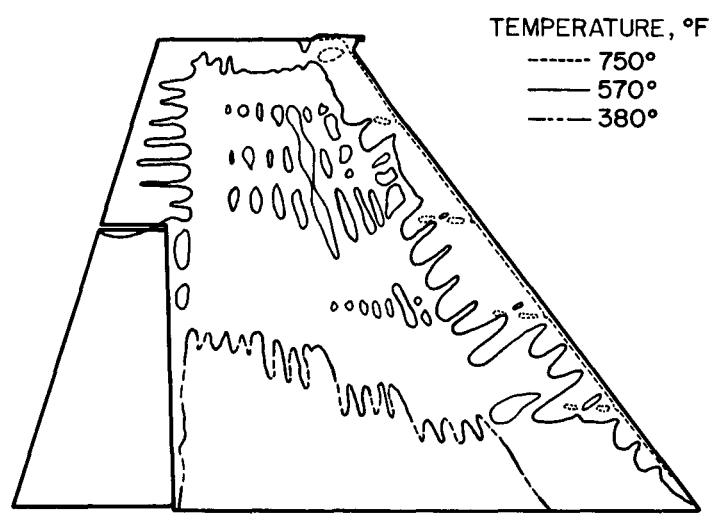


Figure 17

4. STRUCTURAL DYNAMIC EXPERIENCES OF THE X-15 (U)

By Gareth H. Jordan, Norman J. McLeod
NASA Flight Research Center

and Lawrence D. Guy
NASA Langley Research Center

N71-75447

INTRODUCTION

The X-15 is the first airplane that has been designed and flight tested in which the structure was designed to operate in a high-temperature environment, and it is the first airplane to make extensive use of high-temperature materials. The design, manufacture, and flight testing of the X-15 have added impetus to wind-tunnel and analytical studies that have advanced the state of the art in several fields of structural dynamics.

This paper reviews the structural dynamics problems that influenced the design of the structure and discusses the experiences that have been encountered during the flight tests.

The areas discussed include the noise environment produced by the jet engines of the B-52 airplane and the XLR99 rocket engine, the buffet characteristics both of the B-52/X-15 combination and of the X-15 airplane alone, classical flutter, and panel-flutter experiences during the flight program. Where problems have been encountered that led to structural modifications, the modifications are shown.

DISCUSSION

First, the experiences encountered with the B-52/X-15 combination and with the ground handling of the X-15 airplane are discussed.

Noise

Noise surveys indicated that the B-52 jet engines at 100-percent power would produce a noise environment approaching 158 decibels in the area to be occupied by the X-15 tail surfaces. These data were available at the time the design was fixed, and the fatigue life of the horizontal and vertical tails in this environment was questioned. Siren tests were initiated to determine the fatigue life of these structures, and the results of these tests indicated that the fatigue

Preceding page blank



life was unacceptable. North American Aviation, Inc., tested structural modifications that resulted in an appreciable increase in the fatigue life and initiated a retrofit of these modifications in the structure.

Consideration was also given to operating the B-52 jet engines next to the X-15 airplane at 50-percent power during take-off to minimize the noise environment. The measured noise levels produced by these operating conditions are shown in figure 1. The tip of the horizontal tail is exposed to a noise level of about 158 decibels and the sides of the vertical tail are exposed to a noise level of about 144 decibels. Increasing the B-52 jet-engine power to 100 percent would raise these levels by about 6 to 10 decibels.

A second noise source that was considered was that of the rocket engine during ground runs which was estimated to be higher than that of the B-52 jet engines. Measured noise levels produced by the XLR99 engine with the flame shield in place, shown on the right side of figure 1, are 148 decibels on the vertical tail and 156 decibels on the horizontal tail.

In order to check further on the fatigue life of the structure, additional tests were made with the B-52 jet engines as the source of the acoustic load. These tests were made with the B-52 jet engines at reduced take-off power, as shown on the left side of figure 1, and no failures were found even in the original construction after 20 hours of exposure. The results of these tests indicated that the original construction had an acceptable fatigue life in the noise environment of the B-52 jet engine at reduced power. Take-off with reduced power on the engines next to the X-15 airplane was not desirable, however, from an operational standpoint. Calculations indicated that the modified structure would have an acceptable fatigue life in the noise environment produced at 100-percent power; therefore, 100-percent power has been used on all engines for take-off throughout the flight program.

The modifications made to the vertical tail for acoustic fatigue are shown in figure 2. On the left is the original construction and on the right is the modified construction. The modifications consisted of increased rivet diameter, incorporation of dimpled-skin construction rather than countersunk rivets, and an increase in the gage of the corrugated ribs along the edge where they are flanged over to attach to the cap strip. Modifications to the horizontal tail consisted of increased rivet diameter and dimpled construction.

Initial captive flights were made with the original construction before retrofit of the modifications was accomplished and structural failures were found in the upper vertical tail after the third captive flight. The failures were similar to the failures that occurred during the siren tests and consisted of failure of the corrugated ribs where

they are flanged over to attach to the cap strip. The most extensive failure was a complete separation of the rib from the flange for approximately 18 inches on the side away from the B-52 jet engines. Subsequent investigation showed, however, that the failures were largely a result of a previously unsuspected source - the turbulence created by the X-15 pylon and the B-52 wing cutout.

Figure 3 shows the upper vertical tail located in the cutout of the trailing edge of the B-52 wing. On the left is the upper vertical tail in the wing cutout, as viewed over the upper surface of the B-52 wing. On the right is a rear view of the upper vertical tail in the wing cutout. The X-15 pylon and the blunt surface ahead of the X-15 upper vertical tail should be noted. Pressure measurements were made on the sides of the B-52 wing cutout to measure the environment of the vertical tail and these results are shown in figure 4. The magnitude of the pressure fluctuations ΔP plotted against dynamic pressure increases with dynamic pressure and has a value of about 40 percent of dynamic pressure and a frequency of about 100 cps. These pressures converted to equivalent noise levels have a value of about 160 decibels at a dynamic pressure of 300 psf and 154 decibels at a dynamic pressure of 150 psf. Estimates of the fatigue life of the modified construction indicated an acceptable fatigue life in this environment. The modified tail is still subjected to the high-turbulence environment during captive flight and no further difficulty has been experienced to date.

Buffeting

Another area in which the B-52/X-15 combination was of concern was the effect of the X-15 airplane on the buffet characteristics of the B-52 airplane. Wind-tunnel tests indicated that the buffet characteristics of the B-52 airplane would be essentially unaffected by the addition of the X-15 airplane and would not be a problem. Flight experience has shown this to be true. The B-52 limit buffet boundary in terms of normal-force coefficient C_N plotted against Mach number is shown in figure 5. It was originally planned to launch the X-15 airplane at $M \approx 0.78$ at an altitude of 38,000 feet and initial launches were made within the lower shaded area. In order to increase the performance of the X-15 airplane and for safety considerations, the launch conditions have been raised to Mach numbers greater than 0.8 at an altitude of 45,000 feet, and subsequent launches are within the upper shaded area shown in figure 5. The launch conditions currently used are just below the flight-determined buffet boundary for the B-52/X-15 combination, and no problems due to buffeting have been encountered even though the buffet boundary has been penetrated slightly with the X-15 airplane aboard.

The remainder of the paper will be devoted to some of the problems and experiences with the X-15 airplane alone. The buffet boundary

established for the X-15 airplane is shown in figure 6 in terms of normal-force coefficient C_N plotted against Mach number. The data were taken from the normal acceleration at the airplane center of gravity and represent the onset of buffeting.

At subsonic and transonic speeds, the X-15 buffet boundary is similar to that of other low-aspect-ratio, thin-winged airplanes. The X-15 airplane usually penetrates the buffet boundary slightly during round-out after launch before accelerating to supersonic speed and usually encounters some mild buffet after completing the supersonic portion of the flight. Buffeting has not been a problem in the X-15 flights, but flight within the buffet region is generally avoided.


Throughout the flight program the airplane has experienced vibration from various sources. These vibrations have been felt by the pilot and have been referred to as buffeting. The vibration that is felt by the pilot has been attributed to causes other than aerodynamic buffeting. Early in the flight program, panel flutter of the fuselage side fairings caused a heavy vibration throughout the airplane. The stability-augmentation system has also been responsible for heavy vibration due to structural feedback from the horizontal tails. The flight records have also indicated a mild vibration at many regions throughout the flight envelope at a frequency which approximately corresponds to the horizontal- and vertical-tail natural frequencies. It is anticipated that a planned modification to the control system consisting of incorporating a pressure differential feedback valve to the control surface actuators will alleviate this problem.

Classical Flutter

Classical flutter was discussed in the July 1958 conference on the X-15 airplane. The components in which flutter considerations influenced the design are shown as shaded areas in figure 7 and include the horizontal and vertical tails and landing flaps. Adequate wind-tunnel tests were made on the various components to provide proof tests to 30 percent above the design dynamic pressure of 2,500 psf. No indication of flutter has been experienced in flight to date.

Panel Flutter

Panel flutter, on the other hand, has occurred in flight and has required modification of extensive areas of the fuselage side fairing and vertical tails which are shown as shaded areas in figure 8. The side-fairing panels consisted of a series of flat rectangular panels stiffened by a corrugated inner skin with the corrugations oriented normal to the flow. This orientation was chosen to allow thermal



buckling and thus minimize thermal stresses, but of course it is not desirable from a panel-flutter standpoint. With respect to the vertical tail, the skin panels were unsupported over a length of about 60 inches with a rib spacing of about 6 inches. This resulted in long narrow panels having length-width ratios of about 10.

At the time that the structural design of the X-15 airplane was fixed, some information was available in regard to panel flutter. Application of the available results to determine the flutter characteristics of long narrow panels and corrugation-stiffened panels, such as those found in the vertical tail and the side fairing of the X-15, respectively, was uncertain. Thus, the initial design was not influenced by panel-flutter considerations.

Panel flutter of the fuselage side-fairing panels was experienced early in the flight program, however, and resulted in a severe vibration felt throughout the airplane. Strain gages were installed on the side-fairing panels, and panel flutter was detected at dynamic pressures as low as 650 psf and identified as the source of vibration. Wind-tunnel tests on a full-scale side-fairing panel were initiated in the Langley Unitary Plan wind tunnel. During these tests, the panel flutter that was measured was in good agreement with the flight measurements. At the completion of these tests, cracks were found which originated at drain holes in the corrugations and extended outward to the base of the corrugation. Inspection of the airplane revealed several panels which had similar fatigue cracks. Previous wind-tunnel and analytical studies had indicated that a simple modification would be effective in preventing panel flutter on this type of panel. The modification, shown in figure 9, consisted of a hat-section stiffener riveted to the corrugations and extending in the streamwise direction. This modification was installed on the test specimen and tested in the Langley Unitary Plan wind tunnel. These tests served to clear the airplane for flight up to dynamic pressures of 2,000 psf. Proof tests were later conducted in the Langley 9- by 6-foot thermal structures tunnel under conditions of aerodynamic heating at dynamic pressures up to 3,250 psf and cleared the airplane for flight to dynamic pressures of 2,500 psf. A total of 38 side-fairing panels, ranging in size from 12 by 15 inches to 23 by 34 inches, were stiffened in this manner on each X-15 airplane for panel flutter.

Panel flutter of the vertical tail also became of concern during proof tests to clear the airplane for classical flutter. Consequently, a second series of tests on the vertical stabilizer was planned to investigate panel flutter. Tests were made in the Ames 9- by 7-foot tunnel at a Mach number of 1.7 and dynamic pressures up to 1,300 psf. Flutter was obtained on the skin panels with a length-width ratio of 10 and also on the closure rib. As a result of these tests, the affected panels were stiffened by North American Aviation, Inc., and flights with

the stiffened stabilizer were restricted to dynamic pressures no greater than 1,500 psf at Mach numbers up to 3.0.

Additional tests were then conducted on full-scale ventrals in the Langley 9- by 6-foot thermal structures tunnel and were to be culminated by proof tests. These tests disclosed other areas of the external skin also susceptible to panel flutter within the flight environment of the X-15 airplane. The additional skin areas included both unstiffened panels and corrugation-stiffened panels similar to the side-fairing panels.

Results of these and other investigations have led to the establishment of a panel-flutter envelope shown in figure 10. In this figure the

flutter parameter $\left(\frac{E\sqrt{M^2 - 1}}{q}\right)^{1/3} \frac{t}{l}$ is plotted as a function of length-width ratio l/w . The area under the curve is the flutter region and the area above the curve is free of flutter. The results of panel-flutter measurements in flight made on the flat rectangular panels on the vertical tail of the X-15 airplane are also shown in the figure. It is interesting to note the agreement between the flight data and the previously established envelope.

More recent unpublished experimental data tend to move the flutter boundary upward for a wide range of length-width ratios. The flutter results for the corrugation-stiffened panels indicate that correlation for such orthotropic panels on the basis of equivalent isotropic plates is still uncertain. Attempts to correlate the flutter characteristics of these orthotropic panels have been made on the basis of an effective thickness and width, but correlation has not been satisfactory due to the uncertainties in the determination of the effective values.

The modifications made to the vertical tail for panel flutter are shown in figure 11. The modification consists of J-section stiffeners riveted longitudinally on the inner surface of the skin at the center line of the panel. In addition, lateral stiffeners were riveted to the skin near the panel centers and tied into the longitudinal stiffeners. Tests have shown that lateral stiffeners are ineffective in preventing flutter unless they are firmly restrained against rotation about the line of attachment to the panel. Other areas of the vertical tail in which panel flutter was experienced were on the corrugation-stiffened panels, similar to the side-fairing panels. The fix consisted of a single, light-weight hat section riveted to the backs of the corrugations along the longitudinal center line. Proof tests were made on a full-scale ventral incorporating all modifications for panel flutter. These tests were made at a Mach number of 3.0, a dynamic pressure of 3,250 psf, and a stagnation temperature of 660° F, with no evidence of flutter.

During the remaining flights of the X-15, in which dynamic pressures as high as 1,600 psf have been achieved, no further panel-flutter problems have been encountered.

CONCLUDING REMARKS

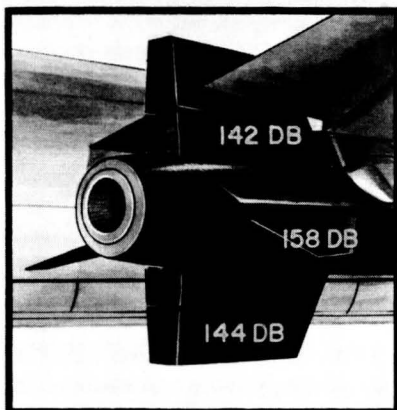
In summary, the structural dynamic problems anticipated during the design of the X-15 have been reviewed briefly, and the actual flight experiences have been described.

Considerable time and effort were expended in finding solutions and providing modifications to the airplane which alleviated the structural dynamic problems encountered. It is of interest to note that the modifications have been relatively simple and that a major portion of the effort has been required to determine the source of trouble and to proof test the modification.

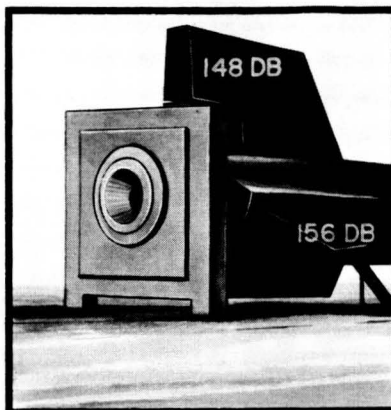
For future vehicles it is desirable to have theoretical methods for prediction of panel flutter or experimental means for defining prototype characteristics on the basis of model test results. Theoretical prediction of panel flutter is still uncertain, particularly for long narrow panels and corrugation-stiffened panels. The flight experience of the X-15 airplane and the research work initiated by the X-15 program have, however, made a major contribution toward understanding the panel-flutter problem.



MEASURED NOISE ENVIRONMENT



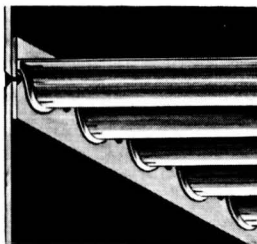
B-52 ENGINES AT
50% POWER



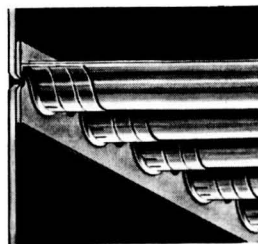
XLR99 ENGINE WITH
FLAME SHIELD

Figure 1

STRUCTURAL MODIFICATIONS FOR ACOUSTICS



ORIGINAL
CONSTRUCTION



MODIFIED
CONSTRUCTION

Figure 2



VERTICAL TAIL IN B-52 WING CUTOUT

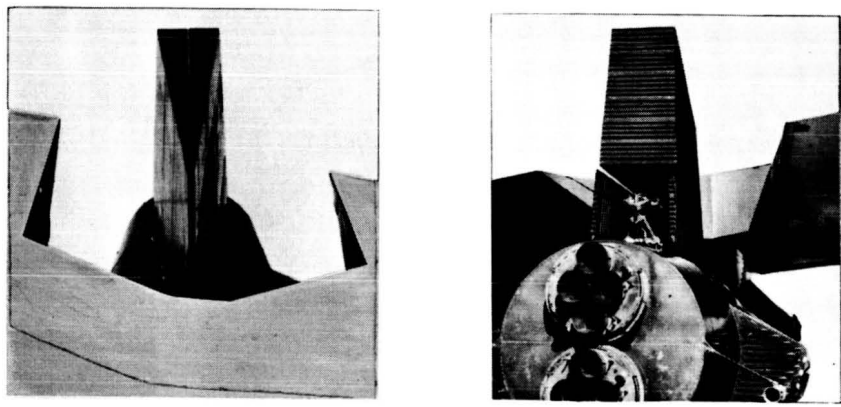


Figure 3

FLUCTUATING PRESSURES IN B-52 WING CUTOUT

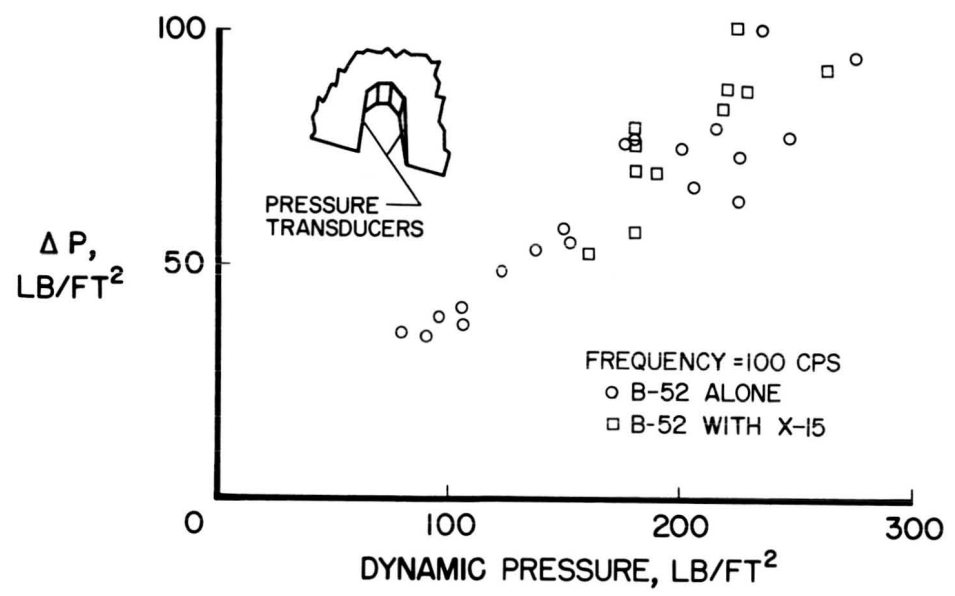


Figure 4

COMPONENTS DESIGNED BY FLUTTER CONSIDERATIONS

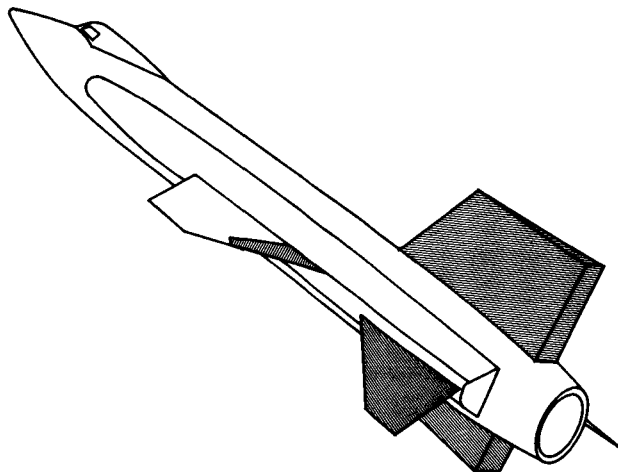


Figure 7

AREAS AFFECTED BY PANEL FLUTTER

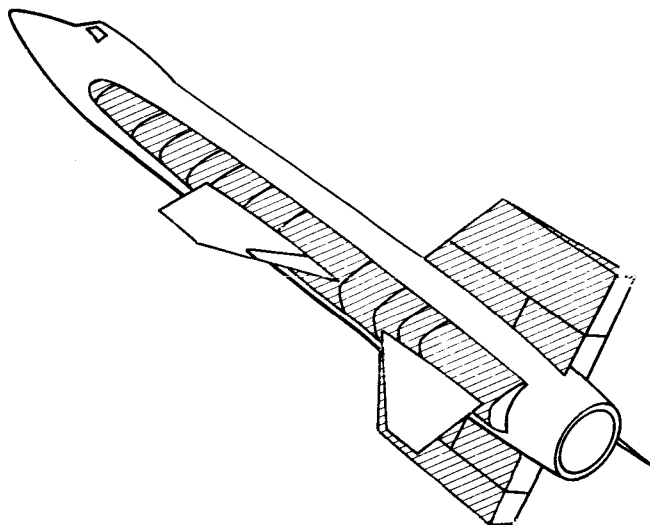
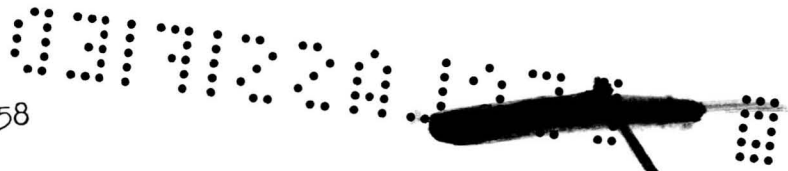


Figure 8





STRUCTURAL MODIFICATION FOR PANEL FLUTTER SIDE FAIRING

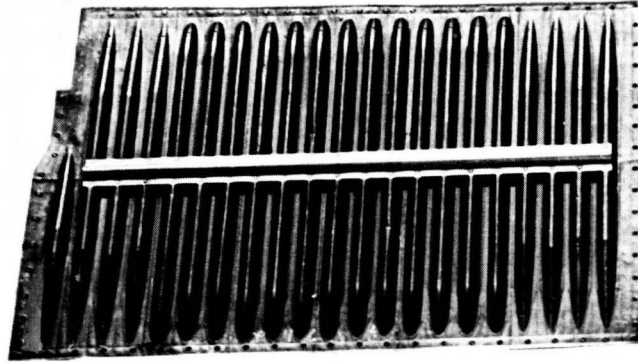


Figure 9

PANEL FLUTTER FLAT PANELS

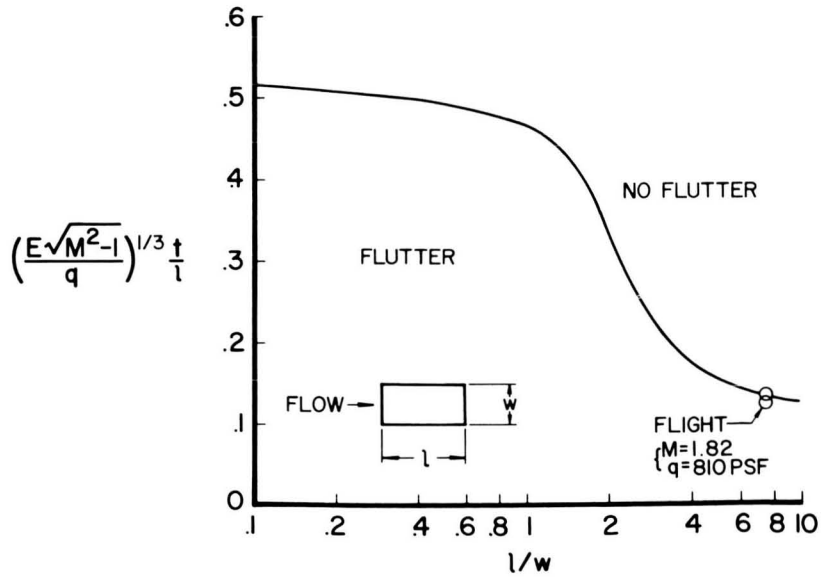
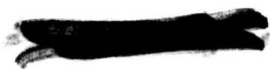


Figure 10



STRUCTURAL MODIFICATION FOR PANEL FLUTTER
VERTICAL TAIL

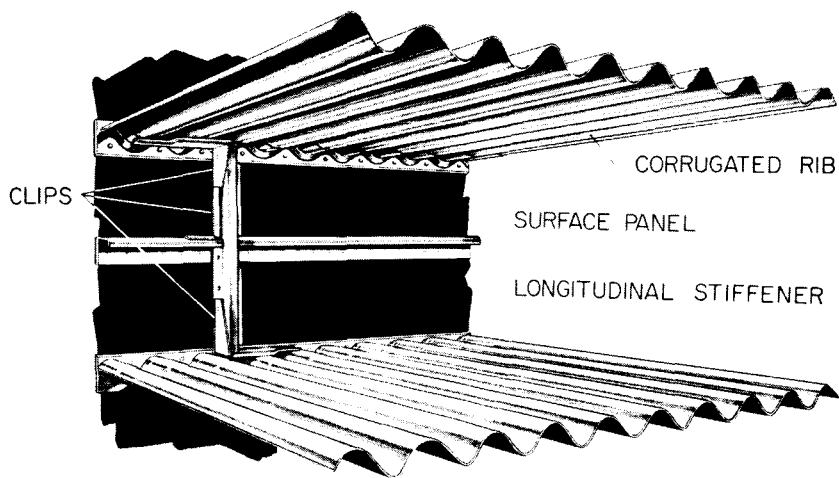


Figure 11



5. LANDING LOADS AND DYNAMICS OF THE X-15 AIRPLANE (U)

By James M. McKay and Eldon E. Kordes
 - NASA Flight Research Center

N71-75448

INTRODUCTION

One of the major problems that must be considered in the design of glide reentry vehicles is the provision for a safe landing on return. Landing-gear systems for these vehicles must meet all the usual requirements and, in addition, must be able to withstand the temperatures resulting from reentry. Also, if adequate ground steering is not provided, the landing-gear system must give good stability during the run-out. The X-15 marks the beginning of a class of reentry vehicles with a landing gear that is designed to meet these requirements. The X-15 landing-gear system consists of a main gear with steel skids placed well back on the fuselage, along with a conventional, nonsteerable nose gear placed well forward.

Because the landing-gear configuration represents a marked departure from previously used configurations, the present paper has been prepared to report on the landing loads experience of the X-15. A further purpose of this paper is to review the dynamics of landing and to present results of a recent theoretical study of the effects of various parameters on the landing loads. The landing flare maneuver, the slide-out characteristics, and a more complete description of the design problems arising during the initial test flights are covered in other papers by White, Robinson, and Matranga (paper no. 9) and Greene and Benner (paper no. 23).

DISCUSSION

Because of the airplane configuration, the landing characteristics of the X-15 are somewhat unusual. A trace of a typical landing sequence is illustrated in figure 1. The sketch at the top of the figure shows that a nose-high attitude is established just prior to main-gear touchdown. The airplane weight, wing lift, and tail loads are indicated by the arrows on each sketch; and the springs represent both the main and nose landing gear. During main-gear contact, the airplane rotates and impacts on the nose gear, as shown in the second sketch. During nose-gear compression, a second reaction occurs on the main gear, as indicated in the third sketch. It is significant to mention that this second reaction is far greater than the first, as will be shown subsequently. The airplane then rests on both gears for the slideout, as shown in the bottom sketch.

~~Preceding page blank~~

PRECEDING PAGE BLANK NOT FILMED

Thus far, 45 landings have been made with the X-15. The first four pointed out certain deficiencies in gear design. The principal deficiency can be brought out by reference to figure 2, which shows one of the main gears of the X-15 and also serves to indicate the unusual nature of the gear operation. The gear consists of a steel skid and an Inconel X strut which is attached to the fuselage by trunnion fittings and through bell crank arms to shock struts inside the fuselage. The skids are free in pitch and roll, but are fixed for parallel alignment. Drag braces are attached to the fuselage ahead of the trunnion fitting and to the skid at the strut-attachment pin. The bungee springs are used to keep a nose-up position of the skids just before landing. During flight the skids and landing-gear struts are folded forward against the outside of the fuselage. After release, they are extended simply by gravity and air loads.

The main changes that were made in this main-gear arrangement were simply to replace the shock struts by struts having greater energy-absorbing characteristics and to "beef up" the gear back-up structure somewhat. These changes were brought about mainly because the gross weight of the airplane had increased and also because the down-load on the elevator during landing was found to be greater than that taken into account in design.

In a discussion such as this, it is, of course, appropriate to mention the fourth landing which was an emergency landing made after an engine explosion. It is significant to mention that the failure of the fuselage which occurred at that time was not attributed to a design error; rather, it resulted because the airplane landed in an overweight condition because all the fuel could not be jettisoned, and further because of a high nose-gear load caused by foaming of the gas and oil mixture in the shock strut. A permanent solution to the foaming problem was achieved by using a floating piston inside the strut to separate the gas and oil. With these main changes, the last 41 landings have been without major incident.

Next, some of the loads results are to be discussed. During the X-15 program, the airplane has been instrumented to measure gear loads, gear travel, and accelerations. Figure 3 shows the main-gear shock-strut force and travel measured on a typical landing. The upper curve is the strut travel and the lower curve is the strut force, measured from time after main-gear touchdown. At touchdown, the angle of attack α_0 was 8° , the sinking speed V_{V_0} was 3 feet per second, and the landing weight was 14,500 pounds. The sketches at the top of this figure are used to help to identify the landing sequence. The important point to notice is that both the shock-strut force and travel are appreciably higher during the second reaction on the main gear following

the nose-gear touchdown than for the initial portion of the landing. These high values are due to several factors, primarily to the main-gear location well back of the airplane center of gravity and to the pronounced aerodynamic down-load on the tail, the negative wing lift during this portion of the landing, and the airplane inertia loads. The increasing air load on the tail is brought about by two sizable increases in angle of attack, namely, the rotation of the airplane onto the nose gear, and a change in the wind-flow direction to nearly horizontal. Experience with the X-15 has shown that the horizontal-tail angle, and hence the tail loads are also increased by the stability augmentation system as the airplane pitches down. For convenience, the time history of only one gear is shown since, for all cases, the landings have been nearly symmetrical and, in all landings, both skids were solidly on the lakebed before nose-gear touchdown occurred.

The influence of airplane sink speed on main-gear response for many landings with the modified gear system is shown in figure 4. Airplane vertical travel at the main gear, and shock-strut force for the first- and second-peak values are presented in terms of airplane sink speed at initial touchdown. Values measured at the first peak are shown by circles and at the second peak by squares. These data are for angles of attack between 4° and 11° , and ground speeds at touchdown between 145 and 238 knots. Notice that there is good correlation between sink speed and the measured quantities at the first peak. The important points to bring out are that the values at the second peak are independent of sink speed, and as the sink speed increases, the values at the first peak approach those of the second. No definite correlation for the first peak has been found between vertical travel or shock-strut force and angle of attack or forward speed at touchdown.

The influence of airplane sink speed on nose-gear response is shown in figure 5. Nose-gear contact velocity, shock-strut travel, and vertical reaction are presented for various airplane sink speeds. The results indicate that there is little change in the measured quantities with airplane sink speed. The large magnitudes of the quantities are, of course, due to the rapid rotation of the airplane after the initial touchdown. The loads resulting from the high nose-gear contact velocities cause high but acceptable accelerations on the pilot during this phase of the landing. However, the lack of any indicated trend with initial sink speed is probably due to the absorption by the main gear of a larger portion of the total energy during the first peak at the higher airplane sink speeds.

Experience during the program has shown that the pilots tend to land the X-15 in a similar way on each flight. Therefore, the effect of many of the variables cannot be determined from the experimental data. In order to study the effects of such quantities as horizontal-

tail loads, skid friction coefficients, gear location, and initial touchdown conditions on the gear response, a theoretical study has been conducted. This analysis was carried out on an analog computer with four degrees of freedom: main-gear motion, nose-gear motion, fuselage pitch, and vertical translation. Results from the calculations are compared with X-15 data in figure 6, where the time history of the main-gear-skid vertical reaction is shown for a typical landing. The initial conditions are angle of attack α_0 of 8° , airplane sink speed V_{V_0} of 3 feet per second, and airplane landing weight W of 14,500 pounds. The method used for obtaining the skid reaction from data of an actual landing necessarily resulted in faired values, as indicated by the solid line. The dashed curve is used to show the calculated values. Although there is a slight time difference at the second peak, the magnitude of the maximum first and second reactions are seen to agree extremely well. The good agreement between calculated and measured results gives confidence in the ability of the analysis to determine the X-15 landing response.

Attention is next directed to the downward-acting horizontal-tail load. This load is sizable and has a marked influence on the vertical reaction on the main-gear skid. The analysis has been used to calculate its effects and the results are shown in figure 7, where skid vertical reaction is given as a function of airplane sink speed for an initial angle of attack of 8° . The results, along with some experimental data, are shown for both the maximum first reaction and the maximum second reaction per skid. The dashed curves apply to the condition where the elevator position is held constant at -4° during the landing. The solid curves are for the condition where the elevator position varies uniformly from the angle of trim of -4° at touchdown to -15° at nose-gear contact. The latter condition is one that usually exists for actual landings of the X-15 airplanes. The differences between the solid and dashed curves are due to the increased tail loads associated with the difference in elevator position. Note the large decrease in the magnitude of the second reaction obtained by keeping the elevator angle small. In fact, a greater reduction in load would be expected with the horizontal tail rotated to a positive angle, leading-edge up, at the instant of main-gear contact. These results show the desirability of including an automatic system to control the elevator positions after touchdown, and hence, to reduce the second reaction on the main-gear system.

Several different types of skids have been proposed for reentry-type vehicles, including wire-brush skids. One of the main differences in the skids is in the value of the skid coefficient of friction. The influence of the skid coefficient of friction on the landing response has been calculated and the results are shown in figure 8. The skid and the nose-gear vertical reaction are presented as a function of airplane sink speed. The solid curve shows the results for a skid friction

coefficient of 0.33, which is representative of the skid on the X-15 airplane. The dashed curve is for a friction coefficient μ of 0.70, which is typical of the values for a wire-brush skid. The results indicate that increasing the coefficient of friction tends to reduce the vertical skid reaction slightly and, as might be expected, to increase the nose-gear vertical reaction. Even though the vertical reactions are not appreciably affected by increasing the coefficient of friction, the drag loads would be affected to a larger degree.

Another factor that would be expected to affect the gear loads is the location of the main gear with respect to the airplane center of gravity. The next results are intended only to show the effect of moving the main-gear location and should not be interpreted to imply any change to the X-15. This effect has been calculated by using X-15 parameters, and results are shown in figure 9 for two positions of the main gear. The skid and nose-gear vertical reactions are shown again as a function of airplane sink speed. The solid curve is for a gear distance L_M of 15.9 feet aft of the center of gravity, which is the value for the X-15; and the dashed curve represents the results obtained by moving the gear to a position one-third of the distance to the center of gravity ($L_M = 11.3$ ft). The results indicate that the second reaction on the main gear is not affected to a great extent; however, the effect of moving the gear forward increases the first reaction in such a way that, at the higher sink speeds, the values of the first and second reaction approach each other. The results do show that moving the main gear forward reduces the nose-gear vertical reaction. It can be seen that a change in the gear position to a little over 11 feet does not have as much effect as might be expected. However, other results not shown here indicate that if the gear is moved still closer to the center of gravity, there is an appreciable reduction in the second main reaction; thus, a configuration representing that of a present-day fighter aircraft is approached, wherein the first reaction is the one that is critical. The analytical program is being continued to study the effects of other parameters on the landing-gear requirements for reentry vehicles.

CONCLUDING REMARKS

The landings with the X-15 airplane have shown that the main-gear loads, measured during the second reaction after nose-gear contact, are several times larger than the loads experienced during the initial phase of the landing. The large loads during the second main-gear reaction are attributed to the main-gear location as well as to the large tail loads, the negative wing lift, and the airplane inertial loads after nose-gear touchdown. The high nose-gear contact velocities



due to the airplane pitching down result in high nose-gear loads, and, consequently, in high accelerations on the pilot during this phase of the landing. Calculated results are used to show that the main-gear reaction can be reduced by proper control of the elevator angle during touchdown. Theoretical results show that increasing the skid coefficient of friction reduces the main-gear reaction slightly, but increases the nose-gear reaction. The calculated results also show that moving the main gear forward increases the first main-gear reaction but reduces the nose-gear reaction, which would be typical of the condition for present-day fighter aircraft. Finally, the present gear system of the X-15 has proven adequate, in general, and has required very little attention.



X-15 TOUCHDOWN SEQUENCE

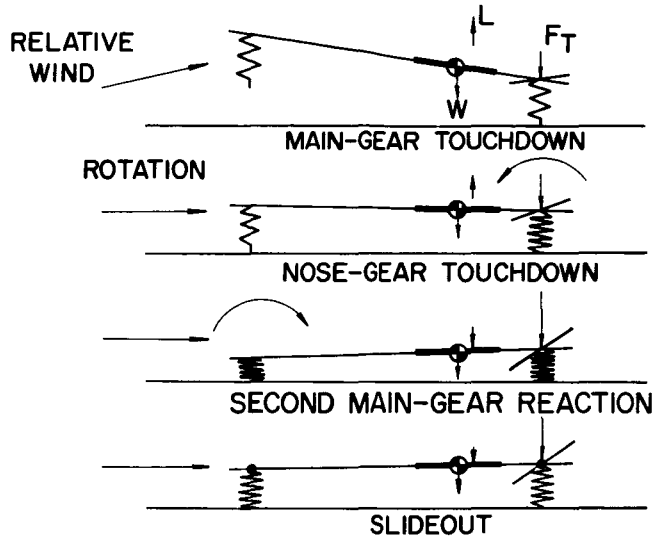


Figure 1

X-15 MAIN LANDING GEAR

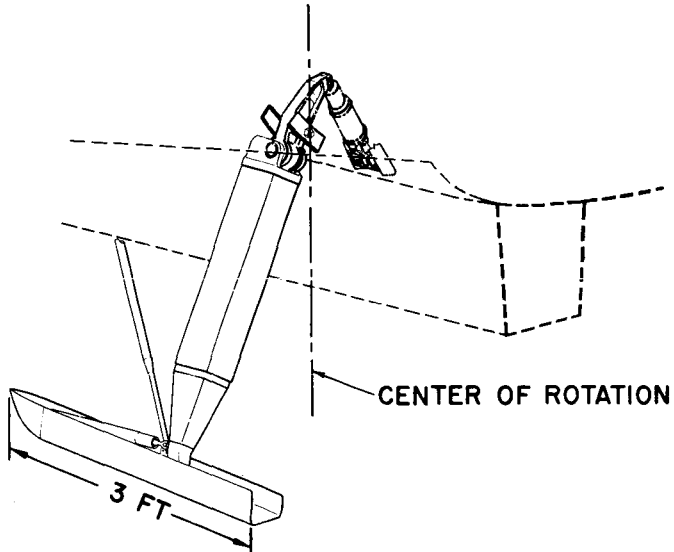


Figure 2

MAIN-GEAR SHOCK-STRUT FORCE AND TRAVEL

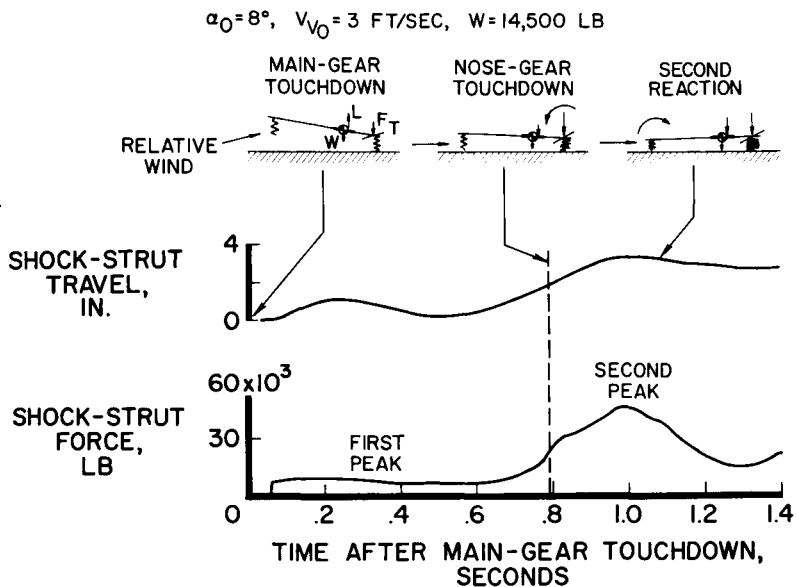


Figure 3

INFLUENCE OF AIRPLANE SINK SPEED ON MAIN-GEAR RESPONSE

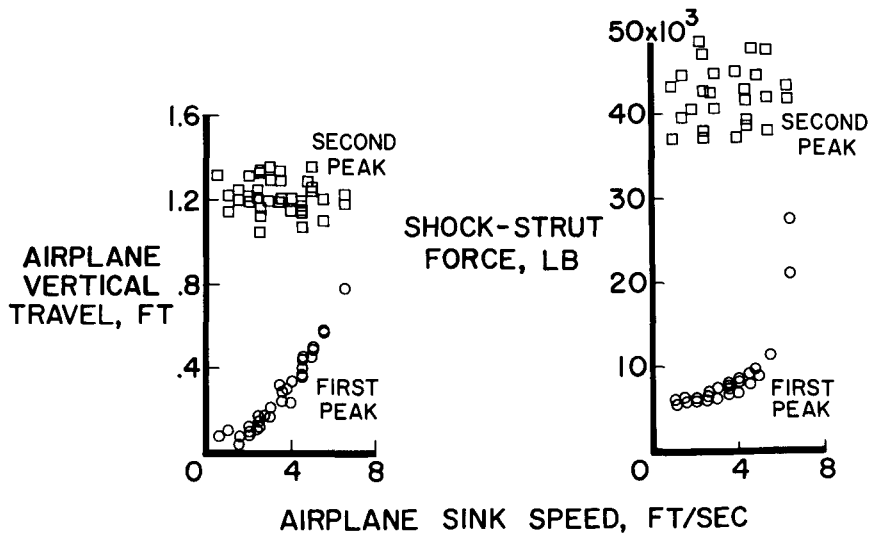


Figure 4

INFLUENCE OF AIRPLANE SINK SPEED ON NOSE-GEAR RESPONSE

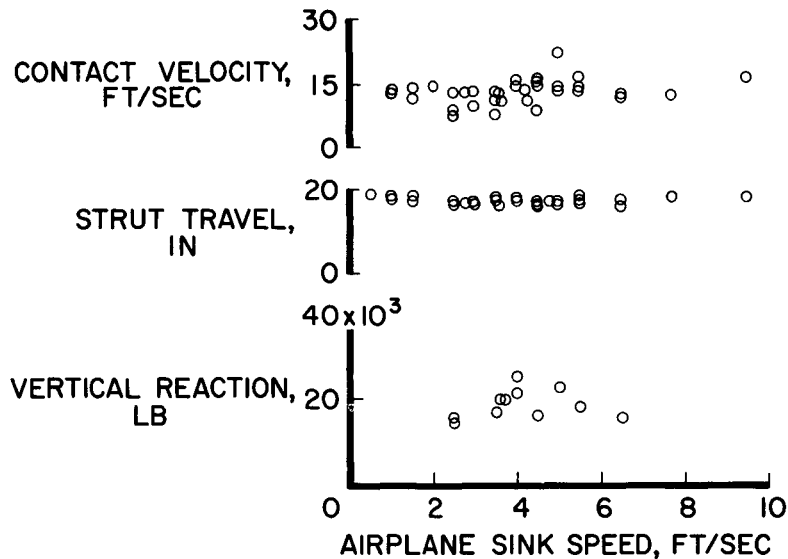


Figure 5

MAIN-GEAR-SKID VERTICAL REACTION

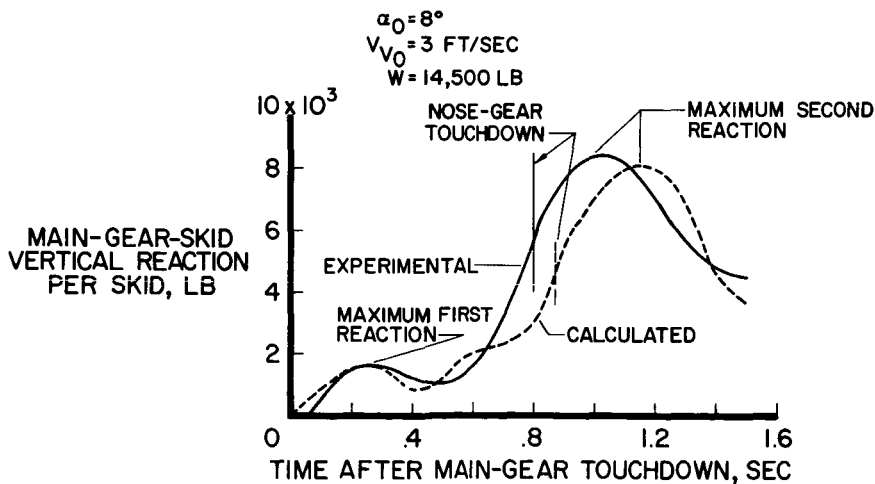


Figure 6



**INFLUENCE OF TAIL LOAD ON
 MAIN-GEAR-SKID VERTICAL REACTION**
 CALCULATED RESULTS

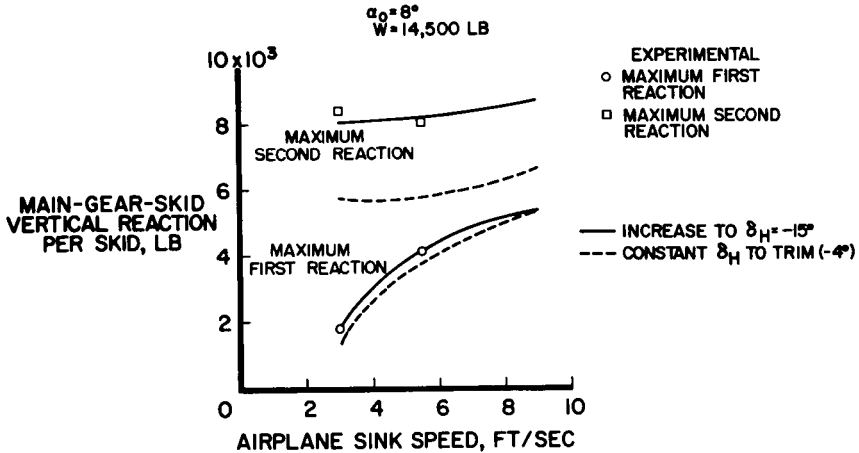


Figure 7

**INFLUENCE OF SKID-FRICTION COEFFICIENT ON
 MAIN- AND NOSE-GEAR VERTICAL REACTION**
 CALCULATED RESULTS

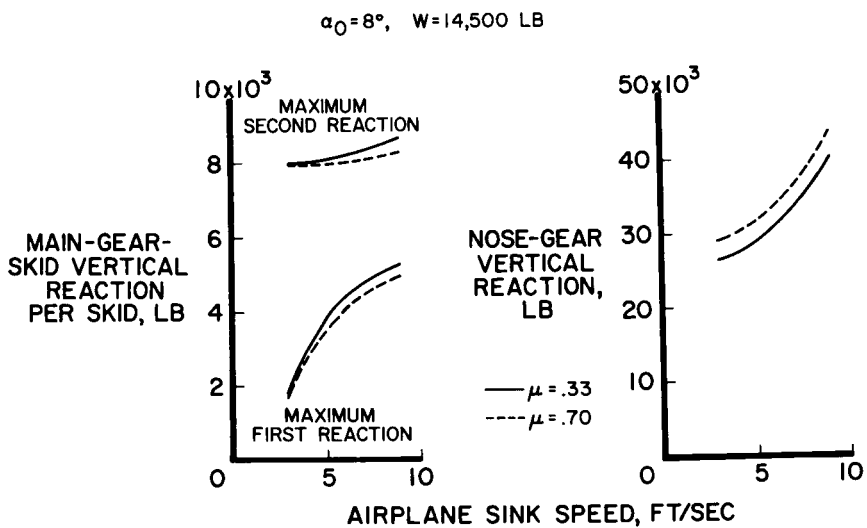


Figure 8

INFLUENCE OF MAIN-GEAR LOCATION ON MAIN- AND NOSE-GEAR VERTICAL REACTION CALCULATED RESULTS

$\alpha_0 = 8^\circ$, $W = 14,500$ LB

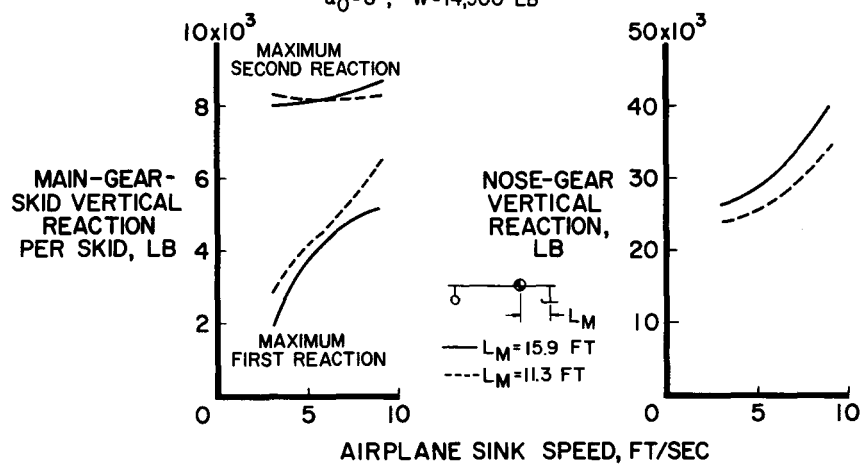


Figure 9



6. AERODYNAMIC FORCES ON COMPONENTS OF THE X-15 (U)

By Earl R. Keener and Chris Pembo

NASA Flight Research Center

N71-75449

INTRODUCTION

In the design of aerospace vehicles which are required to maneuver in the atmosphere, prime factors for consideration are the magnitude and distribution of aerodynamic forces. The design forces and force distributions for the X-15 airplane were obtained from an extensive series of wind-tunnel tests in a relatively unexplored region, as reported at the July 1958 conference on the X-15 airplane. An attempt has been made in the flight research program to verify some of the force measurements with both pressure and strain-gage measurements. This paper presents a summary of the flight force data obtained to date. The data are compared with the wind-tunnel results and with some of the more familiar theoretical methods and approximations.

Before proceeding into the discussion, the flight envelope of the X-15 airplane in terms of Reynolds number plotted against Mach number is shown in figure 1. The solid line shows the maximum performance envelope as determined by a dynamic pressure of 2,500 psf at a maximum Mach number and an altitude of 250,000 feet. From this envelope it is anticipated that the flight Reynolds numbers (based on the mean aerodynamic chord of the wing) will range from nearly 50×10^6 to below 10,000 at altitudes above 250,000 feet. The current flight envelope extends over a Reynolds number range from about 40×10^6 down to 60,000. The cross-hatched area shows the flight test area for aerodynamic force characteristics. The area is limited by measurement accuracy to altitudes below about 100,000 feet, corresponding to Reynolds numbers greater than about 5×10^6 . Wind-tunnel measurements of component forces and surface pressures were obtained at the Reynolds numbers and Mach numbers shown. The bar on the left represents tests at six Mach numbers at nearly constant Reynolds number.

SYMBOLS

C_{N_α} normal-force-curve slope, $\partial C_N / \partial \alpha$

$C_{N,WF}$ wing-fuselage normal-force coefficient

~~PRECEDING PAGE~~ blank

PRECEDING PAGE BLANK NOT FILMED

$C_{N,WP}$	wing-panel normal-force coefficient
c	local wing chord of uncambered section, measured parallel to plane of symmetry
c_{av}	average chord of wing panel
c_n	wing-section normal-force coefficient, $\int_0^1 \frac{p - p_\infty}{q} \alpha \frac{x}{c}$
h	geometric altitude
M	free-stream Mach number
p	local static pressure
p_∞	free-stream static pressure
q	free-stream dynamic pressure
S_F	planform area of the fuselage
S_W	total area of the wing
S_{WP}	area of the exposed wing panel
x	chordwise distance rearward of leading edge of local chord
α	angle of attack

DISCUSSION

The normal-force characteristics of the exposed wing panel will be discussed first. Pressure measurements are shown for a wing station near the midsemispan in figure 2. Flight data are shown for an angle of attack of 10° at Mach numbers of 4.7 and 5.4. The wind-tunnel data are shown for comparison at a Mach number of 4.7. In addition, the figure includes wind-tunnel data for a Mach number of 7.0. A section profile is shown for this wing station. The wing section is a modified NACA 66-005 airfoil, for which the leading-edge radius was increased to 0.375 inch and the trailing-edge thickness was increased to 1-percent chord.

At a Mach number of 4.7, the wind-tunnel data demonstrate that generally good agreement has been obtained between flight and wind-tunnel pressure measurements. At this Mach number it was shown at the July 1958 Conference on the X-15 airplane that the fuselage bow shock crosses the wing near the midsemispan. The effect of the bow shock may be seen on the lower surface by comparing the experimental data with shock-expansion theory for the isolated wing. The experimental data show a pronounced compression as a result of the presence of the bow shock near this station. The data at Mach numbers of 5.4 and 7.0, however, agree with the theory for the isolated wing; thus, it is indicated that the midspan is exposed to the free-stream conditions by the inboard movement of the bow shock.

Figure 3 shows the wing-panel spanwise load distribution at a Mach number of 4.7 and angles of attack of 10° and 15° . Both the flight and wind-tunnel data were obtained from pressure measurements at three span stations from which the values of the load parameter $c_n(c/c_{av})$ were obtained by integration. The flight and wind-tunnel data are seen to be in reasonable agreement. Included in this figure is the linear theory for the isolated wing for comparison with the experimental distributions. The theory is shown by the solid line adjusted in level to pass through the data at the midsemispan. The data show that the shape of the distribution of loading can be roughly predicted at these angles of attack by the linear theory for the isolated wing.

The wing-panel normal-force-curve slope as a function of Mach number for low angles of attack is presented in figure 4. Most of the flight data presented were obtained from strain-gage data. Several points (square data symbols) are also shown which were obtained from flight pressure measurements by integration of span load distributions similar to those of figure 3. The data are compared with linear supersonic theory for the isolated wing. The reduction in slope at supersonic Mach numbers agrees favorably with the linear theory. In addition, the data indicate that the normal force of the wing is about the same as that of an isolated wing for the range of data shown.

It is of interest to mention that the strain-gage data in figure 4 were obtained by using the Bakelite type of gage that has been employed in previous flight research programs. It had been expected that these gages would no longer be useful after the airplane had once exceeded a Mach number of about 4, because of the high temperature. However, the ground calibrations performed after the last flight, which exceeded a Mach number of 6, have shown that the gages still were functioning satisfactorily, even though temperatures above 500° F were experienced in the vicinity of some gages. For the data shown, the duration of time covered by the angle-of-attack change was short enough that temperature changes were small.

Figure 5 summarizes the normal-force-curve slopes for trimmed conditions in the angle-of-attack range from 0° to 5° for the horizontal tail, the wing, the wing-fuselage combination, and the complete airplane. The wing data are the same as those shown in figure 4; however, the coefficients shown in figure 5 are all based on the total wing area of 200 square feet. The slopes shown for the horizontal tail are those obtained from the variation of the balancing-tail load with angle of attack. The balancing-tail loads were obtained from strain-gage measurements during maneuvers, which, in turn, were corrected to zero pitching acceleration to obtain the conditions for balance. Figure 5 can be used to illustrate relative values of component loads for most flight conditions, since the airplane is nearly symmetrical about the horizontal plane. In general, the horizontal-tail load in trimmed flight is about 10 percent of the total airplane load throughout the test range of supersonic speeds. For the portion of the flight program so far completed, maximum horizontal-tail loads have been well within the design limits.

The normal-force values shown in figure 5 for the wing-fuselage combination were obtained by subtracting the values for the horizontal tail from those for the total airplane. Note that the normal-force slopes for the wing are considerably smaller than those for the wing-fuselage combination. This probably is due to a large extent to effects of the fuselage sidefairings.

Figure 6 shows the ratio of the wing-panel load to the wing-fuselage load as a function of Mach number, as determined from the data of figure 5. Included in this figure are two approximations based on the planform areas shown. The first approximation of 0.54 is the ratio of the wing-panel area to the total wing area. This approximation is often used at transonic speeds as a rough estimate. The second ratio shown of 0.27 is the ratio of the wing-panel area to the total wing-fuselage planform area. This approximation may be considered to be roughly applicable at hypersonic speeds. In spite of the rather large scatter in the data, it may be seen that the trend of measured values is to decrease with increasing Mach number from a level near the transonic approximation to a level near the hypersonic approximation.

Figure 7 shows the fuselage pressure distributions over the upper and lower surface of the airplane. The conditions shown are for a Mach number of approximately 4.7 and angles of attack of 0° and 16° . It may be seen that the wind-tunnel and flight data are in general agreement at both angles of attack. It is of interest to note the usefulness of the tangent-cone approximation in predicting the positive pressure coefficients. In addition, the two-dimensional Prandtl-Meyer expansion is useful at this Mach number in roughly predicting the negative pressure coefficients, approaching a vacuum over the canopy.

Figure 8 shows the pressures on the vertical tail caused by deflecting the speed brakes 35° . The condition shown is for a Mach number of 5.7 at an angle of attack of 0° . Pressures are shown at three stations on the upper vertical tail and at one station on the lower. Wind-tunnel results at a Mach number of 4.7 are also presented. The speed-brake hinge line is located at a value of x/c of 0.65. It may be seen that there is general agreement between wind-tunnel and flight data. The pressures are about the same on both the upper and lower speed brakes. The effect of the speed brakes does not extend appreciably forward or outboard, a fact which is attributed to their low aspect ratio.

Similar data for an angle of attack of 15° are shown in figure 9. Both flight and wind-tunnel data are for a Mach number of 4.7. At this angle of attack the upper speed brake has little effect. This effect is associated with the general blanketing of the upper vertical tail by the wing-fuselage flow field. In contrast, the lower speed brake obtains a higher pressure at an angle of attack of 15° than at an angle of attack of 0° . The large pressure rise still does not result in extensive flow separation ahead of the brake.

CONCLUDING REMARKS

In conclusion, generally good agreement has been obtained between the flight and wind-tunnel measurements for the angle-of-attack range covered to date. In future flights the pressure and strain-gage measurements will be extended to higher angles of attack, where interference and nonlinear effects are the predominant flow characteristics.

FLIGHT ENVELOPE

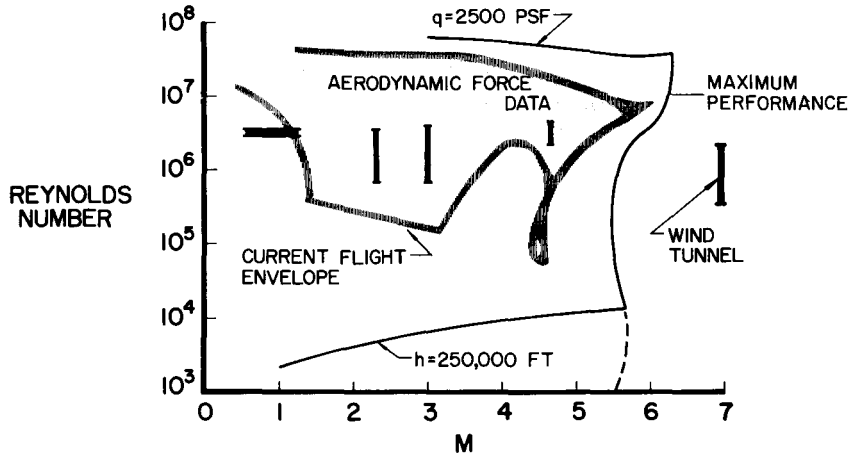


Figure 1

WING PRESSURE DISTRIBUTION
MIDSEMI SPAN
 $\alpha = 10^\circ$

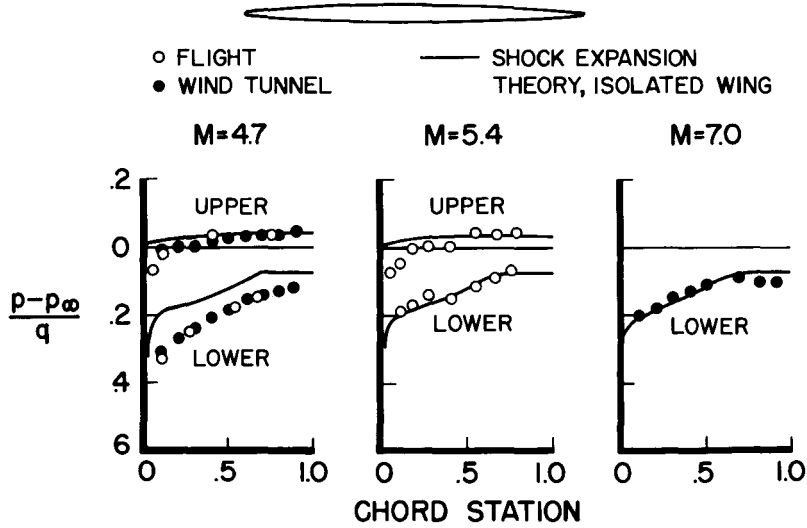


Figure 2

WING-PANEL SPAN-LOAD DISTRIBUTION M=4.7

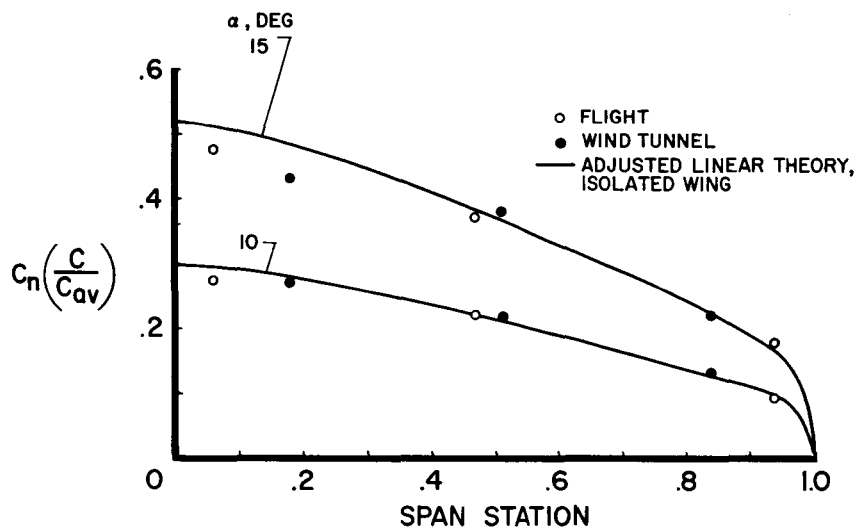


Figure 3

WING-PANEL NORMAL-FORCE-CURVE SLOPE $\alpha=0^\circ$ TO 5°

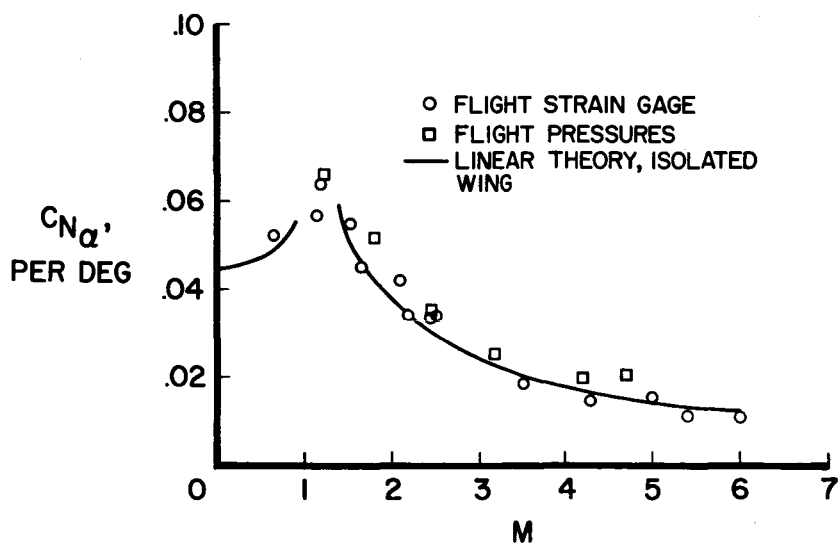


Figure 4

DIVISION OF LOADS

$\alpha = 0^\circ$ TO 5°

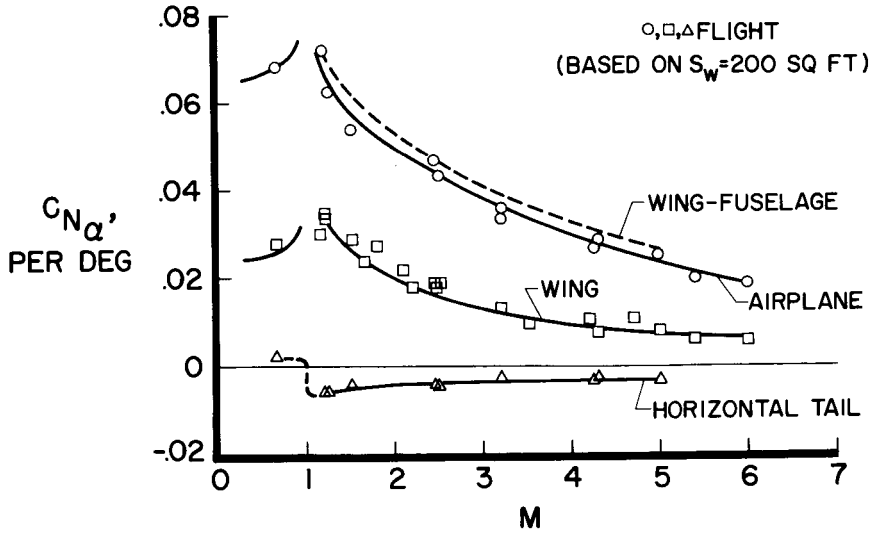


Figure 5

RATIO OF WING-PANEL LOAD TO WING-FUSELAGE LOAD

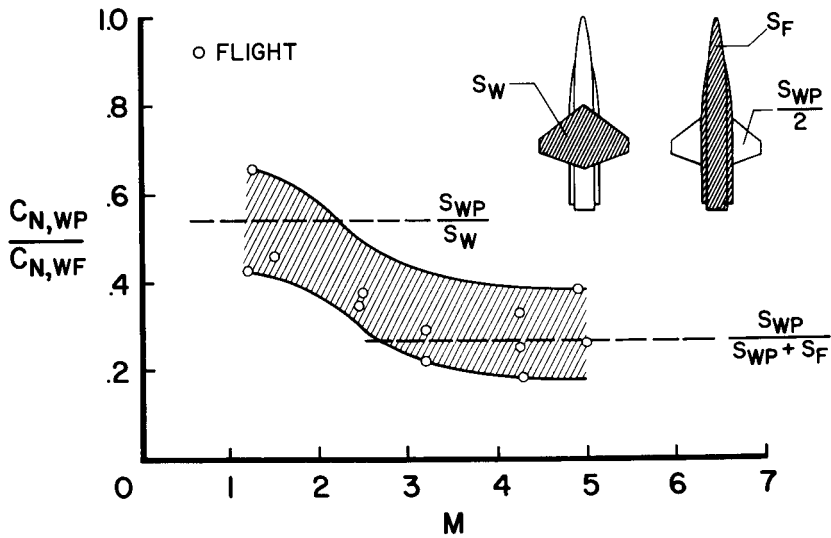


Figure 6

FUSELAGE PRESSURE DISTRIBUTION

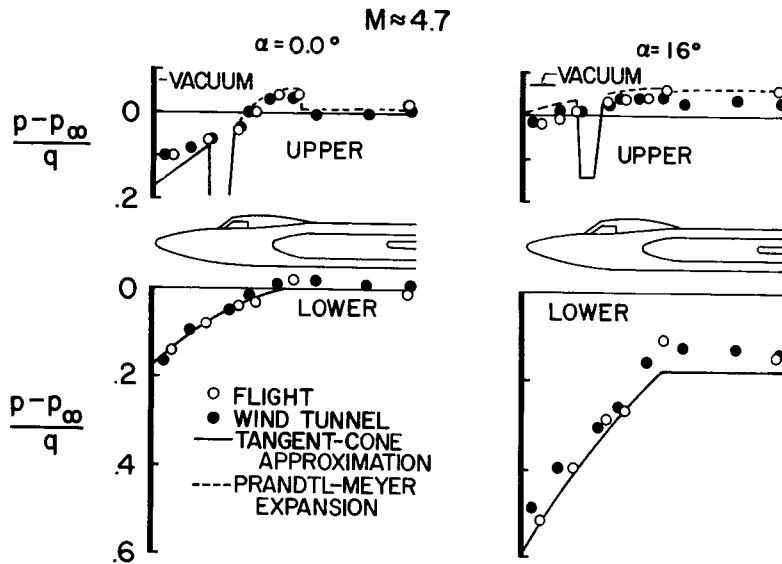


Figure 7

VERTICAL-TAIL PRESSURE DISTRIBUTION SPEED BRAKES DEFLECTED 35°

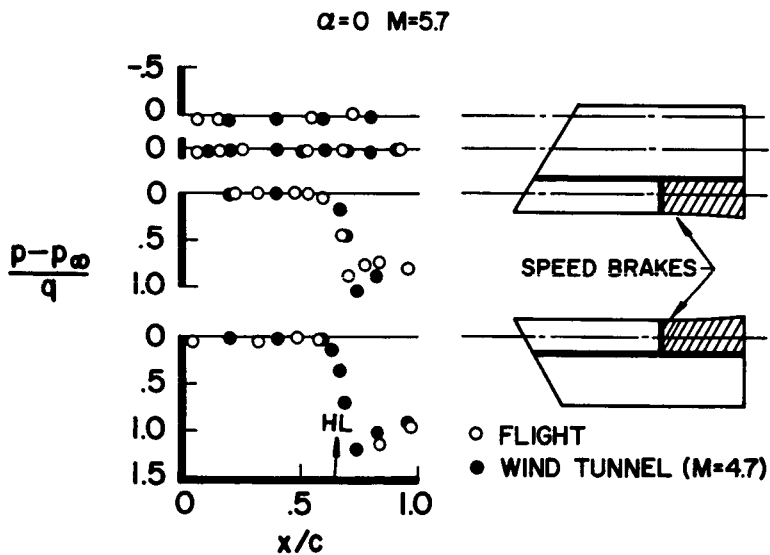


Figure 8

VERTICAL-TAIL PRESSURE DISTRIBUTION SPEED BRAKES DEFLECTED 35°

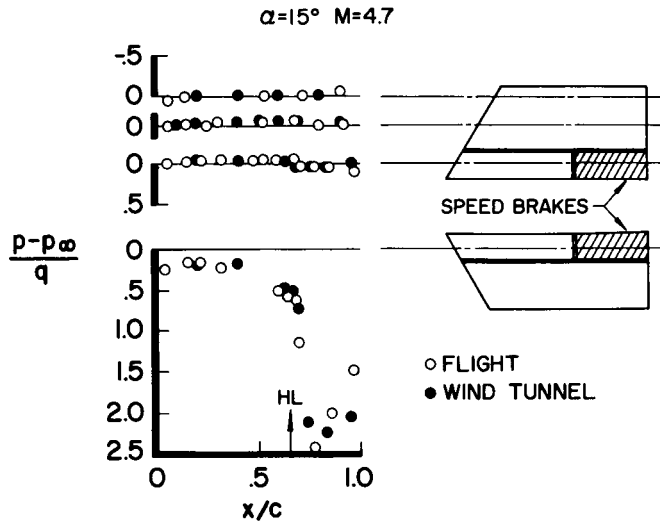


Figure 9

CONFIDENTIAL
N71-75450⁸³

7. A COMPARISON OF FULL-SCALE X-15 LIFT AND DRAG CHARACTERISTICS
WITH WIND-TUNNEL RESULTS AND THEORY (L)

By Edward J. Hopkins
NASA Ames Research Center

David E. Fetterman, Jr.
NASA Langley Research Center

and Edwin J. Saltzman
NASA Flight Research Center

SUMMARY

Data on the lift and drag characteristics of the X-15 airplane obtained in flight are shown to be in agreement with wind-tunnel-model data for Mach numbers up to 5. Existing theoretical methods are indicated to be adequate for estimating the X-15 minimum drag but underestimated the drag due to lift and overestimated the maximum lift-drag ratio. Two-dimensional theory is shown to be adequate for predicting the base pressures behind surfaces having very blunt trailing edges, such as those on the vertical tail of the X-15.

INTRODUCTION

Recent flights made by the X-15 airplane up to a Mach number of 6 permit comparisons to be made between flight and wind-tunnel results and existing supersonic and hypersonic theories throughout a Mach number range not heretofore covered. For aircraft having surfaces with extremely blunt trailing edges such as are found on the X-15 airplane, the base drag represents a very large portion of the minimum drag. Therefore, the base drag measured in flight on the various components of the X-15 airplane, including the vertical fins, the side fairings, and the fuselage, will be compared with the base drag measured on a wind-tunnel model. The adequacy of two-dimensional theory for predicting the base pressures behind surfaces having very blunt trailing edges is also shown.

7



SYMBOLS

C_L	lift coefficient
C_D	drag coefficient
C_{D_B}	base-drag coefficient
$\frac{dC_D}{dC_L^2}$	average slope of the drag-due-to-lift factor measured between $C_L = 0$ and C_L for maximum lift-drag ratio
$\Delta C_{D_{SB}}$	speed-brake drag-coefficient increment
L/D	lift-drag ratio
M	free-stream Mach number
R	Reynolds number based on free-stream conditions and body length (49.83 ft, full scale)
T'	reference temperature
T_w	wall temperature
T_{ad}	adiabatic wall temperature
p_B	base pressure
C_{p_B}	base-pressure coefficient
δ_H	horizontal-tail deflection
α	angle of attack

Subscripts:

MIN	minimum
MAX	maximum

85

DISCUSSION

The lift and drag flight data to be shown were obtained during power-off gliding flights in which gradual push-down, pull-up maneuvers were performed. Examination of the flight records indicated that negligible or zero pitching acceleration was encountered during this flight maneuver. Accelerometers were used to determine the lift and the total drag. A more detailed description of the method for obtaining flight drag data is given in reference 1. The flight data to be presented herein include some of the data of reference 2, which were limited to Mach numbers below 3.1, and data obtained in recent flights. Full-scale flight drag measurements should be conducted under prescribed conditions which are best suited for the particular airplane and instrumentation system. Such conditions did not exist for some of the maneuvers included in this paper. For this reason, the X-15 flight drag results cannot be considered final until data from such prescribed maneuvers have been obtained.

Typical drag characteristics obtained during power-off flight at Mach numbers of 3 and 5 are shown in figure 1. For some of the flight results to be presented, it was necessary to extrapolate the drag curves to obtain values of the minimum drag since the lift coverage was insufficient to define the entire drag curve.

Except for the minimum drag coefficient, the trimmed lift and drag characteristics for the wind-tunnel models were derived from reference 3 and unpublished data¹ on the 0.020-scale model tested in the Langley Unitary Plan wind tunnel at Mach numbers of 2.29, 2.98, and 4.65. Also, increments of drag for the speed brake were taken from references 4 and 5. Recent tests have been conducted in the 8- by 7-foot test section of the Ames Unitary Plan wind tunnel to measure the minimum drag of the 0.067-scale model of the X-15 airplane with the boundary layer tripped by distributed roughness particles placed a constant distance from the leading edge of all wing and tail surfaces. The distance selected for fixing transition was 5 percent of the average chord of the exposed wing surface, since this distance corresponded approximately to the average length of laminar flow as measured in flight at a Mach number of 3. The boundary layer was also tripped on the fuselage and the side fairings at this same distance. The drag of the roughness particles was evaluated from separate measurements of the drag of the model with particles of several different sizes and was subtracted from the total drag. This model was also equipped with the nose boom and all other protuberances, including the camera fairings, antennas,

¹The pitching-moment results from this investigation on the 0.020-scale model were confirmed by the results recently obtained on the 0.067-scale model in the Ames 8- by 7-foot wind tunnel.

retracted landing skids, pitot probe, and exhaust vents found on the flight airplane. Base pressures were measured on the side fairing, the fuselage, and the upper and lower vertical fins to facilitate comparisons between the experimental and theoretical values of the minimum drag with the base drag removed. The minimum drag is compared on this basis since no known methods are available to account for the interference effects from the wakes of the blunt surfaces on the base drag.

In order to make a valid comparison between wind-tunnel and flight results, it is necessary to adjust the skin-friction drag, which is included in the wind-tunnel data, to values corresponding to flight Reynolds numbers. The results for extrapolating² the minimum drag as measured in the wind tunnel by the T' method of references 6 and 7 to flight Reynolds numbers at Mach numbers of 2.5 and 3 are shown in figure 2. For this extrapolation, the recovery temperature was assumed to be that for an adiabatic smooth flat plate having a turbulent boundary layer and a recovery factor of 0.88. At flight Reynolds number for the Mach number of 3, the increment of drag calculated to account for the difference between the skin-friction drag of an adiabatic flat plate and that for a flat plate having the minimum temperature measured on the rearward portion of the fuselage is also shown. A more exact skin-friction correction to the extrapolated minimum drag for an adiabatic flat plate at flight Reynolds number should, of course, take into account the different temperatures which would exist on each of the components of the X-15. However, because of the relatively small skin-friction increment shown, which represents a temperature differential of 438°F ($T_{ad} = 538^{\circ}\text{F}$, $(T_w)_{MIN} = 100^{\circ}\text{F}$), the effect of these different component temperatures does not appear to be too significant at Mach numbers of 3 and below. At Mach numbers above 3, however, this increment of skin friction would become larger, because of the greater difference between the adiabatic wall temperature and the actual temperatures of the X-15 surfaces. For the Mach numbers shown, the T' method appears to give a satisfactory extrapolation of the minimum drag from wind tunnel to flight for the Reynolds numbers considered here. In figure 2 the flight data have a small increment of drag subtracted because the airplane did not have zero horizontal-tail deflection for zero lift coefficient. No such adjustment was made to any other data to be presented.

The effect of Mach number on the minimum drag with the base drag removed is shown in figure 3. In calculating the skin-friction drag by the T' method at the higher Mach numbers and corresponding Reynolds

²In the extrapolations to flight conditions shown herein, it was assumed that the wave-drag coefficient did not vary with Reynolds number. This assumption was confirmed by calculations which indicated that boundary-layer-displacement effects were negligible on the X-15 configuration at Mach numbers of 3 and below.

numbers, the skin temperature was considered to be the maximum which would be calculated for the central portion of the wing during a prescribed (not actual) flight maneuver. The effect of heat transfer and radiation on the surface temperature was considered. These maximum calculated temperatures, together with the flight conditions corresponding to the flight data presented in figure 3, are as follows:

M	R	T _{wMAX} , °F
1.1	82 × 10 ⁶	448
1.4	115	511
1.5	115	534
1.9	80	635
1.9	63	655
2.1	62	705
2.3	118	829
2.5	62	835
2.6	95	866
3.0	57	994
3.3	58	1,109
4.0	70	1,267
4.3	22	1,357
5.0	19	1,597
5.0	12	1,662
6.0	33	1,649

The wave drag of the surfaces and the fuselage for the supersonic theory was computed on an electronic computing machine by the method of Holdaway and Mersman given in reference 8. This method is based on the theory of reference 9. The wave drag of the protuberances such as the camera fairings, retracted skids, standard NASA airspeed boom, hypersonic flow-direction sensor when used, and antennas was estimated separately from reference 10 and is included in the wave-drag increments shown.³ For hypersonic theory, the wave drag of the fuselage, the hypersonic-flow-direction sensor, the blunt leading edges, and the protuberances was calculated from Newtonian theory (e.g., ref. 11). At the lowest Mach numbers, the sum of the skin-friction and the wave drag from supersonic theory shows good agreement with the flight points, but at the higher Mach numbers this theory underpredicted the flight data. Hypersonic theory shows general agreement with the flight data between Mach numbers of 4 and 6.

³In general the X-15 was equipped with the standard NASA airspeed boom at a Mach number of 3 and below and with the hypersonic flow-direction sensor at higher Mach numbers.

The average value of the trimmed drag due to lift as measured at low lift coefficients is presented for power-off flight as a function of Mach number in figure 4. For the wind-tunnel and theoretical values of the drag due to lift, the center of gravity was assumed to be located at its average position for flight, 22 percent of the mean aerodynamic chord. For both the supersonic and hypersonic theories, the mutual interference factors for the wing-body and the tail-body combinations were estimated from reference 12. The lift-curve slopes for the wing and tail alone were calculated by linear theories given in references 13 and 14 for the supersonic theory. For hypersonic theory, the lift of these components was calculated from the shock-expansion theory for two-dimensional flat plates with a correction applied for the three dimensionality of the flow from the charts in reference 15. The effect of the expansion flow field from the wing on the tail lift was accounted for in the hypersonic theory by the method described in reference 16. Since the negative dihedral placed a large portion of the horizontal tail below the wing vortex field, no interference effects from the wing vortices on the tail lift were considered for either theory. In both theories, the drag due to lift was considered to be equal to the lift of the surface times the flow angle relative to the surface; thus, no leading-edge thrust was assumed. Up to a Mach number of about 5, the wind-tunnel data show excellent agreement with the flight data. This result is representative up to an angle of attack for $(L/D)_{MAX}$, since insufficient flight data were available at the higher attitudes. Both theories, however, underestimate the flight drag due to lift throughout the Mach number range.

Some insight into the factors that contribute to these low theoretical estimates can be gained from figure 5, which shows the trimmed lift and horizontal-tail deflection as a function of angle of attack at a Mach number of about 5 for power-off flight. The wind-tunnel data show general agreement with flight data. Both theories give good predictions of trimmed lift coefficient but considerably underestimate the tail deflections for trim; hence the theoretical estimates of the drag due to lift are low. (See fig. 4.) The difficulty of predicting the tail inputs is believed to be due primarily to the effect of the gap between the horizontal tail and the side fairing, which progressively increases with tail deflection, and also to the complex flow field existing behind the wing. In the theories no gap effects were considered. However, as mentioned previously in the hypersonic theory, downwash and local dynamic-pressure variations on the horizontal tail were determined from considerations of the shock-expansion field behind the wing.

The trimmed maximum lift-drag ratio is shown as a function of Mach number in figure 6. The theoretical curves are based on the estimated values of wave drag, friction drag, and drag due to lift just discussed.

In addition, the base drag, which must be included, was assumed to be the same as that measured in power-off flight. The wind-tunnel data show excellent agreement with the flight values. The theories, however, overestimated the flight $(L/D)_{MAX}$, primarily because of the underestimated drag due to lift.

In all the foregoing comparisons either the base drag was removed from the total drag, or the base drag measured in power-off flight was assumed. The various components of the base drag are now considered. It should be noted that all of the full-scale base-drag or base-pressure-coefficient data which follow (figs. 7 to 10) are for the XLR99 engine installation. However, for some of the preceding figures there are flight data, at $M \leq 3$, representing the XLR11 or interim rocket engine installation. Where this is the case, base drag from the XLR11 installation applies.

The base-drag coefficients measured on the vertical fins, the side fairings, and the fuselage are shown as a function of Mach number both for power-on and power-off flight conditions in figure 7. In each sketch the shaded areas are the areas being considered. It can be seen that engine operation significantly affected the pressures on the fuselage and the vertical fins but had a much smaller effect on the pressures for the side fairing. The wind-tunnel data are somewhat below the power-off flight results, probably because of the influence of the sting support.

Ratios of base drag to minimum drag as measured on each of the base components in power-off flight are shown in figure 8. It can be seen that the vertical fin is the largest contributor to the base drag, contributing even more than the fuselage. Note that the total base drag decreases from about 60 percent of the total minimum drag at a Mach number of about 1.5 to about 17 percent at a Mach number of 5.2.

The average base pressure measured in power-off flight on the upper vertical fin is shown as a function of Mach number in figure 9. The theoretical curve for the two-dimensional theory of Korst (ref. 17) has been verified by past wind-tunnel tests on relatively thin wings with blunt trailing edges. It is noteworthy that base-pressure characteristics for surfaces as blunt as the vertical fin of the X-15 (ratio of chord to thickness of 5.5) were also adequately predicted by two-dimensional theory. At Mach numbers above 4, the flight base-pressure coefficients approach the limiting curve ($p_B = 0$). At Mach numbers above 5, the hypersonic approximation of base-pressure coefficient $(-1/M^2)$ gives reasonable agreement with the flight results.

The base pressures measured on the fuselage and the side fairing are compared with values from the two-dimensional theory of Korst and with values for a body of revolution (without fins) according to Love (ref. 18) in figure 10. It can be seen that the two-dimensional theory, particularly at Mach numbers between about 2 and 3, gives a better estimate of the flight base pressures than Love's curve. The fact that the fuselage base pressures agree better with the two-dimensional theory than with Love's curve is probably associated with the wake interference from the blunt vertical fins and the side fairings.

The increment of drag produced by deflecting the speed brakes 35° is shown as a function of Mach number in figure 11. The increments of drag measured in the wind tunnels show general agreement with those measured in flight. Between Mach numbers from about 3 to 5, Newtonian theory gives a good estimate of this drag increment. It can be seen that the increment of drag from the speed brakes approximately equals the minimum drag at the low Mach numbers and is about 35 percent greater at a Mach number of 5.5.


CONCLUDING REMARKS


Throughout the Mach number range considered, up to a Mach number of about 5 and in the low angle-of-attack range, wind-tunnel trimmed lift and drag obtained on models showed excellent agreement with flight results on the X-15. Furthermore, at least up to a Mach number of 3 and for the Reynolds number range considered herein, flight data indicate that reasonable values of the full-scale minimum drag can be obtained from extrapolations of wind-tunnel results to flight Reynolds numbers, provided that the condition of the boundary layer is known and that a representative wind-tunnel model is tested, even to the extent of including all the protuberances found on the full-scale airplane. Existing theoretical methods were adequate for estimating the X-15 minimum drag; these theories, however, underestimated the drag due to lift and overestimated the maximum lift-drag ratio. This result was due primarily to the inability of the theories to predict the control-surface deflections for trim. It was also shown that two-dimensional theory, which has been known to predict the base pressures on relatively thin wings with blunt trailing edges, also predicts satisfactorily the base pressures behind the extremely blunt vertical surface of the X-15.



91

REFERENCES

1. Beeler, De E., Bellman, Donald R., and Saltzman, Edwin J.: Flight Techniques for Determining Airplane Drag at High Mach Numbers. NACA TN 3821, 1956.
 2. Saltzman, Edwin J.: Preliminary Full-Scale Power-Off Drag of the X-15 Airplane for Mach Numbers From 0.7 to 3.1. NASA TM X-430, 1960.
 3. Penland, Jim A., and Fetterman, David E.: Static Longitudinal, Directional, and Lateral Stability and Control Data at a Mach Number of 6.83 of the Final Configuration of the X-15 Research Airplane. NASA TM X-236, 1960.
 4. Franklin, Arthur E., and Lust, Robert M.: Investigation of the Aerodynamic Characteristics of a 0.067-Scale Model of the X-15 Airplane (Configuration 3) at Mach Numbers of 2.29, 2.98, and 4.65. NASA TM X-38, 1959.
 5. Leupold, Mathias J., and Freeman, Elizabeth M.: A Second Series of Supersonic Force Tests on the Full-Span Model X-15 for North American Aviation, Incorporated. Rep. 200, Naval Supersonic Lab., M.I.T., Sept. 1958.
 6. Sommer, Simon C., and Short, Barbara J.: Free-Flight Measurements of Turbulent-Boundary-Layer Skin Friction in the Presence of Severe Aerodynamic Heating at Mach Numbers From 2.8 to 7.0. NACA TN 3391, 1955.
 7. Bertram, Mitchel H.: Calculations of Compressible Average Turbulent Skin Friction. NASA TR R-123, 1962.
 8. Holdaway, George H., and Mersman, William A.: Application of Tchebichef Form of Harmonic Analysis to the Calculation of Zero-Lift Wave Drag of Wing-Body-Tail Combinations. NACA RM A55J28, 1956.
 9. Jones, Robert T.: Theory of Wing-Body Drag at Supersonic Speeds. NACA Rep. 1284, 1956. (Supersedes NACA RM A53H18a.)
 10. Hoerner, Sighard F.: Fluid-Dynamic Drag. Publ. by the author (148 Busted Drive, Midland Park, N.J.), 1958.
 11. Griminger, G., Williams, E. P., and Young, G. B. W.: Lift on Inclined Bodies of Revolution in Hypersonic Flow. Jour. Aero. Sci., vol. 17, no. 11, Nov. 1950, pp. 675-690.
- 

- 92
12. Pitts, William C., Nielsen, Jack N., and Kaattari, George E.: Lift and Center of Pressure of Wing-Body-Tail Combinations at Subsonic, Transonic, and Supersonic Speeds. NACA Rep. 1307, 1957.
 13. Lapin, Ellis: Charts for the Computation of Lift and Drag of Finite Wings at Supersonic Speeds. Rep. No. SM-13480, Douglas Aircraft Company, Inc., Oct. 14, 1949.
 14. Eichelbrenner, E. A.: Portance Des Ailes En Flèche Aux Vitesses Supersoniques. La Recherche Aéronautique (O.N.E.R.A.), No. 25, Jan.-Feb. 1952, pp. 19-20.
 15. Harmon, Sidney M., and Jeffreys, Isabella: Theoretical Lift and Damping in Roll of Thin Wings With Arbitrary Sweep and Taper at Supersonic Speeds - Supersonic Leading and Trailing Edges. NACA TN 2114, 1950.
 16. Dugan, Duane W.: Estimation of Static Longitudinal Stability of Aircraft Configurations at High Mach Numbers and at Angles of Attack Between 0° and $\pm 180^{\circ}$. NASA MEMO 1-17-59A, 1959.
 17. Korst, H. H.: A Theory for Base Pressures in Transonic and Supersonic Flow. Jour. Appl. Mech., vol 23, no. 4, Dec. 1956, pp. 593-600.
 18. Love, Eugene S.: Base Pressure at Supersonic Speeds on Two-Dimensional Airfoils and on Bodies of Revolution With and Without Fins Having Turbulent Boundary Layers. NASA TN 3819, 1957. (Supersedes RM L53C02.)
- 

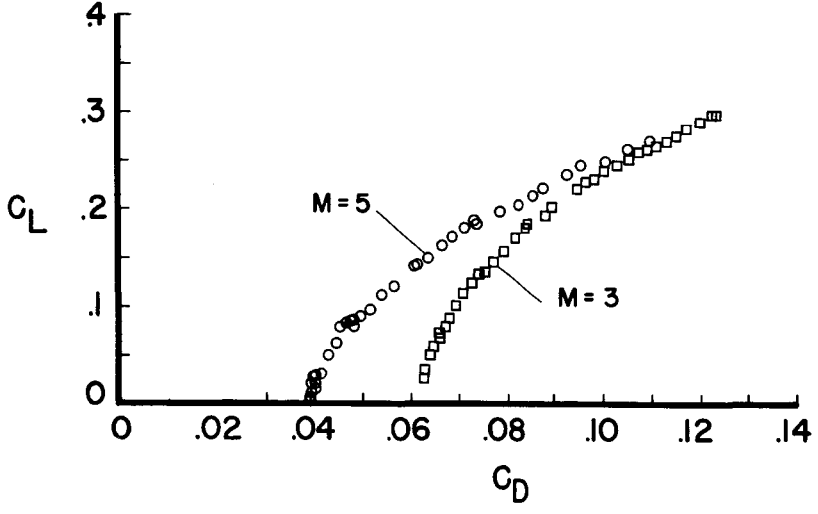


Figure 1

EFFECT OF REYNOLDS NUMBER ON
MINIMUM DRAG

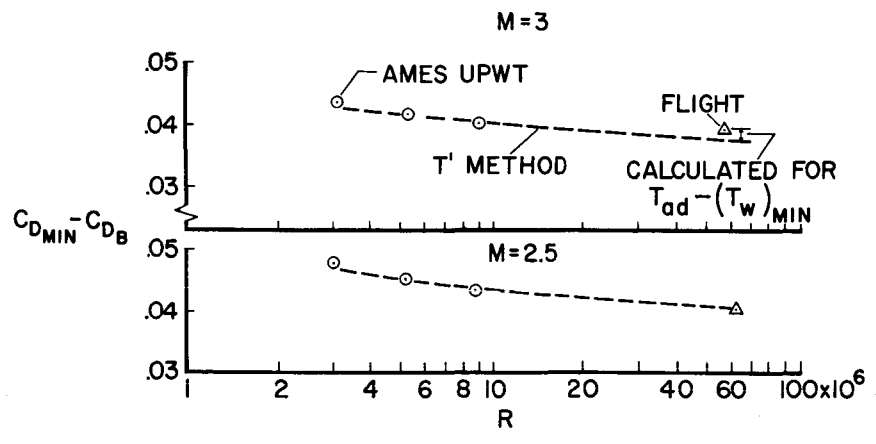


Figure 2

EFFECT OF MACH NUMBER ON MINIMUM DRAG POWER OFF

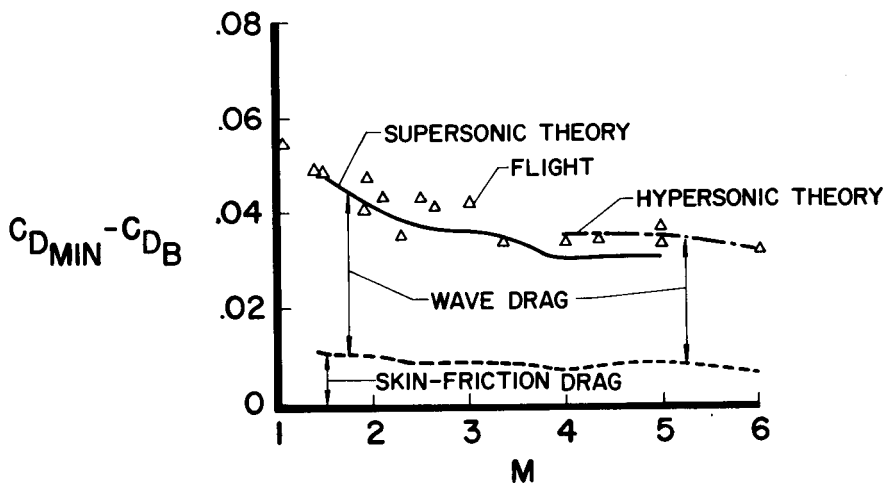


Figure 3

EFFECT OF MACH NUMBER ON THE TRIMMED DRAG DUE TO LIFT POWER OFF

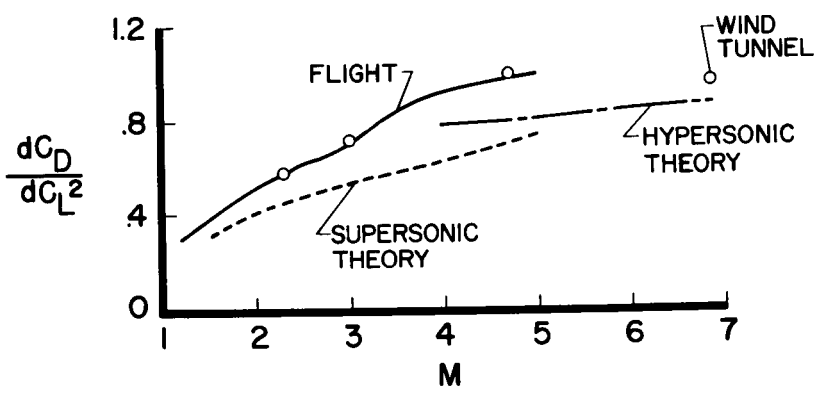



Figure 4



TRIMMED LIFT AND HORIZONTAL-TAIL DEFLECTIONS
POWER OFF
M=5

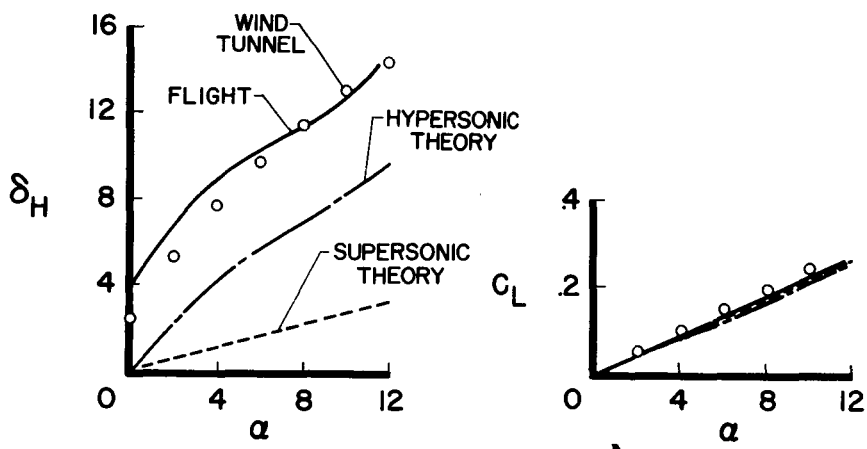


Figure 5

EFFECT OF MACH NUMBER ON THE TRIMMED
MAXIMUM LIFT-TO-DRAG RATIO
POWER OFF

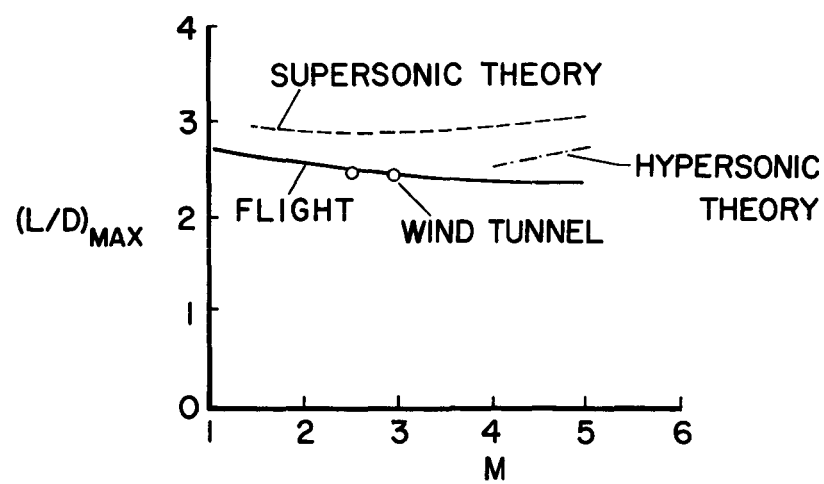


Figure 6



BASE-DRAG VARIATION WITH MACH NUMBER

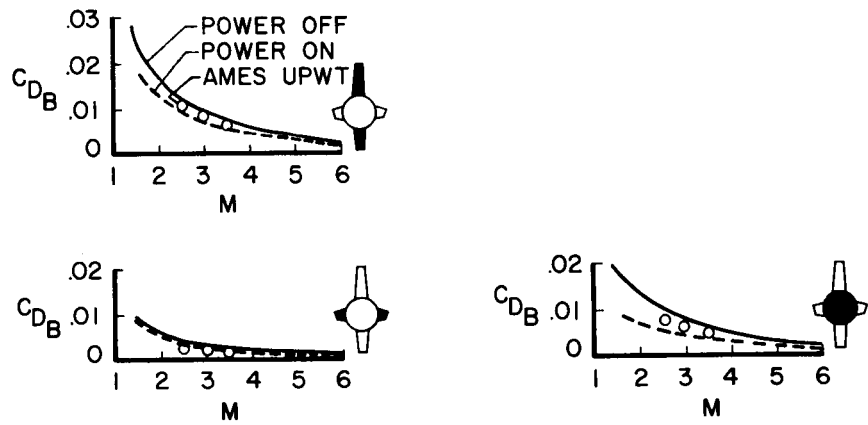


Figure 7

EFFECT OF MACH NUMBER ON RATIO OF BASE DRAG TO MINIMUM DRAG POWER OFF FLIGHT

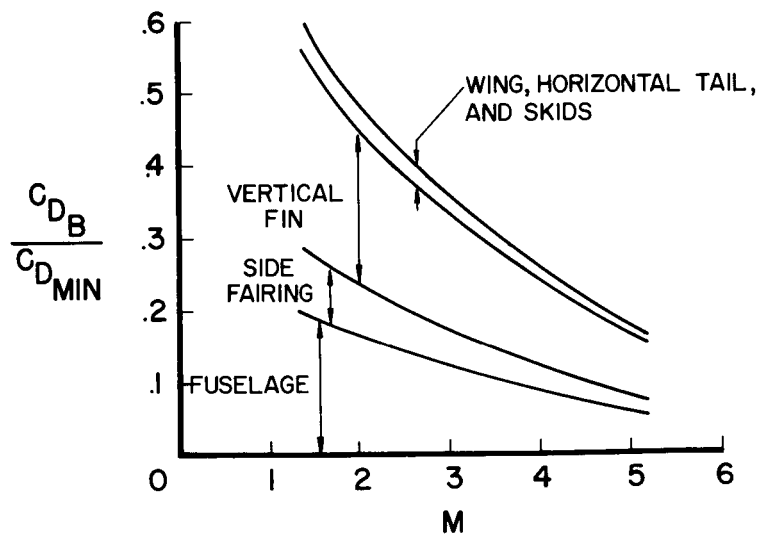


Figure 8

BASE PRESSURES FOR UPPER VERTICAL FIN

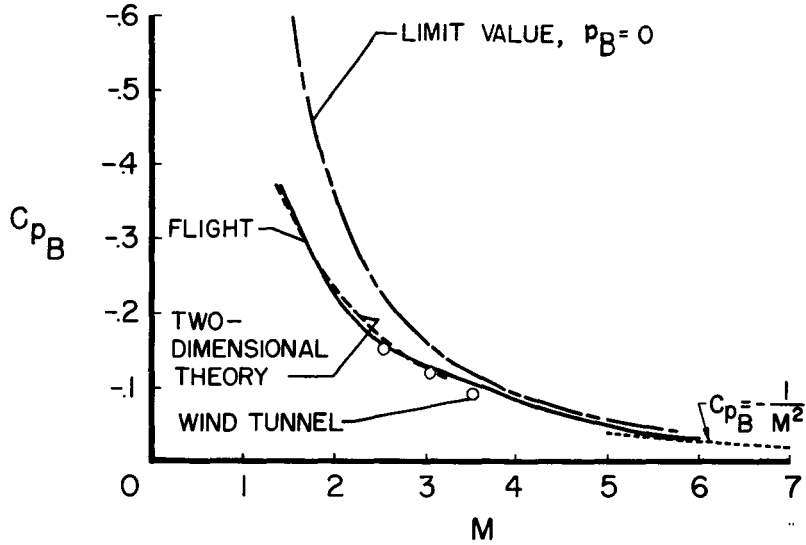


Figure 9

FUSELAGE AND SIDE-FAIRING BASE-PRESSURE COEFFICIENTS POWER OFF

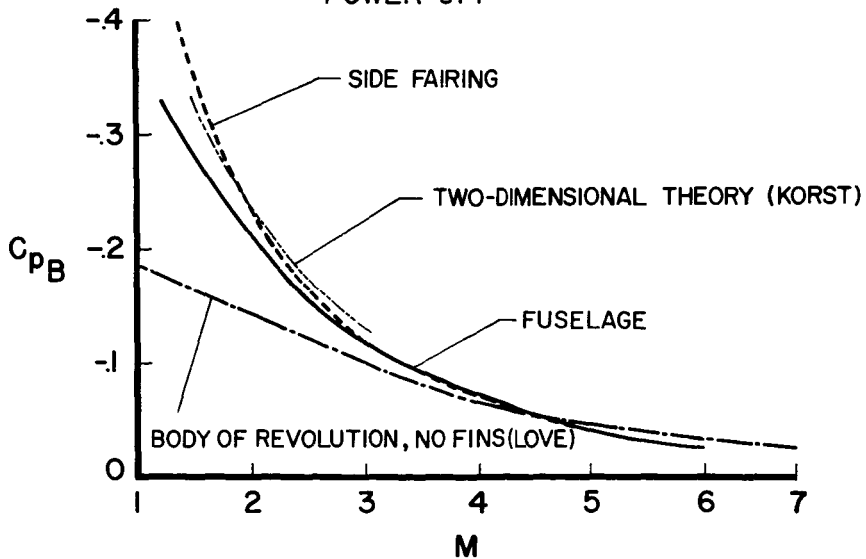


Figure 10

SPEED-BRAKE DRAG INCREMENT POWER OFF

$$\Delta C_{D_{SB}} = C_{D_{SB \text{ OPEN}}} - C_{D_{SB \text{ CLOSED}}}$$

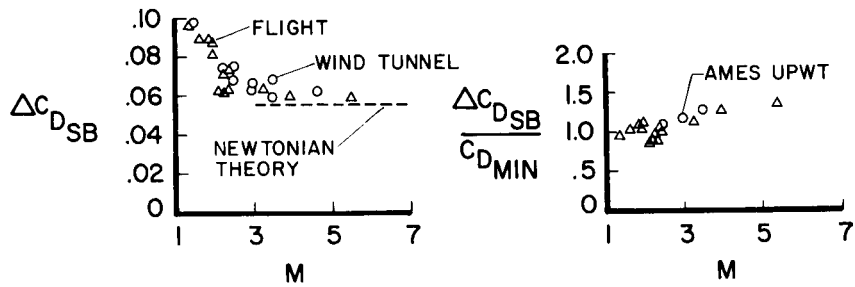


Figure 11



████████████████████ 14-057100
99

8. STABILITY AND CONTROL DERIVATIVE CHARACTERISTICS

OF THE X-15 (W) N71-7545 M

By Harold J. Walker and Chester H. Wolowicz

NASA Flight Research Center

INTRODUCTION

A thorough knowledge of the stability and control derivative characteristics is, of course, a fundamental requirement in planning the first flights of an airplane in new and unfamiliar areas. Although wind-tunnel tests normally provide the bulk of this information, a partial in-flight verification of the wind-tunnel data in a known environment is always desired before proceeding to the more critical areas. In keeping with this approach, three basic objectives may be listed for the current X-15 derivative program, as follows:

- (1) Establish basic trends for flight planning
- (2) Confirm wind-tunnel results and design criteria
- (3) Clarify troublesome flight-control areas

The items listed also comprise the main topics for discussion in this paper. First to be considered is a step-by-step in-flight buildup of the basic stability and control trends necessary in order that the highest possible safety and realism can be achieved in projecting each follow-on flight. These trends, as indicated in item 2, also serve as a basis for confirming many of the original design considerations, including the wind-tunnel and theoretical studies leading to the present configuration. Finally, in item 3, a knowledge of the derivatives would certainly be required in clarifying and correcting any troublesome flight-control problems, which, of course, are not entirely unexpected in a program of this nature.

DISCUSSION

It is desirable to call attention to several of the factors which were particularly problematical in reaching a finally acceptable configuration and which, therefore, are of immediate concern in the flight program. These factors were discussed in some detail at the July 1958


████████████████████

8

conference on the X-15 airplane and, as shown in figure 1, are related primarily to the strong shock fields that are generated at high angles of attack in the upper speed range. Shown on the left is the marked asymmetry in effectiveness that occurs between the upper and lower vertical tails as angle of attack is increased. Further information on these effects is presented in reference 1. This asymmetry, of course, has its source in the high dynamic pressure field surrounding the ventral fin on the lower side, and the highly expanded flow over the dorsal on the upper side. The relative effectiveness of the two surfaces, as shown, can be approximated from two-dimensional relationships by the ratio of the dynamic pressure q times the lift-curve slope CL_{α} for the local shock flow to that for the free stream. The combination of high ventral effectiveness (shown at the top) and low dorsal effectiveness (shown at the bottom) can be expected to generate some irregularity - to be shown subsequently - in the effective dihedral and yaw control characteristics. The present tail configuration with approximately 45 percent of the total exposed area below the fuselage was selected as the best compromise for averting an excessive dihedral effect at low speeds while at the same time providing adequate directional stability during powered flight at high Mach numbers and altitudes. The adequacy of this arrangement for the entire flight envelope could, of course, be proven only under actual flight conditions.

The second effect, on the right in figure 1, is seen to be the rather diverse nature of the downwash ϵ at the horizontal tail. The results shown were estimated from two-dimensional shock-flow relationships obtained by David E. Fetterman, Jr., of the Langley Research Center, and also originate in the high degree of asymmetry in flow conditions above and below the fuselage at high Mach numbers. The small upflow at low angles of attack, followed by an increasing downwash at the higher angles of attack, will lead to a nonlinear unstable trend in the longitudinal characteristics. This trend is further intensified as the leading edges of the horizontal tail at negative trim settings gradually penetrate the region of high dynamic pressure due to the wing compression shocks. Also, an increased pitch-control effectiveness will accompany the rise in dynamic pressure. Some evidence of these effects is discussed subsequently, although rather little flight testing has thus far been conducted under the conditions where these effects are most prevalent.

A third shock effect, not shown here but discussed in reference 1, is the gradual growth of a nonlinear trend in the lift-curve slope for the wing and tail surfaces as hypersonic speeds are approached. This trend can also be calculated from two-dimensional shock-flow relationships and is such as to compensate for much of the stability loss due to the wing downwash and compression effects.




An overall survey of the areas in which flight measurements of the derivatives have thus far been made is shown in figure 2. The angle-of-attack and Mach number coverage in relation to the overall flight envelope is indicated by the shaded region. Also included as a matter of interest, is an outer boundary - the dashed line - representing the limits to which the airplane has actually been flown. Although the derivative coverage is uniformly shaded, the measurements are actually somewhat spotty in many areas and are limited largely to the static stability and control effectiveness. In particular, there is a scarcity of data at the higher Mach numbers and angles of attack, where many of the basic problem areas lie. This, therefore, is the area in which much of our future testing will be focused.

As to the methods employed in the flight program for extracting the derivatives, a somewhat simplified approach in general was taken. Approximate relationships based on measurements of the frequency, damping ratio, and certain amplitude ratios were found to be adequate for control-fixed dynamic responses. Where control inputs were also involved, an analog matching technique was applied. These various methods are described more fully in reference 2. In general, the body-axes coordinate system has been employed throughout the analysis.

Longitudinal Derivatives

Three representative examples of the longitudinal static stability characteristics as derived from gradual pull-up maneuvers are presented in figure 3. Shown here are the angle-of-attack variations of normal-force coefficient C_N and stabilizer incidence δ_h for approximately trimmed flight at a transonic, a supersonic, and a low hypersonic Mach number. The wind-tunnel data are also included as represented by the faired lines. In general, the trends of the data with increasing Mach number are as expected, and the flight and wind-tunnel results are seen to be in fairly good agreement. At the sonic Mach number a nonlinear trend in the apparent stability, as given by the stabilizer trim variation, was confirmed in flight. At the highest Mach number (Mach 5) there is also some evidence of the previously mentioned nonlinear trend in the lift-curve slope. A fair degree of stability is still evident for this Mach number, although some tendency toward reduced stability is observed in the upper angle-of-attack range. This effect is an example of the destabilizing influence of the downwash and dynamic pressure as angle of attack is increased at high Mach numbers.

The effect of Mach number on the lift and stability characteristics as determined from dynamic (or pulse-type) maneuvers is summarized in figure 4. The slope C_{N_α} is given at the top, and the stability derivative dC_m/dC_N , which is also a direct measure of the static



margin in terms of the mean aerodynamic chord, is given at the bottom. For the angle-of-attack ranges represented, good agreement is noted among the various data with the exception of the calculated stability in the high angle-of-attack range. A discrepancy is noted here at Mach numbers above 3, which is attributed to neglecting the nonlinear downwash and dynamic-pressure effects mentioned earlier. The results indicate that, in general, the anticipated levels of stability have been realized in flight, at least in the regions of the envelope covered so far.

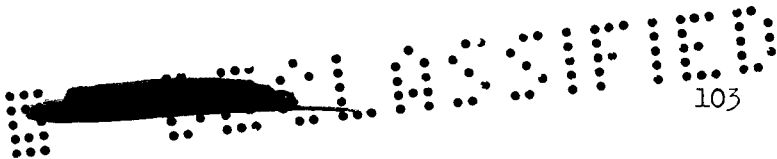
Some typical results for the longitudinal control effectiveness are presented in figure 5. Here again, in general, the results from wind-tunnel tests and theory agree fairly well with the flight data. The peak effectiveness is noted to occur at a slightly lower Mach number than the peak stability shown in figure 4. The opposing trends in the intermediate Mach number range, one rising and the other diminishing, produce a noticeable transonic speed instability.

The trim characteristics for the maximum and two intermediate negative stabilizer settings are presented in figure 6. A potential trim capability approaching α_{TRIM} of 30° is noted at peak speeds, although, in general, very little flight data have been obtained so far in the high angle-of-attack range. The data that are available, however, seem to be generally in good agreement with the wind-tunnel predictions. The marked rise in trim capability above Mach number 3 again is caused by the nonlinear downwash and wing compression effects at high angles of attack.

The last remaining derivative of interest for the longitudinal mode, the damping derivative, is summarized for a moderate angle-of-attack range in figure 7. The derivative $C_{m\dot{q}} + C_{m\dot{\alpha}}$ is more difficult to isolate than the static derivatives, particularly in the supersonic range where the natural damping of the airplane is quite low. The flight and predicted results, however, are in fair agreement. The marked decline in the damping at supersonic speeds is indicated on the right-hand plot, where the damping ratios corresponding to the various derivative points on the left are shown for a moderate dynamic pressure. The damping ratio ζ is seen to drop well below 0.1 at Mach numbers above 2 and some form of damping augmentation must be provided.

Lateral Directional Derivatives


As is so often the case, the lateral-directional modes pose the greater variety of stability and control problems. The major ones were discussed in some detail at the July 1958 conference on the X-15 and



were mentioned briefly at the beginning of this paper. The two most important derivatives affecting these modes are, of course, the directional stability and dihedral effect, which are presented in figure 8. Representative variations of the two derivatives with angle of attack, as determined from both flight and wind-tunnel tests, are presented for a low and a high supersonic Mach number. The flight data for $C_{n\beta}$ are somewhat low in some areas, but otherwise generally confirm the wind-tunnel predictions. The results show that distributing a large portion of the vertical-tail area below the fuselage allows a relatively low dihedral effect to be achieved at the lower Mach number. The static directional stability $C_{n\beta}$, however, diminishes substantially with increasing angle of attack. At the higher Mach number, the dihedral derivative, although still small, is seen to be of opposite sign. This unfavorable trend has a very pronounced effect on the closed-loop dynamic stability which will be discussed in some detail in a subsequent paper. The cause for this positive trend is, of course, the previously mentioned asymmetry in effectiveness between the upper and lower vertical tails. As expected, the directional stability is lower at the higher Mach number but, due to the high intensity of the wing and bow compression shocks, is seen to increase rather than diminish with increasing angle of attack.

The influence of the dihedral derivative on the Dutch roll stability for the two Mach numbers, 1.9 and 4.0, is illustrated in figure 9. The Dutch roll stability is represented here by the parameter $(C_{n\beta})^*$ and is given approximately by the relationship shown in the figure. (See refs. 3 and 4.) For comparison, the wind-tunnel values for $C_{n\beta}$ (the dashed line) are carried over from figure 8. It is especially important to note that the ratio of the moments of inertia about the yaw and roll axes in the second term of the equation is a large quantity (approximately 22), and thus the influence of the dihedral derivative is seen to be greatly magnified as angle of attack is increased. For the lower Mach number, 1.9, the dihedral derivative is negative, so that the static stability is augmented. For the higher Mach number, 4.0, on the other hand, the positive values of the dihedral derivative are seen to detract quite substantially from the basic stability.

One possible method for alleviating the adverse dihedral effect at the higher Mach numbers is to remove the lower rudder. This effect for Mach number 4.0 is shown in figure 10. The rudder-off configuration is represented by the dashed lines, which show that the sign of $C_{l\beta}$ has been reversed in a favorable direction as desired. The directional stability parameter $C_{n\beta}$, as anticipated, has also been markedly



degraded, although much of the loss indicated can be regained by opening the speed brakes. The effect of the lower rudder on the Dutch roll stability $(C_{n\beta})^*$ is shown in the right-hand plot, where a considerable improvement attributable to the favorable dihedral effect is indicated at the higher angles of attack even though the speed brakes are closed. It should be mentioned that for Mach numbers less than about 2.2, the dihedral derivative is normally negative at all angles of attack, and the stability of the basic airplane is generally superior to that for the rudder-off configuration.

The directional stability and dihedral effect for the rudder-on configuration are summarized in figures 11 and 12. Data are presented for both open and closed speed brakes (as indicated by the solid and open symbols), and corresponding results from wind-tunnel tests and theory are included. The results for the directional stability (fig. 11) indicate that the design levels have been essentially realized in flight, although the trend of the flight data is somewhat low at supersonic Mach numbers. There is also an apparent scatter in the flight increment for $C_{n\beta}$ due to speed-brake deflection in the lower angle-of-attack range. This scatter is believed to be due in large part to differences in angle of attack within the range from 2° to 6° , although the wind-tunnel data for this increment show relatively little sensitivity to angle of attack.

The flight data for the dihedral derivative $C_{l\beta}$ in figure 12 generally appear to confirm the wind-tunnel measurements for both angle-of-attack ranges. The speed-brake effect for this derivative is seen to be relatively small and to lie within the scatter of the data.

As would be expected, most of the various effects due to shock interaction and removal of lower rudder are also reflected in the control characteristics for the lateral-directional modes. Time does not permit a complete review of these effects; however, a summary of the results for the basic airplane at low angles of attack is given in figure 13. The yaw and roll control effectiveness $(C_{n\delta_v}$ and $C_{l\delta_a})$, as well as the cross coupling derivatives $(C_{l\delta_v}$ and $C_{n\delta_a})$ are included and, except in one area, the flight and predicted results are generally in accord. The exception is seen to be the low trend in the yaw-control effectiveness at Mach numbers above 2 which appears to coincide approximately with the reduced directional stability noted in figure 12.

At this point, only the lateral and directional damping characteristics remain to round out the derivative presentation. The damping

trends for this mode, however, are found to be much the same as those for the longitudinal mode considered earlier. It suffices therefore to point out that the lateral-directional damping also decays to very low levels at supersonic speeds and that damping augmentation must be provided.

CONCLUDING REMARKS

It can be stated that the X-15 flight program thus far has established fairly well-defined derivative trends for Mach numbers approaching the design limit. With few exceptions, these trends have agreed well with the wind-tunnel predictions. Also, many of the basic stability and control design parameters have been confirmed in a substantial portion of the overall flight envelope. The gradual development of these basic trends from one flight to the next has, in fact, generated a high level of confidence in proceeding to the more critical flight areas during the past several months. No serious flight-control problems have thus far been encountered in the longitudinal mode; however, one serious deficiency in the lateral-directional mode has been observed in the form of an adverse dihedral effect at high Mach numbers and angles of attack. Further studies and tests are, of course, planned for the high Mach number and angle-of-attack ranges to reveal any further flight-control problems that may exist in these more critical areas and to fill out the remainder of the flight envelope.

REFERENCES

1. Walker, Harold J., and Wolowicz, Chester H.: Theoretical Stability Derivatives for the X-15 Research Airplane at Supersonic and Hypersonic Speeds Including a Comparison With Wind-Tunnel Results. NASA TM X-287, 1960.
2. Yancey, Roxanah B., Rediess, Herman A., and Robinson, Glenn H.: Aerodynamic-Derivative Characteristics of the X-15 Research Airplane as Determined From Flight Tests for Mach Numbers From 0.6 to 3.4. Prospective NASA TM.
3. Moul, Martin T., and Paulson, John W.: Dynamic Lateral Behavior of High-Performance Aircraft. NACA RM L58E16, 1958.
4. Taylor, Lawrence W., Jr.: Analysis of a Pilot-Airplane Lateral Instability Experienced With the X-15 Airplane. NASA TN D-1059, 1961.



PROMINENT SHOCK-FLOW EFFECTS

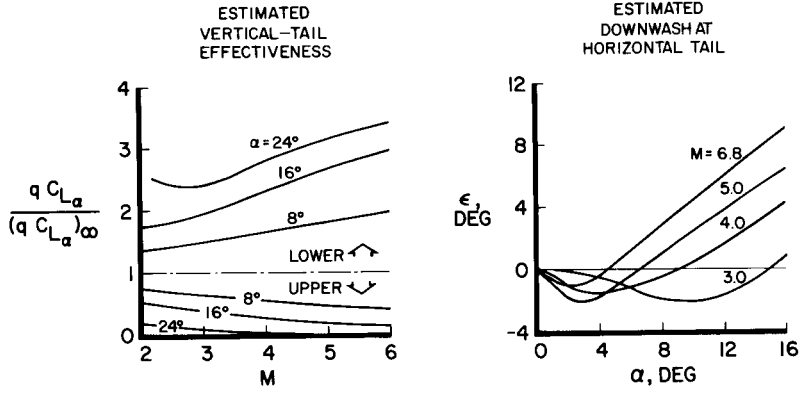


Figure 1

FLIGHT COVERAGE

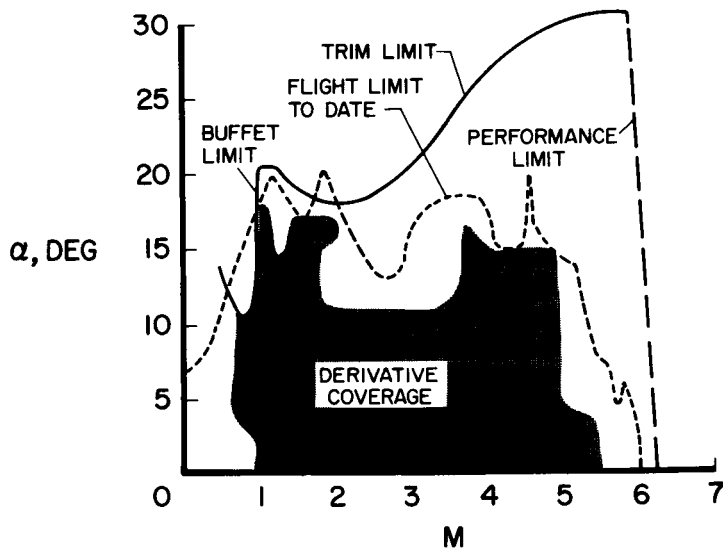


Figure 2



LONGITUDINAL STATIC STABILITY

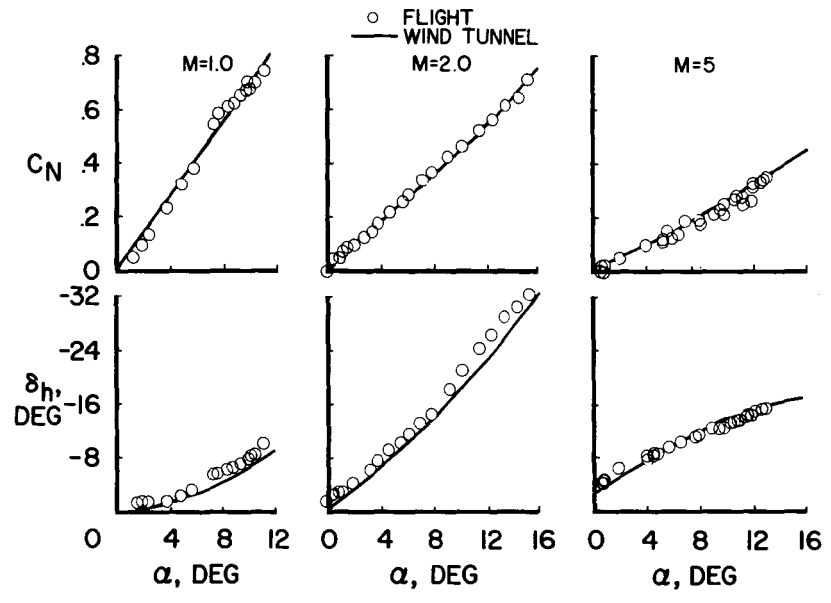


Figure 3

SUMMARY OF LONGITUDINAL STABILITY

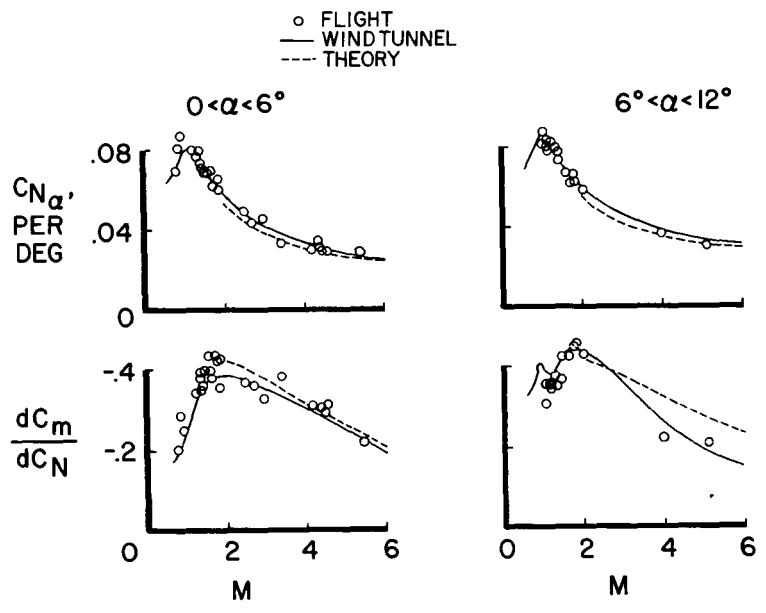
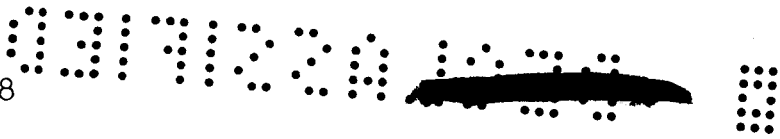


Figure 4



LONGITUDINAL CONTROL EFFECTIVENESS

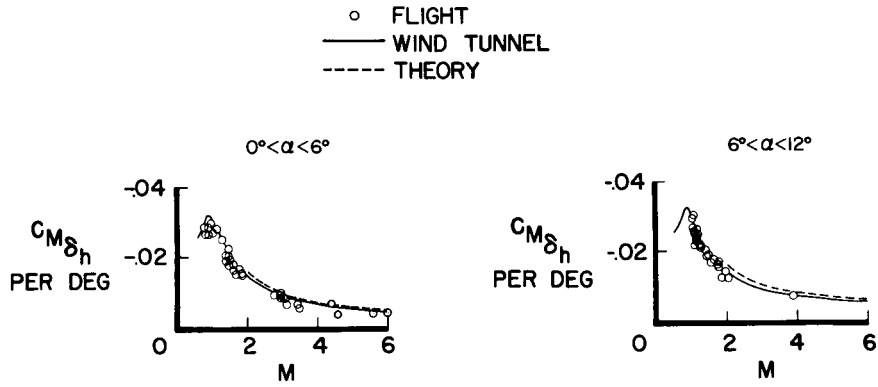


Figure 5

TRIM CAPABILITY

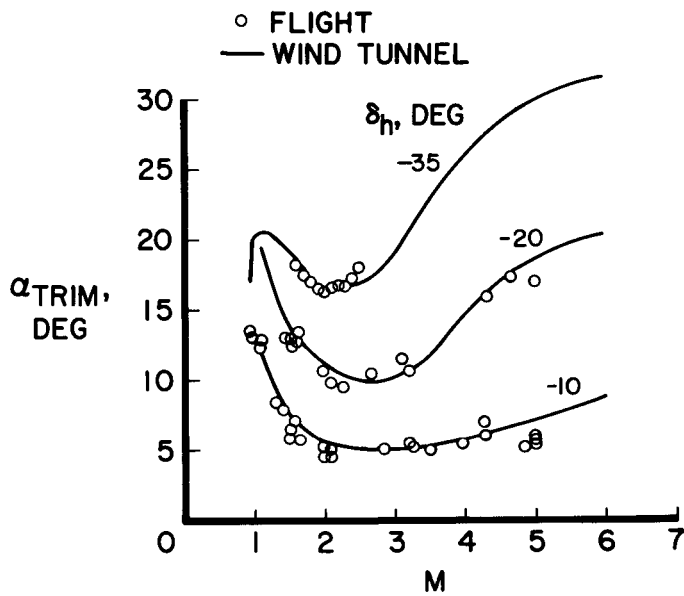


Figure 6



LONGITUDINAL DAMPING

$0^\circ < \alpha < 6^\circ$

○ FLIGHT
 — WIND TUNNEL
 - - - THEORY

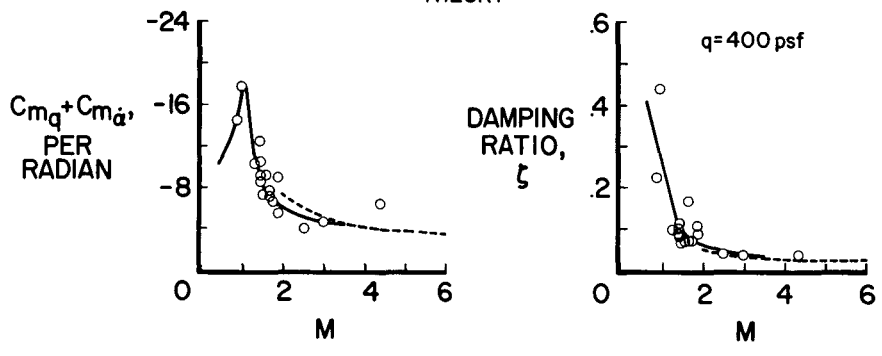


Figure 7

LATERAL-DIRECTIONAL STABILITY

— WIND TUNNEL ○ FLIGHT

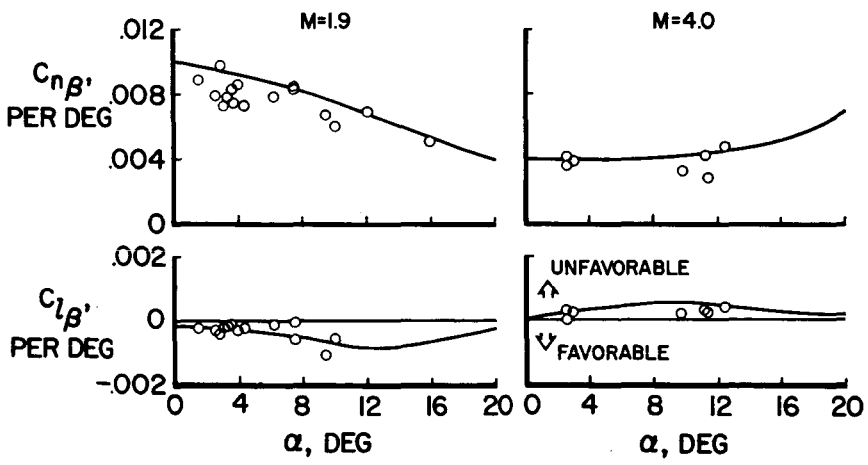
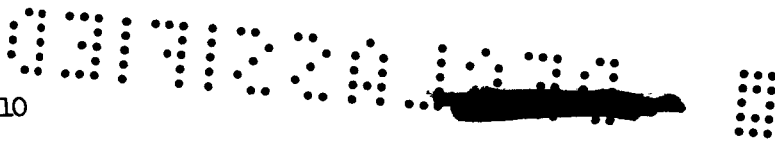


Figure 8



DUTCH ROLL STABILITY

$$(C_{n\beta})^* = C_{n\beta} - \alpha \frac{I_z}{I_x} C_{l\beta} \approx \frac{\omega^2}{qSb/l_z}$$

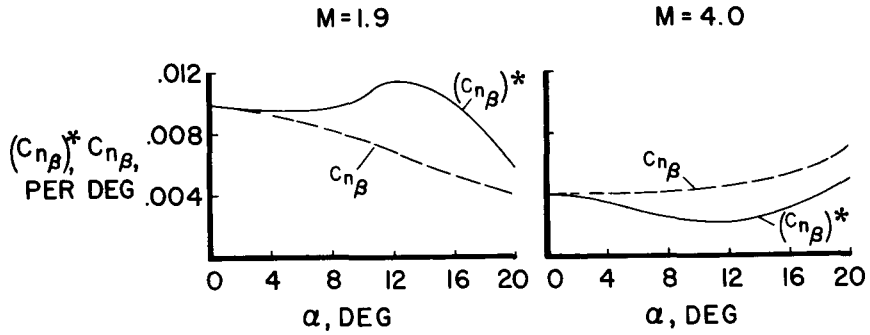


Figure 9

EFFECT OF LOWER RUDDER ON LATERAL-DIRECTIONAL STABILITY

SPEED BRAKES CLOSED M=4.0

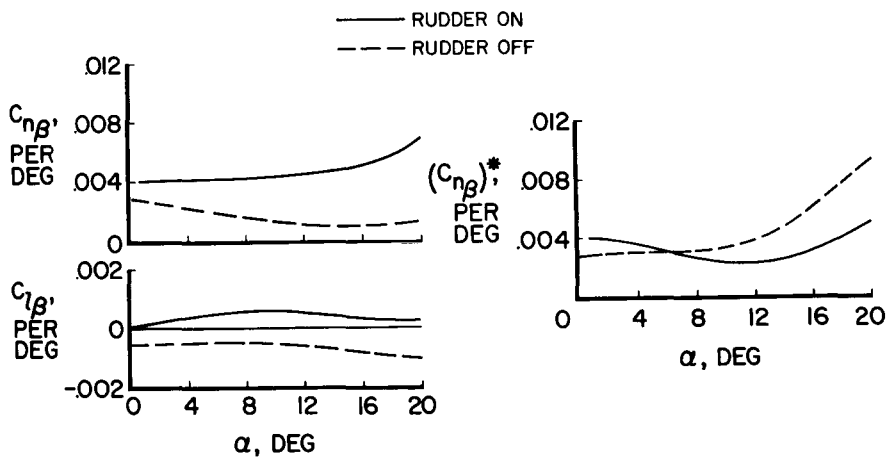


Figure 10



$C_{n\beta}$ SUMMARY

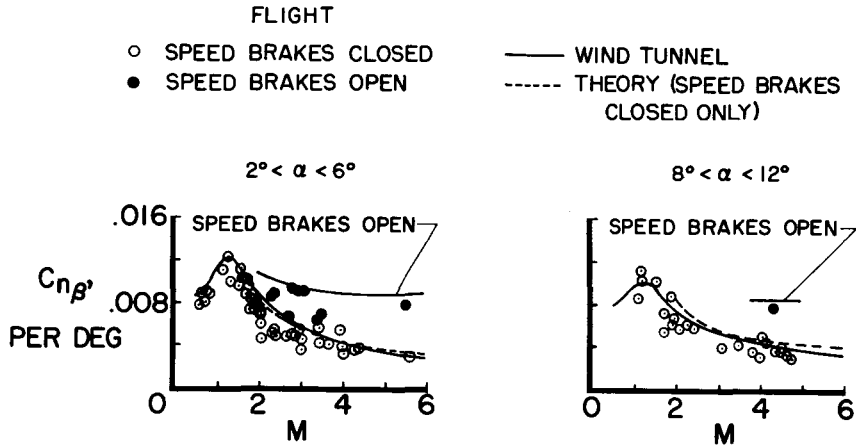


Figure 11

$C_{l\beta}$ SUMMARY

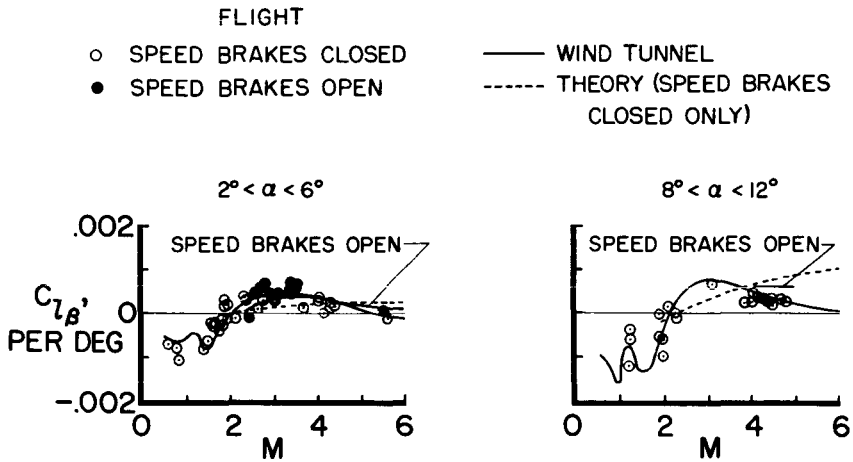


Figure 12



SUMMARY OF LATERAL-DIRECTIONAL CONTROL

$0^\circ < \alpha < 5^\circ$

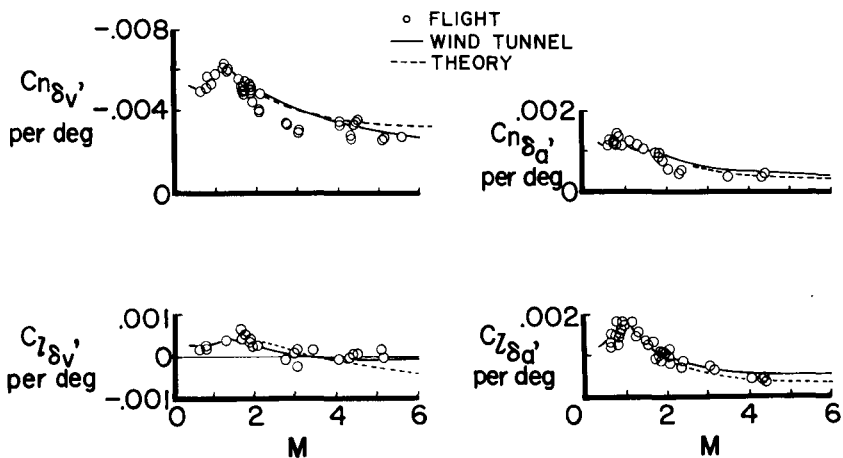


Figure 13

CONFIDENTIAL

9. RÉSUMÉ OF X-15 HANDLING QUALITIES (L)

By Robert M. White
Air Force Flight Test Center

N71-75452

Glenn H. Robinson, and Gene J. Matranga
NASA Flight Research Center

SUMMARY

The handling qualities of the X-15 research airplane have been assessed from pilots' opinions, with verification in many cases by data acquired during flights. Areas of interest covered are the launch, climbout, ballistic, reentry, and landing phases of flights made to date.

INTRODUCTION

The concept of aircraft handling qualities has been specified since World War II to provide certain performance features, such as rolling velocity and stall warning, and a desired level of static and dynamic stability to allow the pilot to fly the aircraft with relative ease. Although great efforts have been made to assign quantitative values to these parameters, many of the results on how the airplane flies are assessed through pilot opinion. Both pilots and engineering analysts might do well to accept this thesis, for to quote one well-used text book (ref. 1) on the subject: "The desired magnitude of dihedral effect has never been very successfully determined. From the analysis of many stability and control flight tests, it has become apparent the pilot likes to have some dihedral effect, but not too much."

This résumé covers in broad aspects many of the handling features of the X-15 from its launch to landing. Some conclusions can be drawn, but many comments regarding handling-quality specifications for hypersonic and high-altitude flight must wait until future flights are made and their data are thoroughly examined.

SYMBOLS

- a_l longitudinal acceleration, g units
- a_n normal acceleration, g units

[Redacted]

g	acceleration due to gravity
L/D	lift-drag ratio
M	Mach number
P_{MAX}	maximum angular rolling velocity, deg/sec
\dot{q}	angular pitching acceleration, deg/sec ²
\bar{q}	dynamic pressure, lb/sq ft
\bar{q}_{MAX}	maximum dynamic pressure, lb/sq ft
$(W/S)_{av}$	average wing loading, lb/sq ft
α	angle of attack, deg
α_{TRIM}	trim angle of attack, deg
β	angle of sideslip, deg
δ_h	horizontal tail deflection, deg
ζ	damping ratio
θ	pitch angle, deg
$\Delta\phi_{MAX}$	maximum roll angle increment, deg
ω_n	natural frequency in pitch, radians/sec

THE X-15 COCKPIT

Since frequent reference will be made to the pilot's cockpit, some of the salient items used for display and control can be examined by reference to figure 1.

The display is conventional in that it shows in standard fashion the operating level of many of the aircraft and engine systems. The flight phase is monitored chiefly from the inertial system which provides readout in altitude, velocity, and aircraft attitude. Additions from the "q" sensor ball nose provide pointers and cross bars that

allow the pilot a reading of angle of attack and vernier indications of angle of attack and sideslip. A prime reliance is placed on the attitude indicator in three axes, inasmuch as the earth's horizon is quickly lost as an outside reference during the high pitch angle climb experienced on all flights. Simplicity is the key, and many small changes have been made continually to improve display, as requested by the pilots, to give a readable display in the rapid cross checks that a pilot makes in a fast-moving situation.

Control is afforded in several ways. Aerodynamic control is provided by a conventional center stick or by an interconnected side stick so positioned as to allow pilot control without inadvertent or adverse inputs from acceleration forces. Reaction control for attitude control at low dynamic pressure is given by a simple controller on the left side of the cockpit that allows inputs in roll, pitch, and yaw.

LAUNCH AND CLIMBOUT

Two areas common to all flights, the launch and initial climbout, have been studied in detail. The launch is characterized by two prominent features, first a sudden departure from the B-52 pylon, yielding a zero g peak normal acceleration, and second an abrupt rolloff to the right that rarely exceeds a 10° to 15° change in bank angle. The release is what might be expected and, after the very first experience, is of no concern to the pilot as normal 1.0g flight is regained within 2 seconds. The rolloff at launch stops as the X-15 emerges from the B-52 flow field. Since the bank-angle change is small, it is easily and quickly corrected. Launch has been made by using either the center or side aerodynamic control stick with equal satisfaction in both cases. In addition, launch has been made with the control neutral, correcting the rolloff as it occurred, and with small lateral-control input to counteract the roll before it could develop. Both cases have been acceptable and resolve into individual pilot's technique and preference.

Immediately after launch the engine is fired and the climbout begins. Assume for a moment that a long delay occurs before engine ignition, which has been true on several occasions. The pilot glides at an angle of attack of 8° , which is near the best lift-drag ratio for glide; the aircraft responds well and is free of buffet. If angle of attack is increased to 10° , a mild buffet onset is immediately detected, which allows the pilot to make corrections well in advance of a stall condition. The aerodynamic qualities, then, at 45,000 feet, Mach number 0.8, and at maximum weight are considered excellent. Very quickly after engine light-off, supersonic speed is reached and an angle of attack of 10° is maintained to rotate the airplane to a climbout pitch

angle that is established by the mission requirement. Buffet is absent above Mach 1.0, but a nosedown trim change occurs between Mach numbers 1.1 and 1.4. Figure 2 illustrates this trim change. Note that the piloting task in the low-supersonic-speed range calls for constant angle of attack. It is seen that in order to maintain constant α the pilot must trim in substantial up stabilizer. Frequently, the speed change is so rapid (approximately 6 seconds from Mach numbers 1.1 to 1.4) that the pilot has difficulty keeping up with the trim change and as a result the angle of attack in this speed range is usually lower than desired. The trim change is mild, however, and has not received the objections from pilots that have often been given to the more abrupt trim change in the transonic region below Mach number 1.0 that occurs on many jet aircraft.

CONTROL CHARACTERISTICS

Figure 3 presents the details of an altitude mission which reached 217,000 feet and which enables many comments to be made pertinent to X-15 flight control characteristics. After initial rotation at an angle of attack of 10° , a constant pitch angle of 32° is established and maintained to burnout where the acceleration along the longitudinal axis a_L reached 3.6g. From engine burnout until the reentry the aircraft follows a ballistic trajectory, and two unique features that occurred are weightlessness experienced by the pilot for about 2 minutes and the requirement that reaction controls be used since dynamic pressures have decreased to a minimum of 3 pounds per square foot at peak altitude. This part of the flight is followed by the reentry maneuver, which terminates when the aircraft rotates to level flight after experiencing, as in this case, normal acceleration a_n of 3.8g, longitudinal acceleration of -2.2g, and peak dynamic pressure in excess of 1,400 pounds per square foot.

The portion of the profile during exit is particularly pleasing to the pilot since the airplane is very stable and the damping appears adequate, even with roll and yaw dampers failed. The increase in acceleration along the longitudinal axis during the thrust period reaches a maximum of 3.6g at burnout. The g-level, although certainly noticeable to the pilot, has not been high enough to provide any adverse comment in regard to impairing the pilot's ability to perform his essential tasks. Thrust termination during flight occurs when the pilot stops the engine or when burnout results from propellant exhaustion. In all cases there have been no transient aircraft motions, and thrust misalignment has not been a factor of concern. The stabilizer is trimmed to maintain an angle of attack of 0° . This change in trim is complete at approximately 145,000 feet, where \bar{q} has decreased to 26 pounds

per square foot. At this point a decay in response to aerodynamic control is easily noted by the pilot, and reaction controls are then employed. The reaction controls proved to be very effective, aircraft response to inputs in roll and yaw were good, and the response in pitch was more than desired and caused some difficulty in damping the pitch oscillations.

Ballistic Control Characteristics

The motions in the ballistic flight region can best be illustrated by the time history shown in figure 4, which includes that part of flight at dynamic pressures of less than 10 pounds per square foot. Plotted are the angle of attack and airplane pitching acceleration \dot{q} which developed as a result of the reaction-control use. All reaction-control inputs were essentially in the proper direction to damp the airplane motion except at one point where the angle-of-attack oscillation experienced its largest excursion. At this point an input was made that reinforced the increase in angle of attack, but immediately afterward the pilot was able to damp the oscillation adequately to maintain the desired angle of attack. Although the longitudinal control task was complicated by the presence of an out-of-trim stabilizer condition, the results are indicative of control difficulties that can be encountered with an acceleration-command reaction-control system. Since this figure presents results of the first and only significant reaction-control experience with the X-15, proper longitudinal control trim and pilot experience are expected to yield an improvement in airplane attitude control at low dynamic pressure. The excursions in sideslip were contained to acceptable limits by using reaction control. Similar results were evident in bank-angle control. Lateral-aerodynamic-control inputs were used at low dynamic pressure with no apparent response compared with the good response and control afforded by reaction control. Pilot technique in this region was use of reaction control in one axis at a time.

Zero g, while apparently an interesting area to consider, has had no noticeable effect on the pilot control task for the approximate 2 minute period during which the weightless state was experienced.

The presentation for control is provided by cross bars shown in figure 5 to allow flying at prescribed values of angles of attack and sideslip. As can be seen, these bars are incorporated within the face of the attitude indicator which additionally provides roll information for control inputs. Inasmuch as the pilot is presently manually controlling attitude about three axes without any damping system, the instrument presentation is considered adequate since all information is displayed centrally and minimizes scanning and instrument cross-check.

Control During Reentry

The reentry maneuver is perhaps the most interesting from the pilot's standpoint, since it is flown at relatively higher angles of attack and under the rapidly changing conditions of dynamic pressure, temperature, velocity, with the associated changes in aircraft stability and responses. The maneuver actually begins as the aircraft passes through 180,000 feet (see fig. 3) where the stabilizer is trimmed to a value that will maintain reentry normal acceleration. The reaction control is used to establish the reentry angle of attack.

The time history shown in figure 6 begins immediately after the stabilizer has been trimmed for reentry. With the stabilizer constant and the angle of attack raised to 10° , the normal acceleration a_n increases to approximately $2g$ as the dynamic pressure \bar{q} increases. The angle-of-attack decrease results from a repositioning of the stabilizer to maintain the reentry acceleration until level flight is regained at just above 60,000 feet. Returning to the point where reentry angle of attack was reached, but just prior to significant change in dynamic pressure, a sideslip oscillation developed but was low enough in magnitude and frequency to be disregarded by the pilot, particularly since it damped adequately as \bar{q} increased. Before leaving this area, it is interesting to point out that the static simulations and the Johnsville centrifuge program contributed to very good training for these conditions so that the actual reentry did not result in a completely new or unexpected flight experience.

Other Control Features

Several features, common to all flights, can be noted prior to a discussion of the terminal and landing phase of the X-15.

The speed brakes have been used in a large number of areas throughout the speed and altitude range, under thrust, and after engine shutdown. Except for incremental use in the landing pattern, they have always been extended symmetrically, that is, with equal brake deflection for the segments both above and below the fuselage, and opened to full deflection. During extension there is a mild trim change. Aside from the trim change, no undesirable aircraft motions have been experienced with speed-brake use; they are extremely effective, and there has never been a report of buffet due to speed-brake deflection.

Lateral control of the aircraft has been effected by differential deflection of the horizontal stabilizer, that is, the so-called "rolling tail." This method of lateral control has been excellent on the X-15. The pilot is not aware of what specific type of lateral control is

allowing the roll motion. His only concern is in being able to get the aircraft response he calls for when deflecting the control stick. Figure 7 contains many representative points obtained in flight and illustrates the comparatively low roll rates and moderate bank-angle changes associated with performing the X-15 mission. From experience to date, the rolling tail has provided a good rolling control for the X-15, and there have been no undesirable aircraft motions coupled in any axis because of lateral-control deflection. It is true that inertial coupling is a factor under specific conditions of dynamic pressure, angle of attack, and rolling velocity, but no attempt has been made to verify such predictions by specific roll-performance flight tests, aside from determining lateral effectiveness and using roll control only as required on any particular flight.

The stability augmentation system which provides rate damping about all axes has had significant effect on pilot opinion. During early flights below a Mach number of 3.5, moderate gains were used. Pilot opinion expressed a desire for a stiffer aircraft, particularly in pitch and roll and flights above $M = 3.5$ have used considerably higher gains. In general, pilot opinion of the augmented handling qualities in the Mach number range from 2.5 to 6.0 has been quite favorable. It is interesting to note that at angle of attack of 8° and above with low damper gain and particularly with roll or roll and yaw dampers off, the pilot has great difficulty in controlling the lateral and directional motions to prevent divergence. The primary cause of the control difficulty is due to an adverse dihedral effect which is present at Mach numbers above 2.3. This problem area has received a great deal of attention, and the paper by Petersen, Rediess, and Weil (paper no. 10) completely summarizes the area of unaugmented X-15 lateral and directional characteristics. With dampers set at high gain, however, the lateral and directional characteristics have been acceptable to the highest angle of attack explored thus far (approximately 17°).

The pilot ratings (P.R.) for longitudinal controllability are summarized in figure 8 as a function of frequency ω_n and damping ratio ζ , and these results are compared with criteria developed by the Ames Research Center (ref. 2) from simulator studies conducted on reentry vehicles. The X-15 flight data obtained during powered and unpowered flight are shown by circular symbols (according to pilot rating) whereas the comparative Ames results are indicated by the lines. Most of the X-15 points have satisfactory ratings including one of the two points representing damper-off conditions. In general, the correlation between the X-15 flight points and the Ames criteria are good. It appears however, that the damper-off points were rated in flight more favorably than would be predicted from simulator results.



The side aerodynamic control stick designed for the X-15 has received the usual critical analysis associated with a departure from the conventional control. The following list includes most of the factors considered:

- Force gradients - sensitivity
- Dead band - centering
- Control harmony
- Utility at high acceleration
- Controller geometry and location
- Trim control

As experience using the side stick was gained and modifications were attempted to make each factor fully acceptable to the pilot, most features included in the initial design were found to be satisfactory. All pilots agree to its utility value at high acceleration; however, the location of the control in relation to the pilot's arm position proved most critical. A modification allowed the selection of five different positions, which provided for adjustment of the control stick, fore or aft prior to flight, to satisfy an individual pilot's desire. The trim control remains controversial, and further evaluations will seek the best compromise between a wheel or button control and its best location on the stick. In general, the control has been most desirable on many occasions and has been used entirely on some flights from launch to landing.

LANDING TECHNIQUES

The final phase of each flight is, of course, the landing. This area has progressed from one receiving a great deal of concern and attention in the first flights to routine operation based on the experience, procedures, and techniques developed.

Prior to and during the X-15 flight program, landing simulations have been made using the F-104 airplane. With predetermined settings of the lift and drag devices and the engine thrust, the lift-drag ratio is established to match that of the X-15. This experience allowed the pilots to establish geographic checkpoints and key altitudes around the landing pattern; pilots thus become familiar with the position and timing required in the pattern by the low lift-drag ratio. At present, prior to each X-15 flight, the pilot devotes an entire F-104 flight to approaches and landings in what is considered satisfactory preparation and practice for the landing maneuver.

As concerns the space positioning of the X-15 for a landing pattern, figure 9 illustrates a wide range of conditions in altitude at the high key and lateral dispersion from the touchdown point. This figure indicates the flexibility allowed the pilot in maneuvering to a designated touchdown point. This flexibility is primarily attributed to several factors. The pattern is normally flown at an indicated airspeed of 300 knots, and the handling qualities, including the control-system use and the airplane responses, are considered excellent. If less sink rate is desired, the aircraft can be flown at an indicated airspeed of 240 knots for best L/D; and if necessary, excess altitude can be lost at constant airspeed by use of the speed brakes. Although rates of sink average 250 feet per second and have been as high as 475 feet per second prior to landing flare, none of the pilots have considered these values to be a limiting factor in the pattern.

A summary of flare characteristics is shown in figures 10 and 11. Note once again the wide range of conditions that a pilot can choose to arrive at a similar landing. The flare-initiation altitude shown in figure 10 has generally averaged less than 1,000 feet but covers a wide range of airspeeds.

In figure 11, the average vertical velocity at the flare runs between 100 and 180 feet per second, which is usually at a lower rate of sink than that for steady glide. This reduction is generally a result of deceleration during the approach. Aside from airspeed control, the cues that a pilot uses are all external. A landing point is chosen and the flare point is selected so that the remaining energy will carry the aircraft to the intended touchdown spot. The flare altitude is not selected from the altimeter, but from the pilot's own estimate of the height necessary to reduce the sink rate and arrive level in close proximity to the ground. It is significant that as flight progressed, the flare speeds increased, not to seek better handling qualities, which are good throughout, but to gain more time after the flare to make configuration changes, correct trim changes, and then execute the landing at acceptable values of angle of attack, sink rate, and proximity to the intended landing point.

Pertinent touchdown parameters are presented in figures 12 and 13. As is shown in figure 12, most landings have been accomplished with vertical velocities of less than -5 feet per second at angles of attack between 6° and 8° . Ground effect, while noted in some cases, has not been a significant factor in the pilot's analysis of the landing. In each of the last 20 landings a specific spot has been used for the intended touchdown point. In figure 13, all but four landings have been grouped within $\pm 1,200$ feet of that spot. This degree of precision is considered to be very good. The landing summary shown reveals an average slideout distance from touchdown of 5,000 to 6,000 feet. The

shortest distance can be achieved by using full aft longitudinal control and flap retraction to place the greatest load on the skids, and full deflection with speed brakes for added drag. In addition to good inherent directional characteristics on the ground, the pilot has used lateral-control inputs to provide greater load on one skid and achieve some measure of directional control.

In summary of the landing information, it is considered important to indicate that the pilot, provided an aircraft with good control and handling qualities as represented in the X-15 in the landing pattern, can intercept the pattern at any one of its key positions, can make adjustments based on his experience, judgment, and reactions to the many cues available, and can complete a satisfactory landing in close proximity to a designated landing spot with the power off, low L/D airplane. Experience with the X-15 has included landings with various dampers inoperative, a few recent landings using only the side arm controller, and one recent landing with one wind-shield outer panel shattered to the point of being opaque, with an attendant compromise in the pilot's visibility and the landing task. These landings have been equally satisfactory and are grouped with the other data presented.

CONCLUSIONS

This summary of X-15 handling qualities has been, in general, an expression of pilot opinion, verified in many cases by the data acquired, rather than an attempt to compare with specifications. Obviously the main concern in expanding the flight envelope to design speed and altitude has been a detailed analysis of each forward step taken so that it could be achieved safely. With these missions completed, flights can now be performed within the flight envelope with an aim to gathering handling-quality data as it compares or relates to formulating detail specifications.

Concerning the question as to whether there have been new regions in which the X-15 has been flown that have indicated a significant change in handling-quality specification as they are known today, the answer, as might be suspected, is no. In this sense the performance of the X-15 can still be related with that of certain of the century-series fighters, despite their vast performance differences. The pilot still desires an excellent control system, insists on the aircraft responding to his inputs at the rates he desires, and is quite displeased with undamped oscillations about any axis. Certain differences as to what the pilot desires may show up whether he is flying an X-15 or an operational fighter. When proceeding in unexplored regions in an X-15, pilots prefer having damping in roll and a high longitudinal

CONFIDENTIAL

damping, probably because it gives a feeling of security to have a solid airplane. In the fighter excessive damping might inhibit the ease with which a pilot can track a target. In the past, the impression of what the pilot prefers has been translated into design specifications regarding handling qualities, and from pilot experience in the X-15 program it seems apparent that much of the same procedures will be used for hypersonic and aerodynamic reentry vehicles in the future.

REFERENCES

1. Perkins, Courtland D., and Hage, Robert E.: Airplane Performance Stability and Control. John Wiley & Sons, Inc., c.1949.
2. Creer, Brent Y., Heinle, Donovan R., and Wingrove, Rodney C.: Study of Stability and Control Characteristics of Atmosphere-Entry Type Aircraft Through Use of Piloted Flight Simulators. Paper No. 59-129, Inst. Aero. Sci., Oct. 5-7, 1959.

[Redacted]

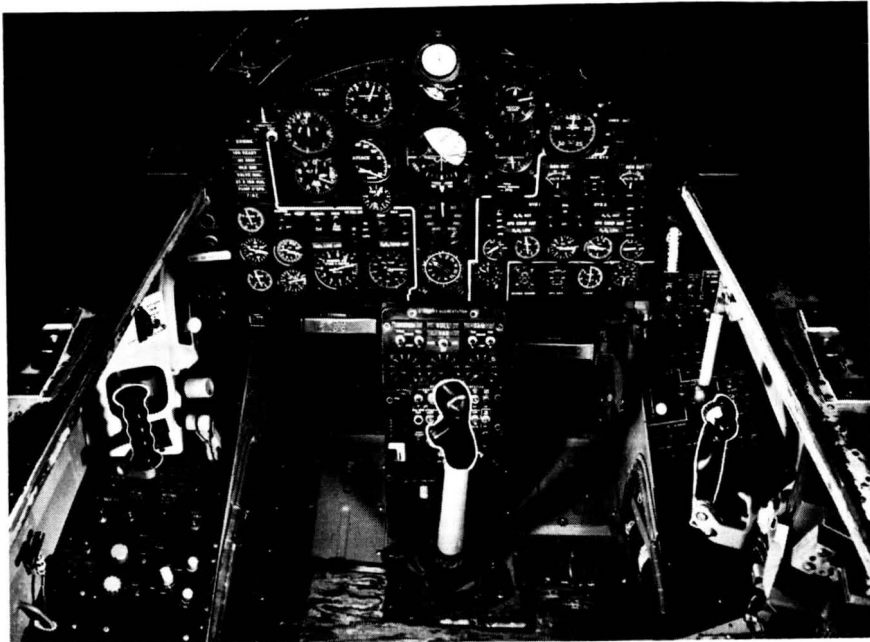


Figure 1

LONGITUDINAL TRIM CHARACTERISTICS

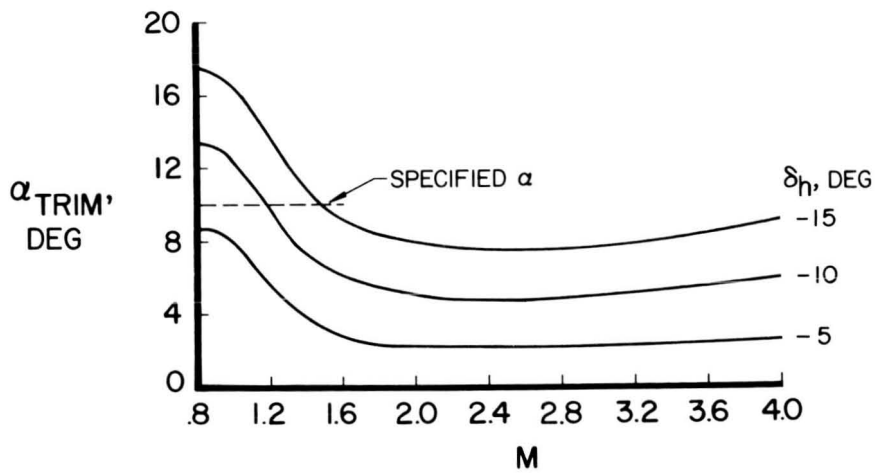


Figure 2

REPRESENTATIVE ALTITUDE MISSION

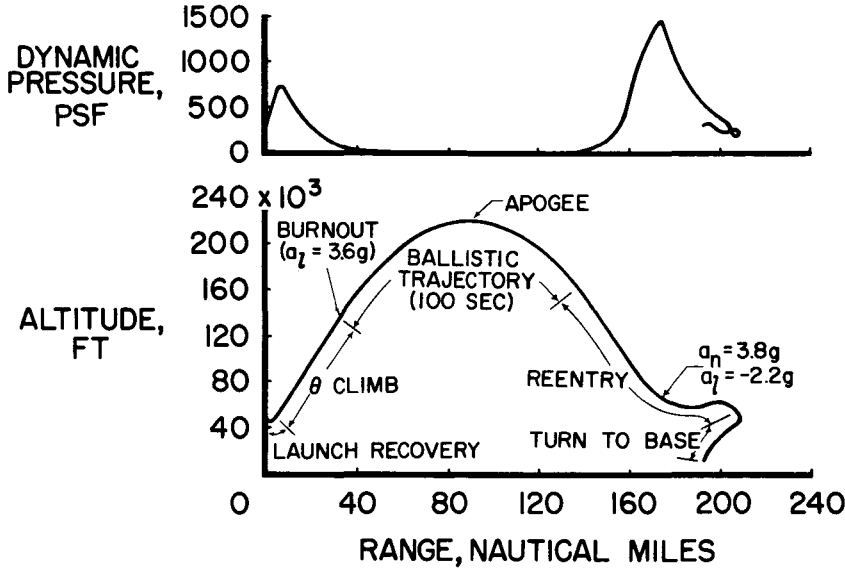


Figure 3

REACTION-CONTROL UTILIZATION

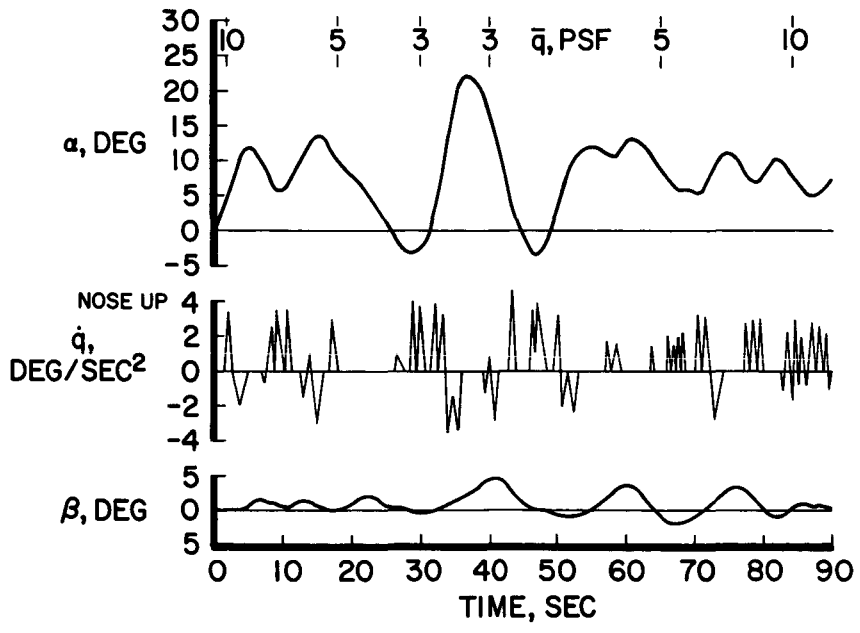
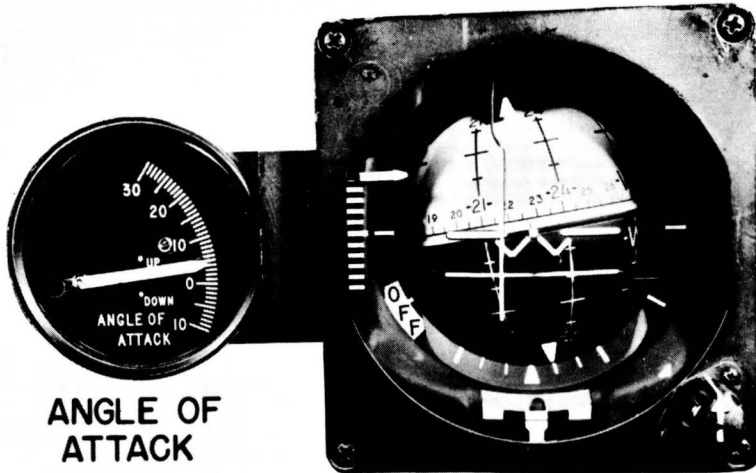


Figure 4



X-15 AIRPLANE ATTITUDE DISPLAY



ANGLE OF ATTACK

AIRPLANE ATTITUDE
3-AXIS BALL

Figure 5

REENTRY TIME HISTORY

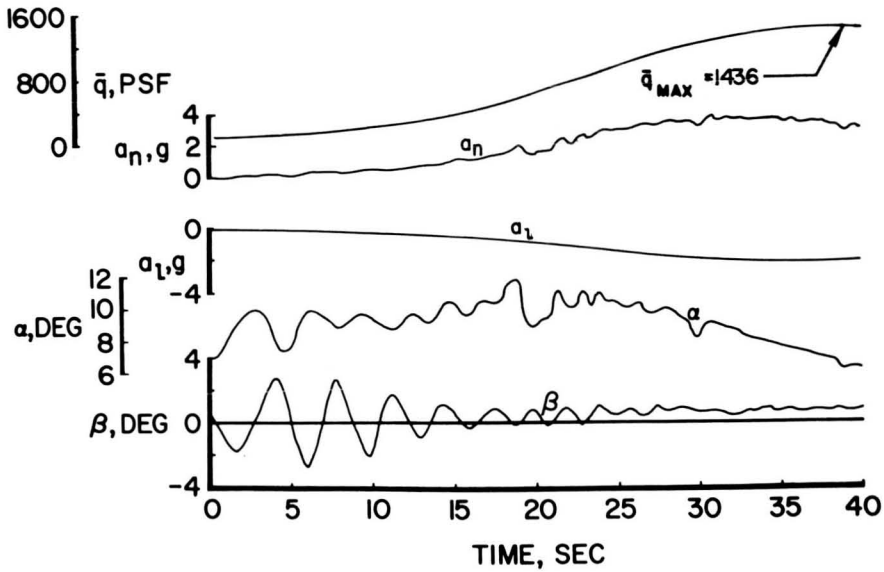


Figure 6

X-15 LATERAL-CONTROL UTILIZATION M=2.5 TO 5.5

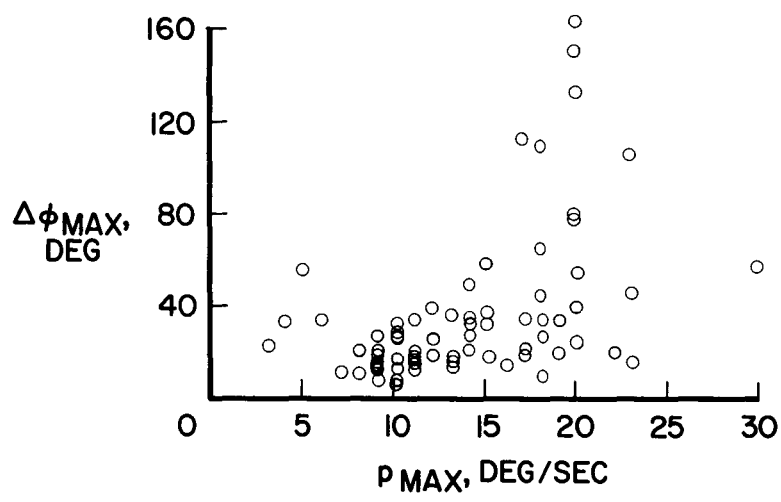


Figure 7

SUMMARY OF X-15 LONGITUDINAL HANDLING QUALITIES M=2.5 TO 5.5, q̄=100 TO 1,400 PSF

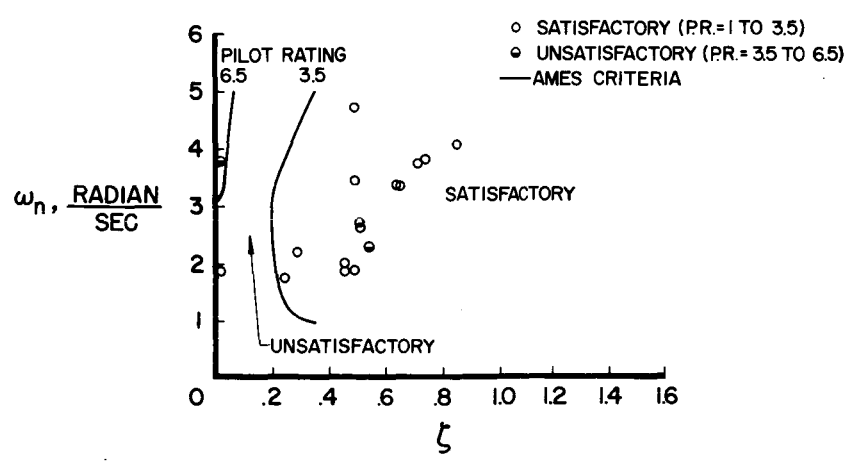


Figure 8

SUMMARY OF X-15 LANDING PATTERN

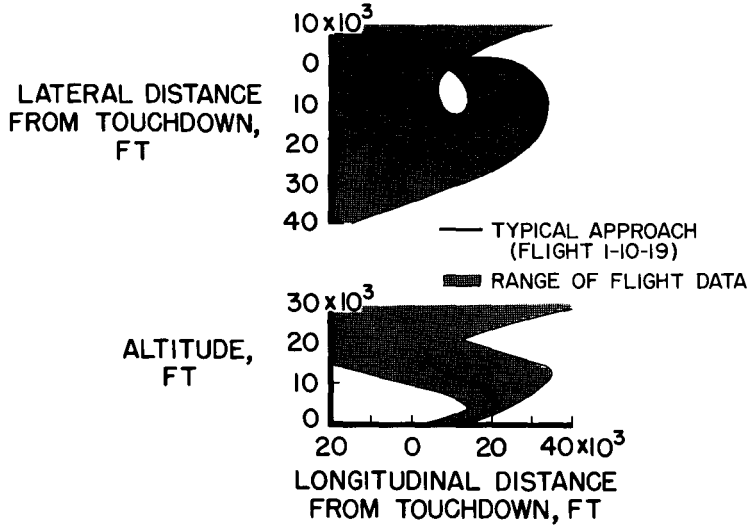


Figure 9

X-15 FLARE-INITIATION ALTITUDE

$$(W/S)_{av} = 73 \text{ PSF}$$

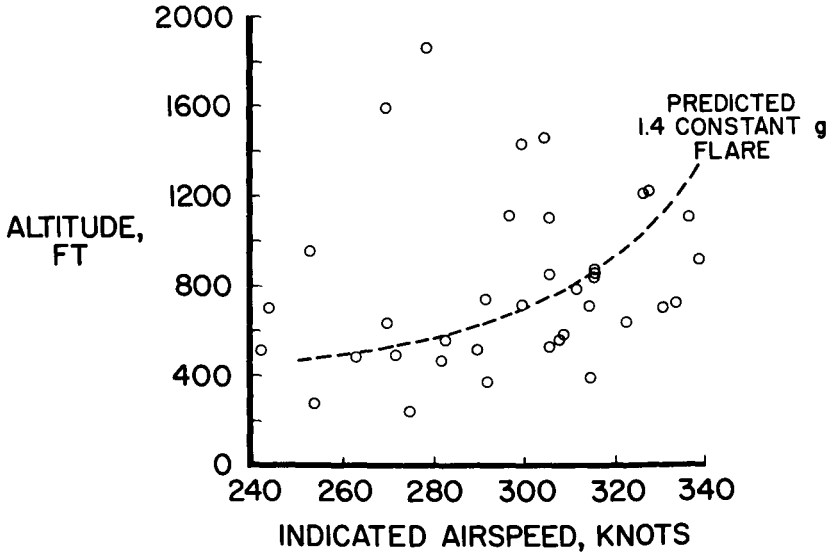


Figure 10

X-15 GLIDE CONDITIONS AT FLARE INITIATION

$(W/S)_{AV} = 73 \text{ PSF}$

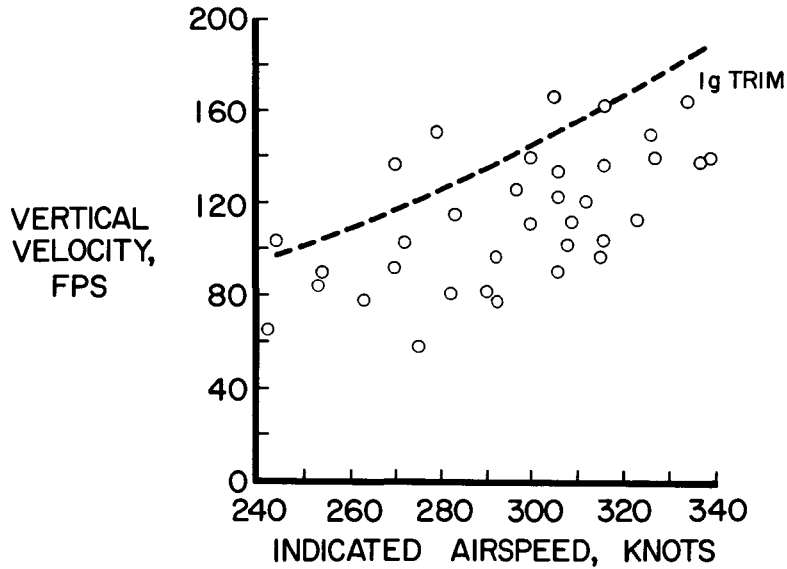


Figure 11

X-15 TOUCHDOWN PARAMETERS

$(W/S)_{AV} = 73 \text{ PSF}$

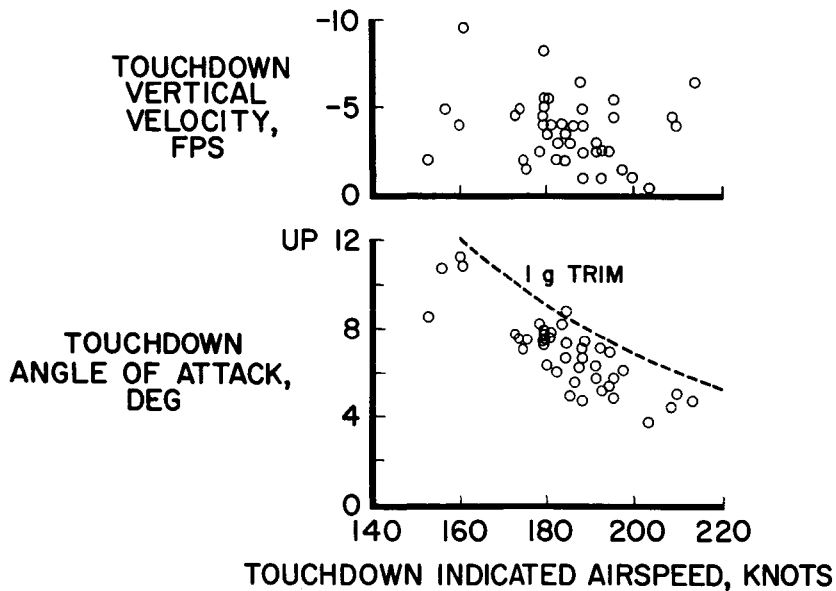


Figure 12

X-15 TOUCHDOWN AND SLIDEOUT DISTANCES

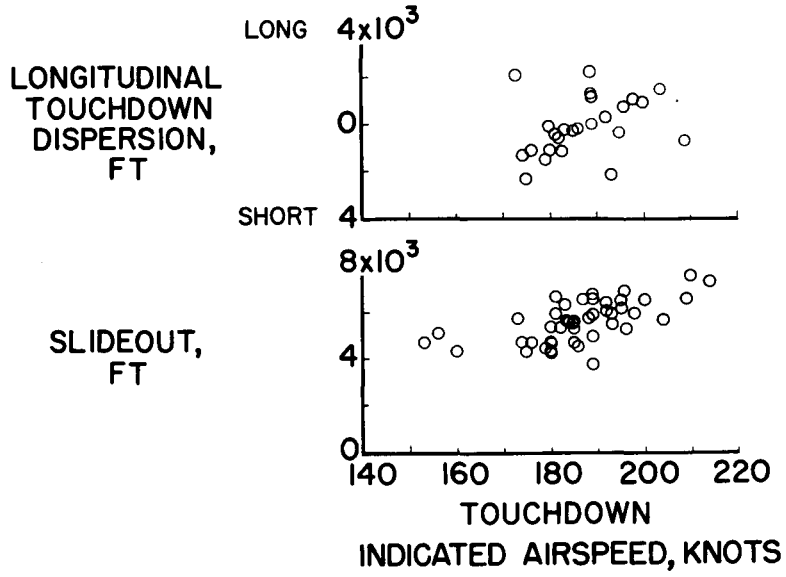


Figure 13

N71-75453

131

10. LATERAL DIRECTIONAL CONTROL CHARACTERISTICS

By Forrest S. Petersen, Herman A. Redless, and Joseph Weil

NASA Flight Research Center

SUMMARY

The deterioration of lateral directional controllability with roll damper off and the pilot performing a lateral control task is explained. The problem area was defined by fixed-base and airborne simulators and verified by closed-loop analysis in which a human transfer function represents the pilot. A parameter which will predict the problem area for the X-15 airplane is developed. The means considered to alleviate the control problem in the X-15 airplane are also discussed.

INTRODUCTION

As indicated in reference 1, a primary area of concern has been the lateral directional dynamic instability with roll damper off. This condition corresponds to the potential emergency situation created by a stability-augmentation-system failure since the X-15 airplane is intended to perform all its missions with the stability-augmentation system in operation.

Considerable effort has been expended in the investigation of the control problem which might follow a roll-damper failure. These investigations have utilized both fixed and airborne simulators, closed-loop theoretical analysis, and actual flight tests of the X-15 airplane. It is the purpose of this paper to review the results of these efforts as well as the courses of action considered to alleviate the problem.

SYMBOLS

b	wing span, ft
C_2	cycles to double amplitude
$C_{1/2}$	cycles to one-half amplitude
c_1, c_2, c_3	constants of a general third-order equation

$$C_l = \frac{\text{Rolling moment}}{qSb}$$

$$C_n = \frac{\text{Yawing moment}}{qSb}$$

$$C_{l\beta} = \frac{\partial C_l}{\partial \beta}$$

$$C_{n\beta} = \frac{\partial C_n}{\partial \beta}$$

I_X moment of inertia about principal X-axis, slug-ft²

I_Z moment of inertia about principal Z-axis, slug-ft²

K_P pilot gain

$$K_P' = K_P L \delta_a$$

$$L = \frac{\text{Rolling moment}}{I_X}, \text{ per sec}^2$$

$$L_p = \frac{\partial L}{\partial p}$$

$$L_\beta = \frac{\partial L}{\partial \beta}$$

$$L_{\delta_a} = \frac{\partial L}{\partial \delta_a}$$

M Mach number

m mass, slugs

$$N = \frac{\text{Yawing moment}}{I_Z}, \text{ per sec}^2$$

$$\dot{N}_p = \frac{\partial N}{\partial p}$$

$$N_r = \frac{\partial N}{\partial r}$$

$$N_\beta = \frac{\partial N}{\partial \beta}$$

$$N_{\delta_a} = \frac{\partial N}{\partial \delta_a}$$

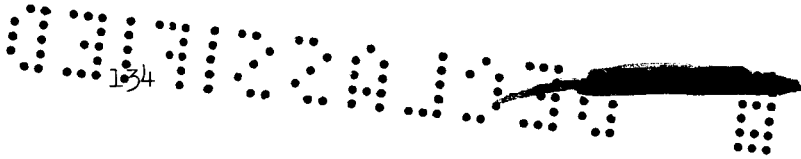
- p roll rate, deg/sec or radians/sec
- q dynamic pressure, lb/sq ft
- r yaw rate, radians/sec
- S wing area, sq ft
- s Laplace transform variable
- s_i roots of transfer function (i = 1,2,3,...)
- t time, sec
- V forward velocity, ft/sec

Y $\frac{\text{Side force}}{mV}$, per sec

$$Y_\beta = \frac{\partial Y}{\partial \beta}$$

- α angle of attack, deg or radians
- α₀ trim angle of attack of principal axis, radians
- β angle of sideslip, deg or radians





- δ_a aileron deflection, deg or radians
- ζ_ϕ damping ratio of the numerator of the airplane transfer function in roll
- ζ_ψ damping ratio of short-period Dutch roll mode
- τ_1 pilot time constant, sec
- τ_ϕ time constant in roll, sec
- ϕ bank angle, deg or radians
- θ_i pole angle or zero angle ($i = 1, 2, 3, \dots$)
- $\omega_{n\phi}$ undamped natural frequency of the numerator of the airplane transfer function in roll, radians/sec
- $\omega_{n\psi}$ undamped natural frequency of short-period Dutch roll mode, radians/sec

Subscripts:

- e error
- ref reference
- P pilot

GENERAL REMARKS

It became apparent early in six-degree-of-freedom simulations of reentries from altitude missions with the roll damper off that uncontrollable combinations of Mach number and angle of attack were frequently encountered. Stick-fixed stability analysis had not indicated that these uncontrollable conditions would be encountered. Figure 1 shows the uncontrollable area with the roll damper off in terms of angle of attack plotted against Mach number as determined from extensive fixed-base simulator work. The criteria used in defining the uncontrollable area was actual loss of control. As a result, no fine line of demarcation between controllable and uncontrollable is implied or shown. The lighter shaded area indicates that the pilot was able to fly for longer periods of time before loss of control occurred. In the darker shaded areas loss of control is very rapid. Since the airplane is uncontrollable in



the shaded area, no data with the stability-augmentation system of the X-15 airplane off were anticipated in this area. However, by using T-33 and F-100C variable-stability airplanes as in flight simulators, several points within this area have been extensively evaluated.

To obtain flight verification in the X-15 airplane, pilots were instructed on several flights to explore the fringes of the predicted uncontrollable region. Figure 2 shows the flight conditions on one such flight in relation to the uncontrollable area. Figure 3 shows the airplane motions which occurred along this flight path. At the beginning of the flight path and time history, the airplane was at an angle of attack of approximately 7° and the pilot turned the roll and yaw dampers off. Lateral motions immediately began to build up, so he reduced the angle of attack. The motions subsided and angle of attack was again increased. Once again the motions began to build up, and the angle of attack had to be reduced. Although the pilot was holding on to the center stick, he was not consciously making any lateral-control inputs. However, there were lateral-control inputs as shown in the figure.

Figure 4 shows the destabilizing effect of two types of pilot inputs in a time history for an F-100C variable-stability airplane. In the first portion of the time history, the pilot attempted to hold the stick fixed as in the previous time history. As in the time history with the X-15 airplane (fig. 3), there is a definite lateral-control input and a resultant divergent oscillation. During the center portion of the time history, the pilot released the stick and the oscillations were obviously damped. In the last portion the pilot attempted to control bank angle in a conventional manner; that is, lateral-control inputs are generally proportional to bank angle and in a direction to keep bank-angle excursions low. The similarity of the inadvertent lateral inputs and divergent oscillation in the first part of the time history to those in the last portion should be noted.

ANALYSIS OF THE LATERAL CONTROL PROBLEM

Analytic closed-loop investigations of the X-15 (see fig. 5) have been conducted and indicate that the uncontrollable region can be predicted. The following transfer function, developed in reference 2 and used in reference 3, closely approximates the control inputs of a pilot applying lateral control proportional to bank angle plus a lead:

$$\frac{\delta_a(s)}{\varphi(s)} = K_P(1 + 0.57s) \tag{1}$$

No directional control is considered during reentry conditions of rapidly changing dynamic pressure, angle of attack, and Mach number. The rolling moments resulting from directional control vary greatly in magnitude and even change sign. This precludes effective use of directional control during reentry.

It is shown in reference 3 that the characteristic equation of the pilot airplane system (see fig. 5) is obtained by combining the pilot transfer function with the transfer function for roll response to lateral-control inputs as follows:

$$\frac{K_P L_{\delta_a} (1 + 0.57s) \left[s^2 + (-N_r - Y_\beta)s + N_\beta - L_\beta \frac{N_{\delta_a}}{L_{\delta_a}} + N_r Y_\beta \right]}{s^4 + (-Y_\beta - N_r - L_p)s^3 + (N_\beta - \alpha_0 L_\beta + Y_\beta N_r + Y_\beta L_p + N_r L_p)s + (-L_p N_\beta + \alpha_0 L_\beta N_r - Y_\beta N_r L_p)s} = -1 \quad (2)$$

which is of the form,

$$\frac{K_P (1 + 0.57s) (s^2 + 2\zeta_\varphi \omega_{n\varphi} s + \omega_{n\varphi}^2)}{s \left(s + \frac{1}{\tau_\varphi} \right) (s^2 + 2\zeta_\psi \omega_{n\psi} s + \omega_{n\psi}^2)} = -1 \quad (3)$$

The closed-loop stability of the system is then determined by solving for the roots of equation (2). In figure 6 the neutral stability of the X-15 airplane defined by the roots of equation (2) is compared with the uncontrollability envelope previously shown. The area within this boundary is predicted to be unstable with the pilot in the loop and is in reasonable correlation with the simulator results.

An analysis of this general type of control problem has been performed in reference 4 by using root locus methods, and the specific control problem of the X-15 airplane has been analyzed in reference 3 with the same methods. A portion of the analysis of reference 3 is briefly repeated herein to describe a useful parameter which relates the severity of the control problem to familiar aerodynamic derivatives and provides a better understanding of the problem.

Figures 7(a) and 7(b) present typical root loci of the pilot-airplane transfer function in roll (the left-hand side of equation (3)) for controllable and uncontrollable situations, respectively. The complex poles represent the stick-fixed Dutch roll stability. The line drawn from the complex pole to the complex zero (locus of the roots) represents the changing stability of the pilot-airplane system with increasing pilot gain. In figure 7(a), the pole is above the zero and, therefore, the locus closes in the controllable direction; however,

when the zero is above the pole the locus closes in the uncontrollable direction and may cross over into the unstable right half of the plane. The difference between the distances of the zero and pole from the origin $\omega_{n\phi} - \omega_{n\psi}$ is suggested as an indication of the possibility of an uncontrollable condition. For aircraft with low lateral-directional damping, as in case of the X-15 airplane, this difference can be closely approximated by the following equation:

$$\omega_{n\phi} - \omega_{n\psi} \approx \frac{L_{\beta} \left(\alpha_0 - \frac{N_{\delta_a}}{L_{\delta_a}} \right)}{2\omega_{n\psi}} \quad (4)$$

When $\omega_{n\phi} - \omega_{n\psi}$ is negative, as in figure 7(a), this control problem does not exist; however, other types of lateral-control problems may or may not exist. If it is positive, as in figure 7(b), this type of control problem will exist if the value of $\omega_{n\phi} - \omega_{n\psi}$ is sufficiently large and the basic airplane damping is low enough.

It is shown in the appendix that the maximum decrement of damping which the pilot might provide when $\omega_{n\phi} - \omega_{n\psi}$ is positive is approximately proportional to $\omega_{n\phi} - \omega_{n\psi}$ for the X-15 airplane. An increasing positive value of this parameter represents an increasing decrement in the damping of the closed-loop pilot-airplane system. A cumbersome but more exact expression is given in the appendix (eq. (A9)).

In a paper by Walker and Wolowicz (paper no. 8) it was shown that the X-15 airplane above a Mach number of 2.3 has undesirable positive values of $C_{l_{\beta}}$. The aileron cross-coupling term $\frac{N_{\delta_a}}{L_{\delta_a}}$ of equation (4) is a small quantity; therefore, the positive product of L_{β} and α_0 predominates. Figure 8 shows that, whereas in the angle-of-attack range from 5° to 15° , the X-15 airplane is predicted to be nearly neutrally stable, the addition of the pilot in the loop deteriorates the stability markedly so that an oscillation doubles the amplitude in one-half of a cycle at $\alpha = 12^{\circ}$. The pilot-airplane curve was calculated by using equation (A9).

Simulator studies have shown that this controllability parameter (eq. (4)) correlates well with pilot opinion for the X-15 airplane. Figure 9 shows the variation of pilot ratings with the values of $\omega_{n\phi} - \omega_{n\psi}$. The conditions for the X-15 airplane were selected and flown

158 [REDACTED]

in five degrees of freedom which gave the values of $\omega_{n\phi} - \omega_{n\psi}$ as

indicated in the figure. It is seen that there is a definite deterioration of pilot opinion with increasing positive values of the parameter. This parameter is not presented as a general criterion for all lateral-directional control problems but rather as a means of explaining the type of controllability problem which is discussed in this paper. It can be used for indicating the possibility of the specific type of control problem existing in other aircraft if the assumptions used in its derivation are compatible with the particular aircraft.

POSSIBLE METHODS OF ALLEVIATION OF LATERAL CONTROL PROBLEM

As soon as it was suspected that a large portion of the flight envelope for the X-15 airplane was uncontrollable with lateral-stability augmentation off, investigations were initiated to find ways of alleviating the problem. The first method tried, probably because it would have been the easiest to implement, was pilot-display quickening. Sideslip and bank angle presentations were quickened by including yaw rate and roll rate, respectively. Various quickening gains were used in the investigation on the fixed-base simulator, but no combination which significantly improved the pilot's ability to handle the instability was found.

Arthur F. Tweedie of North American Aviation, Inc., and Lawrence W. Taylor and Richard E. Day of NASA Flight Research Center independently investigated the use of ailerons to control sideslip angle for certain types of airplane instabilities. Figure 10 shows a time history illustrating the use of a nonconventional control technique which evolved from these investigations and showed considerable promise on a fixed-base simulator. The first part of the time history shows once again the destabilizing effect of conventional lateral-control inputs. In the last part of the time history, a method called the β technique was used. It consists of sharp, lateral-control inputs to the left, as the nose swings left through zero sideslip, and vice versa. At this time $\dot{\beta}$ is maximum. The pilot flies hands-off except when making the lateral pulses. This is desirable in flight because of the instability induced by the inadvertent inputs associated with merely holding on to the center stick.

Figure 11 shows a comparison of the effectiveness of the β technique on fixed-base and airborne simulators with the center stick. The solid line represents pilot opinion of using conventional lateral-control techniques on either simulator. The short dashed line represents pilot opinion of using the β technique on the fixed-base simulator. The longer dashed lines represent pilot opinion of the β technique in

[REDACTED]

the F-100C. Fixed-base ratings indicated considerable improvement with this technique. However, experience in the F-100C indicated that the improvement achieved in terms of pilot opinion of the handling qualities was greatly reduced as the roll-damper gain was reduced to zero. Use of the side-arm controller in the X-15 airplane has provided some relief from the destabilizing effect of inadvertent inputs present with the center stick and makes the β technique more effective. Figure 12 shows the uncontrollable area and indicates regions in which pilots have successfully flown the X-15 airplane with the side-arm controller by using the β technique with roll damper intentionally off. Pilots feel that they were able to fly sufficiently well in the shaded area of figure 12 to permit a successful reentry from a flight to an altitude of 250,000 feet. Previous experience with the center stick indicated the controllable angle of attack to be considerably lower. All X-15 pilots are well versed in the use of the β technique. Its usefulness may, however, be even less than was indicated when the pilot has the task of maintaining bank-angle excursions from zero to small values as he does in a reentry. Furthermore, a lateral input in the wrong direction, which is a conceivable mistake with other problems clamoring for the pilot's attention, could be disastrous.

As was indicated in a previous paper by Walker and Wolowicz (paper no. 8) recent efforts have been directed toward the evaluation of the handling qualities of the X-15 airplane with the lower rudder off. Figure 13 shows the variation of $C_{l\beta}$ and $C_{n\beta}$ with Mach number at an angle of attack of 12° with the lower rudder on and off. The upper portion of the figure shows that desirable negative values of $C_{l\beta}$ are realized throughout the Mach number range at this angle of attack with the lower rudder off as contrasted with undesirable positive values of $C_{l\beta}$ with the lower rudder on at all Mach numbers above about 2.3. This favorable value of $C_{l\beta}$ is not realized without a reduction in $C_{n\beta}$ as is shown in the bottom half of figure 13. However, as was pointed out in the derivative paper by Walker and Wolowicz (paper no. 8), the Dutch roll stability is increased by negative values of $C_{l\beta}$.

Figure 14 shows the uncontrollable areas in terms of angle of attack and Mach number as predicted by fixed-base simulators with lower rudder on. Figure 15 shows the predicted uncontrollable area based on closed-loop analysis and fixed-base simulator studies for the lower rudder off. The solid lines in figures 14 and 15 indicate the conditions followed just prior to and during reentry on a typical altitude mission. With the lower rudder on, a considerable portion of the reentry from an altitude mission is within the uncontrollable region as shown in figure 14. Figure 15 shows that a reentry conducted with the lower rudder off

does not penetrate the predicted uncontrollable region. The flight conditions flown on the X-15 flight with the lower rudder off are shown as dashed lines in figure 15. In the limited area explored on this flight, the flying qualities were as good as or better than those predicted by the fixed-base and airborne simulators. However, as predicted, the flying qualities at low angles of attack were worse with the lower rudder off than with the lower rudder on. Additional flights are being planned in the X-15 airplane to evaluate further the handling qualities with lower rudder off. If these tests continue to indicate favorable trends and no severe problem areas are uncovered, the configuration with the lower rudder off may offer undeniable advantages for the high angle of attack, reentry portion of an altitude mission.

Since control characteristics are reasonably good with the stability-augmentation system on, one way in which the potential problem area can be improved is by reducing the chance of a critical augmentation failure. This is to be accomplished by dualization of certain components in the augmentation system.

CONCLUDING REMARKS

In conclusion a serious lateral directional control problem with the lower rudder on and the roll damper off at high angles of attack has been uncovered. The problem is caused primarily by negative dihedral effect and was not revealed until the inputs of the pilot were used with airplane stability to determine closed-loop stability. The use of a transfer function which represents the inputs of a pilot performing a lateral-control task permits calculation of the degree of pilot-airplane instability. Although special control techniques have not completely alleviated the problem, they have provided sufficient improvement when utilizing the side stick to allow flight in the fringes of the uncontrollable region. Removal of the lower rudder appears promising as a means of alleviating the lateral directional instability at high angles of attack associated with a roll damper failure. Finally additional reliability will be obtained by dualization of certain components in the stability augmentation system.

DECREMENT IN DAMPING DUE TO THE PILOT

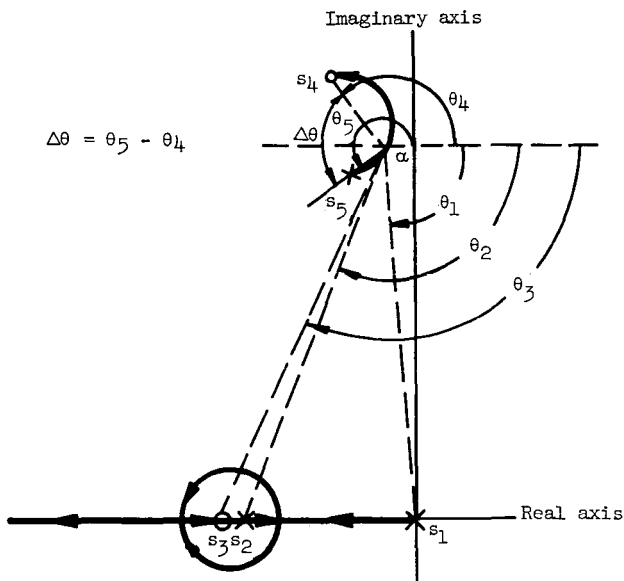
The controllability parameter developed in reference 2

$$\omega_{n\phi} - \omega_{n\psi} \approx \frac{L\beta \left(\alpha_0 - \frac{N\delta_a}{L\delta_a} \right)}{2\omega_{n\psi}} \quad (A1)$$

will be used in the derivation of an expression for the maximum decrement in damping which a pilot might provide while performing a lateral-control task. This derivation assumes the following:

- (1) The damping in roll and the Dutch roll damping are low.
- (2) $\omega_{n\psi} \gg \omega_{n\phi} - \omega_{n\psi}$
- (3) The pilot-time constant τ_1 is less than an order of magnitude different from the roll-mode time constant.

These assumptions are compatible with the characteristics of the X-15 airplane and the derivation of equation (A1). First it is necessary to establish that the root locus (see ref. 5) from the complex pole to the complex zero is approximately a semicircle, as shown in the following sketch, under these assumptions:



142
By definition of root locus at some point a on the locus,

$$\Sigma\theta = 180^\circ$$

also

$$\Sigma\theta = \Sigma \text{ Pole angles} - \Sigma \text{ Zero angles}$$

that is,

$$\Sigma\theta = \theta_1 + \theta_2 + \theta_5 - \theta_4 - \theta_3 = 180^\circ$$

Because of assumption 1,

$$\theta_1 \approx 90^\circ$$

Because of assumption 3,

$$\theta_2 \approx \theta_3$$

Therefore,


$$\Sigma\theta \approx 90^\circ + \theta_5 - \theta_4 \approx 180^\circ$$

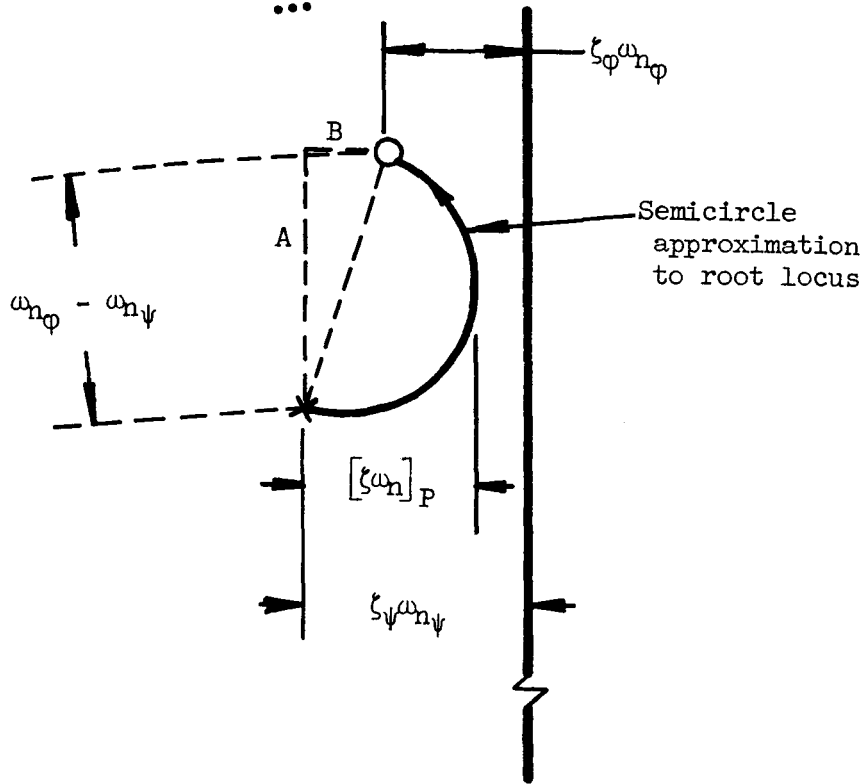
or

$$\Delta\theta = \theta_5 - \theta_4 \approx 90^\circ$$

therefore the locus is approximately a semicircle. Note that $\theta_1 \approx 90^\circ$ and $\theta_2 \approx \theta_3$ both provide conservative answers because deviations from these approximations for the X-15 airplane are in the direction to increase $\Delta\theta$; thus, the actual stability will be greater than the semicircle approximation.

The maximum pilot-damping decrement, $[\zeta\omega_n]_P$, is derived with the aid of the following sketch:





Simple geometric relations show that

$$[\zeta\omega_n]_P = \frac{1}{2} \left(B + \sqrt{B^2 + A^2} \right) \quad (A2)$$

where

$$A \approx \omega_{n\phi} - \omega_{n\psi} \quad (A3)$$

and

$$B = \zeta_{\psi}\omega_{n\psi} - \zeta_{\phi}\omega_{n\phi} \quad (A4)$$

144
 By comparing equations (2) and (3) in the discussion it can be seen that

$$\zeta_{\phi} \omega_{n_{\phi}} = -N_r - Y_{\beta} \quad (A5)$$

In order to obtain an expression for $\zeta_{\psi} \omega_{n_{\psi}}$, the third-order equation which is reduced from the denominator of equation (2) must be solved. A good approximate solution to a third-order equation of the form,

$$s^3 + c_1 s^2 + c_2 s + c_3 = 0 \quad (A6)$$

when $c_3 \ll c_2$, as is the case for the X-15 airplane, is to assume a real root to be

$$s_1 = -\frac{c_3}{c_2}$$

and then solve by synthetic division. This method yields the following approximate expressions when small terms are neglected:

$$\zeta_{\psi} \omega_{n_{\psi}} \approx \frac{1}{2} \left[(-N_r - Y_{\beta}) + (L_p - N_r) \left(\frac{\alpha_o L_{\beta}}{N_{\beta} - \alpha_o L_{\beta}} \right) \right] \quad (A7)$$

and

$$\omega_{n_{\psi}}^2 \approx N_{\beta} - \alpha_o L_{\beta} \quad (A8)$$

Substituting equations (A5), (A7), and (A8) into equation (A2) and reducing to simplest form leads to the following expression for the maximum damping decrement the pilot might provide:

$$[\zeta \omega_n]_P \approx \frac{1}{2} \left\{ \frac{\alpha_o L_{\beta} (L_p - N_r)}{2 \omega_{n_{\psi}}^2} + \sqrt{\left[\frac{\alpha_o L_{\beta} (L_p - N_r)}{2 \omega_{n_{\psi}}^2} \right]^2 + \left[\frac{L_{\beta} \left(\alpha_o - \frac{N \delta_a}{L \delta_a} \right)}{2 \omega_{n_{\psi}}} \right]^2} \right\} \quad (A9)$$

For the X-15 airplane at moderate to high angles of attack, the term

$$\frac{\alpha_0 L_\beta (L_p - N_r)}{2\omega_{n\psi}^2}$$

is generally smaller than the remaining term and the following can be used for a first approximation:

$$[\zeta\omega_n]_P \approx \frac{L_\beta \left(\alpha_0 - \frac{N_{\delta_a}}{L_{\delta_a}} \right)}{4\omega_{n\psi}} = \frac{\omega_{n\phi} - \omega_{n\psi}}{2} \quad (A10)$$

0371209103 [REDACTED]

146

REFERENCES

1. White, Robert W., Robinson, Glenn H., and Matranga, Gene J.: Résumé of X-15 Handling Qualities. Prospective NASA paper (see paper no. 9 of this compilation).
2. Taylor, Lawrence W., Jr., and Day, Richard E.: Flight Controllability Limits and Related Human Transfer Functions as Determined From Simulator and Flight Tests. NASA TN D-746, 1961.
3. Taylor, Lawrence W., Jr.: Analysis of a Pilot-Airplane Lateral Instability Experienced With the X-15 Airplane. NASA TN D-1059, 1961.
4. Ashkenas, Irving L., and McRuer, Duane T.: The Determination of Lateral Handling Quality Requirements from Airframe - Human Pilot Studies. WADC Tech. Rep. 59-135, ASTIA Doc. No. AD 212 152, U.S. Air Force, June, 1959.
5. Evans, Walter R.: Control-System Dynamics. McGraw-Hill Book Co., Inc., New York, 1954.

[REDACTED]

LATERAL-DIRECTIONAL PROBLEM AREA ROLL DAMPER OFF

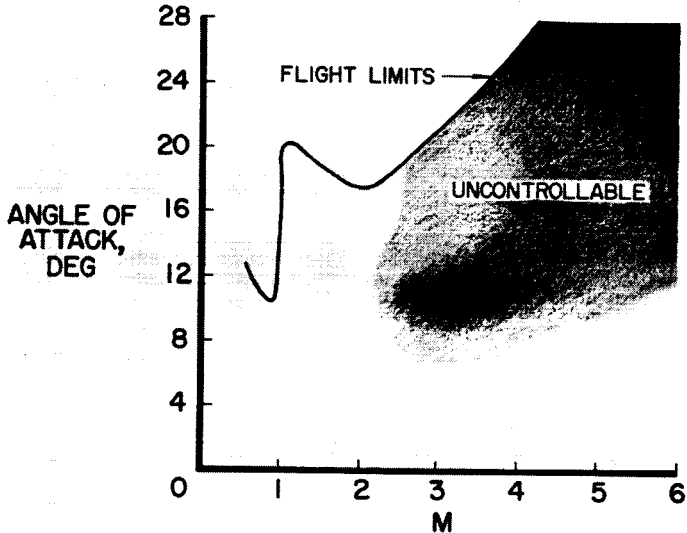


Figure 1

INITIAL FLIGHT STUDY ROLL DAMPER OFF

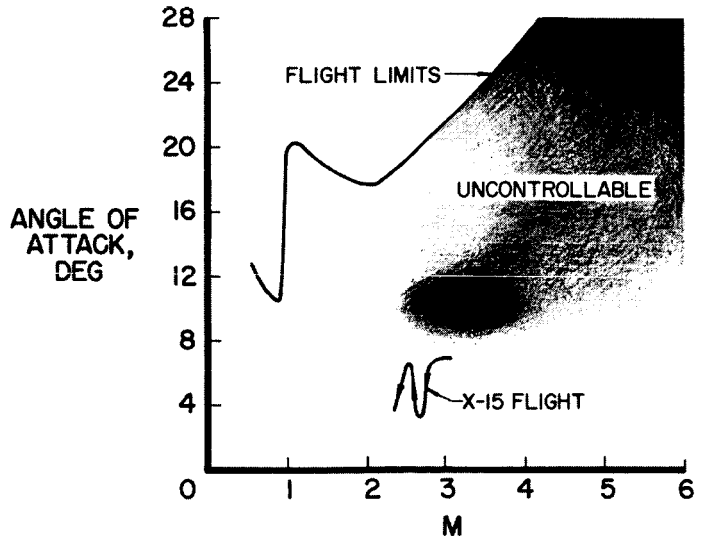


Figure 2

ANGLE-OF-ATTACK EFFECT ON X-15 CONTROLLABILITY X-15 FLIGHT - ROLL DAMPER OFF CENTER STICK

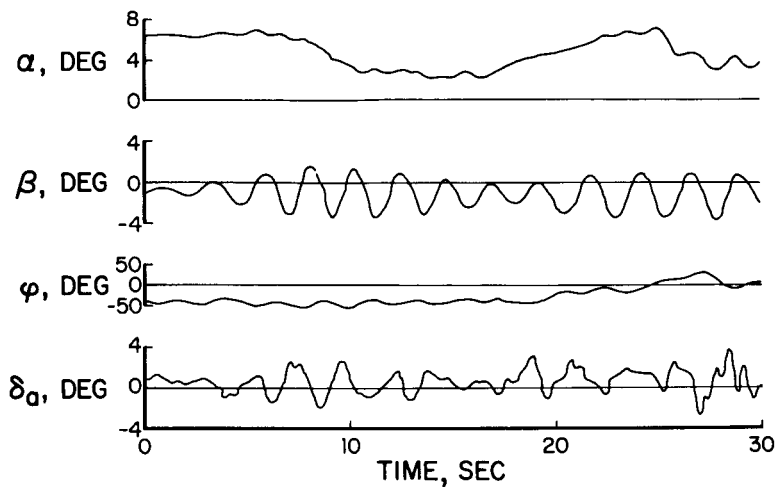


Figure 3

EFFECT OF PILOT ON CONTROLLABILITY F-100C VARIABLE-STABILITY AIRPLANE

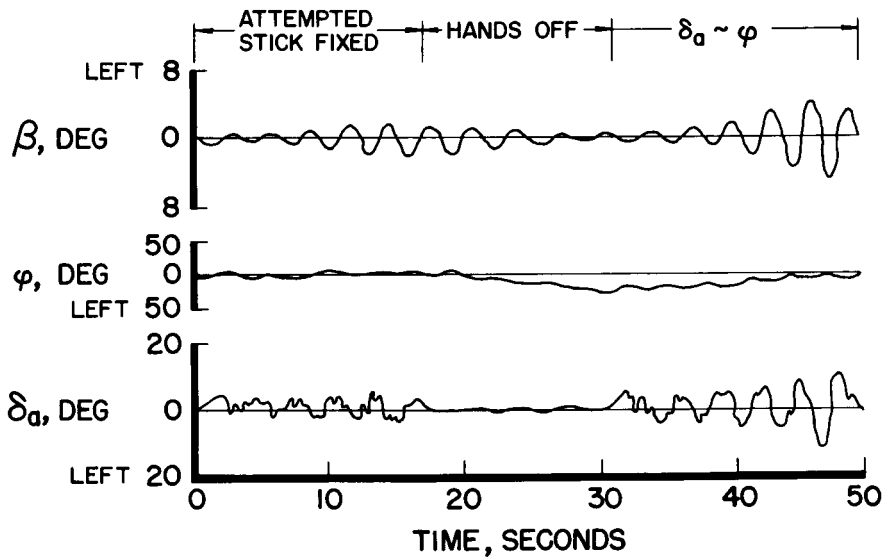
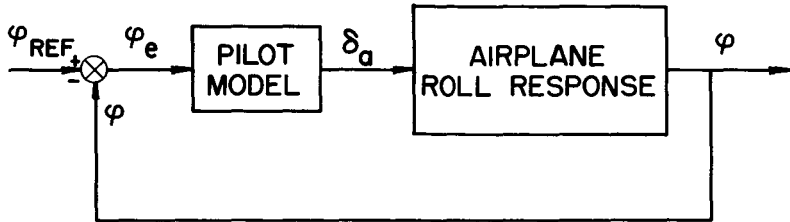


Figure 4



PILOT-AIRPLANE CLOSED-LOOP SYSTEM FOR LATERAL CONTROL



PILOT MODEL $\frac{\delta_a(s)}{\varphi_e(s)} = K_P(1 + \tau_I s)$

AIRPLANE ROLL RESPONSE $\frac{\varphi(s)}{\delta_a(s)} = \frac{L \delta_a (s^2 + 2\zeta_\varphi s + \omega_{n\varphi}^2)}{s(s + \frac{1}{\tau_\varphi})(s^2 + 2\zeta_\psi \omega_{n\psi} s + \omega_{n\psi}^2)}$

Figure 5

COMPARISON OF CALCULATED AND SIMULATED CONTROLLABILITY BOUNDARIES

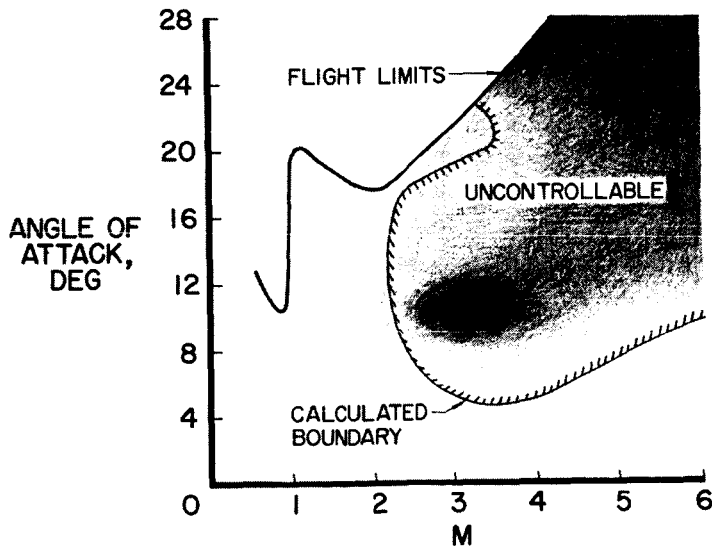


Figure 6

ROOT-LOCUS EXPLANATION OF CONTROL PROBLEM

- ZEROS
- × POLES
- COMPLEX ROOT FOR A SPECIFIC PILOT GAIN

$$\omega_{n\phi} - \omega_{n\psi} \approx \frac{L_{\beta} \left(\alpha_0 - \frac{N_{\delta a}}{L_{\delta a}} \right)}{2 \omega_{n\psi}}$$

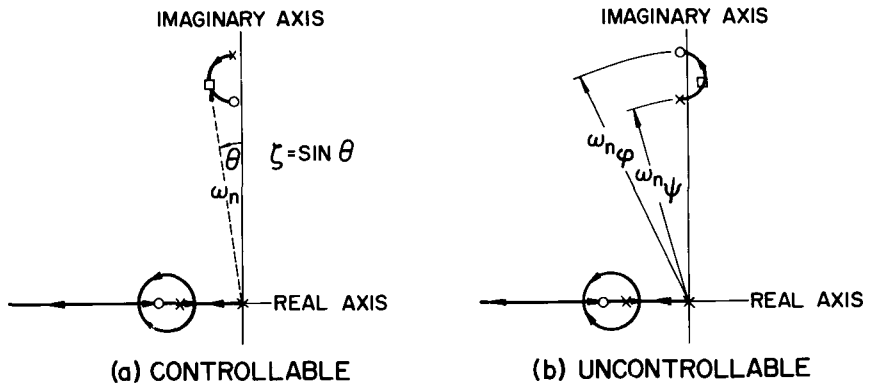


Figure 7

ANALYSIS OF THE PROBLEM

M=3.5, q=400 PSF

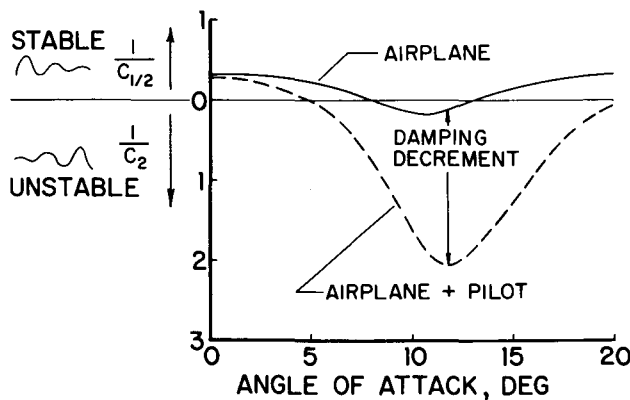


Figure 8

CORRELATION OF PILOT OPINION AND CONTROLLABILITY PARAMETER FIXED-BASE X-15 SIMULATOR

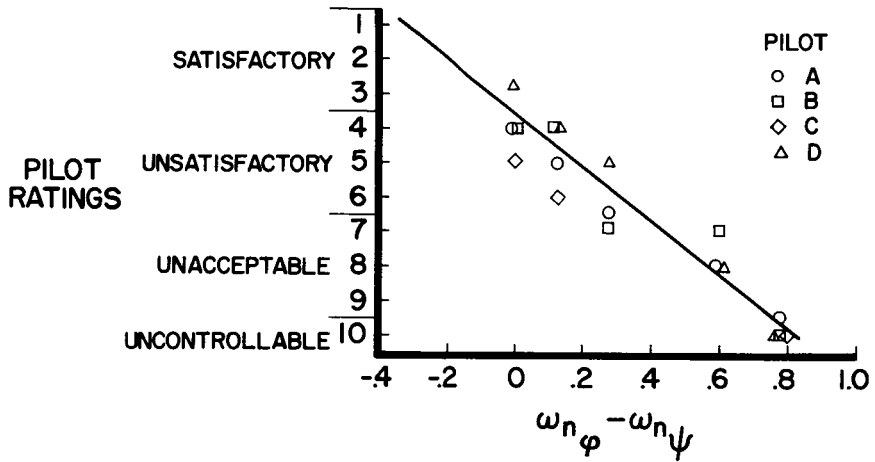


Figure 9

ILLUSTRATION OF $\dot{\beta}$ CONTROL TECHNIQUE FIXED BASE X-15 SIMULATOR

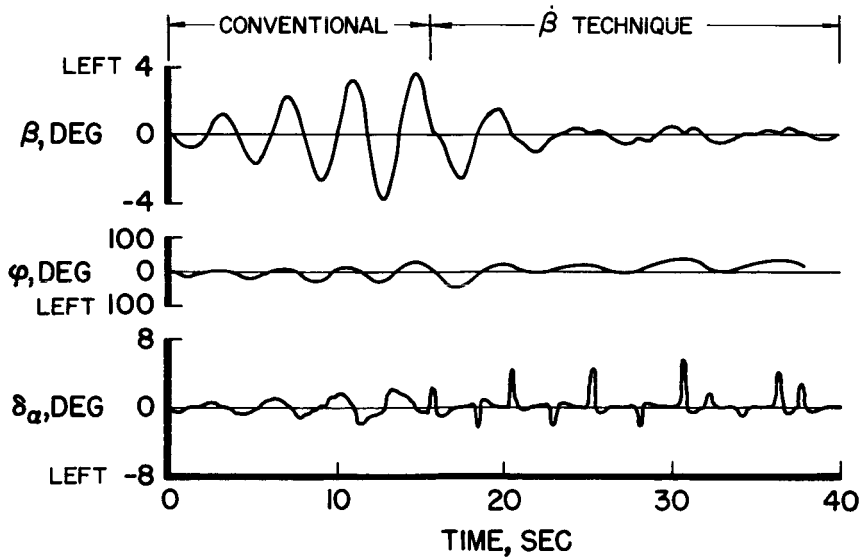


Figure 10



EFFECT OF MOTION CUES ON
 β CONTROL TECHNIQUE
 CENTER STICK, $M=3.5$, $\alpha = 10^\circ$

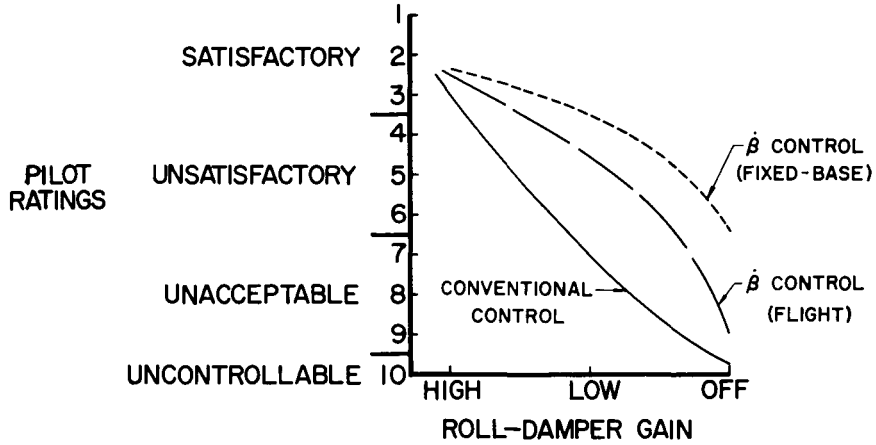


Figure 11

X-15 FLIGHT STUDIES WITH SIDEARM
 CONTROLLER
 ROLL DAMPER OFF

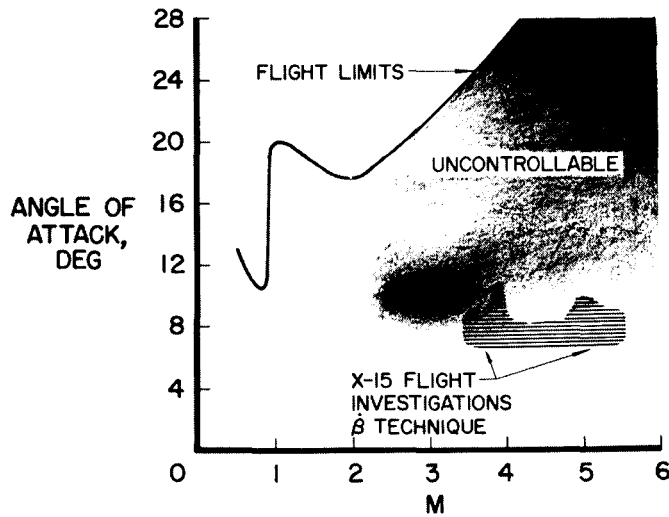
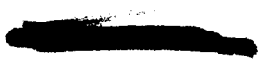


Figure 12



EFFECT OF LOWER RUDDER ON DERIVATIVES WIND-TUNNEL DATA, $\alpha = 12^\circ$

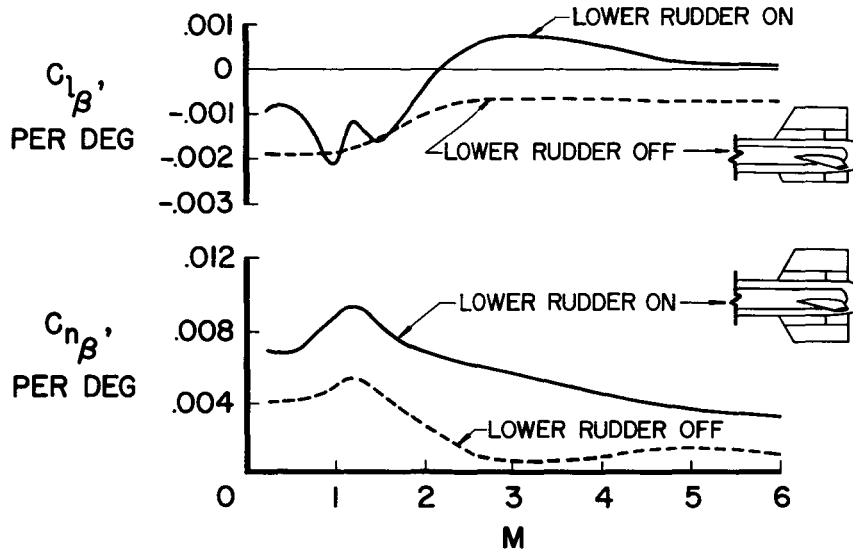


Figure 13

RELATION OF REENTRY TO CONTROLLABILITY BOUNDARY

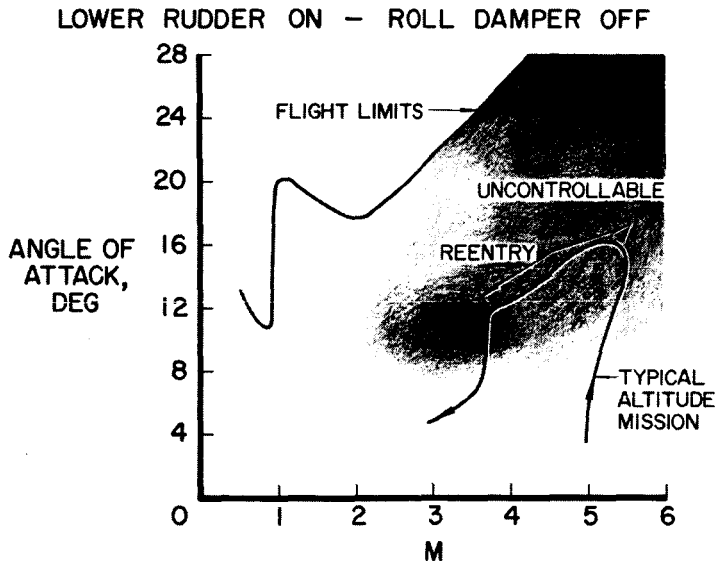


Figure 14

RELATION OF REENTRY TO CONTROLLABILITY BOUNDARY LOWER RUDDER OFF - ROLL DAMPER OFF

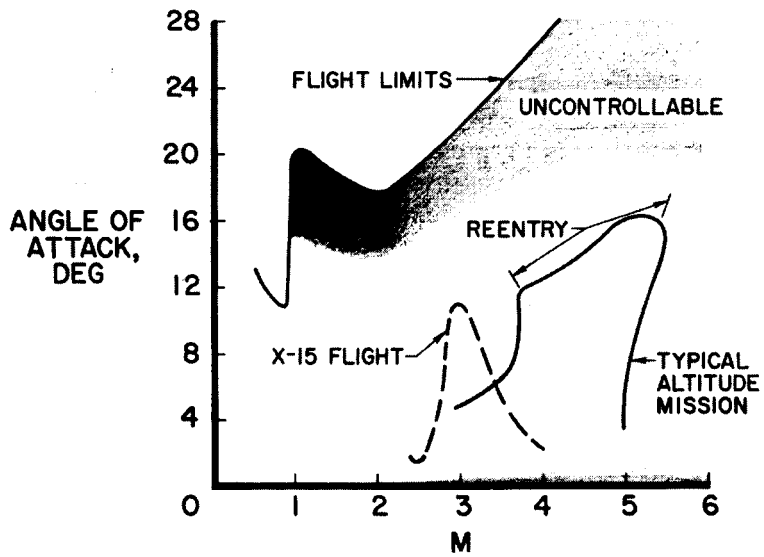


Figure 15

11. X-15 MISSION PLANNING AND OPERATIONAL PROCEDURES (U)

By Robert G. Hoey
Air Force Flight Test Center

and Richard E. Day
NASA Flight Research Center

N71-75454

INTRODUCTION

The philosophy of the X-15 flight-test program thus far has been to expand the flight envelope to the maximum speed and design altitude as rapidly as practical and simultaneously to obtain as much detailed research data on the hypersonic environment as possible. The envelope expansion program has been performed on an incremental performance basis; that is, each successive flight is designed to go to a slightly higher speed or altitude than the previous flight, thus permitting a reasonable extrapolation of flight-test data from one flight to the next and also building a backlog of pilot experience. The mission planning and operational procedures associated with the program are discussed in this paper. The effect on flight planning of systems reliability, stability limitations, and ranging considerations are also discussed. General piloting techniques and pilot training are mentioned.

DISCUSSION

First, the tools which are available to perform the flight-planning and pilot-training task for the X-15 program are examined. The prime tool is a six-degree-of-freedom analog simulator shown in figure 1. This simulator was constructed by North American Aviation, Inc., during the design and development stage of the X-15 program and was subsequently transferred to the NASA Flight Research Center for use during the flight-test program. This simulator is quite complete including actual hydraulic and control system hardware. Another primary pilot-training tool has been the F-104 airplane which is used by the pilots to practice low L/D landings. Digital computers have been of value in performing temperature-prediction calculations prior to each flight. Variable-stability airplanes have also been available during the test program.

One factor which had a significant effect on flight planning was the development status and demonstrated reliability of the subsystems on the X-15 airplane. Lack of duality in the stability-augmentation system required that flights be performed in such a manner as to provide for the safe return of the pilot and the aircraft in the event of

stability-augmentation malfunction. Inasmuch as the flow direction sensor, reaction control system, and inertial platform system were newly developed for the X-15 airplane, they could not be relied upon as primary flight instruments until reliability had been demonstrated.

Two flight-envelope expansion programs, one with the XLR11 engines and another with the XLR99 engine, were to be performed. The predicted flight envelope for the two configurations is shown in figure 2. A maximum velocity of about 3,300 ft/sec and a maximum altitude of 133,000 feet were predicted for the XLR11 powered configuration. A maximum velocity of slightly over 6,000 feet per second was predicted for the XLR99 powered configuration; and although the performance capability exceeds the design altitude of 250,000 feet, this altitude was chosen as an objective for completing the envelope expansion program.

Prior to the delivery of the X-15 airplane, a general handling-qualities study was performed on the X-15 analog simulator. The results of this study are summarized in figure 3. The hatching represents areas of instability, and flight in these areas is uncontrollable with or without the stability-augmentation system. The shaded area represents a region of uncontrollability with the stability-augmentation system (SAS) off. The details of this controllability problem have been discussed in the previous paper by Petersen, Rediess, and Weil (paper no. 10), and the only pertinent comment here is that considerable flight-planning effort was expended to insure that these areas could be avoided or investigated under controlled conditions on all flights.

Before the first cross-country flight of the X-15 airplane could be attempted, it was recognized that intermediate emergency lakes must be provided so that the pilot was always within gliding range of a landing site. A study was then performed, again on the analog simulator, to determine the overall range capabilities of the airplane. A simultaneous survey was conducted to locate all of the usable dry lakes in the area north and east of Edwards Air Force Base along the High Range. A summary of this study for the XLR99 powered configuration is shown in figure 4. Burning time is plotted against distance from the launch point. The solid curve represents the position of the airplane at any time during the powered portion of the flight. The dashed curve on the right represents the maximum forward-range potential of the airplane at any instant to a high key altitude of 20,000 feet. The dashed curve on the left represents the maximum rearward-range capability after performing a 180° turn, again to an altitude of 20,000 feet. For example, for a premature shutdown at 55 seconds the airplane is at the point shown in the example plan view and can perform a turn to arrive at a point 30 miles from launch, or it can glide straight ahead to a point 160 miles from launch; however, it cannot land at the lake which it is overflying at that instant. The usable emergency dry lakes were then spotted along the abscissa, and lakes were selected which provided

overlap throughout the entire flight. The general shape of these curves changes somewhat depending on the type of flight profile flown; however, the general spacing of the emergency lakes is not greatly affected. For the XLR11 powered configuration the range potential increases much more slowly than for the XLR99 powered configuration and closer spacing of emergency lakes was thereby required. The launch lakes selected and intermediate emergency sites are shown in figure 5. All flights with the XLR11 engine could be made either in the local area around Rogers Dry Lake or from the Silver Lake launch site. Envelope expansion flights with the XLR99 engine could be flown from Silver, Hidden Hills, and Mud Dry Lakes. After the lakes had been selected, the right to use the lakes was acquired and runway outlines were marked on the surface of each lakebed.

Once the predicted performance, ranging, and handling qualities of the airplane were well understood, the task of defining the piloting techniques required to reach the performance objectives was undertaken. The intent here was to make the best possible use of the pilot's presentation and to depend heavily on the most reliable information in the cockpit using the less dependable indications for cross checks during the flight or as backup information in the event of failure of a prime system. The analog simulator was invaluable in determining optimum piloting techniques. During most of the program with the XLR11 engine the airplane was equipped with a standard nose boom which provided accurate values of angle of attack, airspeed, and pressure altitude to the pilot. Piloting techniques were based on these parameters, and the resulting flight profiles were much like those of previous research airplanes, such as the X-2. The flow-direction sensor was installed for the XLR99 powered flights, and the sole source of velocity and altitude information to the pilot was then from the inertial platform. It was believed that the reliability of these indications from the inertial platform had not been adequately demonstrated to allow them to be used as prime instruments. Therefore, engine burning time was reverted to as the prime reference during the powered portion of the flights with the XLR99 motor.

A typical XLR99 altitude mission is shown in figure 6. The technique and pilot cues which have been devised to accomplish this mission will be examined next. Immediately after launch the pilot rotates to an angle of attack α of 10° , lights the engine, and throttles immediately to 100-percent thrust. The angle-of-attack indicator as shown in figure 7 is the primary instrument used during this roundout; however, a successful roundout can also be accomplished by using either the accelerometer or the stabilizer position indicator on the trim knob. The angle of attack of 10° is maintained until the desired exit pitch angle θ of the airplane is reached (32° for the flight shown). This occurs approximately 28 seconds after engine start. A pitch null vernier on the three-axis attitude ball allows the pilot to

[REDACTED]

preselect the desired pitch angle and fly it precisely during the exit phase. The pilot then maintains a constant pitch attitude until the engine shutdown time is reached.

At the extreme pitch angles required the pilot cannot see the horizon and, therefore, must rely on the attitude indicator to maintain proper heading and to keep wings level, as well as to maintain the desired exit pitch angle. A stop watch has been installed in the cockpit which is actuated by the main propellant valves to indicate engine burning time to the pilot and is used to initiate the engine shutdown. Obviously, a constant throttle setting must be used with this technique. The inertial platform system indications of velocity and altitude provide additional cues to the pilot during the powered portion of the flight as do radar altitude and time communications from the ground. The engine shutdown time and exit pitch angle are the two performance items over which the pilot has the most effective control during powered flight. These two parameters are adjusted during the planning phase so as to attain the desired peak altitude yet still complete the entry within a nominal range which corresponds to one of the launch and emergency lake complexes mentioned earlier. After engine shutdown the stabilizer is trimmed to zero and the reaction-control system is used to control the vehicle over the top. The prime cues used by the pilot during this portion of the flight are the attitudes from the three-axis ball and the angle-of-attack α and angle-of-sideslip β cross pointers which are also displayed on the same indicator. The entry conditions are established by trimming the stabilizer position to the desired value as indicated on the trim knob and then by using the reaction-control system to set up the desired angle of attack on the angle-of-attack gage. This angle of attack is maintained until the normal acceleration n_z reaches 4.0g and the remainder of the pullup to level flight is performed at 4.0g with the accelerometer as the prime indicator.

A typical speed flight is shown by the dashed curves of figure 6. The initial rotation and climb is performed in the same manner as the altitude profile. After 39 seconds of burning the pilot pushes over to 0g and maintains 0g until the shutdown time is reached. After engine shutdown a rudder pulse is usually performed at low angle of attack followed by subsequent data maneuvers at increasing angles of attack in order to obtain stability and control data for the complete envelope. The angle-of-attack indicator is usually used to establish the trim conditions for these data maneuvers; however, the stabilizer-position indicator can also be used. All speed buildup flights have been flown along the same general powered flight profile with higher peak velocities being obtained by either extending the engine burning time slightly or extending the speed brakes prior to shutdown. This greatly simplifies the temperature-prediction technique since direct extrapolation of flight-test data is possible from one flight to the next.

The pressure instruments, (pressure-altitude, airspeed, and Mach number indicators) are used only after the airplane is subsonic to perform the landing pattern and the landing.

The pilot preparation which is accomplished prior to each flight will now be examined. The six-degree-of-freedom analog simulator is used to acquaint both the pilot and the ground controller with the required piloting technique and general timing of the proposed flight. The normal flight profile is generally flown several times and changes suggested by the pilot are incorporated into the flight plan. After the pilot is familiar with the normal mission, off-design missions are flown to acquaint the pilot with the overall effect of variations in the critical control parameters. (See fig. 8.) Variations in engine thrust or engine shutdown time are simulated. For example, an error in total impulse of 120,000 lb-sec, which can result from either a 2-second error in burning time or a 1,500-lb error in average thrust, will result in a difference in peak altitude of approximately 10,000 feet. An error in pitch angle of 2° during the exit phase will result in a peak altitude difference of approximately 12,000 feet. A reduction in angle of attack of 1° or 2° during the roundout increases the average dynamic pressure during powered flight and, therefore, reduces the overall performance significantly.

The following simulated emergency conditions are next practiced by the pilot: (1) engine failures, (2) inertial-platform failures, (3) flow-direction-sensor failures, (4) radar and/or radio failures, (5) stability variation, and (6) stability-augmentation failures. Premature engine shutdowns are performed at the critical points in the flight to acquaint the pilot with the optimum technique required to either return to a lake behind him or to fly to an alternate lake ahead of him. Simulated failures of the inertial platform presentation are practiced and alternate techniques for either completing the normal mission or, at least, for safely returning the vehicle and pilot are devised. Normally, failure of the velocity or altitude readout does not affect the flight; however, in the event of an attitude presentation failure an immediate pushover must be initiated to a pitch angle of approximately 18° where the pilot again has the horizon in sight. Simulated flights with the flow-direction sensor inoperative are also practiced. In general, all missions can be completed without the angle-of-attack or sideslip indications by using normal-acceleration, attitudes, and stabilizer position indications; however, the pilot does not have as precise control of the flight conditions. Radar and communications failures are also practiced to assure that the flight can be accomplished with only the information available in the cockpit. For flights into critical-stability areas, simulated missions are performed with the stability of the analog altered to reflect the most pessimistic combination of errors which might exist in the predicted

stability derivatives. Last but not least, single- and multiple-channel failures of the stability-augmentation system are examined to determine the ground rules to be used for each flight. In most cases, a single failure of the pitch or yaw channel can be tolerated and the mission can be completed in a normal manner. Failure of the roll damper, however, creates a critical situation especially for high-altitude flights where an entry must be performed. This single item has created by far the most concern during the X-15 flight-test program. The controllability study in the previous paper by Petersen, Rediess, and Weil (paper no. 10) indicated that the airplane could not be controlled above an angle of attack of approximately 7° with the roll damper inoperable. For any altitude above 200,000 feet, an angle of attack greater than 7° is required during the entry to avoid exceeding the maximum dynamic-pressure limits of the airplane. Three possibilities have been examined for successfully accomplishing an entry with the roll, or roll and yaw damper inoperable. The first possibility is to jettison the lower vertical fin which improves the handling qualities appreciably at high angles of attack but at the expense of degraded handling qualities near zero angle of attack. The second possibility is the use of the β technique which has been discussed in the previous paper by Petersen, Rediess, and Weil (paper no. 10); and, although all X-15 pilots have mastered the technique on simulators, it is not considered a final answer to the problem. The third possibility is the dualization of the roll damper which is presently being undertaken but will take some time to accomplish. Pilot practice is, therefore, concentrated in the first two areas. The β technique is practiced during entries with the stability-augmentation system off, and entries with the lower vertical fin off are performed on the simulator. For flights to altitudes below 200,000 feet, entries at an angle of attack of 7° with the stability-augmentation system off are also practiced.

An important pilot-training device for the landing phase of X-15 flights is the F-104 airplane. The use of the airplane in preparing for X-15 flights has been covered in a previous paper by White, Robinson, and Matranga (paper no. 9).

In addition to these preparation procedures which are performed prior to each and every flight, additional training procedures have also been used. A centrifuge program was performed in June 1958 which verified that the pilot could successfully control the airplane under the predicted acceleration environment. Prior to his first flight in the airplane, each pilot went through a ground dry run with the X-15 airplane mated to, or in the vicinity of, the B-52 airplane. The purpose of this dry run was to permit the pilot to become familiar with the complete prelaunch check list and cockpit procedures. Engine runs on the Propulsion System Test Stand at Flight Research Center were also performed by each pilot prior to his first X-15 airplane flight. Variable-stability airplanes have been used to simulate the handling

qualities of the X-15 airplane at various flight conditions to provide more realistic motion cues to the pilot.

Although the pilot is undeniably in complete control of the flight, the ground monitoring station performs an important function in the support of X-15 flight operations. It is equipped with displays of the radar data and selected channels of telemetered data. The primary function of the ground-control station are shown as follows:

- (1) To monitor the subsystems operation during the flight and advise the pilot of any discrepancies noted
- (2) To position the B-52 airplane over the desired launch point at the desired time by advising the B-52 pilot of course corrections and countdown time corrections prior to launch
- (3) To time the engine operation as a backup for the onboard stop watch and to advise the X-15 pilot of heading corrections, radar altitudes, and position during the flight
- (4) To monitor and evaluate stability and control parameters
- (5) To monitor the pilot's physiological environment
- (6) To provide the X-15 pilot with energy-management assistance in the event of a premature engine shutdown or other off-design condition
- (7) To direct air search and rescue operations in the event of an emergency

Normally, all important information in the control room is passed on to the pilot through the ground controller; however, other ground-control personnel have the capability to transmit directly to the pilot in the event of extreme emergency where insufficient time is available to relay the information.


In order to supply energy-management advice to the pilot as rapidly as possible, some special techniques and equipment are presently being incorporated. The analog simulator was used to define the optimum piloting techniques required to obtain the maximum forward and reverse range from various flight conditions. These techniques are fairly well standardized and understood by the X-15 pilots. A small analog computer has been mechanized to store the precomputed maximum range capabilities as a function of forward velocity, vertical velocity, and altitude. Radar values of these parameters are fed into the system and the resulting range footprint to a high key altitude of 20,000 feet is displayed on a scope-type map presentation. The ground controller can then tell at a glance which lakes are within the range capability at any particular instant. Three modes of operation are used. The normal mode shows the total attainable ground-area footprint which is essentially a cardioid in shape. The other two modes indicate the instantaneous airplane position or heading by a single dot or line. A simplified system by using the same basic principle but with a family

of curves drawn on the map instead of the scope presentation has been in use on all flights to the present time.

Some flight results are examined to evaluate the planning and pilot training. Figures 9 and 10 show a comparison between the maximum altitude and maximum speed profiles as predicted and those actually flown with the XLR11 engine. The comparison is considered rather good and very near optimum, especially since maximum performance for both flights were obtained on each pilot's first attempt and on his fourth flight in the X-15 airplane. Figures 11 and 12 show comparisons between predicted speed and altitude profiles with the XLR99 engine and the actual flight profiles. The overshoot in actual velocity and altitude flight is a result of a 2-second delay in shutting down the engine. It should be understood that the cockpit stop watch did not work on this particular flight and that at this point in the trajectory the airplane is accelerating at approximately 100 ft/sec^2 . The pilot was, therefore, relying on a ground time callout to shutdown the engine and the resulting delay was responsible for the discrepancy. In general it has been found that the control of flight profile is not as precise with the XLR99 engine as with the XLR11 engine, primarily as a result of the larger accelerations. After each flight a performance "match" is simulated on the analog computer with the actual angles of attack and thrust values which were experienced on the flight. Analog-computer matches of these two flights are also shown in figures 11 and 12. The overall performance of the simulator is shown to be rather close to that of the airplane. The only changes which have been made to the simulator as a result of flight-test data have been weight- and burning-time alterations. No alterations to the predicted performance and stability derivatives have been required.

Several anticipated malfunctions, such as stability-augmentation failures, engine failures, stop-watch malfunctions, inertial-system malfunctions, and radar and radio malfunctions have occurred during the test program thus far. The anticipated controllability problems have also been verified in flight. The value of the analog simulator in defining techniques and training the pilots to allow completion of the missions under these adverse conditions is undeniable.

Several unexpected incidents have also occurred during the program which have justified the decision to perform an incremental-performance envelope expansion program. On the maximum speed flight with the XLR11 engine at a Mach number of 3.3, the cockpit seal was burned slightly due to the canopy lifting and allowing hot stagnation air to reach the rubber seal. On the first flight with the XLR99 engine to a Mach number of 4.2, side-panel buckling was encountered as a result of differential heating. Wing leading-edge skin buckling was also encountered as a result of local aerodynamic heating at Mach numbers on the order of 5.0. A poor aerodynamic seal around the nose gear door



resulted in some minor internal damage due to aerodynamic heating at a Mach number of 5.3. A severe airplane vibration induced by the stability-augmentation system was experienced on an interim altitude flight at a Mach number of 3.8. Since all of these items were discovered on lower velocity flights under less critical conditions, they have been corrected without significantly affecting the test program. Any of the incidents listed could have resulted in major damage to the airplane if maximum speed or altitude had been attempted on the first flight and could possibly have resulted in loss of the airplane.

CONCLUDING REMARKS

In conclusion, the expansion of the X-15 flight envelope is being performed according to the planned program. All predictions of stability, performance, and flight trajectories have been within expected accuracies. Controllability problems predicted by analog simulator data were verified in flight. General piloting techniques developed on the analog simulator have proven to be satisfactory in flight. Ground-control functions have proven to be of value in assisting the B-52 and X-15 pilots. Pilot-training procedures have proven to be adequate for a program of this type. The use of the analog simulator to establish pilot cues and timing and allow the pilot to practice until the techniques become routine has considerably eased the total piloting task, thereby improving his ability to obtain more precise flight data in the time available. Predictable emergency conditions or off-design missions have been encountered during the program, and in each case simulator training has contributed greatly to the pilots' ability to complete the mission. The two most valuable training devices have been the fixed-base six-degree-of-freedom analog simulator and the F-104 in-flight landing pattern simulator. Other training devices, such as the centrifuge and variable stability airplane, have contributed to the overall pilot experience level, but are not considered necessary for continuous use on a flight-by-flight basis. Unexpected problems, primarily in the area of aerodynamic heating, have also been encountered; however, neither pilot nor flight vehicle safety has been compromised due to the incremental performance philosophy of envelope expansion testing.

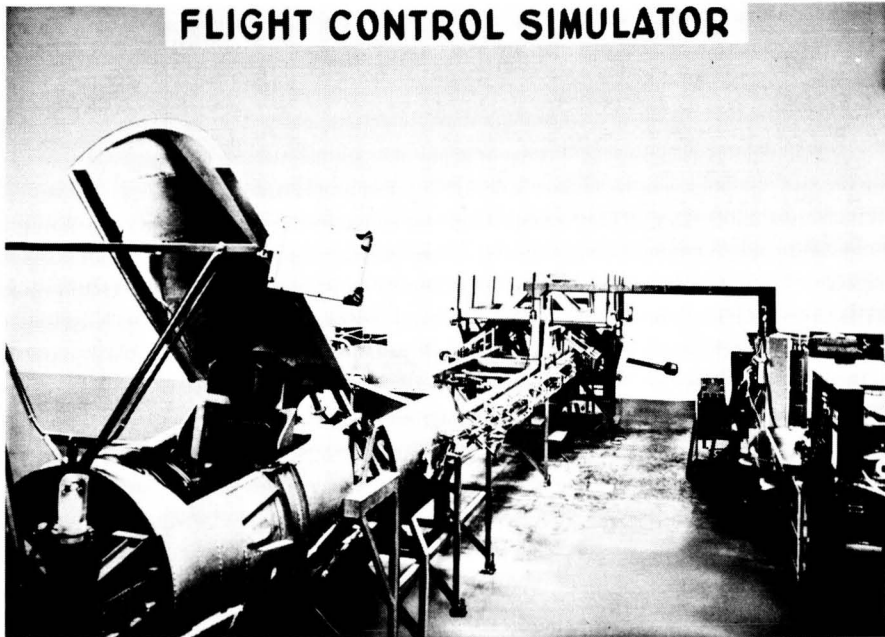


Figure 1

X-15 PERFORMANCE ENVELOPE

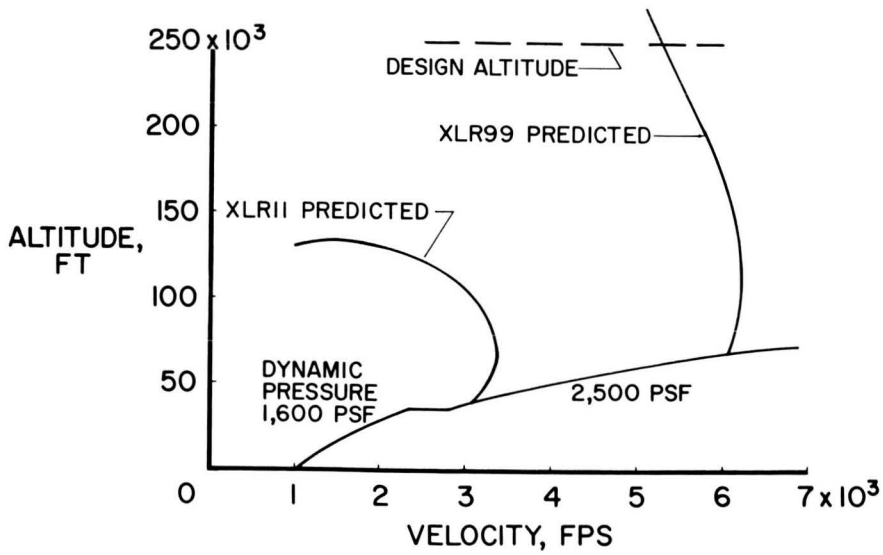


Figure 2



STABILITY AND CONTROL SUMMARY

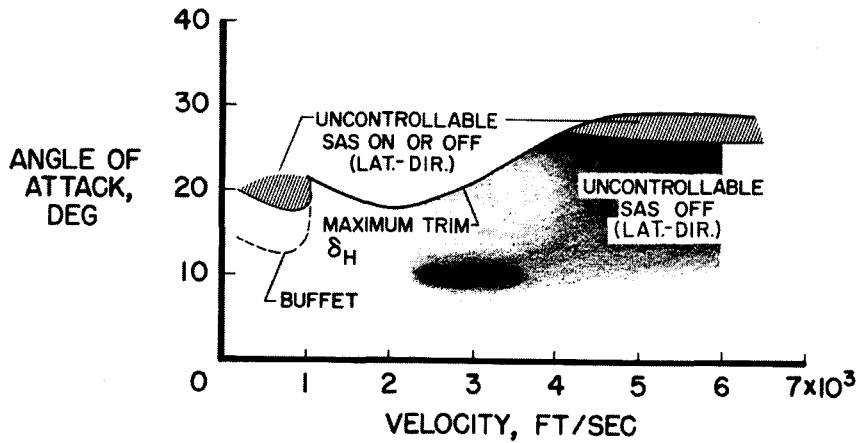


Figure 3

XLR99 RANGING

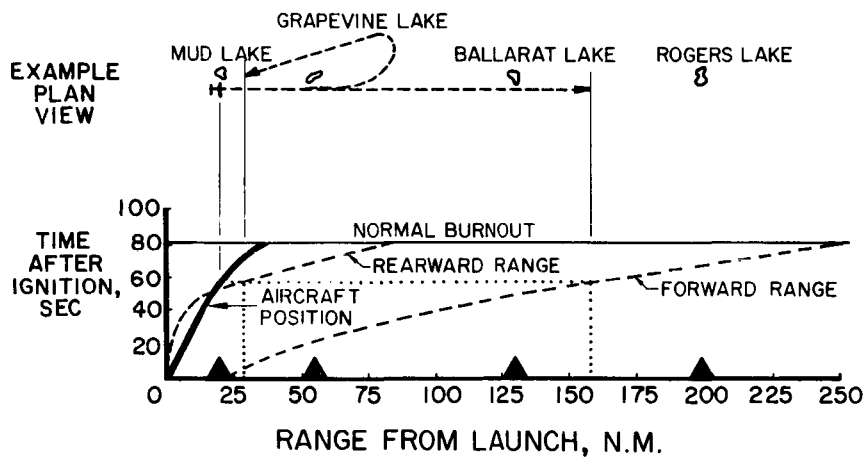


Figure 4



LAUNCH AND EMERGENCY LAKE COMPLEX

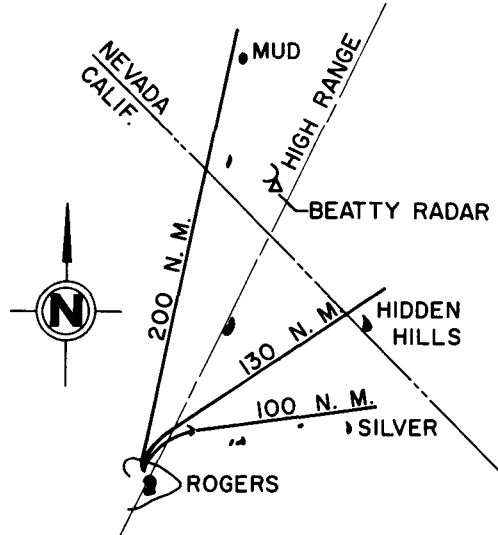


Figure 5

XLR99 ALTITUDE MISSION SPECIFIED PROFILE

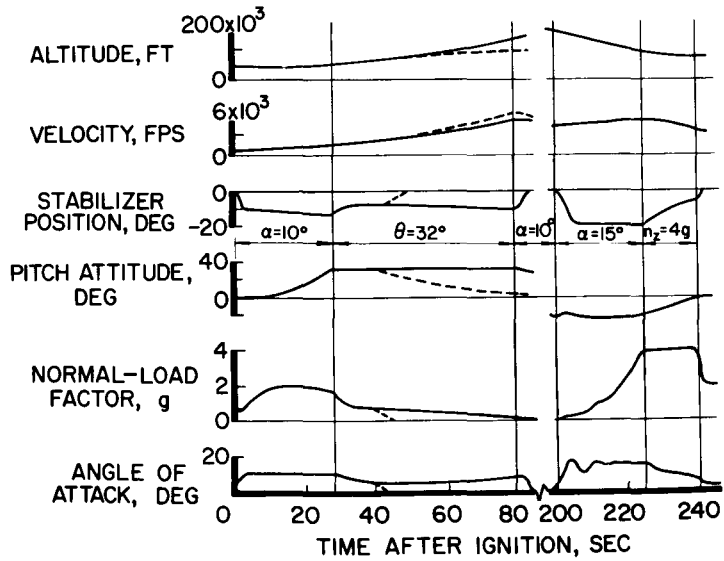


Figure 6



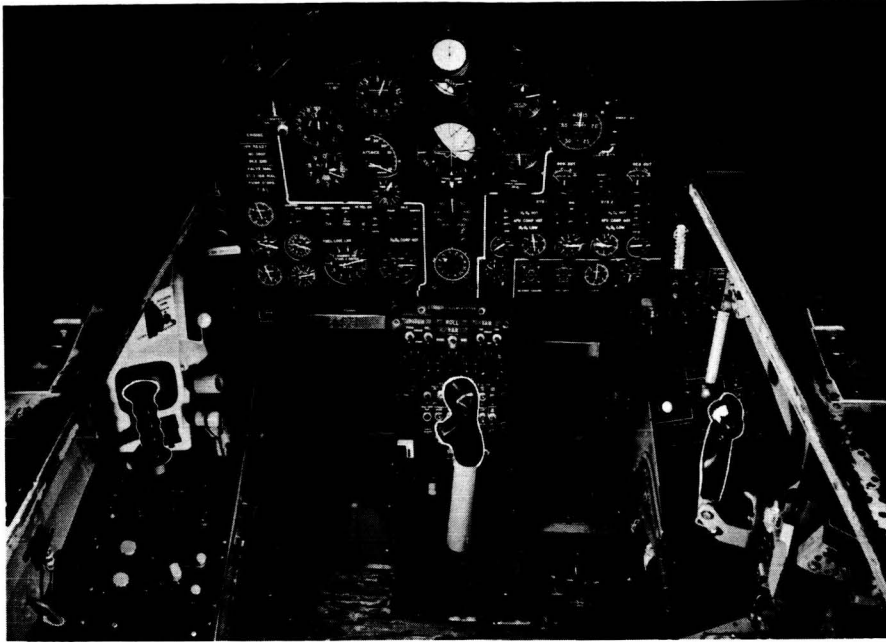


Figure 7

XLR99 ALTITUDE - MISSION PROFILE

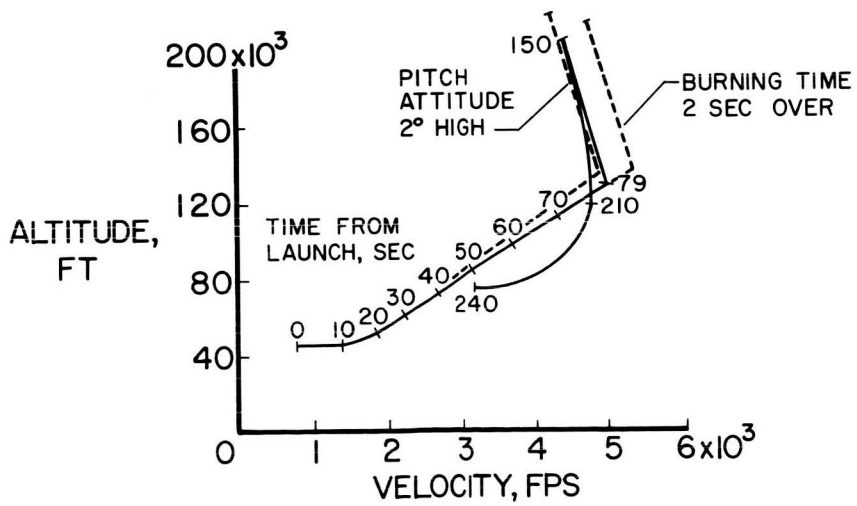
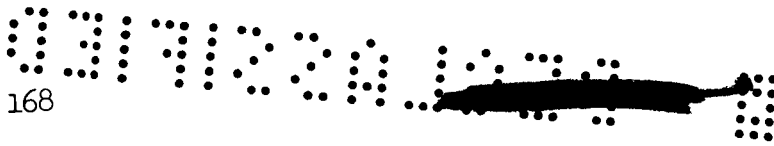


Figure 8



XLR II PERFORMANCE COMPARISON MAXIMUM ALTITUDE

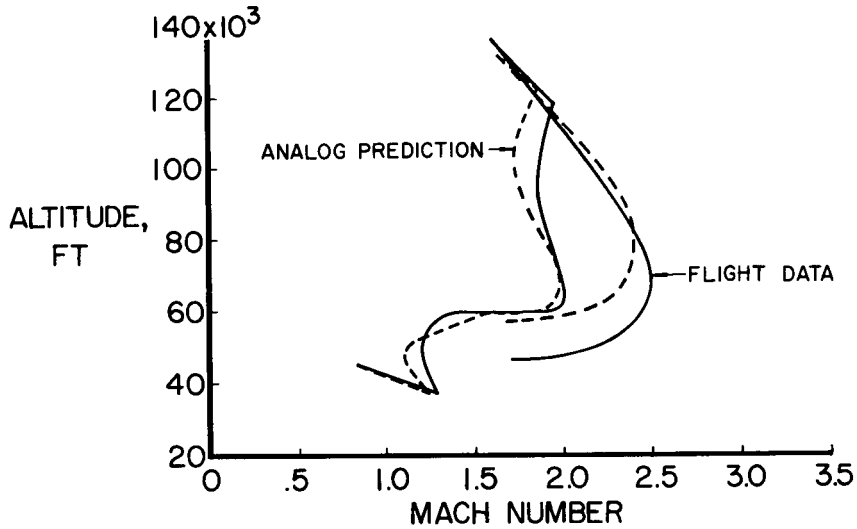


Figure 9

XLR II PERFORMANCE COMPARISON MAXIMUM SPEED

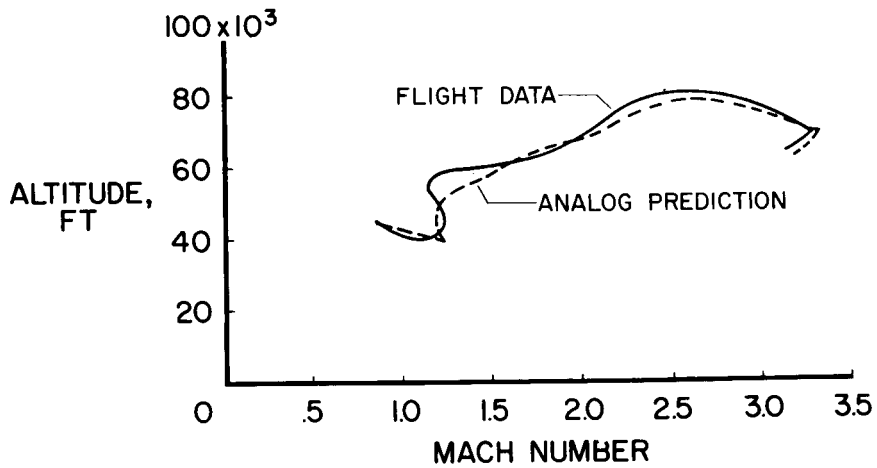


Figure 10



ALTITUDE - FLIGHT PERFORMANCE COMPARISON XLR99 ENGINE

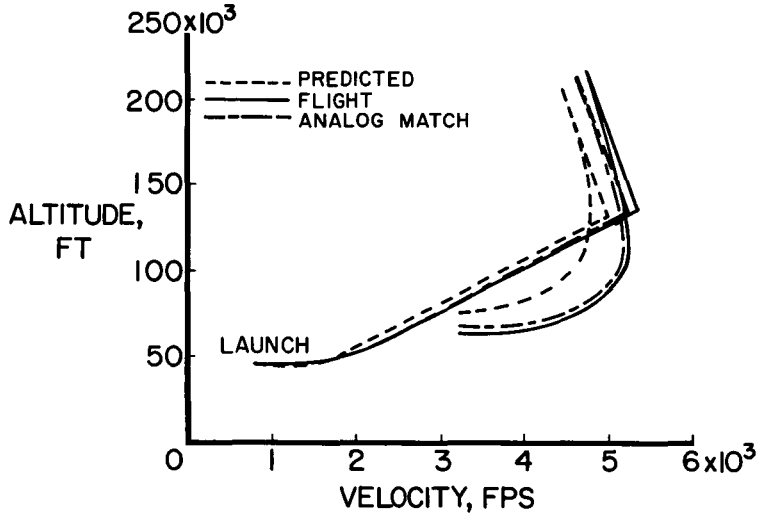


Figure 11

SPEED - FLIGHT PERFORMANCE COMPARISON XLR99 ENGINE

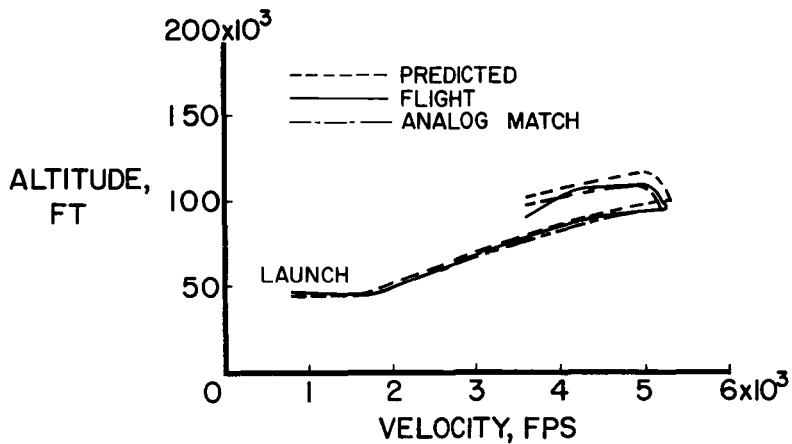
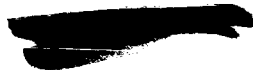


Figure 12



171

12

12. X-15 STABILITY AUGMENTATION SYSTEM (4)

By Lawrence W. Taylor, Jr.
NASA Flight Research Center

and George B. Merrick
North American Aviation, Inc.

N71-75455



SUMMARY

This paper describes the basic damper system currently installed in the X-15, discusses some of the problems encountered during its development and flight testing, and reviews briefly the system reliability.

INTRODUCTION

The proposed performance goals of the X-15 research vehicle made it obvious in the early stages of its development that stability augmentation would be required. In figure 1 the flight envelope of the X-15 is compared with that of a typical century series aircraft. Dampers were necessary in these military aircraft and it was clear from the estimated speed and altitude that the X-15 would have similar requirements. It was also believed that any system installed to augment the stability should emphasize simplicity and reliability. For these reasons a simple three-axis damper system was proposed which would not include multiple sensors, complicated automatic gain scheduling, or sophisticated automatic control modes.

This paper describes the basic damper system currently installed in the X-15, discusses some of the problems encountered during its development and flight testing, and reviews briefly the system reliability.

SYMBOLS

- $C_{l/2}$ cycles to damp to half-amplitude
- $C_{l\delta_a}$ aileron control effectiveness
- $L\delta_a$ roll control power
- q dynamic pressure

PRECEDING PAGE BLANK NOT FILMED

Preceding page blank

- δv vertical-tail deflection
- $\Delta\phi$ peak-to-peak amplitude of limit cycle in roll
- ζ damping ratio

SYSTEM CONFIGURATION

A functional diagram of the stability augmentation system (SAS) built by Westinghouse is shown in figure 2. The essential components of the pitch, roll, and yaw channels of the system are indicated as gyros, cockpit gain selectors, electronics, and servos. The outputs of the servos go to their respective control surfaces. Unique features of the system are cockpit gain selection and the inner connection required for operation of the left-hand and right-hand horizontal stabilizers, which provide both pitch and roll damper input. Also shown is a yaw rate input to the roll axis. This interconnection is necessary for stability at high angles of attack primarily due to the high roll input of the lower rudder. The gain-selector settings of 8, 6, 8, indicated for pitch, roll, and yaw, respectively, are the normal settings.

Positive control of failures is emphasized by providing complete fail safety. Figure 3 shows a schematic diagram of the yaw axis monitoring arrangement which is typical of the pitch and roll channels also. A complete duplication from gyro pick-off to servo input is provided in a working channel and a monitor channel. This arrangement allows a continuous comparison of system performance in the two channels. Automatic shutoff of the affected channel with rapid servo centering is accomplished when a 10-percent variation exists between the working and monitoring channels. Because of the high dynamic performance of the servo cylinder, it was not necessary to duplicate its dynamics in the monitor channel. A simple, constant gain, auxiliary SAS is being fabricated for the X-15, which will serve as a backup in the event of a failure of the primary stability augmentation system.

RELIABILITY

Information concerning the failures experienced thus far with the stability augmentation system is shown in figure 4. The number of accumulated failures is plotted against the total number of hours during which the systems have been functioning, both on the ground and in the air. There is also a scale showing the total number of flights including aborted flights. The lower scale is necessarily nonlinear because, for example, more ground hours per flight were put on the systems in preparation for the earlier flights than for the later flights. The top curve includes all failures accrued during both ground

and flight operation and should be used primarily as logistics information. Note that the failure rate, given by the slope, has greatly diminished. The breakdown given by the bar graph on the right shows the module failures to be the largest single source of system failures. Next is ship's wiring, with miscellaneous other failures accounting for the remainder of the total.

The lower curve represents only the failures which have occurred in flight, "in flight" being defined as the time from take-off of the B-52 to landing of the X-15 or X-15/B-52 combination in case of an abort. The in-flight failures breakdown is shown also on a bar graph at the right of the figure. These failures resulted from the malfunction of one electronic module, three instances of broken ship's wiring, and three malfunctioning gain switches. Of these 7, 6 were traceable to human error and were damaged on the ground but did not result in failures until airborne. Considering only the electronic module failure in 78 flights, and no in-flight failures in the last 13 flights, it can be said with confidence that SAS has proven to be reliable.

LIMIT CYCLES

Some of the development problems are now considered. In the first studies using the X-15 flight simulator, unwanted limit cycles or continuous oscillations, sustained by SAS, were observed. The limit cycles were caused by hysteresis and rate limiting which produce considerable phase lag. The phenomenon was later observed in flight though at first it was not noticed by the pilots. An illustration of the magnitude of the limit cycle is shown in figure 5. The peak-to-peak amplitude of the limit cycle is plotted against the roll control power which is proportional to both dynamic pressure and aileron control effectiveness. The roll damper gain is 0.3 deg/deg/sec or a setting of 6. The circles denote the early flight data. Shown as squares are limit cycles measured on the ground by using an analog computer to close the aerodynamic loop around the X-15 airplane. The solid line gives the calculated limit-cycle characteristics. These calculations were made by using a mathematical model of the nonlinear actuator which included hysteresis, dead band, and rate limiting. Notice the extreme increase in the limit-cycle amplitude predicted at large values of control power. A flight was made to verify these limit-cycle characteristics at large values of this roll-control parameter. Figure 6 shows a time history of roll rate and aileron deflection during the severe roll limit cycle. The frequency of this limit cycle was about 3.2 cps and the amplitude was about 1° total change in bank angle. This was considered by the pilot to be quite objectionable which is due in part to the motion of the control stick caused by surface rate limiting. Notice that the amplitude of this limit cycle was not constant but changed due to control input and a

tendency to beat. Figure 7 shows again a comparison of the limit-cycle characteristics obtained in flight and those calculated, the data of the special flight having been added. Although the critical value of I_{σ_a} appears to be somewhat higher than that calculated, a drastic increase in bank-angle amplitude would result if the control power were allowed to increase much further.

As a means of reducing the limit cycles to an acceptable amplitude, the SAS electronic filter was modified, with the result in the limit-cycle characteristics shown in figure 8. The reduced lag of the modified filter greatly reduced the amplitudes of the limit cycles so that the problem was essentially eliminated. The most extreme values of control power did not give objectionable limit cycles.

Although the discussion of the limit cycles thus far has been concerned with roll, the limit cycles also exist at some flight conditions in pitch and yaw as well, but to a lesser degree. The limit cycles in pitch and yaw occur at frequencies closely related to the natural frequency of the airplane and do not have the critical nature of the roll limit cycles.

VIBRATION

Although the modified filter greatly improved the problem with limit cycles of 1 to 3 cps in roll, a new problem arose. It became apparent during tests on the ground that it was possible to excite and sustain a system-airplane vibration at 13 cps with the modified filter. A breadboard of the modified filter was flown at high damper gains, but the pilot failed to excite the vibration. After touchdown, however, during the rollout, a severe vibration was encountered and SAS had to be turned off. This experience led to the belief that the vibration would only occur on the ground. To prevent recurrence on the ground, a switch which automatically lowered the gain to a safe level when the landing gear was extended was incorporated in the airplane. Five flights later the sense of security engendered was shaken, literally. Figure 9 shows a portion of a time history during reentry from a 170,000-foot-altitude mission. It is obvious that a 13-cps vibration is present in all traces - left and right SAS links, left and right surface deflections, and roll rate. The pilot reported the vibration to be the most severe that he had ever encountered or ever wants to. The shaking was triggered by pilot inputs at low dynamic pressure (130 lb/sq ft) and continued until the SAS gain was reduced slightly and dynamic pressure had climbed to 1,000 lb/sq ft. Fortunately, the amplitude of the shaking was limited by rate limiting of the control-surface actuators. An analysis of the problem was conducted to find an explanation for this behavior.




Figure 10 illustrates the mechanics of the phenomenon. The lightly damped horizontal stabilizer surfaces, here represented by the flexible beams with masses, were excited at their natural frequency (13 cps) by the pilot inputs to the control system. The inertial reaction of the fuselage to this vibration was picked up by the gyro, so that the SAS was able to sustain the vibration with inputs to the control surfaces.

Because of the closed-loop nature of the problem, restrictions in the allowable gain exist at the structural frequencies as is shown in figure 11. Presented is system gain as a function of frequency for three filters, all at a SAS gain setting of 6. If the curves intersect these boundaries which represent restrictions in gain at the structural frequencies of the horizontal tail at 13 cps and 30 cps, then a sufficient condition exists for a sustained oscillation. The modified filter used during the previously discussed altitude flight intersects the first boundary; a vibration, therefore, would be expected at 13 cps. The original filter presently in use is shown to be free of the 13-cps vibration but produces unacceptable limit-cycle characteristics at critical flight conditions. One way to avoid both problems is to use a notch filter. This filter was designed to give a minimum phase lag at limit-cycle frequencies and a maximum of filtering at the surface resonant frequencies.

An additional fix is a pressure feedback valve for the surface actuator, which would augment the structural damping of the horizontal surfaces. Referring again to figure 11, the use of the pressure feedback valves would lift the restrictions in gain to values outside the range of gain for SAS. Pressure feedback valves would allow further improvement of the limit-cycle characteristics because of the reduced phase lag associated with removing the notch filter. Both the notch filter and pressure-feedback valve are currently being developed for use in the X-15.

SAS EFFECTIVENESS

A few words pertinent to the effectiveness of SAS are in order. Other contributors to this conference have indicated the need for and the large improvement in lateral-directional handling qualities produced by SAS. Figure 12 illustrates the adequacy of the damping of the unaugmented and augmented X-15 airplane in pitch. The coordinates are velocity and altitude, and the solid lines indicate the boundaries of the flight envelope of the X-15 airplane. In this lower region, the pitch damping of the unaugmented airplane is acceptable, less than one cycle being required to damp to half amplitude ($\zeta \approx 0.1$). The augmented airplane has as much damping over the entire aerodynamic region. In the

ballistic region aerodynamic control becomes ineffective and the use of reaction controls is required. To provide damping in this region a reaction augmentation system or RAS has been designed and is to be installed in the airplane. This system uses the reaction control rockets to provide damping about all three axes. Although the airplane can be and has been flown by the pilot without augmentation in the ballistic region, RAS is expected to improve greatly the control characteristics of the airplane. More important, it will provide a good backup damping system for SAS during the setup for the reentry portion of high-altitude flights.

A more advanced flight-control system has been developed for evaluation in the X-15 airplane. This system is discussed in the paper by Johannes, Armstrong, and Hays (paper no. 13 of this conference).

CONCLUSIONS

The design objectives of a simple reliable stability augmentation system have been achieved. The reliability of the electronic components in flight has been good and approaches the design objective. Limit-cycle problems predicted on the simulator have been verified in flight. A vibration problem not anticipated was encountered in flight with a modified shaping and was traceable to structural SAS interaction. Two acceptable means of eliminating these problems have been developed for incorporation into the X-15 airplane. In short, the overall experience with this system has been favorable and the improved vehicle characteristics available with SAS have enabled the pilots to investigate with confidence many areas which without stability augmentation would be uncontrollable.

ENVELOPE COMPARISON

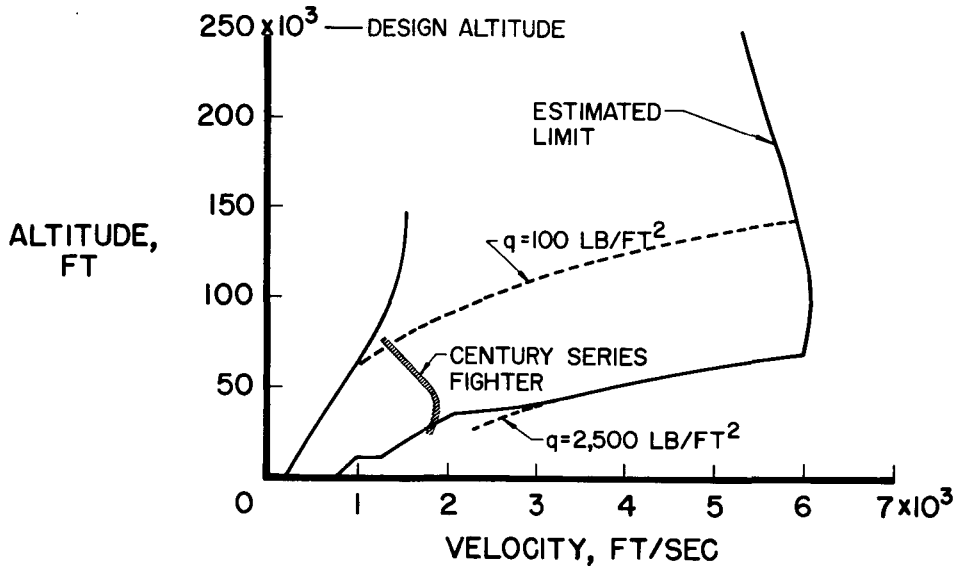


Figure 1

FUNCTIONAL DIAGRAM OF SAS

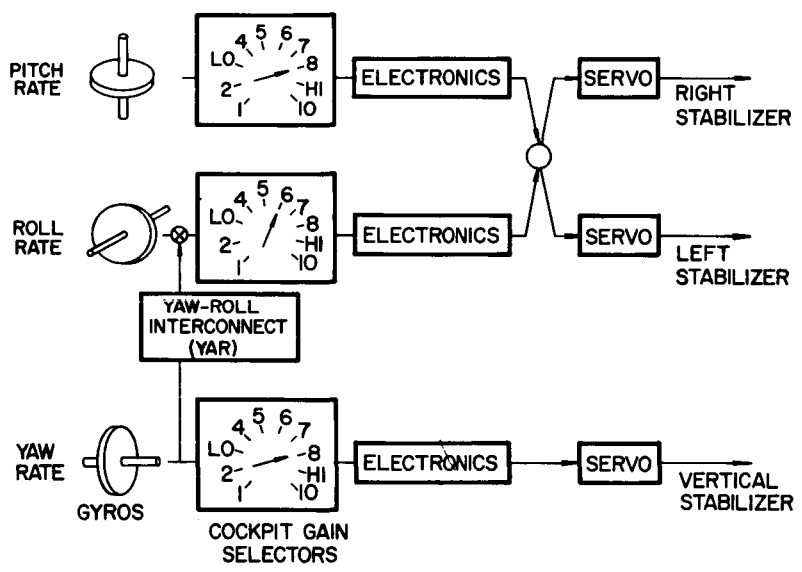


Figure 2

CONFIDENTIAL

FAIL-SAFETY PROVISIONS YAW AXIS (TYPICAL)

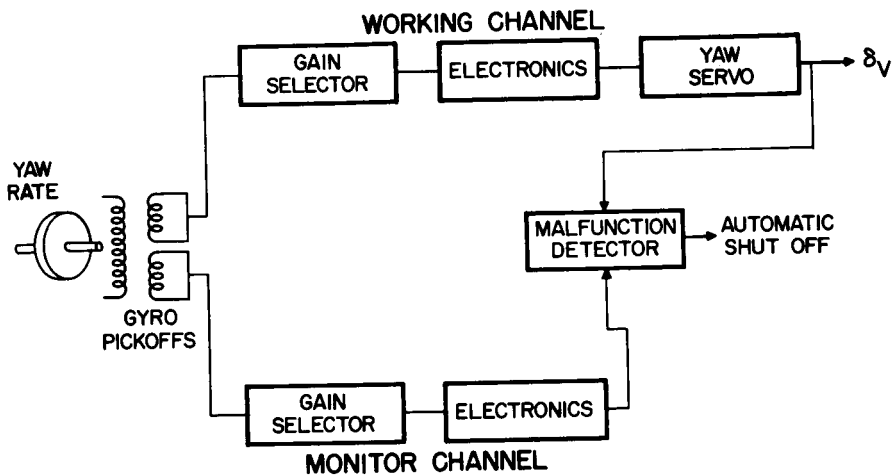


Figure 3

SAS FAILURES

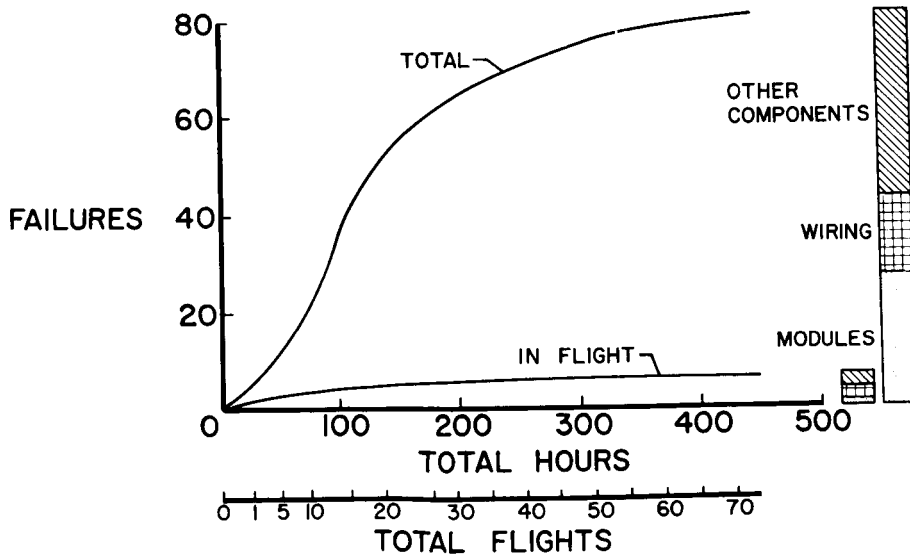


Figure 4

CONFIDENTIAL

EARLY ROLL LIMIT-CYCLE DATA

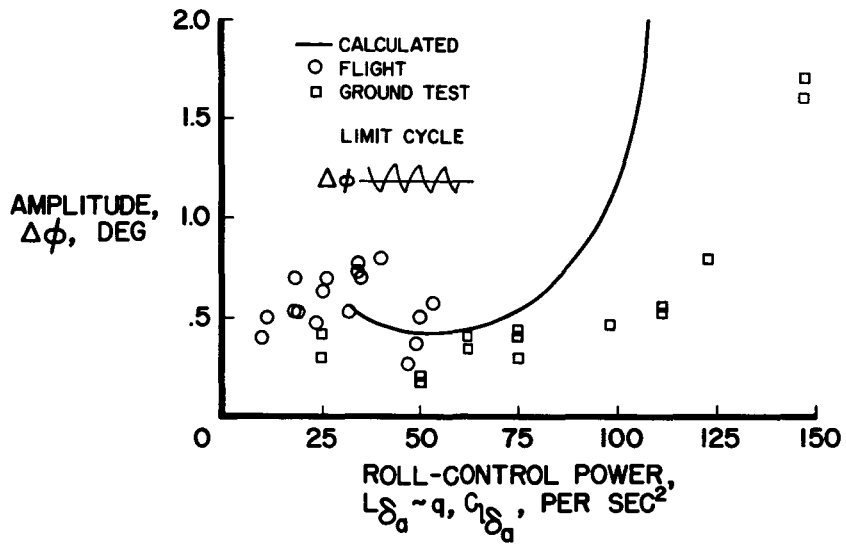


Figure 5

TIME HISTORY OF SEVERE ROLL LIMIT CYCLE

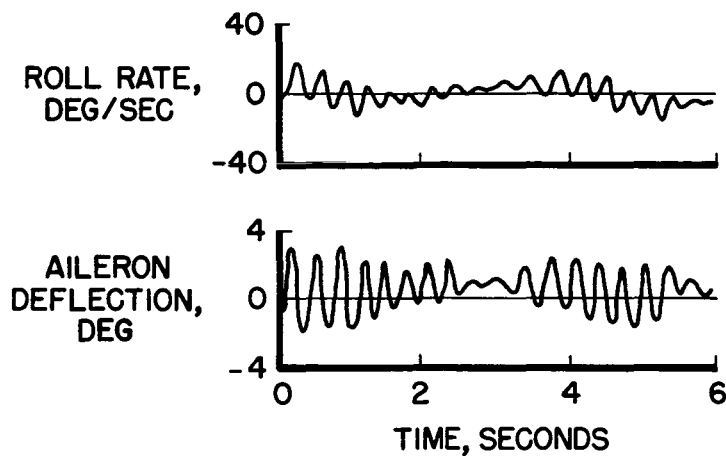


Figure 6

CONFIDENTIAL

COMPARISON OF CALCULATED AND FLIGHT ROLL LIMIT CYCLES

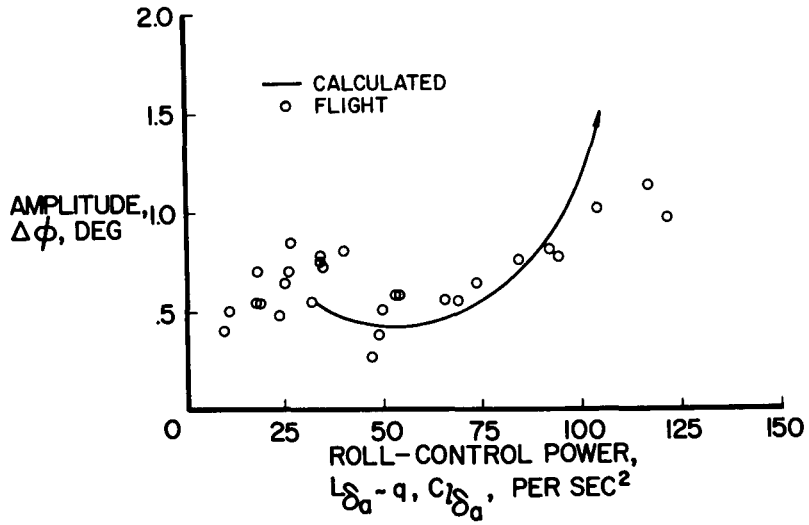


Figure 7

EFFECT OF MODIFIED FILTER ON ROLL LIMIT CYCLE

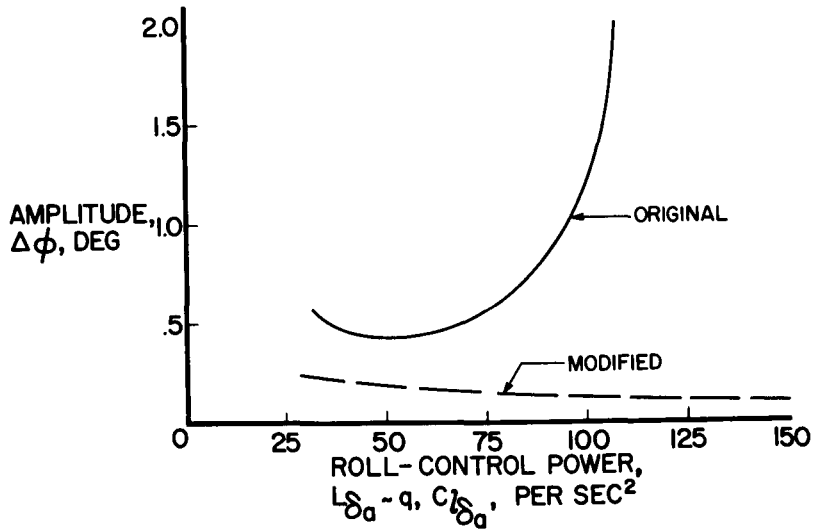


Figure 8



TIME HISTORY OF IN-FLIGHT VIBRATION

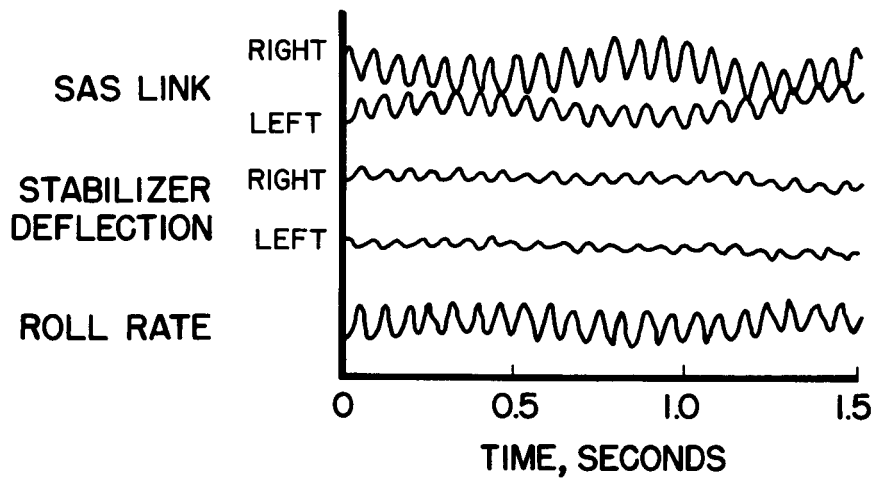


Figure 9

MECHANISM OF VIBRATION

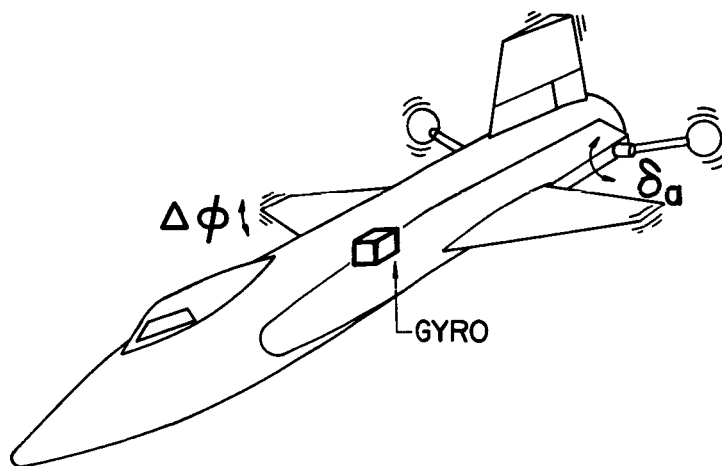


Figure 10



CONFIDENTIAL

EFFECT OF FILTERS ON HIGH-FREQUENCY STABILITY

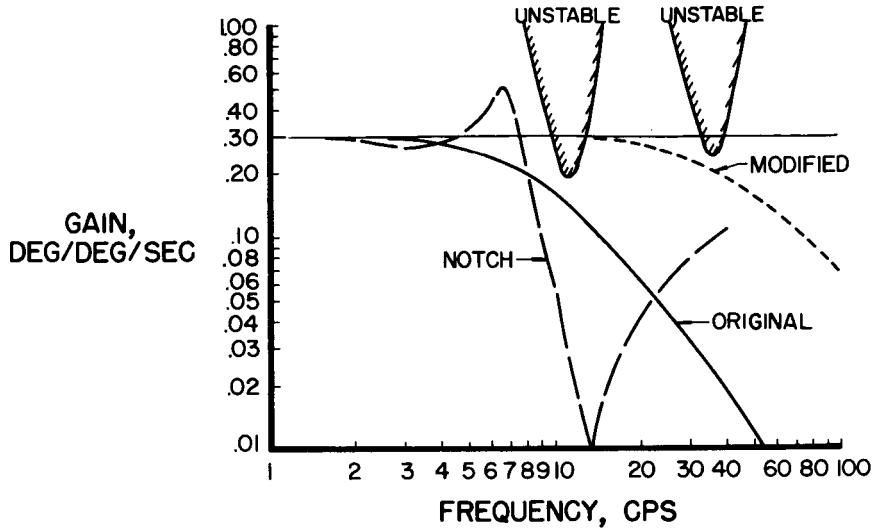


Figure 11

EFFECT OF SAS ON LONGITUDINAL DAMPING

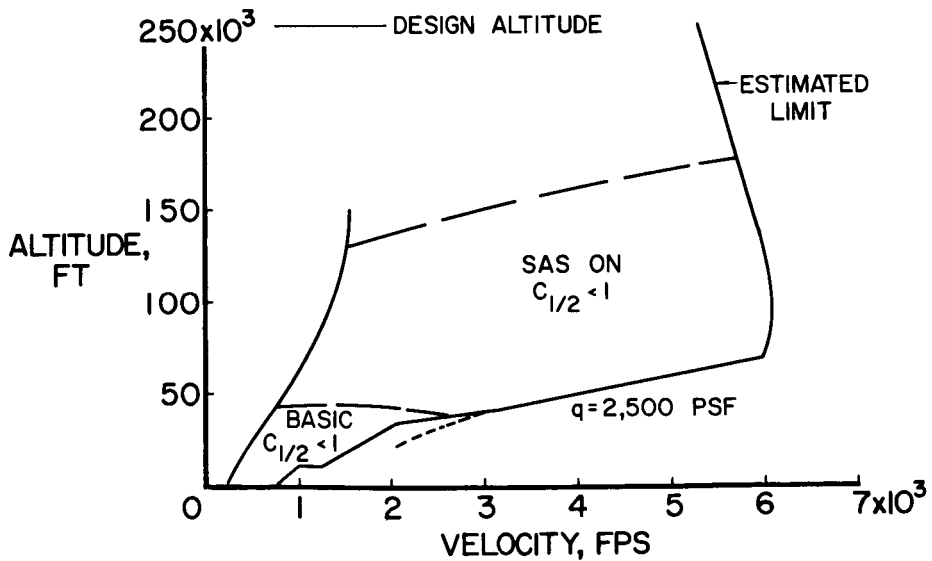


Figure 12

CONFIDENTIAL

Declassified by authority of
Classification Change Notice
Dated ** 2/14/62

DECLASSIFIED- 1/31/68
AUTHORITY: TAINE TO SHAUKLAS
MEMO: PS: 2840 dated 2/6/68

13. DEVELOPMENT OF X-15 SELF-ADAPTIVE FLIGHT-CONTROL SYSTEM (W)

By Robert P. Johannes
Aeronautical Systems Division, U.S. Air Force

N71-75456

~~████████████████████~~ Neil A. Armstrong
NASA Flight Research Center

and Thomas C. Hays
Aeronautical Systems Division, U.S. Air Force



In-house studies conducted at Wright-Patterson Air Force Base in 1956 convinced the Flight Control Laboratory, Aeronautical Systems Division, of the theoretical feasibility of designing a self-adaptive flight-control system. As the name implies, such a system would automatically adapt itself in order to provide essentially constant damping and frequency of the aircraft in combination with the control system as the vehicle encountered flight conditions of varying aerodynamic control-surface effectiveness. Conventional flight-control systems adjust their gains as functions of measured and computed air data; however, these functions require extensive flight test to perfect, have to be reestablished for even minor aircraft configuration changes, and result in complex and unreliable systems. Since future vehicles will require high reliability as well as satisfactory operation on the first flight and will be operating where adequate air data will probably not be available, a new approach to flight-control-system design was definitely needed. To this end a number of study contracts were awarded in 1957 which soon led to flight-test programs testing adaptive concepts in F-94 airplanes by the Massachusetts Institute of Technology and the Minneapolis-Honeywell Regulator Company. Minneapolis-Honeywell continued this effort with a company funded flight-test program for testing the system in an F-101A airplane.

By 1958 the Flight Control Laboratory was convinced of the potential of self-adaptive techniques; however, the flight profiles of the airplanes used to test the techniques were so limited that the full capabilities of the systems could not be evaluated. In order to demonstrate fully the capabilities of an adaptive system in a true aerospace environment, a program was initiated which would result in flight demonstrations in the X-15 airplane. The X-15 was selected both as the first such vehicle to be available and also as one which would constitute a severe test due to its range and rate of change of such parameters as natural frequency, damping, and surface effectiveness.

Although the primary purpose of the program was to test a self-adaptive technique in a true aerospace environment, it was decided to include in the system certain features which had come to be recognized

Declassified by authority of NASA
Classification Change Notices No. 143
Dated ** 2/14/62

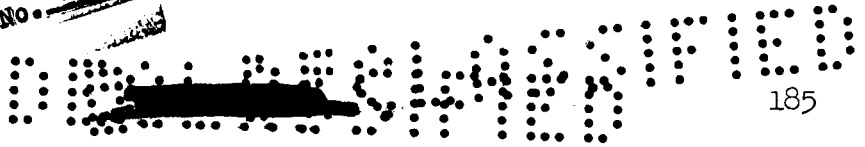


as important by-products of the self-adaptive concept. These features include dual redundancy provisions for reliability, integration of reaction and aerodynamic controls, rate command control, and simple outer-loop hold modes in attitude and angle of attack. Early in 1959 competition proposals were evaluated by the Flight Control Laboratory and the NASA, and as a result the contract was awarded to Minneapolis-Honeywell Regulator Company in June 1959. The MH-96 flight-control system was flown in prototype form in an F-101A at Minneapolis and in the X-15 simulator both at North American Aviation, Inc., and the NASA Flight Research Center; the system is currently installed in the X-15 airplane number 3. The system is expected to be flown in that aircraft this year.

An indication of the scope of the system is illustrated in figure 1. Some of the devices were not supplied under the contract but are standard X-15 items which are part of the overall flight-control system. These include the q-ball, which supplied angle of attack, and the stable platform, which is used for attitude reference. The heart of the system is the adaptive controller, which contains the electronic modules. Two separate rate gyro packages are shown; each contains three rate gyros. In this system basic damping augmentation is provided by attitude rate feedback in all three axes.

In order to provide a common basis for discussion, consider briefly the basic principles of the system operation (fig. 2). Commands are introduced to the actuators through conventional mechanical inputs and simultaneous electrical inputs proportional to stick displacement which are inserted in the pitch and roll channels. The electrical input to each axis is shaped by a simple network which has the dynamic response that is desired of the aircraft in that axis. In the X-15 airplane these networks (called models) are first-order lags with time constants of $1/2$ second in pitch and $1/3$ second in roll. Unfortunately, a single desirable invariant response is very elusive, since pilot opinion varies among pilots, and desirable characteristics for reentry are different from those for landing. Some consideration was given to a variable model but such a model has not been incorporated at this time.

If sufficient lead is added and the gain is increased enough, the remainder of the loop will have a transfer function which approaches "one." When this condition is reached, the response of the aircraft will be that of the model. This is the principle of operation of the MH-96. The gain is automatically increased until the system begins to oscillate at the verge of instability. The gain changer shown in figure 2 operates by monitoring the limit-cycle amplitude and adjusting the gain to maintain constant amplitude. The limit-cycle frequency is determined by the lead compensation and must be higher than the aircraft natural frequency but lower than the lowest aircraft structural frequency. On the X-15 airplane the limit-cycle frequency is approximately 4 cps. Variation in

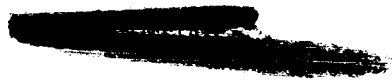


normal yaw-rate gain K_r and associated rudder activity δ_r is shown in figure 3. A tendency for the amplitude limit cycle to increase results in a gain reduction, whereas loss of the limit cycle initiates a gain increase. This characteristic gave rise to a problem which was noted during early simulator tests when a rapid decrease in controller gain was required by the rapid buildup of surface effectiveness during entries. Delays in the gain reduction, partly caused by the hysteresis in the control linkages, resulted in temporary oscillations as high as 3° , peak to peak, at the servo. Modification of the gain computer characteristics has improved the situation, but the problem has not been completely eliminated. There is a possibility, however, that this problem will be of no consequence during flight, since this same behavior was noted on the F-101 when it was used as a ground simulator, but during flight, air turbulence acted to prevent delays in gain reduction.

Another related problem on the X-15 simulator was servo motion reflected back to the stick. This reflection occurred because the servo velocity capability exceeded that of the actuator, so that feedback to the stick occurred and caused oscillations and stick kicks, which were particularly severe at the entry condition previously mentioned. In order to prevent these motions from closing the loop by putting additional inputs to the servos, electrical deadbands were placed in the control sticks and the servos were orificed to limit their velocity. Although this modification reduced the problem of reflected motion in the stick to a great extent, a related problem must be tolerated. In the X-15 airplane, it is possible for the servo velocity to exceed that of the actuator and thereby to allow the actuator to move at its rate limit. If this is the case, the surface is no longer producing the response requested by the servo, and the aircraft is unable to maintain the commanded rate (fig. 4). The symbols used in figure 4 are defined as follows:

- $\delta\phi$ control stick deflection in roll axis
- p rolling velocity
- δ_{aL} left-aileron deflection
- ϕ roll angle
- β sideslip angle

In the small roll step on the left of figure 4, vehicle response follows the model very well. In the large roll step, rate limiting occurs as evidenced by the slope of the surface position trace, and the response deviation from the model is significant. These deviations are reflected also in the coupled axes as evidenced by the large sideslip excursion. In some critical areas this excursion could result in loss of control.




This loss is characteristic of high-gain systems in areas of marginal controllability, however, and is best avoided by refraining from abrupt control inputs in such areas.

As was stated in paper no. 12 by Taylor and Merrick, it was found that an electronic filter was required in the SAS (stability augmentation system) to avoid exciting the lightly damped first bending mode of the horizontal stabilizer in flight. It became apparent that a notch filter would also be required to prevent a similar occurrence with the adaptive flight-control system. A breadboard notch was made on the basis of tests using the SAS and was tested on the X-15 simulator by using strain gages on the beams representing the horizontal stabilizers to provide a feedback similar to that on the airplane. Subsequent tests with the actual airplane made it plain that modes of higher frequency also needed to be filtered. The filtering requirements had now become so great that the associated phase lag at about 3 cps became a major concern. Insignificant limit-cycle oscillations had now become intolerable in all three axes. It is believed that significant progress toward the solution of this problem has been attained by the use of a higher-order filter and by reducing the minimum gains; however, activity in this area is continuing.

A control problem exists whenever motions about one axis couple into another. One solution involves the addition of cross control circuitry. Such an interconnect in the MH-96 commands a roll input proportional to yaw rate to combat the unfavorable effects of a high negative dihedral reported in paper no. 10 by Petersen, Rediess, and Weil. The inverse of this interconnect has been studied on the simulator to reduce the yaw-due-to-roll input with favorable results, but this installation has not yet been made in the X-15 airplane system.

Rate-command control is a feature of the system which has become controversial, particularly in the pitch axis. Rate command is achieved at the expense of the vehicle's affinity for a fixed angle of attack and dynamic pressure, thereby retracting a number of conventional flying qualities. Conventional X-15 trajectories are seldom, if ever, flown where pitch rate is maintained at a constant value and pitch rate is therefore a particularly vexing parameter to handle. The use of constant attitude (pitch rate = 0) or pitch-rate program entries is suggested and is currently being studied. In addition, trajectories may be flown by using the automatic-pilot assist modes and CSS (control stick steering), which are incorporated in the system.

Rate-command trim is an obvious companion to rate-command control and is used in this system. However, this type of trim is considered by some to leave something to be desired. Inasmuch as the servo authority in pitch is only about half the full surface authority from any trim position, automatic trim augments the servo authority by energizing the



trim actuator any time the servo is displaced more than 2° from center so that the servo is permitted to return to center. This technique, which is installed primarily to provide satisfactory outer-loop operation, permits nearly full servo authority for damping and full surface authority for control but invites undesirable cycling. Trim rate has been reduced to minimize cycling in the low dynamic-pressure regions. This disconcerting phenomenon still exists throughout the envelope, however, as is shown in figure 5.

An angle-of-attack ramp is shown with the servo and surface cycling due to trim follow-up. In addition, the control-linkage movement associated with trim follow-up causes cockpit stick movement resulting in occasional inadvertent pilot inputs.

In the development of the MH-96, Minneapolis-Honeywell has made considerable advances toward solving the problem of automatic aerodynamic and reaction control blending. In its present form, the system will allow operation of the vehicle throughout the complete mission with either the right-hand or center stick. The present left-hand stick is retained so that the reaction controls may also be fired manually if desired.

The self-adaptive system provides a simple controls blending technique (fig. 6). The symbols used in figure 6 are defined as follows:

h	altitude
K_q	pitch-rate gain
\dot{q}_{RC}	pitching acceleration due to reaction control
δ_h	horizontal-tail angle
\bar{q}	dynamic pressure

When the gains in all three axes reach 80 percent of maximum, the reaction-control channel is activated. The solenoid valves, which are actuated by electrical commands from the pilot, will not, however, fire until needed; a deadspot upstream allows the aerodynamic controls to be used to the fullest extent to maintain constant response until the pure ballistic condition is approached; then, the thrust limitations of the reaction jets cause a slower response. Even here, however, the rate feedback will provide damping and rate-command operation. On entry, when the gains have fallen to 60 percent of maximum, the reaction-control channel is deactivated. The lower percentage was selected because simulator experience showed that occasional servo activity in the ballistic regime could lower the gain and thereby deactivate the reaction controls.

A significant control-system feature is the redundancy configuration selected to provide the generally incompatible objectives of reliability and fail safety (fig. 7). Extremely high reliability is a requirement because of the low probability of a successful entry from high altitude without augmentation. Fail safety is equally important since a large transient introduced in a high dynamic-pressure region would result in destruction of the vehicle. Completely dual damper channels, where either or both channels may control the axis, are provided. The adaptive feature of the circuitry permits one channel to be lost with little or no loss in system performance, since the remaining gain changer will attempt to provide the additional gain required for limit-cycle appearance. The gain computers are interlocked, when operative, to prevent overcritical gain following a limit-cycle circuit failure and to provide the desired limiting effect for hard-over failures. In the case of model or variable-gain amplifier failure, conventional monitor circuits which disengage both channels were required. This problem combined with the desire of NASA for increased system flexibility led to the addition of parallel fixed gain channels with fail-safe passive circuitry. Since these channels operate simultaneously with the adaptive channels to avoid the reliability and transient penalties of switching, they effectively limit the minimum gain for adaptive operation. These gains must be sufficiently high for satisfactory emergency performance throughout the envelope but must be below critical in the high dynamic-pressure regions. A successful compromise has not been entirely achieved, and the expected flight envelope has been somewhat reduced. Reliability models indicate a damper mean time between failures (MTBF) of 360 hours and a system MTBF of 200 hours. The basic limitation is the servos which have no duality. This compares with a stability augmentation system MTBF of 100 hours. It is interesting to note that the adaptive electronics have a predicted MTBF of 100,000 hours.

The flight-test program is planned so that the MH-96 flight-control system can be demonstrated throughout the X-15 flight envelope and accepted in the shortest possible time consistent with flight safety. A comparison of the handling qualities using the MH-96 flight-control system will be made with the handling qualities using the fixed gain of the stability augmentation system, wherever possible. The evaluation will use many of the same maneuvers performed earlier with the basic control system, including SAS. Conditions of primary interest will be: high dynamic pressure for limit-cycle characteristics, low dynamic pressure for reaction-control operation, and rapidly changing dynamic pressure for gain-changer operation. The program plans are illustrated in figure 8, where the flight sequence is indicated by the circled numbers. The first two flights are planned to evaluate the basic adaptive inner loop and fixed gain operation at moderate dynamic pressures. Outer loops and limiting functions will also be investigated. The third flight to high speed and high dynamic pressure will investigate high angle-of-attack stability. Flight 4 is planned to investigate the low dynamic-pressure region including reaction-control operation. The next flight


objective is the completion of two similar high-performance flights (5 and 6) to 250,000 feet with all portions of the flight-control system operative. Satisfactory system performance on these flights will complete the contractual requirements. The detailed flight research program will be conducted so as to provide comparisons with other control system concepts and to permit determination of the actual value of such concepts as variant response, rate command, and blended controls. Since the system theoretically maintains aircraft controllability to higher angles of attack than does SAS, flight verification is certainly an early objective, since the possibility of extending the altitude capability of the airplane is thereby introduced.

Although the flight-control system is "self-adaptive," and much speculation and some claims have been made about learning machines and self-designing control systems, the system installed in the X-15 by no means developed itself. Although the present self-adaptive technique obviates the need of air data for gain adjustment, it does not eliminate the requirement during design of the system for accurate knowledge of the vehicle sensors, control linkages, structural flexibility, and aerodynamic parameters. In general, however, the self-adaptive feature makes this control system much less sensitive to these factors than conventional systems. The high gain of the system, however, and the requirement for making some performance measurement for self-adaptation cause problems of their own, particularly when combined with peculiarities, such as linkage slop, of the X-15 airplane.

Although the self-adaptive system is a considerable advancement and is being directly applied with minor changes to Dyna-Soar, it is obvious that it is not the last word. This type of system has definite limitations in the amount and type of variation of dynamics it can control, and it still requires a knowledge of the form of the system equations and of the approximate numerical value of system coefficients.

In general, future effort will be directed toward providing methods of design and techniques of control which will permit the designer to build a better control system with less knowledge of the vehicle under control. This is not to say that the designer will not use all available information (or even that all applications require an adaptive system): but it is an attempt to provide systems less dependent on a priori knowledge for successful operation.

In summary, a self-adaptive flight control system is now ready to be flight tested in the X-15, an aircraft whose range of stability, damping, and surface effectiveness will provide a fair challenge to the adaptive concept. A number of problems have been uncovered during the development phase, some of which may be attributed to tailoring the system to the eccentricities of the X-15. These problems, in general, result in degraded system performance due to inherent system constraints



GAIN OPERATION AND SURFACE ACTIVITY

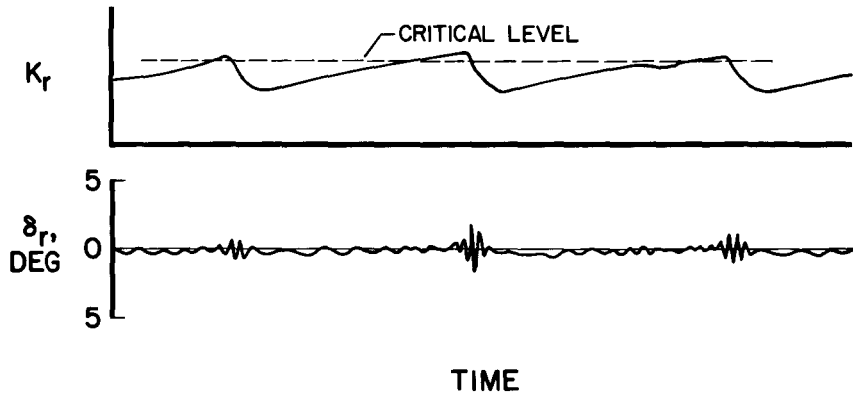


Figure 3

SURFACE RATE LIMITING X-15 SIMULATOR

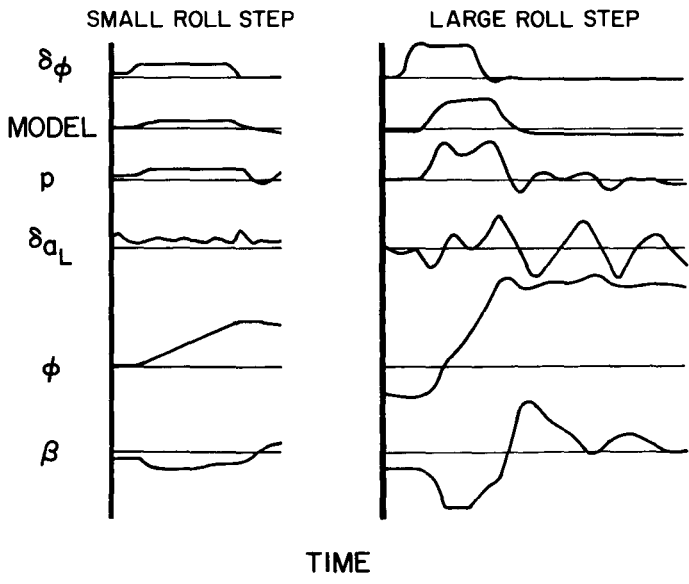


Figure 4



TRIM FOLLOW-UP FEEDBACK

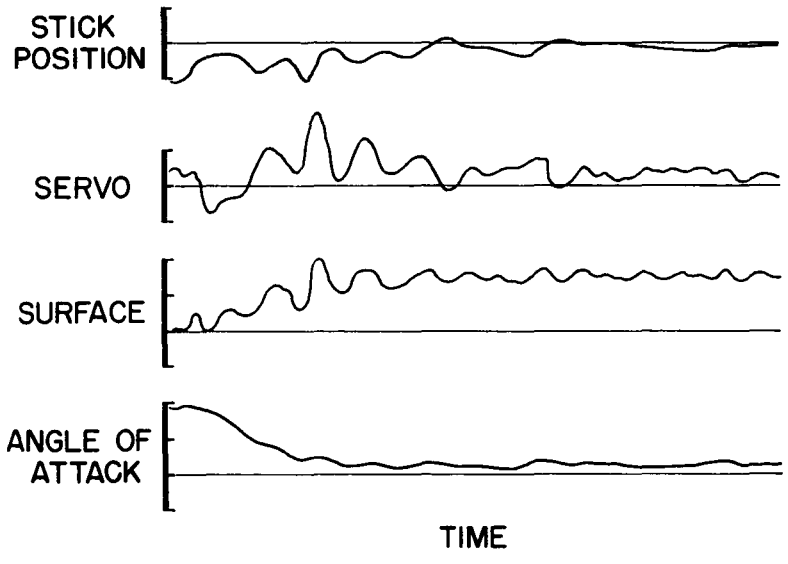


Figure 5

CONTROLS BLENDING

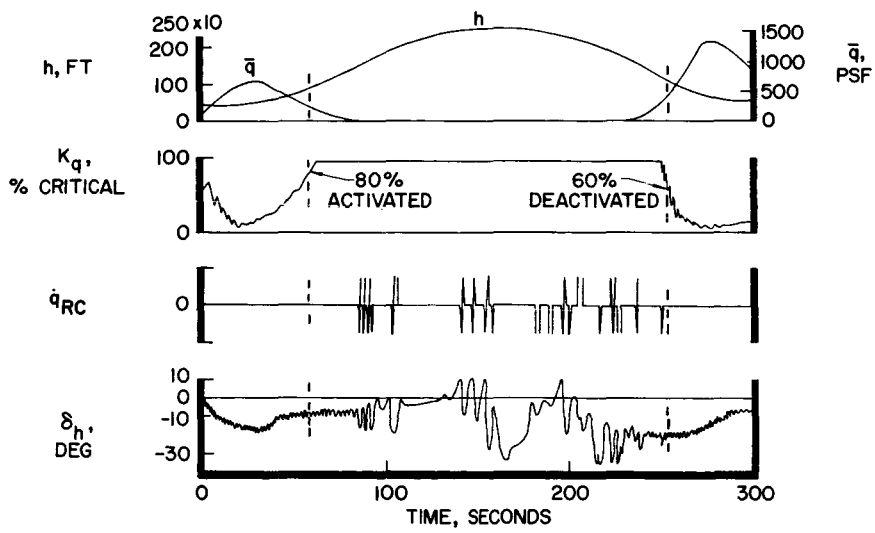


Figure 6

0371001070

N71-75457 195

14. FLIGHT CHARACTERISTICS OF X-15 HYPERSONIC

FLOW-DIRECTION SENSOR (L)

By William D. Mace
NASA Langley Research Center

and Jon L. Ball
NASA Flight Research Center

INTRODUCTION

The expansion of the X-15 powered flight regime beyond Mach numbers of about 3 has required the installation of a specially designed sensor to measure the angles of attack and sideslip. The vane-type sensor commonly used for this purpose is not suitable because of the high temperatures and low pressures encountered by the airplane. Generally speaking, these measurements are required to aid the pilot in the conduct of the flight, particularly during reentry, and also to provide the basic flight data necessary for research purposes.

Based on the conceptual design work done by the NASA, a contract was awarded to the Nortronics Division of the Northrop Aircraft Corporation for the detail design and construction of a prototype and several operational sensors. The characteristics of the prototype model were described at the July 1958 conference on the X-15 airplane. The purpose of this paper is to discuss the experience that has been obtained through the use of this sensor during flight testing of the airplane.

SYMBOLS

C_{NA} normal-force coefficient

M Mach number

P_1, P_2 specific pressures

$\Delta P = P_1 - P_2$

P_T total pitot pressure

T temperature

14

α	angle of attack
β	sideslip angle
γ	flight-path angle
θ	pitch attitude angle
ψ	angular position behind stagnation point

DISCUSSION

The high-temperature flow-direction sensor installed on the nose of the X-15 with the afterbody cover removed is shown in figure 1. The physical size of the instrument is about $16\frac{3}{4}$ inches long, with a ball diameter of $6\frac{1}{2}$ inches, and a base diameter of $13\frac{3}{4}$ inches. The unit weighs about 78 pounds. The internal temperature of the sensor is controlled through the use of liquid nitrogen. The coils through which the coolant circulates are visible in the photograph.

In operation, the sensor is a null-seeking hydraulically actuated, electronically controlled servomechanism. A block diagram of the mechanization scheme employed for control of the sphere is shown as figure 2. Two identical servos are used for independent control in each axis. The servo for only one axis is shown in this figure. The differential pressure between opposing orifices is measured, and the unbalance signal is fed through amplifiers to the hydraulic actuator; this actuator then positions the sphere to balance this differential pressure. The sphere position then is a direct indication of the angle of attack. A synchro transmitter is used to detect the position of the sphere with respect to the airframe, and this signal is fed through an isolation amplifier to the onboard indicating and recording instruments and also to the telemetry link.

Since the dynamic pressure can vary from about 1 pound per square foot to 2,500 pounds per square foot, compensation is required in the servo loop to maintain stability and accuracy. This compensation is provided by measuring the pressure difference between the total-pressure port and one of the angle-sensing ports; the resulting signal is used to adjust the gain in the sphere-positioning servo loop.

The operating characteristics of the sensor are as follows: Range from -10° to 40° in angle of attack, $\pm 20^{\circ}$ in sideslip, and an accuracy based on ground tests within $\pm 0.25^{\circ}$. The unit is capable of continuous

operation at a skin temperature of 1,200° F. The response of the system is essentially flat to about 6 cycles per second, with a maximum velocity limit of about 85° per second.

Since the first sensor was delivered in December 1960, one of them has been installed on each of the 22 flight attempts. Early flights and ground tests indicated several modifications to be desirable to increase the reliability of the instrument. Among these have been the installation of improved, more reliable liquid nitrogen valves, modification of the actuator design to eliminate fluid seepage through a static seal, and the addition of a flow-limiting orifice in the liquid nitrogen line.

A summary of the flight test experience is as follows: There have been 15 drops in 22 attempts with the sensor mounted on the aircraft. Sensor operation has been completely satisfactory on 11 of these drops. On three flights, unwanted oscillations occurred; however, usable data were obtained. These oscillations were caused by feedback from the synchro recorders used initially. Installation of the servo recorders originally intended for this purpose has eliminated this trouble area. And finally, there has been one case in which the sensor response was very poor in one axis. This incident occurred only once during one of the early flights and, as yet, the cause has not been determined. The flight test envelope encompassed by these flights has been discussed in previous papers in this conference.

Figure 3 is representative of the time history of thermocouples located on the sphere. The cooling system provided to maintain the interior temperature at 120° F has not been required on any of the flights to date. The cooling system has cycled, however, but this was a supply-line cooling cycle that maintains liquid nitrogen at the sensor. Maximum temperature measured to date is about 1,100° F.

Now that the flight data have been obtained, the question logically arises, "How good is it?" Since ground facilities with which to test full-scale sensors in the flight environment were not available, other methods of assessing its operating characteristics must be relied on.

These characteristics may be inferred by examining the spread in parameters, such as normal-force coefficient, that have been computed by using in-flight data. (See fig. 4.) This figure presents a comparison between the values of C_{NA} as obtained from vane boom data and ball nose data. Wind-tunnel test results are represented by the solid line. These flight data are a compilation of these values as computed for the same flight conditions for several flights. The spread in the sensor data is less than 1/4° and is in very good agreement with wind-tunnel data at the four Mach numbers shown.

[REDACTED]

In the 1958 conference on the X-15 airplane, a figure was presented that gave the anticipated accuracy of the sensor for dynamic pressures ranging from 1 pound per square foot to 2,500 pounds per square foot. (See fig. 5.) This plot was based on analytical work as well as on tunnel tests on the prototype sensor. In this figure flight data have been superimposed on this plot in the low-dynamic-pressure region. These flight data provide a comparison of the angle of attack as measured by the sensor with the angle of attack as computed by using pitch attitude obtained from the inertial platform and the flight-path angle as derived from radar information. On this basis the maximum difference is less than $3/4^{\circ}$ at a dynamic pressure of 3.5 pounds per square foot.

Since the delivery of five sensors to the NASA Flight Research Center, it is estimated that the equivalent of the full time of one man has been required to maintain and use them. Much of this time has been spent in becoming familiar with the unit. Frequent disassembly and inspection operations have been accomplished to ferret out potentially weak areas and to build confidence in its reliability.

Since the completion of the design effort on this device, some attention has been given to the feasibility of incorporating some modifications with the view of increasing the versatility of the system. For example, the pressure distributions around the sphere have been examined analytically and to some extent experimentally to determine whether stream static pressure could be derived from measurements of the sphere surface pressures. This work indicates that this approach is feasible provided suitable transducers are obtainable.

These studies are by no means complete and further work in this area, particularly in the tunnel testing phase, is anticipated.

CONCLUSIONS

In conclusion then, the flow-direction sensor developed for the X-15 program has been flight tested and has met the design objectives. Although there are some refinements required to optimize the design, for example, increasing the stability margin in the servo to reduce or eliminate limit cycle effects, they are considered to be of a relatively minor nature and do not compromise the sensor operation. Additional work is being done with the view of increasing both the reliability and the versatility of the instrument.

NASA SENSOR INSTALLED ON THE X-15 AFT CONE REMOVED

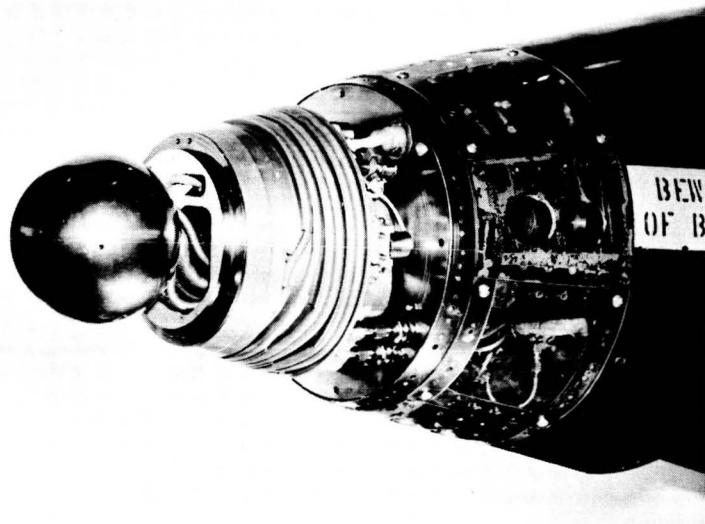


Figure 1

SENSOR MECHANIZATION α OR β AXIS

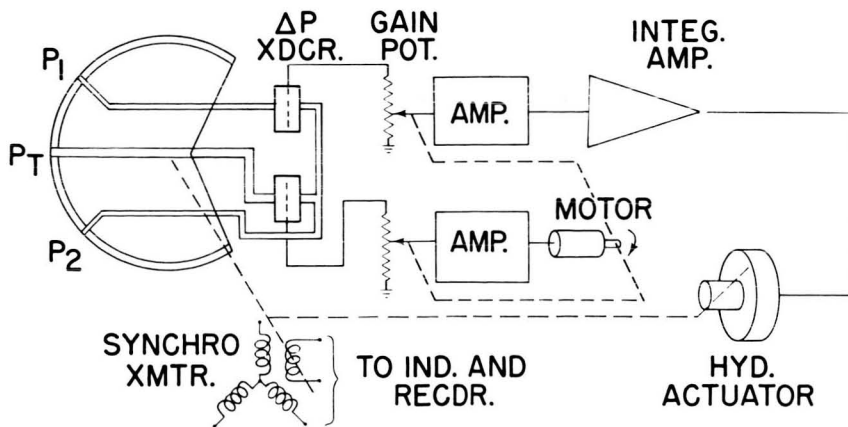


Figure 2

NASA SENSOR SPHERE TEMPERATURES
 MACH NUMBER=5.27 ALTITUDE =107,700 FT

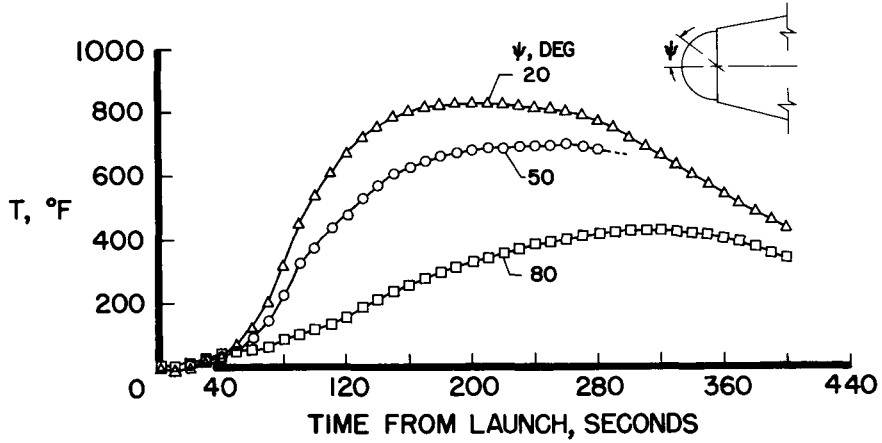


Figure 3

VARIATION OF NORMAL - FORCE COEFFICIENT
 WITH ANGLE OF ATTACK

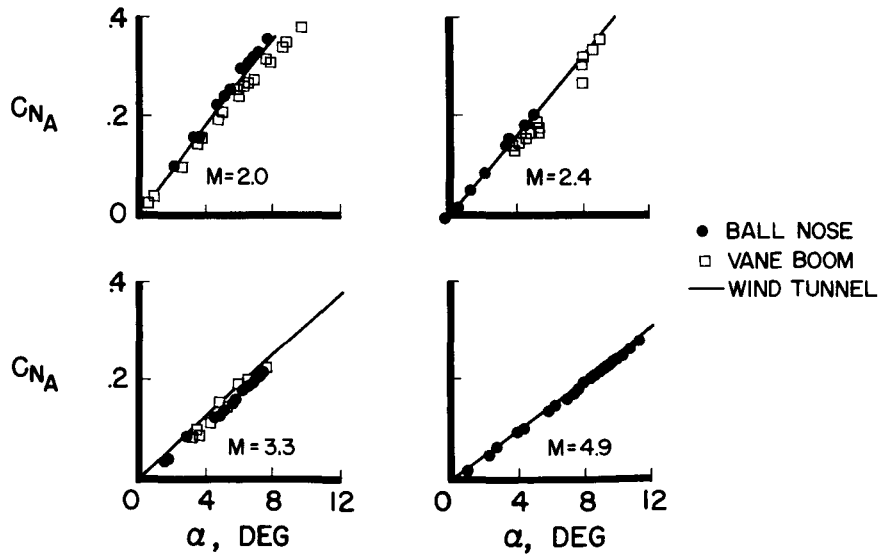


Figure 4

COMPARISON OF ANGLE-OF-ATTACK MEASUREMENTS
AT LOW DYNAMIC PRESSURE

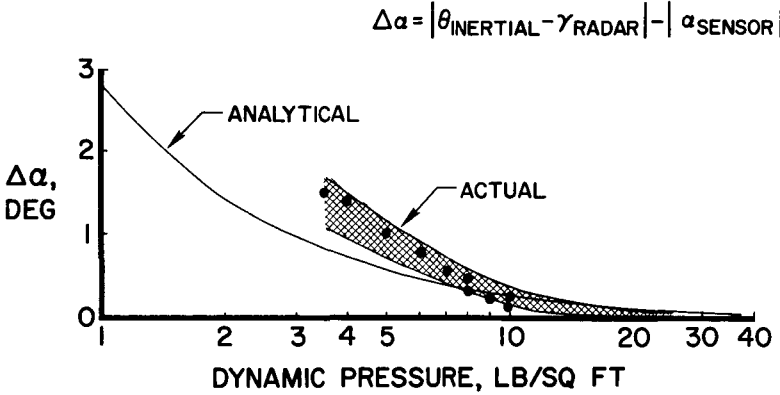


Figure 5



CONFIDENTIAL 205

15. FLIGHT EXPERIENCE WITH X-15 INERTIAL DATA SYSTEM (U)

By Jay V. Christensen
NASA Ames Research Center

and John A. Dodgen
NASA Langley Research Center

N71-75458

INTRODUCTION

The X-15 inertial data system was described in some detail in a paper by M. L. Lipscomb and J. A. Dodgen presented at the July 1958 Conference on the X-15 airplane. The primary reasons for selecting the inertial data system were discussed in that paper. It will be of value to review the system and the more important experience obtained in using the inertial data system in the X-15 program. Areas that are reviewed include those of system modification, alinement experience, reliability, confidence determination, and flight performance.

15

DISCUSSION

The inertial data system was selected to provide the operational and research measurements shown in table I. The accuracies selected represent a compromise between the data desired, the X-15 weight and size restrictions, and the inertial state of the art of the time. The measurements required for pilot displays are the attitudes, height, total velocity, and vertical velocity.

Within 300 seconds after launch, pressure instruments are adequate for vehicle height- and velocity-control data. This is a short amount of time compared with the hour or more that may be required in reaching the launch point. An all-inertial operation from take-off to touchdown would have required a system too heavy and large to be practical for the X-15 operation. An inertial data system with radar damped, in-flight alinement techniques was selected to provide a capability of 300 seconds of velocity and height data and 20 minutes of attitude data. This approach allowed both performance and equipment weight and size to meet the X-15 requirements and was within the state of the art.

Figure 1 shows the integrated system. The inertial data system is basically an earth-slaved, Schuler-tuned, system alined in azimuth to an equivalent guidance equator which is coincident with the radar-range center line of the X-15 airplane. Attitudes, velocities, and height are presented to the pilot with reference to this coordinate system. Major

Preceding page blank

X-15 components include the stabilizer, computer, and pilot's displays. The stabilizer utilizes three self-balancing accelerometers and three single-degree-of-freedom gyroscopes. A four-gimbal system provides complete attitude freedom in all axes. A direct-current analog computer is used for computing velocity and position data and the necessary acceleration corrections. An AN/APN-81 Doppler radar is used as a horizontal velocity reference for alinement to the vertical during carried flight. An N-1 compass is used during the straight and level portions of the carried flight for the heading reference. An NASA pressure instrument is used for the vertical-velocity reference. Position data for confidence checks and initial conditions are obtained from ground radar and a B-52 pressure altimeter. The control panel provides mode control and system performance monitoring and also processes reference information for use in the computer. The selection of this type of inertial system was a joint NASA-U.S. Air Force effort and resulted in a contract with Sperry Gyroscope Co. in June 1957 to build the all-attitude flight data system portion, which included the stabilized reference package, the computer, the pilot's velocity and position read outs, and the B-52 control panel.

Experience has shown that the initial conditions obtained during the in-flight alinement have to be accurate to the design tolerances shown in table II if the required flight-data accuracy is to be obtained. Also, it is quite evident that the flight-data accuracy is not only a function of the X-15 component accuracy and reliability, but it is directly dependent on the accuracy and reliability of the carrier-airplane reference system. The reference-system accuracy not only depends on component design and maintenance, but it is a direct function of the dynamics of the flight profile. Because of the dynamic response of the reference system, it is difficult to maintain the accuracy during climbs and turns. The launch pattern requires a turning climb with a 180° turn just prior to launch. The reduction of adverse effects resulting from this profile required considerable flight experience in developing adequate procedures and control techniques. The effort required in solving this problem has been greater and more important than was originally anticipated.

The operational development of the system will now be discussed. To date a number of engineering modifications have been made to the basic flight data system; however, many of these modifications have been minor and the total effort in this area is reasonable considering the complexity of the equipment. The two hardware modification areas that are discussed are those desired for component improvement and those desired to allow changes in operational and alinement techniques.

In order to provide a more comfortable thermal safety factor in the stabilizer, all critical germanium transistor amplifiers were

changed to silicon. A gyroscope failure at NASA Flight Research Center originally required a stabilizer turn-around at the contractor's facility that would take the unit off flight status for 3 to 6 weeks. In order to insure availability of flight-status units at Flight Research Center, a gyroscope of better quality was substituted. In addition, Flight Research Center has developed a complete repair capability including gyroscope changes. The reference-velocity resolving circuit in the B-52 control panel was modified to minimize alinement errors resulting from transient errors in the heading reference. The velocity indicators were modified to provide a better thermal safety margin with respect to summer operating temperatures.

The more important hardware modifications required by changes in operational and alinement techniques are as follows: (1) cooling capability for ground and taxiing operations, (2) logic circuit for turn-on protection, (3) simulated Doppler velocity reference, (4) slaving time-constant change, (5) ground gyro calibration, (6) ground heading reference, and (7) independent control of alinement loops.

Because cooling for ground and taxi operations was not available, the B-52 airplanes had to be modified to provide this capability. Without cooling and consequently without ground alinement, qualitative evaluation of system performance was not possible during the first 9 months of flight operations.

Originally, inadvertent power application during ground operation could result in seriously damaged units as a result of the ensuing stabilizer tumble and system operation without cooling. A logic circuit was installed and has provided very valuable system protection.

As a result of Doppler reliability problems in the X-15 program, it was necessary to provide a simulated reference velocity for in-flight alinement in case the Doppler failed. This modification has proved to be a very valuable one. When this simulated reference was used, it provided inertial attitudes in every case and in some cases the velocity and height data have also been usable.

Because of transients and dynamics in the reference systems during carried flight, the time constants of the alinement loops were changed and gyro calibration during flight was discontinued in favor of ground gyro calibration prior to taxi. Flight operation is now conducted with the ground-derived calibrations.

The N-1 compass system proved inadequate as a heading reference during ground operation because of errors induced by moving ground equipment and fluctuating electrical loads. Ground heading alinement is now determined by using surveying techniques and is set into the system by using an adjustable synchro reference. The investigations,

[REDACTED]

modifications, and flight checking of modifications had to be carried out on active research flights. Deviations from standard procedures to help isolate inertial-system problems have not been possible. In order to help isolate system-integration problems, an inertial flight-test program utilizing one of the carrier airplanes was initiated in January of 1961. This program substitutes a pod containing the flight data system instead of the X-15 airplane under the pylon of the B-52 airplane. This allowed use of the actual equipment and wiring in the test program. This program is semiactive and has provided worthwhile systems experience.

The original concept was to control all alinement loops simultaneously. Flight experience showed that this concept was not optimum. The basic problem was the transient errors introduced in the reference systems by the B-52 flight profile. These errors resulted in certain periods during which the flight data system was more accurate than the reference systems. Modifications now allow independent automatic and manual control of each alinement loop. A significant increase in system performance has resulted.

Figure 2 shows a direct comparison between inertial velocity data and radar data which were taken from the nineteenth flight of the number 2 X-15 airplane.

Figure 3 illustrates a time history of the mean total velocity difference between the two measurement systems, and was obtained from five flights since July 1961. The smoothed radar data over the X-15 profile have an uncertainty figure of about 75 ft/sec. The inertial data recording technique has an estimated uncertainty of 60 ft/sec. The total root-mean-square measurement uncertainty, shown by the dashed line, is approximately 90 ft/sec. Most of the points fall below the uncertainty level and indicate performance approaching the design specification of 70 ft/sec. This accuracy is well within the X-15 control requirement.

Figure 4 shows a direct comparison of inertial-height data with radar data and was taken from the nineteenth flight of the number 2 X-15 .

Figure 5 is a time history of the mean height difference between the two measurement systems. The data were obtained from five flights since July 1961. The smoothed radar data over the X-15 profile has an uncertainty figure of 1,500 feet. The inertial data measurement technique has an estimated uncertainty of 1,600 feet. The total root-mean-square measurement uncertainty, shown by the dashed line, is approximately 2,200 feet. These data indicate performance which is approaching design specifications and is adequate for aircraft control.

The height divergence which is a characteristic of the vertical loop in all pure inertial systems can be observed in figure 4. The

divergent characteristic of a height-measuring loop in a pure inertial system will be a limiting factor in advanced vehicle applications.

Table III summarizes the complete inertial data system experience since March and July of 1961. The evaluation criterion used is the following: Did the pilot have inertial data presented to him which were adequate for vehicle control? The inertial velocity and height data reflect component and reference system reliability problems, as well as poor initial conditions resulting from operational problems. As an example, the inertial height percentage of 64 represents 4 non-specification flights out of 11, which were the results of an indicator failure, a Doppler radar failure, a stabilizer failure, and one bad flight resulting from initial conditions being out of design specification at the launch point. The velocity percentage of 73 reflects an indicator failure and the same Doppler radar and stabilizer failure just mentioned.

On the six flights since July 1961, the system has demonstrated control quality measurement capability and has very closely approached the design specifications as well. This is illustrated by the second column of percentages. These percentages reflect a continuing improvement in accuracy and reliability as operating, calibrating, and maintenance procedures are refined and unreliable items are eliminated.

Table IV illustrates component reliability since March 1961. The major components listed were classified as having a malfunction if any subcomponent failed in flight in such a manner as to be detected by even minor system performance degradation. Personnel experience and quality control improvements have been the most important factors in improving component reliability.

The important problem of establishing confidence in the system prior to launch and during actual flight will now be considered. At the present time, the inertial attitudes have to be usable or the launch is cancelled. Also, the inertial velocity and height are so desirable that an evaluation of the accuracy of these parameters must be made prior to launch. To provide the pilot with this information is a necessity and is the objective of a series of confidence checks. During carried flight these checks require a close monitor of system outputs in terms of velocity, position, and attitude. For example, inertial total velocity is compared with the B-52 Doppler velocity, inertial height with pressure altitude, and the inertial positions with ground radar positions.

The final attitude evaluation is left to the pilot. If the velocity and position checks confirm that system operation is good, the attitude reference will be accurate to within minutes of arc, but the pilot still checks to establish confidence and confirm the indicator operation.

[REDACTED]

After launch the ground controller transmits velocity and height information from ground radar read outs, and the X-15 pilot cross-checks the inertial indicators to obtain an estimate of system performance in terms of the accuracy and the rate of error propagation. Using these confidence checks, the pilots have demonstrated that they can correctly evaluate the quality of the inertial data.

The problem of evaluating the condition of an inertial system before and during actual flight and determining what data can safely be used for vehicle control is one that is not only important to the X-15 program, but one that will become increasingly important in manned space-vehicle operation. To provide procedures and read outs that will give the pilot confidence in the inertial data is an important part of this problem.

CONCLUDING REMARKS

In conclusion, the flight data system can provide the vehicle-control data for which it was intended, dependent upon the reliabilities of the reference and data systems. The accuracies required from the in-flight alignment appear to be about the best that can be obtained with reasonable operating requirements and procedures. Operational experience with the integrated system has been very important because the more important modifications and techniques were not developed until considerable experience was obtained with the complete system.

The X-15 airplane needs an inertial system to furnish control data as the flight-test envelope continues to expand. It may later be able to make a contribution to the inertial technology by serving as a test-bed for the development of inertial systems for more advanced research vehicles. This potential is presently being investigated. The X-15 airplane is but the first of a number of manned vehicles that will use inertial equipment to fulfill control and guidance requirements.



TABLE I.- MEASUREMENT SPECIFICATIONS

[Time duration: 300 seconds]

Measurements required	Range	Accuracy, rms
Attitude angles, deg . . .	Unlimited	0.5
Height, ft	^a 0-500,000	5,000
Velocity:		
Total, ft/sec	^a ±7,000	70
Down range, ft/sec . . .	^a ±7,000	50
Cross range, ft/sec . .	^a ±3,000	50
Vertical, ft/sec	^a ±5,000	20

^aRequired for pilot displays.

TABLE II.- INITIAL-CONDITION REQUIREMENTS

	Accuracy	Reference
Height	250 ft	Pressure altimeter
Range velocity	10 ft/sec	Doppler radar
Cross-range velocity	10 ft/sec	Doppler radar
Vertical velocity	2 ft/sec	NASA pressure rate of climb
Azimuth	1/2 deg	N-1 compass

TABLE III.- INERTIAL FLIGHT-DATA EXPERIENCE

Initial measurements	Acceptable flight-data percentages since March, 11 flights	Acceptable flight-data percentages since July, 6 flights
Attitude	100	100
Inertial speed	73	100
Inertial height	64	83

TABLE IV.- FLIGHT EXPERIENCE - INERTIAL COMPONENTS RELIABILITY

Component	Reliability percentage, 11 flights since March 1961
Attitude indicator	100
N-1 compass	100
Vertical velocity reference	100
Precision power	100
Cage control	100
Computer	100
Wiring	100
Total velocity indicator	91
Height indicator	91
Control panel	91
Stabilizer	91
Doppler radar	82



INTEGRATED SYSTEM

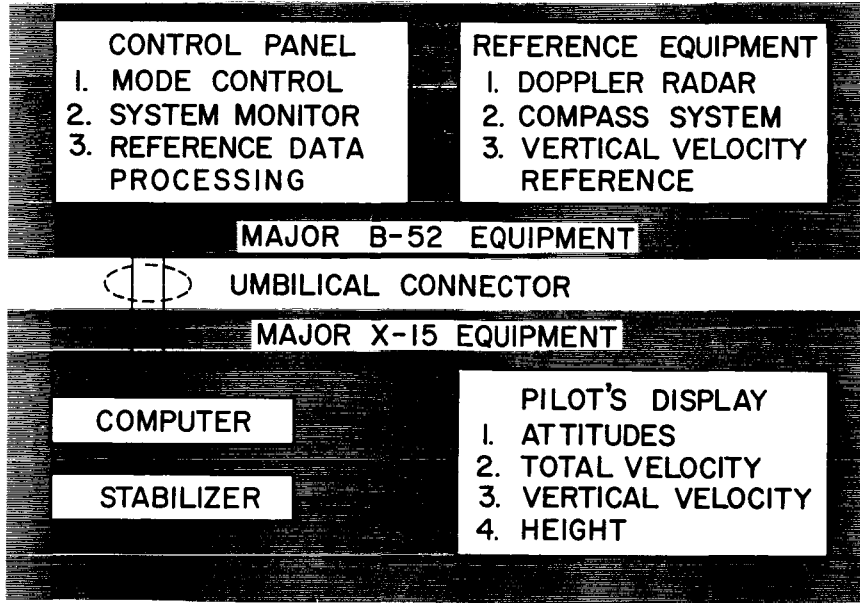


Figure 1

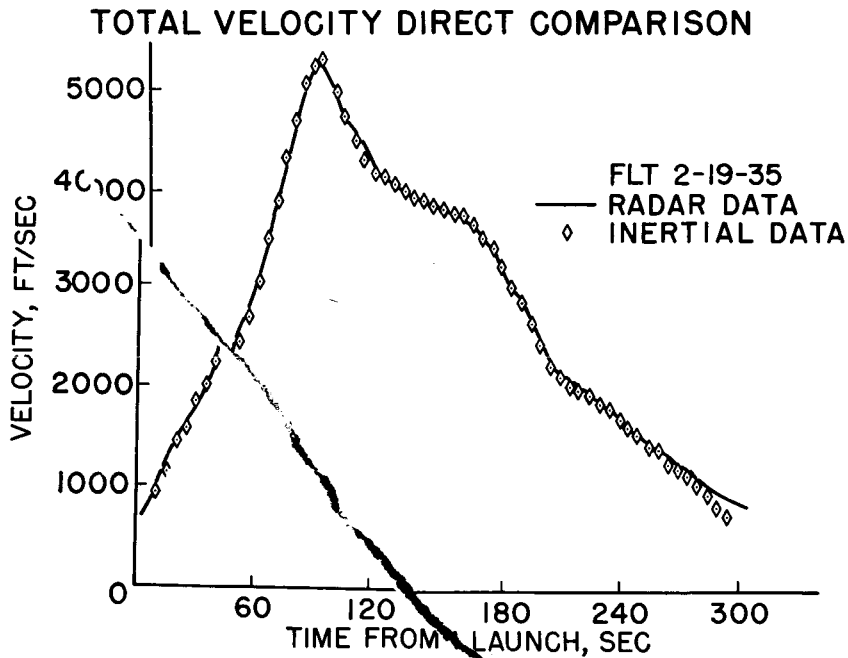


Figure 2

MEAN TOTAL VELOCITY DIFFERENCE INERTIAL VS RADAR 5 FLIGHTS

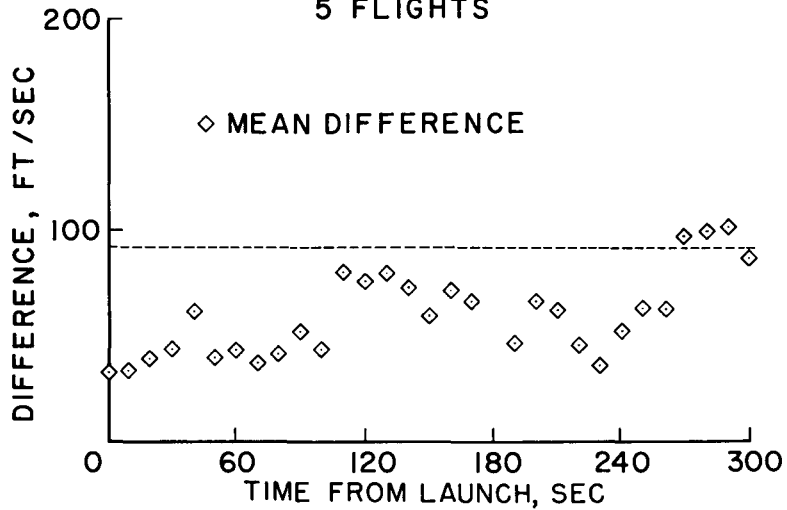


Figure 3

HEIGHT DIRECT COMPARISON

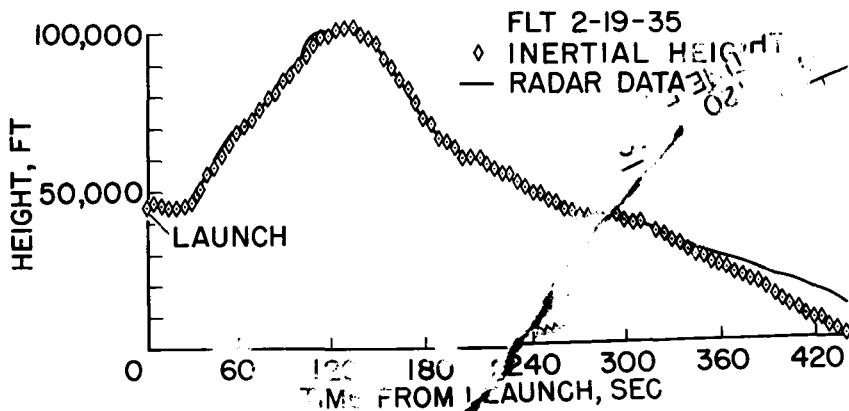


Figure 4

ORIGINAL PAGE IS
OF POOR QUALITY

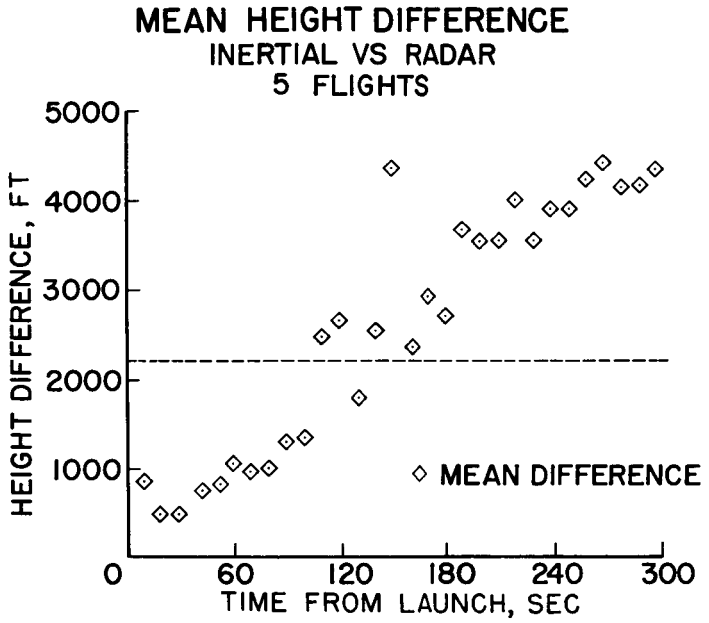


Figure 5

REF ID: A615

16. XLR99 ENGINE OPERATING EXPERIENCE (U)

By Richard G. Leiby
Air Force Flight Test Center

N71-75459

Donald R. Bellman, and Norman E. DeMar
NASA Flight Research Center

INTRODUCTION

The XLR99-RM-1 rocket engine, which was developed specifically for the X-15 airplane, is the largest rocket engine designed from the outset for use in a manned vehicle to be completely controlled by the crew. In order to provide the desired safety and controllability required by the X-15 mission, many unique features were included in the design. Delays in the development of the engine required that the initial X-15 flights be made with an interim engine. However, the first flight with the XLR99 was made in November 1960, and the engine has been used in government flight operations since February 1961. Since the first flight, fifteen flights have been made with the XLR99. This paper summarizes the XLR99 operating experience during the flight program.

GENERAL DESCRIPTION

The procurement specification of the XLR99 presented a number of special requirements listed as follows: Minimum hazard, variable thrust, multiple restart, prelaunch idle, and long life. These requirements are beyond those heretofore normally expected of a rocket engine. They resulted in additional complexity but also provide the engine its unique capabilities. In defining "minimum hazard," the single malfunction concept was employed. The XLR99 was designed so that, under any single condition of malfunction, the engine would create no hazard to the airplane. This safety concept was demonstrated analytically by malfunction analysis and empirically through 47 malfunction tests during the Preliminary Flight Rating Test (PFRT).

The XLR99 provides variable thrust over a continuous range from 50 percent to 100 percent of rated thrust and is capable of more than five restarts without servicing. The turbopump and both igniter stages are operated as an idle mode before launch, so that an operational check of over 90 percent of the engine's components is provided prior to commitment of the X-15 to free flight.

Preceding page blank

16

Of particular interest to the X-15 program is the requirement of long life. The engine life requirement is compared in figure 1 with that for missile engines. In its application as an aircraft engine, the XLR99 was required to accumulate one hour of operation or 100 starts without overhaul, far beyond normal rocket engine life. Note that a logarithmic scale is used. The top shaded area indicates the spread in engine life that is actually being encountered. The design requirement is shown by the point. Data on the present engine are as follows:

Propellants

Engine - liquid oxygen and ammonia
Pump - 90 percent hydrogen peroxide

Dry weight - 910 pounds

Specific impulse

Sea level - 230 seconds
45,000 ft - 265 seconds

Rated thrust

Sea level - 50,000 pounds
45,000 ft - 57,000 pounds

Expansion ratio (area) - 9.8

Rated chamber pressure - 600 psia

Altitude - all altitudes

Attitude - all attitudes

The altitude values of thrust and specific impulse are the more significant since in the research flights the entire period of engine operation takes place at and above this altitude. Engine starts have been demonstrated in the altitude facility of the Arnold Engineering Development Center at altitudes up to 70,000 feet; however, the engine has been designed to operate at any altitude. In regard to attitude, engine operation has been demonstrated at 90° climb, 30° dive, and 45° left and right roll. The engine is shown in figure 2. A 6-percent increase in thrust and efficiency could be achieved through addition of a nozzle extension to expand the gases to an altitude equivalent pressure of 45,000 feet rather than the present 19,000 feet equivalent pressure. However, such a change would result in a significant weight increase with concomitant center-of-gravity effects.



TESTING BACKGROUND

The first complete, flight engine configuration was fired in February 1958, and the Preliminary Flight Rating Test was completed in January 1960. During this program more than 500 minutes of engine operation and over 640 starts were accumulated on 14 engines, utilizing three test stands at the Reaction Motors Division, Thiokol Chemical Corp. The Edwards Propulsion System Test Stand (PSTS), (fig. 3), began operations with the XLR99 in June 1959. This test facility consists of a complete X-15 propulsion system and provides a capability for engine checkout, pilot and maintenance crew familiarization, and limited development firings. To date, over 300 firings have been made in the PSTS. As final confirmation of flight readiness, ground runs in the X-15 at the PSTS facility permit an integrated systems checkout.

PERFORMANCE ACHIEVED

The XLR99 is now operating successfully in the X-15. However, delays in the development program schedule resulted in a decision in September 1958 to freeze the design with a reduced performance requirement rather than to accept further delays in excess of those which could be compensated for by the interim XLR11 propulsion system. Table I shows the resulting specification changes. In addition to the reduction in specific impulse, it will be noted that weight has increased significantly and throttle range has been reduced. Development tests are scheduled for early December 1961 to return the minimum thrust point to the 19,500-pound level.

There is a statistical variation in performance from engine to engine and test to test. Figure 4 is a plot of thrust-chamber data from four engines during PFRT and is in consonance with the performance of flight engines. The present specification specific impulse is superimposed upon these points.

As a part of the PFRT program, two engines were required to accumulate one hour of operation and 100 starts. The requirement was exceeded. The two engines accumulated 64 and 65 minutes, 100 and 137 starts, respectively. Unfortunately, this performance has not continued in field operations. Figure 5 depicts engine service life at Edwards Air Force Base (EAFB). Listed here are all nine flight engines and a ground test engine; Engine serial No. 105 was destroyed in the explosion of X-15 No. 3 on June 8, 1960. The arrows indicate thrust-chamber replacement. Early in the flight program, operations were plagued by several premature chamber failures. These involved

██████████

failure of cooling tube walls and consequent leakage of fuel into the combustion chamber. This problem is discussed in detail in the paper by Hjelm and Bornhorst (paper no. 17). In addition to the premature failures, three flight engine thrust chamber-injector assemblies have been removed for other reasons. Although in these cases the chambers are not lost to the program, the engines have become inactive pending chamber reinstallation or replacement, seriously impairing the spares capability.


Figure 6 is a plot of throttle actuator position and chamber pressure. Although extremely rapid response is not required by the mission, chamber pressure follows the throttle closely. It might be noted that the thrust chamber pressure lags the throttle position by 0.2 to 0.6 seconds.

Figure 7 is interesting as an indication of the times involved in recovery from a malfunction shutdown after launch. These data are taken from a flight made by Major Robert W. White in April 1961 in which a malfunction shutdown occurred almost immediately after launch. Shown are throttle position, fuel-pump pressure, and chamber pressure plotted against time. The igniter idle switch was actuated approximately 20 seconds before launch and pump discharge is up. The fire switch was actuated 1.3 seconds after drop and the throttle was advanced. Pump discharge and chamber pressures were rising when malfunction shutdown occurred. Restart must be delayed to completion of the purge and engine reprime. The fire switch was actuated at 21.9 seconds. When the pilot saw the pump pressure rise he advanced the throttle. It is interesting to note that the throttle motion was stopped as the pilot checked his chamber pressure as he neared the desired thrust level and the two pressure traces clearly reflect this event. The sequence from launch involved approximately 30 seconds and an altitude loss of 8,000 feet as against a good start drop of about 2,000 feet.

FIELD PROBLEM AREAS

Although PFRT was completed successfully, field operations differ from test-stand conditions, and the PFRT experience did not carry over to operations at Edwards. The problem areas which have become prominent are as follows: Vibration, premature chamber failures, pump seal leaks, corrosion, compatibility, and controls.

The most pernicious problem encountered has been the 1,600 cps vibration. A typical trace of the accelerations at one of the engine mounting points is shown in figure 8. The initial accelerations are



low and build up. If the vibration does not exceed 100g at the pickup location, damping occurs. Between 100 and 200g, either damping or divergence can result. Above 200g, divergence always occurs. Therefore, a vibration cutoff was installed to shut down the engine in event of vibration levels above 120g. Inasmuch as there is the possibility of damping in this range, the cutoff includes a 50-millisecond delay to permit this damping and avoid unnecessary shutdowns. The mechanics of this phenomenon have not been determined; however, the incidence rate is known to increase in the higher performing engines and is also aggravated by operation at mixture ratios below design. The incidence rate has been contained within 2 to 4 percent of start attempts through installation of vibration isolators and a quick-change orifice device which permits operations at proper mixture ratios at all times. An interesting facet of this phenomenon is discussed subsequently with regard to compatibility. The vibration situation has not directly delayed flight operations, but is the major contributor to the malfunction shutdown rate during ground operations. A vibration shutdown has not yet occurred in flight.

The premature failure of thrust chambers has produced a direct effect upon engine availability for flight. This problem is discussed in detail in the paper by Hjelm and Bornhorst (paper no. 17).

The pump seal leak involved O-ring deterioration at the pump-fuel casing joint. However, replacement requires removal of the turbine exhaust duct, stator blades, rotor and inlet housing. Thus, O-ring replacement requires 2 to 3 shifts. Just to remove the exhaust ducts necessitates removal and re-safety wiring of 60 bolts. Thus, although the O-ring failure, which results in a steam leak, is not of major significance in itself, repair requires removal of the engine from the aircraft, and time-consuming engine disassembly, directly contributing to flight delays. The deterioration is believed to be due to the longer pump runs utilized in field operations; turbine-case temperatures in the vicinity of the O-ring have been recorded as high as 600° F. An investigation is under way for an improved seal which will withstand higher temperatures. In the interim, pump ground runs are being reduced in duration in an effort to minimize deterioration of the present seals.

Corrosion appears to be largely a result of the unusually long engine life. With a few exceptions, materials used are those reported to be compatible with the propellants. There have been some instances of galvanic action between the magnesium pump case and steel parts with decomposed peroxide as an electrolyte. As is sometimes said, the only thing really compatible with peroxide is more peroxide.

The necessity for component compatibility is not a new idea. In the XLR99 engine, the major component-compatibility requirement has been

██████████

met; that is, the components work together properly. However, the "vernier" mismatch of individual components still occurs. For example, minor speed control difficulties have been corrected by matching of governor and turbopump. This component match is illustrated again by the vibration problem. During initial checkout of engines serial number 108 and 111 on the PSTS, excessive vibration-incidence rate was observed. The igniter in the engine (serial number 108) was replaced and the vibration incidence rate was reduced within acceptable limits. The igniter removed from the engine serial number 108 was then installed in another (serial number 111) and its incidence rate reduced within acceptable limits. Compatibility is not particularly a problem but does produce the usual puzzling inconsistencies.

The difficulties in the control area are primarily in the hydraulic governor system. The servicing procedure is somewhat complicated and often difficult; production tolerances result in metering-valve binding, and the peroxide and hydraulic oil produce some corrosion. The most surprising occurrence was a siege of problems due to governor housing porosity; however, this problem has been resolved by an epoxy impregnation of the castings.

There are also random failures of pressure switches, relays, etc. These are not unexpected nor is the failure rate high; however, they require removal of the control box with resultant delay.

It might be noted that the premature chamber failures and pump seal leaks have contributed directly to flight delays. The problems of corrosion, compatibility, and control are usually corrected at the PSTS and rarely affect flight engines.

FLIGHT EXPERIENCE

Perhaps this discussion of the problem areas and specification deviations has presented an overly dreary picture of the XLR99 engine. In spite of these troubles and in spite of these delays, the engine has performed well in flight and the aircraft has approached its design speed. The mission experiences of the X-15 with the XLR99-RM-1 engine is indicated in the following tabulation:

Launches	Successful	Engine abort prior to launch	Malfunction with restart
15	15	1	3

The table shows that the X-15 has been launched 15 times with the XLR99 aboard and in each case successful engine operation has been achieved. On three occasions malfunction shutdowns occurred in flight, but each time the first restart attempt was successful and no compromise to the mission resulted. It should be borne in mind that the XLR99 has been designed to shutdown in event of malfunction. Unlike its predecessors, no explosion, fire, or other hazardous condition has occurred in flight. None of the emergency landing areas have been used. On one mission only, the engine failed to operate just prior to launch and the flight was aborted; but this was just one among many such aborts from other causes. (Even this lapse demonstrated the advantage of the pre-launch idle mode.)

FUTURE APPLICATIONS

Other than the previously mentioned increase in range of throttleability, there is no active program at the present time for the advancement of the XLR99 rocket engine. There have been several proposals for increasing the performance of the X-15 airplane through injector redesign, addition of a nozzle extension, and conversion to the more dense storable propellants. Several firings have been made with present pump and chamber assembly with the nitrogen tetroxide-mixed hydrazine propellants. The engine has also been proposed for Dyna-Soar air launch tests. However, for the X-15, the research gains must be weighed carefully against the additional development cost and the time extension required to accomplish the changes.

Regardless of these proposals it is believed that the XLR99 engine has demonstrated valuable new concepts in the application of rocket power to manned vehicles. The most significant of these is the "man-rating" concept evolved. The XLR99 does not depend passively upon reliability for pilot safety. An active approach, designed to react to malfunctions, which do occur, was applied. For the X-15, where safety takes precedence, this reaction is a shutdown for those cases where the malfunction could result in a hazardous condition. (Nonhazardous malfunctions do not produce a shutdown.) It is recognized that all manned rocket-powered vehicles cannot use the shutdown for protection. However, the principle evolved (extremely detailed malfunction analysis, idle modes, continuous igniter operation, selected redundancy) can serve to prevent catastrophic malfunction results and allow time for some alternate action on the part of the crew. The concepts demonstrated in the X-15/XLR99 system deserve close study. Their adaptation to other aerospace vehicles will enhance operational safety and thus, mission success.

~~SECRET~~

TABLE I.- XLR99-RM-1 DEVELOPMENT SPECIFICATION CHANGES

	<u>Initial proposal Feb. '56</u>	<u>Spec. 91F June '58</u>	<u>Spec. 91M March '61</u>
Maximum thrust (45,000 ft), lb	57,000	57,000	57,000
Minimum thrust (45,000 ft), lb	19,500	19,500	31,500
Specific impulse (sea level), sec	241	238	230
Specific impulse (45,000 ft), sec	278	272	265
Engine weight (dry), lb	540	856	910
Engine weight (wet), lb	625	990	1,025



ROCKET-ENGINE LIFE

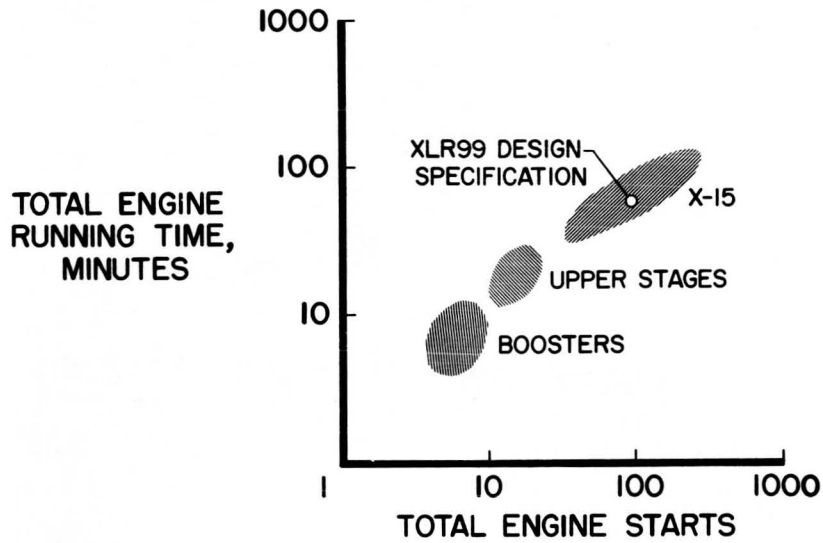


Figure 1

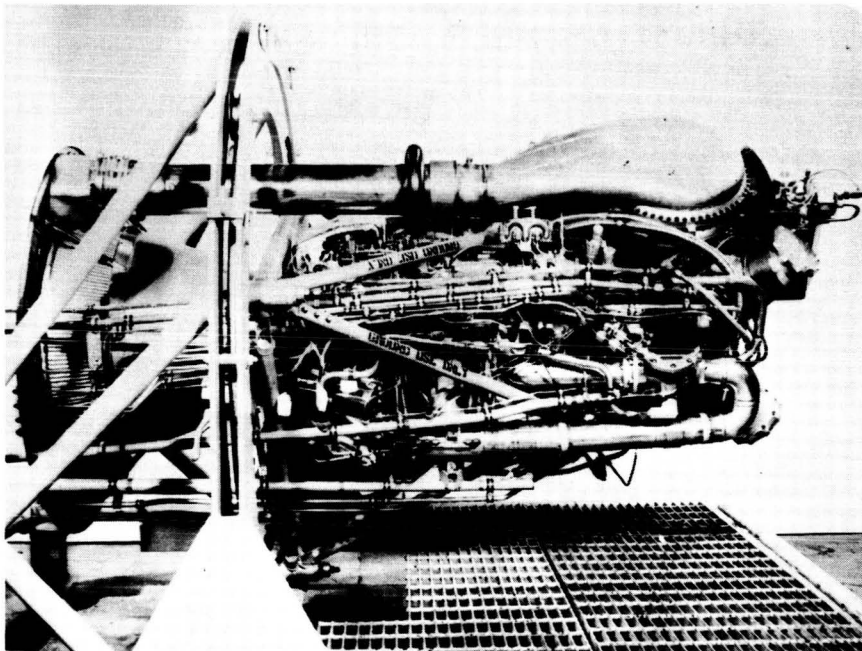


Figure 2

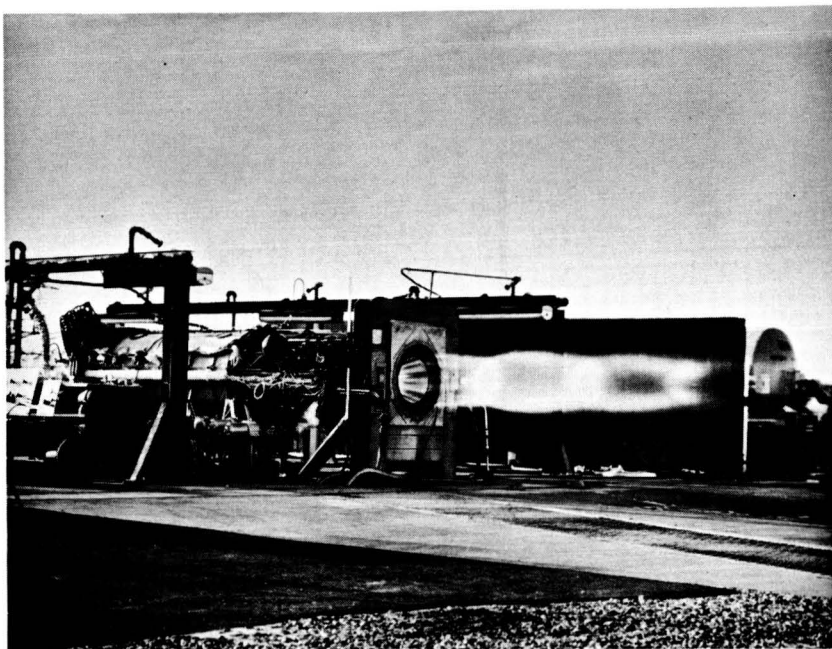


Figure 3

THRUST-CHAMBER PERFORMANCE

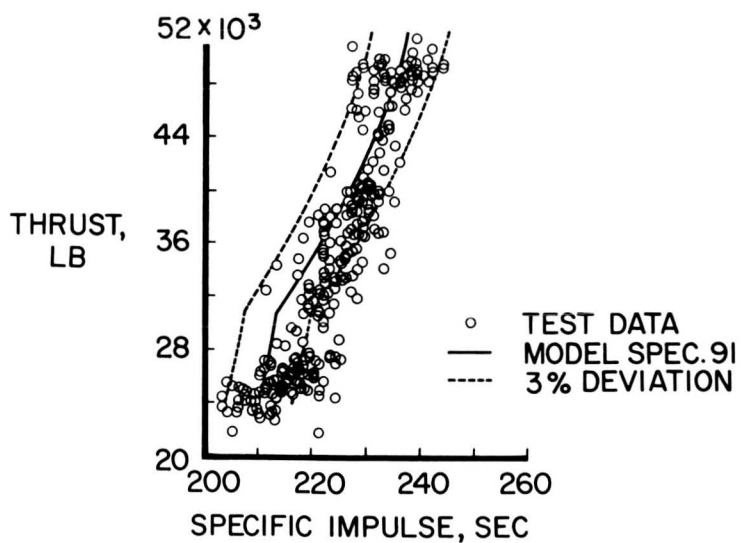


Figure 4

XLR99 ENGINE SHUTDOWN AND RESTART RECORDS

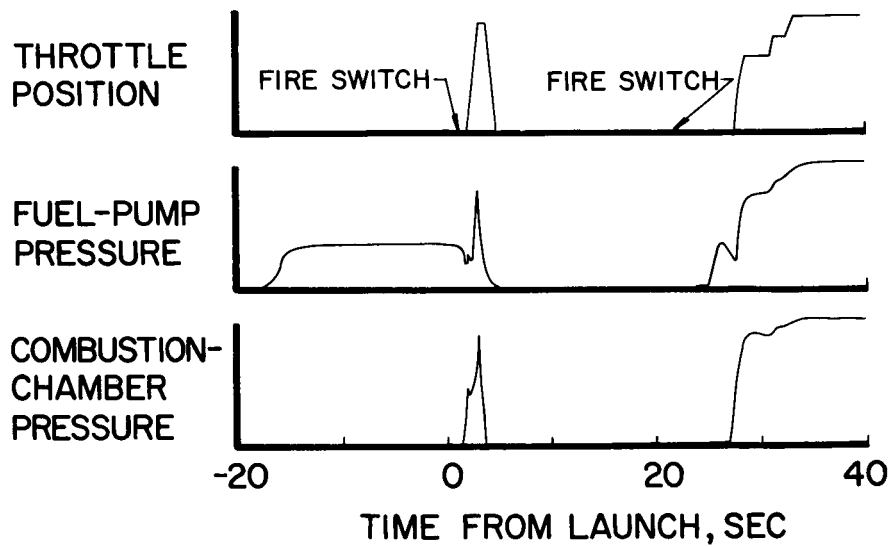


Figure 7

XLR99 ENGINE VIBRATION RECORD

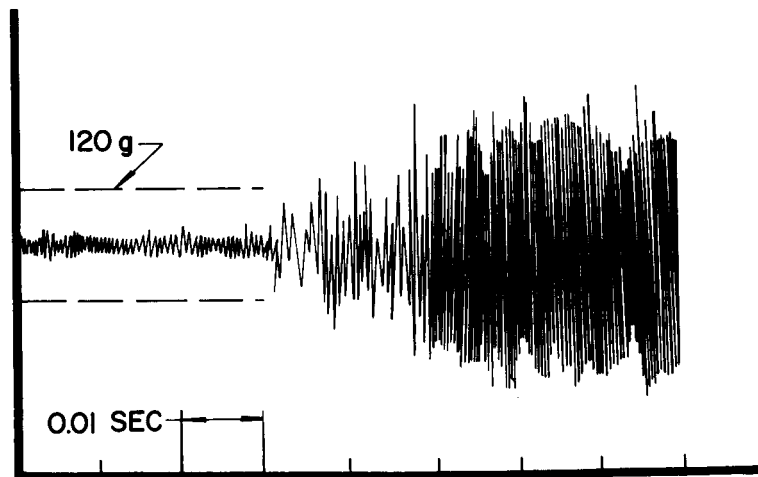


Figure 8

17. DEVELOPMENT OF IMPROVED CERAMIC COATINGS TO INCREASE

THE LIFE OF XLR99 THRUST CHAMBER (L)

By Lawrence N. Hjelm
Aeronautical Systems Division, U.S. Air Force

and Bernard R. Bornhorst
Air Force Flight Test Center

ABSTRACT

This report describes the coating development, laboratory testing, and engine testing program that was performed to solve the problem of premature failure of rocket-engine combustion chambers being experienced in operation of the X-15 system.

BACKGROUND

The XLR99 engine which powers the X-15 airplane, shown in figure 1 as viewed from the rear of the vehicle, is a liquid oxygen, anhydrous ammonia, regeneratively cooled engine. The combustion chamber or nozzle, shown with its characteristic star pattern, is a brazed assembly of 347 stainless steel tubes, formed to shape, through which the anhydrous ammonia flows longitudinally as a coolant. Figure 2 is a photograph of this section showing its construction. The interior surface of the chamber is coated to provide insulation and protection for the tubes from the 5,000° F flame. This coating is generally made up of 0.005 inch of a Nichrome flame-sprayed undercoat with 0.010 inch of Rokide Z flame-sprayed zirconia as an insulating, erosion-resistant top coating.

In service, the Rokide Z coating has been spalling or flaking due to thermal cycling from the large number of engine starts required or from vibration due to an unstable flame. The history of chamber failures is included as table I. The loss of the coating exposes the stainless steel tubes to the heat and erosive effects of the flame. As this exposure occurs, the ammonia within the tubes is overheated locally and boils so that the cooling of the tubes is reduced. The ammonia vapors then attack the tube, and a very brittle nitrated layer is formed. At the same time, the combustion gases begin to melt and erode the tube surface. As this condition persists, the effective thickness of the tube wall is gradually decreased until it finally bursts from cyclic internal pressurization. This situation occurs in the throat of the

nozzle and produces a chamber failure with raw fuel leaking into the chamber from the cracked tube. This process is illustrated in figures 3 and 4.

APPROACH

In January 1961, Materials Central of the Aeronautical Systems Division (ASD) in cooperation with the X-15 Project Office of ASD initiated a study to determine the chamber failure mechanisms and to outline an approach to improve chamber durability. A program to improve the coatings system was developed since the primary cause of failure is loss of the coating. The two possible approaches were to improve the Rokide coating or to develop an improved coating system. Since it was believed that improvements in the Rokide Z coating system would be small and perhaps marginal, the emphasis was placed on the development of a new coating system. At that time, a program with the Plasmakote Corporation¹ already underway to exploit the concept of graded coatings was oriented to solve this specific problem.

A graded coating is a sprayed coating of metal and ceramic in which the composition changes from 100 percent metal at the substrate to 100 percent ceramic at the surface. In this way the weak, sensitive interface between the metal and ceramic layers is removed as illustrated in figure 5. These coatings were produced by spraying mixed powders with an arc-plasma jet and gradually changing the composition by changing the ratio of metal to ceramic powders. Most of the coatings investigated were basically combinations of zirconia with Nichrome, molybdenum, and tungsten. An existing program with the University of Dayton² was oriented to provide realistic techniques for laboratory evaluation for the coatings being developed. Several tests were developed to screen for the most promising coatings. A thermal shock test used 3- by 8-inch plate sections of actual chambers which had been coated with the desired compositions. The ends of this plate were potted in plastic as shown in figure 6 and water was run through the tubes as a coolant. The plate was then cycled ten times at each of nine levels of gradually increasing heat flux produced by the 1/2 inch flame of a nitrogen stabilized, 50 kilowatt arc-plasma jet (3,000° F - 8,000° F). The test in operation is shown in figure 7. Four to six tests were run on each panel and the results were recorded as the number of cycles to fail the coating. Single, 1/2-inch-diameter tubes were also coated and tested in a manner similar to the panel tests. Although these tests turned out to be much less severe than the panel test, these tubes were also used to obtain the relative insulating effect of the coatings by using the tube as a calorimeter and measuring the heat transferred through the coating.

¹Contract AF 33(616)7323.

²Contract AF 33(616)7838.

RESULTS OF LABORATORY EVALUATION

Most of the initial studies were concerned with two gradated coating systems, as described in table II. A great number of additional systems have been evaluated to determine trends or potential of new systems; however, an insufficient number of tests were run to consider the results statistically significant.

It should be noted that the only difference between the two gradated coatings is the primer used over the stainless steel tubes. The thermal shock-test results, in which the two gradated coatings were compared with Rokide Z, are illustrated in figure 8 as the number of cycles to failure.

The extreme spread in life of the Rokide Z system and the high concentration of early failures agreed with engine experience and perhaps indicates nonuniformity in the coating itself. Coating A appears to offer some improvement in life. This can be thought of as an improvement due to coating technique since the materials are the same. However, with coating B a significant improvement is obtained. There were no failures below 43 cycles. This improvement over coating A can only be due to the use of molybdenum as a primer which apparently results in a more adherent, shock-resistant coating.

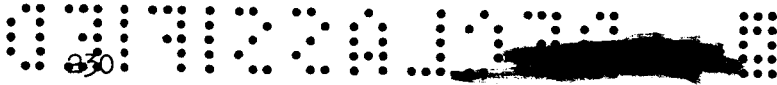
These same test results are plotted in figure 9 to indicate probability of failure at any given number of cycles.

ENGINE TEST PROGRAM

An engine test program was undertaken to evaluate the most promising coatings under actual engine operating conditions. Coating B, which consists of a molybdenum primer with Nichrome gradated to zirconia, was chosen for the first test.

A mock-up of the combustion chamber illustrated in figure 10 was used to determine deposition rates for the spraying process so that the desired coating thickness could be obtained on the actual hardware. The mock-up was constructed of aluminum with panels cut from an old chamber inserted at three positions. This assembly is coated in the same manner as an engine and chamber, and coating thicknesses were measured. The coating thicknesses on the smooth surface are compared with those on the corrugated panels. Proper spraying parameters can then be determined for coating a combustion chamber.

A special fixture was built at NASA Flight Research Center for coating a fully assembled engine. This fixture and the coating operation on the first test engine are shown in figure 11. This figure shows the



engine mounted in rings so that it can be rotated. Figure 12 is a rear view of this operation.


The fixture rotates the engine at various speeds and programs the arc spray gun in and out of the engine from a pantograph arrangement. This procedure allows control of engine rotation and gun position necessary to provide a uniform coating deposit.

The chamber available for the first engine test had failed previously and had one cracked tube, which was welded over. As can be seen from the previously mentioned photomicrographs of failed tubes (figs. 3 and 4), producing a sound, reliable weld in these areas is very difficult because of heavily nitrified layers on the internal cracks.

The gradated coating system applied was chemically similar to the original Rokide Z in that its surface was zirconia backed up by Nichrome. It was therefore assumed that interaction between the coating and combustion products would be similar. In normal operation of this engine, 12 "hot streaks" occur longitudinally through the engine, producing the star pattern mentioned previously. Characteristically, these hot streaks have a white, chalk like surface which may be due to thermal shock of the zirconia particles or hydrogen reduction of the surface with subsequent reoxidation. Several "top coats" of various materials were applied in two circumferential strips just aft of the throat. These were used to determine if the exhaust gases were locally oxidizing and if a more erosion resistant material than zirconia could be used in the engine. These strips consisted of overcoats of tantalum carbide, titanium carbide, titanium nitride, zirconia with 10-percent molybdenum, and zirconia with one percent nickel. Figure 13 is a photograph of the coated chamber, as viewed from the exit cone, showing these test strips.

Prior to the testing of the gradated coating system, a used chamber with a new Rokide Z coating was tested in an old engine to provide directly comparable coating life data. The firing procedure designed for coating evaluation is included in table III. The test data from firing this engine are included in table IV. Loss of the Rokide Z coating in the throat was visible after the second run and progressed until after the seventh start and a total running time of about $5\frac{1}{2}$ minutes. A total of 25 square inches of coating was lost during the test. This progression is illustrated in figures 14 to 16.

The gradated coating was then tested in a similar manner to produce comparable results. The test data from the firing of the gradated coating system are included in table V. As was mentioned previously, this chamber had been leaking and the cracked tubes were welded. After the second run two leaks were evident with no coating loss. Subsequent runs produced



some coating loss around previously leaking areas but none in nonleaking throat areas. After six starts and a total of $5\frac{3}{4}$ minutes, 3 square inches of coating were lost from the leaking areas, slight erosion was evident in nonleaking areas, and chipping of coating surface was evidenced upstream of the throat. This progression can be seen in figures 17 and 18. Due to difficulties, the tests on this engine were stopped.

Figure 19 shows this engine after the test series and illustrates the blackening of the coating that was initiated during the first run. This blackening appeared to be Nichrome "bleed through," since the coating was found to be electrically conductive along its surface. Figure 19 also shows that one top coat, the titanium nitride, did protect the zirconia surface by stopping the chalking action.

A metallographic study was made of sections of this chamber to determine the effectiveness of the top coats and whether there was metal bleed through in the coating. Figure 20 illustrates the character of the original two-layer Rokide Z coating from an old engine. Figure 21 is a section from the throat of the test engine showing the molybdenum primer and Nichrome gradated to a zirconia surface. The top coat of zirconia appears somewhat thin but there is no evidence of metal bleed through. Figure 22 shows the gradated systems with a top coat of zirconia and 10-percent molybdenum used to determine whether molybdenum would oxidize or react in this environment. There is no evidence of attack indicated and the system appears compatible.

Figure 23 shows the gradated system with the titanium nitride top coat which appeared to offer some protection for the zirconia. It can be seen from these photomicrographs that the zirconia had turned black, including areas under the top coats, with no evidence of metal bleed through. It is known, however, that zirconia is easily reduced by hydrogen which causes it to turn black. Moreover, zirconia will dissolve up to 1-percent chromium and in doing so will turn black and become electrically conductive. This would account for the electrical conductivity of the coating and its blackness without any evidence of metal bleed through.

CONCLUSIONS FROM ENGINE TEST

The first engine test has essentially substantiated the results of the coating development program, in that the gradated Nichrome zirconia coating with a molybdenum primer has been demonstrated to be a significant improvement over the original Rokide Z coating system. The evaluation of the several types of top coats indicated that the combustion products were not reactive with the molybdenum zirconia system or the titanium



nitride system. These results allow the development of potentially improved coating systems by replacing Nichrome with molybdenum and through the use of nonreactive top coats.

The metallographic study of the coating after test indicated that the surface blackening had no apparent effect on the usefulness of the coating. Therefore, except for the area of loss, the usefulness of the gradated coating was unimpaired except, perhaps, for some slight surface loss. Although the bulk-fuel temperature-rise data shown in table IV were scanty and will not identify local overheating, there is no indication that the insulation provided by the gradated coating is significantly different from the original Rokide Z system.

It is apparent from the early ruptures of fully coated tubes during the engine test that it will be extremely difficult or impossible to reclaim failed chambers. This fact also points out the importance of early replacement of the coating to prevent internal attack of the tubes. Repeated exposure of uncoated tubes will produce internal and external attack and eventual tube rupture. Therefore, even if a tube is recoated before it leaks, it may easily contain sufficient internal attack to rupture on subsequent pressurization.

FUTURE

The results of the first engine test were encouraging but not completely convincing since the test time was relatively short and long time effects on the coating over a large period of time could not be determined. Nevertheless, due to the urgent need for improved chamber life and because the gradated coating demonstrated a significant improvement for at least 5 minutes, two new chambers have been coated for use in the program. The coating system used is the molybdenum primer and Nichrome gradated to zirconia as in the test engine except that the zirconia top coat thickness has been increased from 0.004 inch to 0.006 inch, and 0.002 inch of titanium nitride has been added as a top coat. An additional old chamber was stripped and recoated with two gradated coating systems and two top coats for the second phase of the engine testing. This testing is currently underway. The coatings in this chamber are molybdenum gradated to zirconia and tungsten gradated to zirconia with top coats of titanium nitride and zirconium diboride. Portions of the chamber were covered during spraying so that each of the coatings with and without top coats will be exposed in the throat area. Longitudinal sections, rather than the circular strips of the previous tests were used so that exposure conditions will be as similar as possible. The compositions of these coatings were chosen for two reasons: First, it was necessary to evaluate quickly the usefulness of

top coats in the throat area and to evaluate the effect of replacing Nichrome with a refractory metal; and second, it was necessary to validate the laboratory tests before proceeding to coating optimization.

The result of the first engine test indicated that the use of high melting-point compounds as top coats could possibly stop the gradual erosion or chalking of the zirconia surface. Titanium nitride stopped the chalking in an area where conditions are much less severe than the throat, and therefore it must be further evaluated to determine its usefulness. Zirconium diboride was also included as typical of another family of compounds which may offer this protection.

Refractory metals were used instead of Nichrome to determine their usefulness under engine conditions. In the first engine test, the top coat which contained 10-percent molybdenum showed no apparent attack or oxidation. It can, therefore, be assumed that the exhaust products are not excessively oxidizing. A refractory metal instead of Nichrome would appear desirable since, in the event of erosion or loss of the coating surface, a refractory metal would offer some protection to the tubes, whereas the Nichrome would very likely melt. By following this reasoning, heavy undercoats of 0.030-inch molybdenum and tungsten were used in the throat of this chamber.

There is some question as to the validity of the thermal shock test for evaluating the top coats or the refractory-metal systems, because the flame can be much hotter than that in the engine and there is some oxidation due to entrainment of air in the flame. The first engine test confirmed the use of thermal shock as a judge of coating capability for the early coatings investigated; however, in subsequent tests on systems with top coats all samples performed poorly. This poor performance may be a result of an inherent shock sensitivity in the system, or it may be that the test is overly severe. The shock-test results on coatings containing refractory metals have been very disappointing. The test results on samples of zirconia gradated with molybdenum have been scattered with a number of early failures. The few samples tested containing tungsten have all shown early failures. This may be due to the fact that the test is somewhat oxidizing because of air entrainment in the nitrogen flame. The titanium nitride top coat was used in the two new chambers because, although the tests indicated early failures were to be expected, they also indicated that only the top coat failed and the failure did not affect the performance of the basic coating. Therefore, the laboratory thermal-shock test results would indicate that the top coats and the coatings themselves that are in the current test engine would all fail very quickly. This engine is being run to determine the validity of these tests and to avoid overlooking promising coating systems because of an overly severe laboratory test.

234

The direction for further coating development work, shown schematically in figure 24, will be dependent upon the outcome to the current engine test. If the coatings perform satisfactorily, the laboratory tests must be modified to be more realistic, and coating development work will be to optimize a system containing molybdenum or tungsten gradated to zirconia with a top coat. If the coatings perform very poorly the thermal shock test will be considered valid and coating development work will be to optimize the earlier type coatings without top coats, and the test will be used to choose the best system. The climax to this program will be an additional engine test of an optimized coating system. This system will then be incorporated into the program for new chambers and for maintenance of existing chambers.

[REDACTED]

TABLE I
XLR99 CHAMBER HISTORY

Serial number	Cycles at crack	Time to failure, min:sec
Failed chambers		
102	86	14:00
42		18:39.7
29		36:47.6
113	85	35:28.5
120		18:45.1
28		
Chambers exceeding rated life		
40	117	46:36.0
116	56	71:52.0
111	206	122:51.0

TABLE II
IDENTIFICATION OF COATING SYSTEMS

Coating designation	Primer	Graduation 1	Graduation 2	Graduation 3	Insulating layer
Rokide Z	0.004-inch Nichrome				0.010-inch Rokide Z (ZrO ₂)
Coating A (Plasmakote)	0.003-inch Nichrome	0.003-inch 70% Nichrome 30% ZrO ₂	0.003-inch 30% Nichrome 70% ZrO ₂	0.003-inch 10% Nichrome 90% ZrO ₂	0.004-inch ZrO ₂
Coating B (Plasmakote)	0.003-inch Molybdenum	0.003-inch 70% Nichrome 30% ZrO ₂	0.003-inch 30% Nichrome 70% ZrO ₂	0.003-inch 10% Nichrome 90% ZrO ₂	0.004-inch ZrO ₂

TABLE III

XLR99 COATING TEST PROCEDURE FOR ENGINE SERIAL NUMBERS 101 AND 6

Run type	Throttle setting, percent	Time at throttle setting, sec
Oxygen-fuel ratio calibration of sea-level orifices	70 50 90 Off	Start 5 5
Engine calibration and functional	70 50 50 70 80 90 100 50 100 50 Off	Start 5 5 5 5 5 5 5 5 5 5
Controllability and restart	70 50 Off 70 100 50 Off	Start + 5 5 10 Restart 5 5
Restart series test no. 1	70 Off 70 50 Off 70 100 Off 70 Off 70 50 Off	Start + 10 10 Restart 10 10 Restart 10 10 Restart + 10 10 Restart 10
Chamber durability (minimum thrust)	70 50 Off	Start 100
Chamber durability (maximum thrust)	100 Off	Start + 60
Maximum thrust restart	70 50 Off 100 Off	Start 10 10 Restart + 40
Restart series test no. 2	70 50 Off 70 50 Off 70 50 Off 70 50 Off 70 50 Off	Start 5 10 Restart 10 Restart 5 10 Restart 5 10 Restart 5 10 Restart 5

TABLE IV

XLR99 CHAMBER COATING TEST DATA FOR CHAMBER SERIAL NUMBER 40 OF ENGINE

SERIAL NUMBER 101 RECOATED WITH ROKIDE Z

[46 min 41 sec operating time before recoating]

Run number	Oxygen-fuel ratio	Run time, min:sec	Total time on coating, min:sec	Rokide Z loss in throat area, sq in.	Run type	Remarks
28-101	1.252	0:5.0	0:5.0	0	Oxygen-fuel-ratio calibration at sea level	Lost data.
29-101	1.252	0:7.9	0:12.9	$\frac{1}{2}$	Oxygen-fuel-ratio calibration at sea level	Faint chalky areas formed in hot streaks.
30-101	1.252	1:09.5	1:32.4	2	Calibration and functional	Chalk growing heavier; 50-percent thrust, $\Delta T = 74^\circ \text{F}$; 70-percent thrust, $\Delta T = 72^\circ \text{F}$; 100-percent thrust, $\Delta T = 69^\circ \text{F}$.
31-101	1.252	0:33.8	2:06.2	$8\frac{1}{2}$	Controllability and restart	Several tubes in most severe lower hot streaks are exposed for about 6 inches to Nichrome; 70-percent thrust, $\Delta T = 65^\circ \text{F}$; 100-percent thrust, $\Delta T = 56^\circ \text{F}$.
32-101	1.252	1:02.3	3:08.5	21	Restart series no. 1	Hot streaks now very well defined with heavy chalk and dark brown fringes. Chalk extends 12 inches downstream from throat. Rokide erosion visible at throat plane over entire circumference. Brown hot streaks extend all way to exit skirt.
33-101	1.252	1:15.5	4:24.0	21	Chamber durability	Ammonia exhaustion shutdown after 76 seconds of run. Short fuel supply due to improper propulsion-system test stand operation; 50-percent thrust, $\Delta T = 90^\circ \text{F}$.
34-101	1.252	1:8.7	5:32.7	25	Chamber durability (maximum thrust)	

¹ ΔT is the temperature rise between fuel pump discharge and jacket outlet banjo.

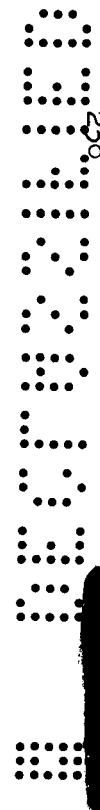


TABLE V

XLR99 CHAMBER COATING TEST DATA FOR CHAMBER SERIAL NUMBER 120 OF ENGINE

SERIAL NUMBER 6 RECOATED WITH COATING SYSTEM NUMBER 1

(GRADATED ZrO_2 AND NICHROME)

[18 min 45.1 sec operating time before recoating]

Run number	Oxygen-fuel ratio	Run time, min:sec	Total time on coating, min:sec	Coating loss in throat area, sq in.	Run type	Remarks
37-006	1.200	0:24.5	0:24.5	0	Oxygen-fuel-ratio calibration at sea level	No coating loss visible. Entire chamber is blackened by apparent Nichrome bleed for about 18 inches downstream of throat plane. Blackened areas extend to exit in hot-streak zones. Chalk has formed in the throat.
38-006	1.250	1:11.5	1:36.0	0	Combined oxygen-fuel calibration, engine calibration, and functional	Two chamber leaks detected, one in number 1 and one in number 9 streak. Neither leak is liquid yet. Blackening may have receded slightly. Small chips have come off over leaks.
39-006	1.250	0:32.2	2:08.2	1	Restart series number	Leak in number 1 streak now liquid. Strip loss on tube crowns in loss area starting from leak chips; 50-percent thrust, ¹ $\Delta T = 65^\circ F$; 100-percent thrust, $\Delta T = 62^\circ F$.
40-006	1.250	1:45.1	3:53.3	2	Chamber durability (minimum thrust)	Still no loss in areas other than in leak area. Orange tinge on TiN patch is due to NH_3 leaks; 50-percent thrust, $\Delta T = 72^\circ F$; 100-percent thrust, $\Delta T = 69^\circ F$.
41-006	1.250	1:04.9	4:58.2	2	Chamber durability (maximum thrust)	Still no noticeable loss in areas other than leak areas. Green tinge in numbers 1 and 9 streaks due to NH_3 leaks. Restart series postponed in interest of safety. Leak appears to have stabilized. Continuity test indicates that black chamber discoloration is electrically conductive; 100-percent thrust, $\Delta T = 62^\circ F$.
42-006	1.250	0:46.0	5:44.2	3	Restart series number for three restarts	Slight crown erosion in other hot streak areas beside leak streaks. Restart series apparently more severe test than durability type. Hydrogen peroxide drain fire on third restart. Engine pulled for chamber replacement and propulsion-system-test-stand repair.

¹ ΔT is the temperature rise between fuel pump discharge and jacket outlet banjo.

0312301030

REAR OF X-15 AIRPLANE WITH SLR99 ENGINE

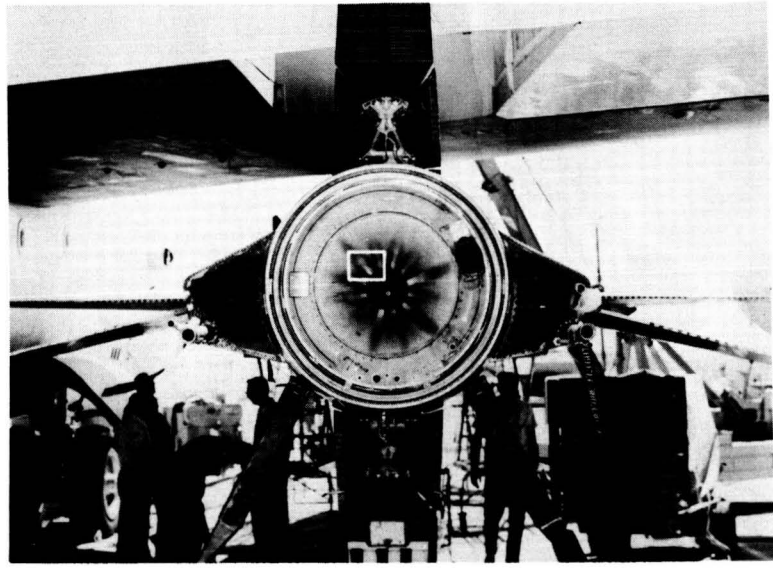


Figure 1

CLOSEUP OF SECTION OF CHAMBER

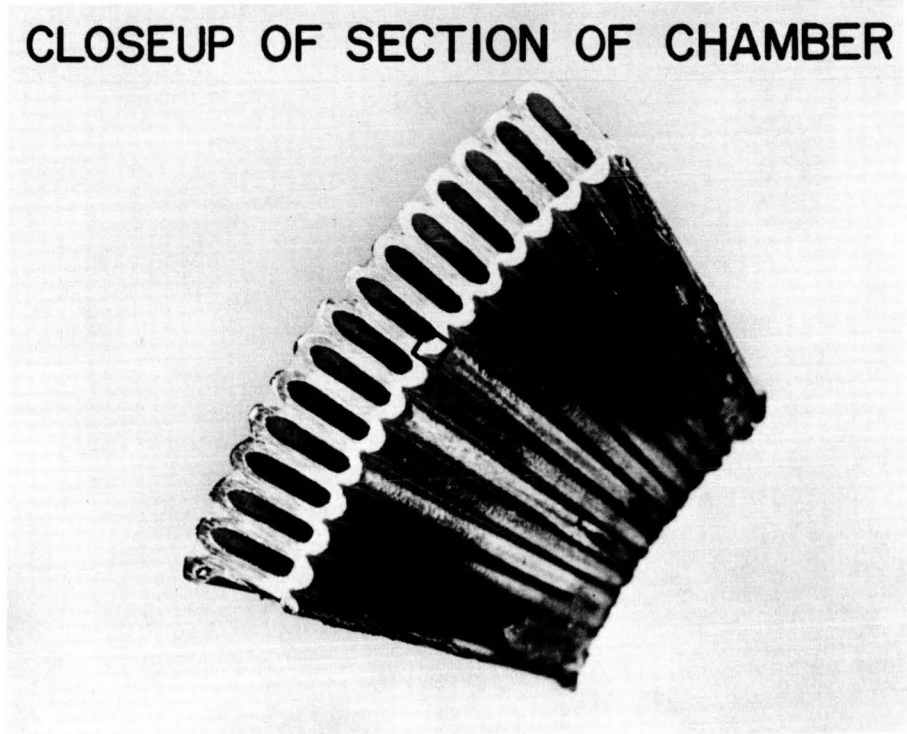


Figure 2



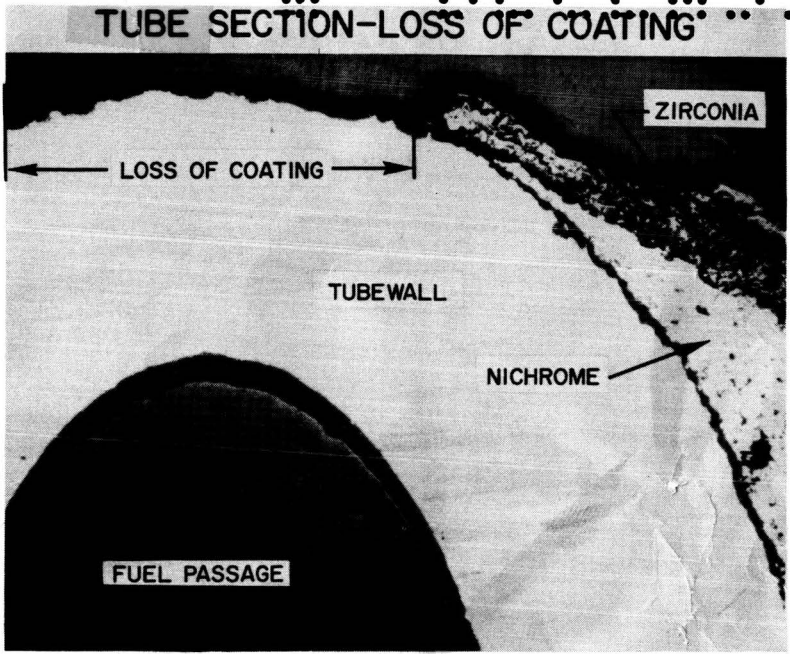


Figure 3

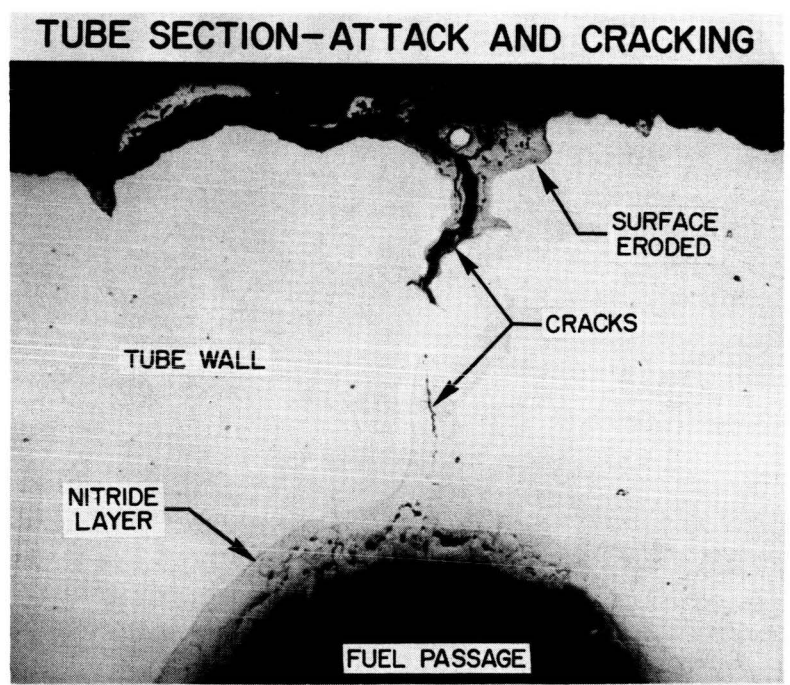


Figure 4

ORIGINAL PAGE
BLACK AND WHITE PHOTOGRAPH

242
0311201030

GRADATED COATINGS

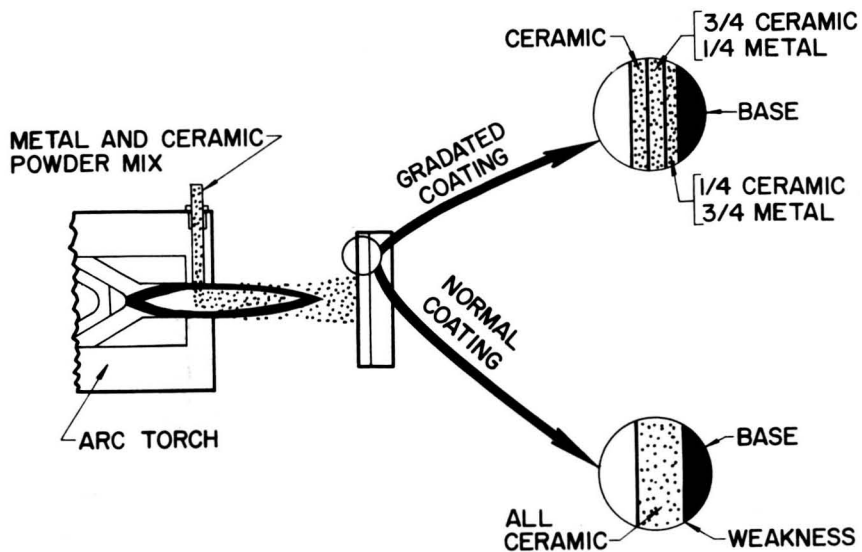


Figure 5

COATED PANEL FOR THERMAL SHOCK TEST

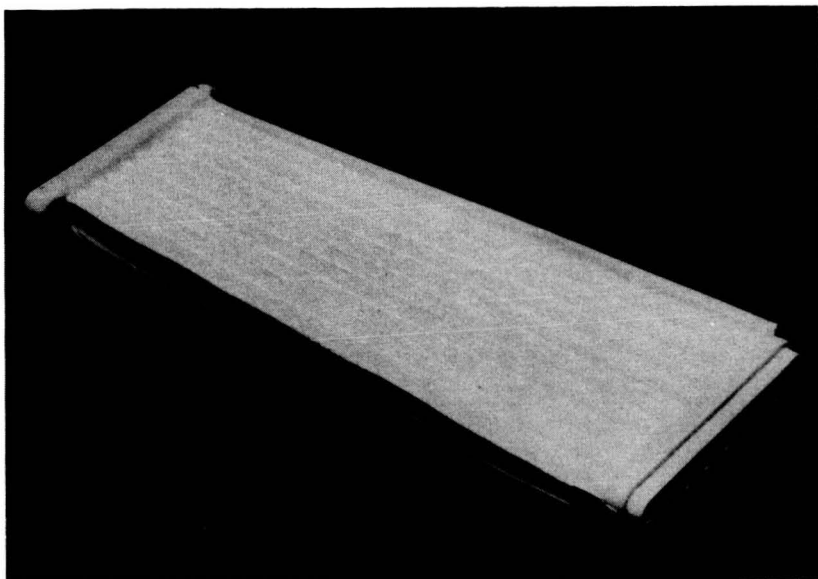


Figure 6



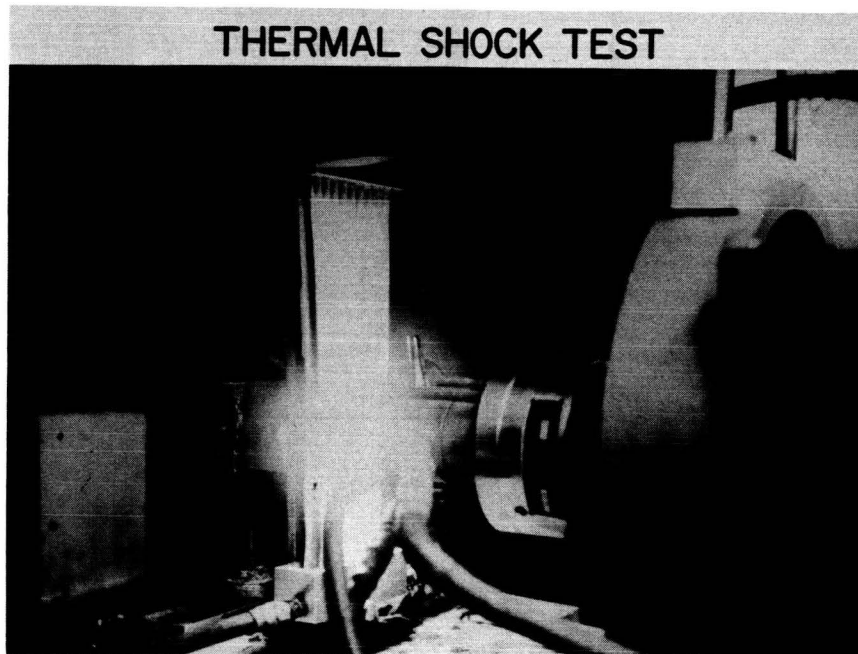


Figure 7

THERMAL SHOCK-TEST RESULTS

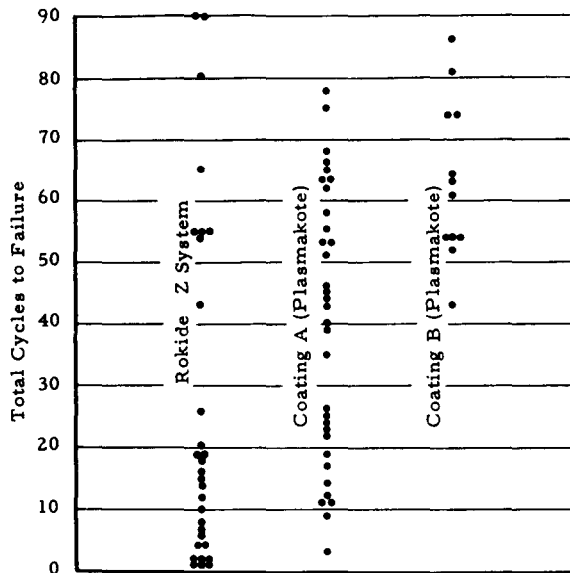


Figure 8

PROBABILITY OF THERMAL-SHOCK FAILURE

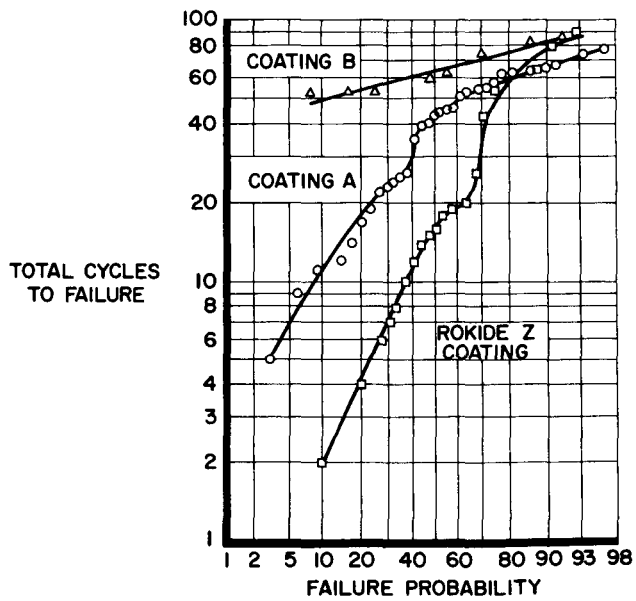


Figure 9

MOCK-UP OF COMBUSTION CHAMBER

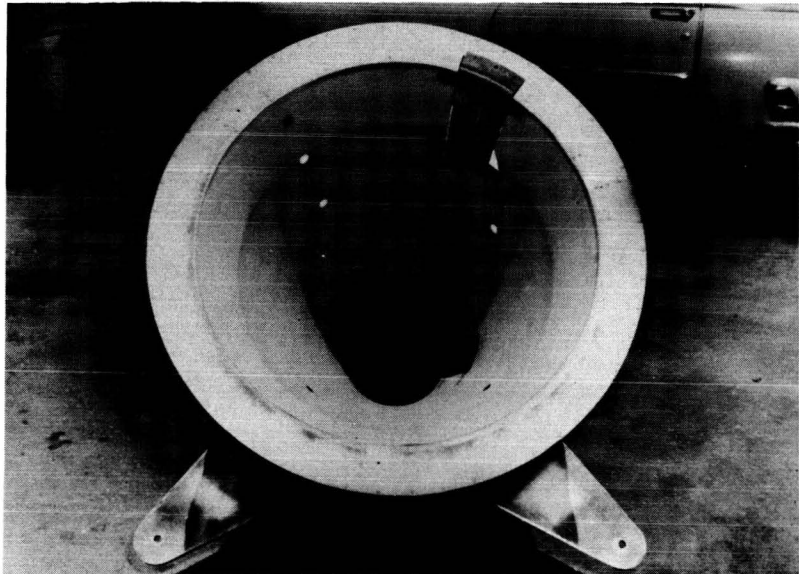


Figure 10

COATING OPERATION - SIDE VIEW

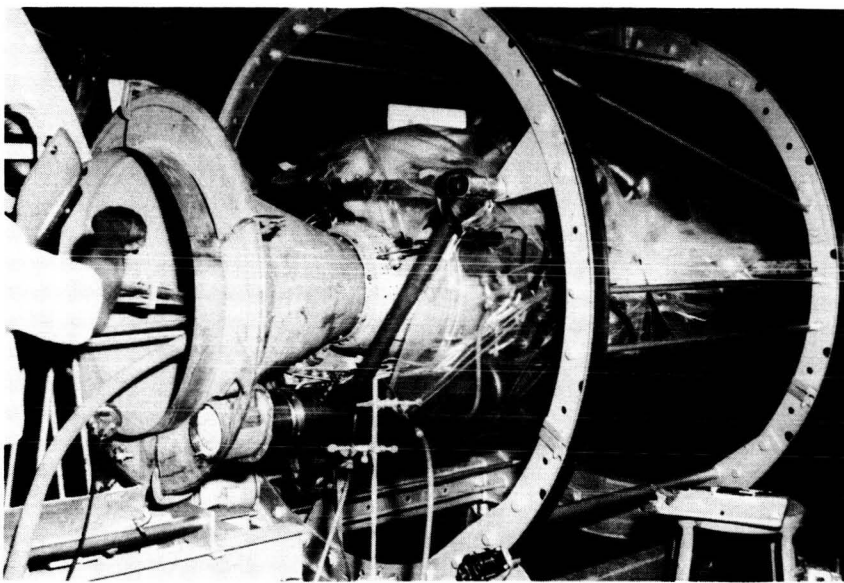


Figure 11

COATING OPERATION - REAR VIEW

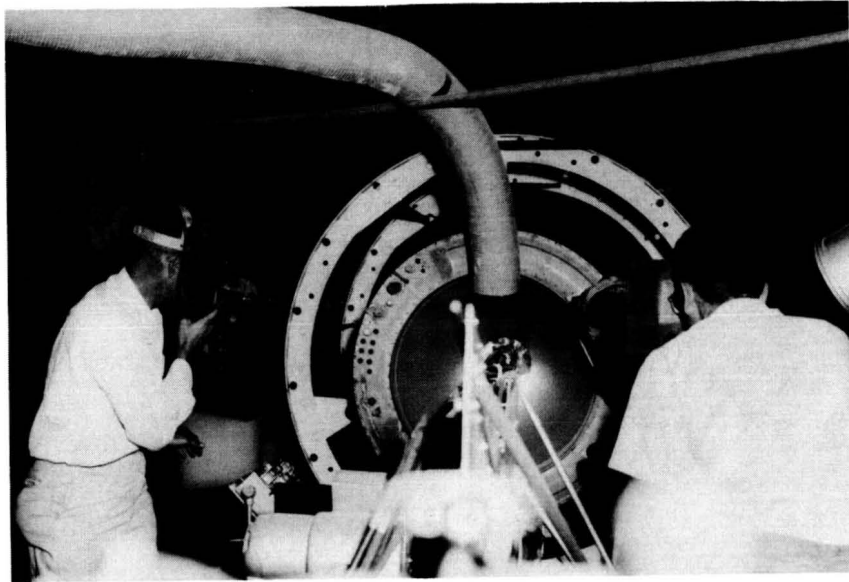


Figure 12

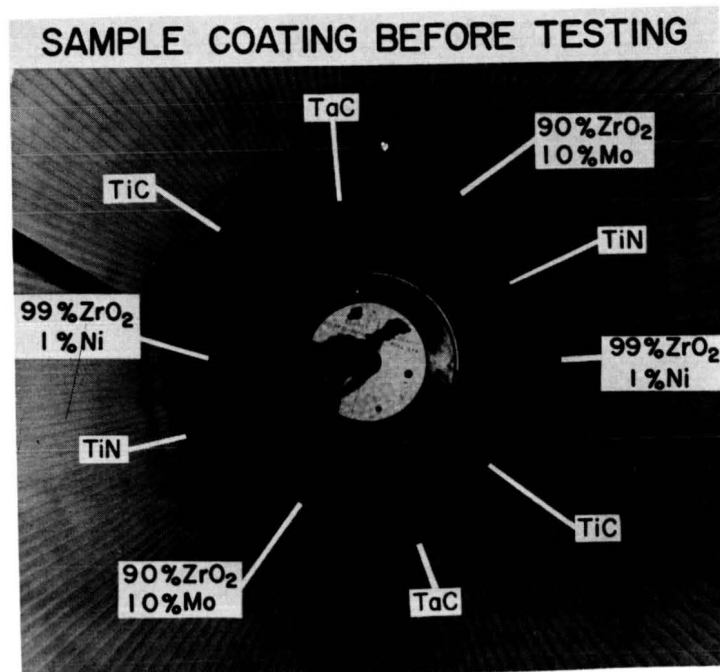


Figure 13

ORIGINAL PAGE
BLACK AND WHITE PHOTOGRAPH

ROKIDE Z COATING AFTER THREE STARTS AND 1-1/2 MINUTES
(2 SQ IN. OF ROKIDE Z LOST)

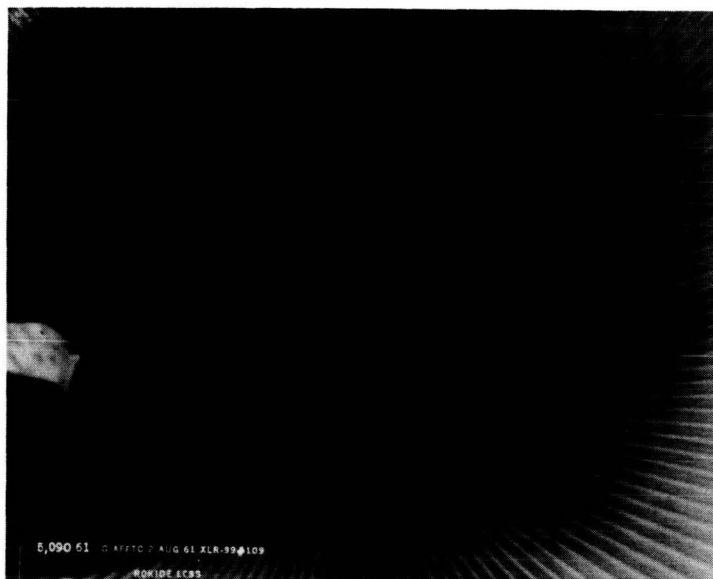


Figure 14

ROKIDE Z COATING AFTER FOUR STARTS AND 2 MINUTES
(8-1/2 SQ IN. OF ROKIDE Z LOST)



Figure 15

ORIGINAL PRINT
BLACK AND WHITE PHOTOGRAPH



ROKIDE Z COATING AFTER TEST - SEVEN STARTS AND
5-1/2 MINUTES
(25 SQ IN. OF ROKIDE Z LOST)

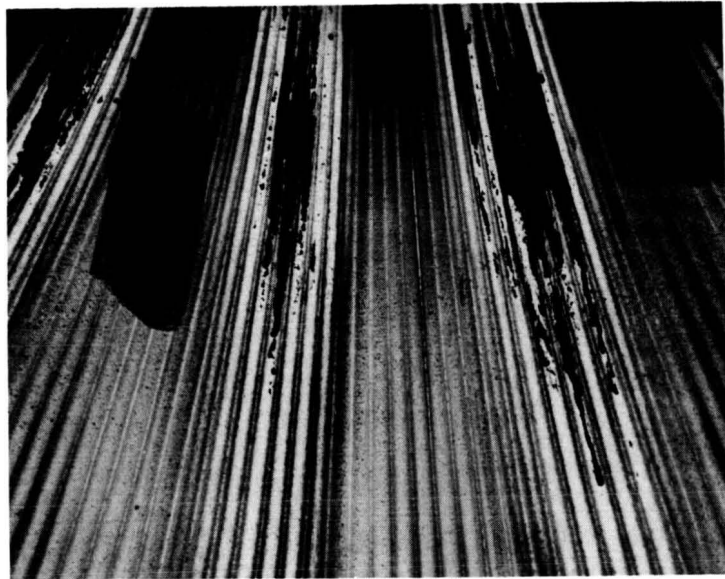


Figure 16

GRADATED COATING AFTER THREE STARTS AND 2 MINUTES
(1 SQ IN. OF COATING LOST)

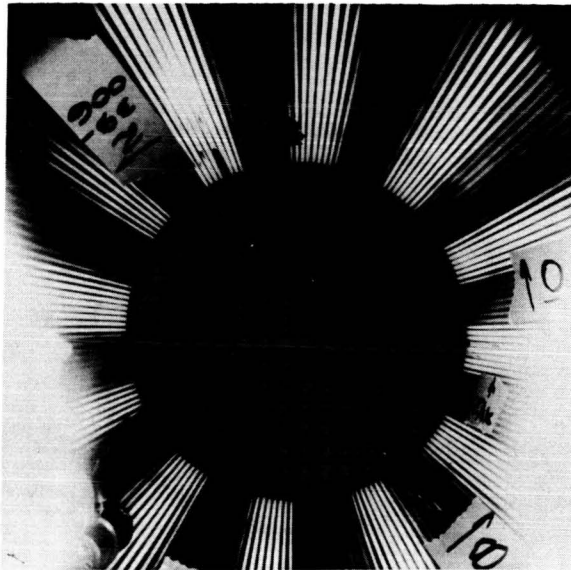


Figure 17

GRADATED COATING AFTER TEST - SIX STARTS AND 5-3/4 MIN
(3 SQ IN. OF COATING LOST)



Figure 18



GRADATED COATING AFTER TESTING

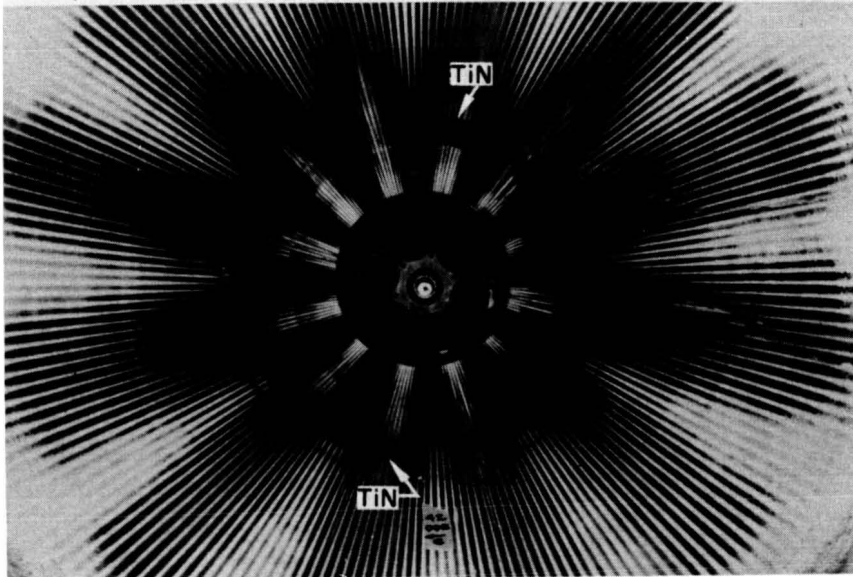


Figure 19

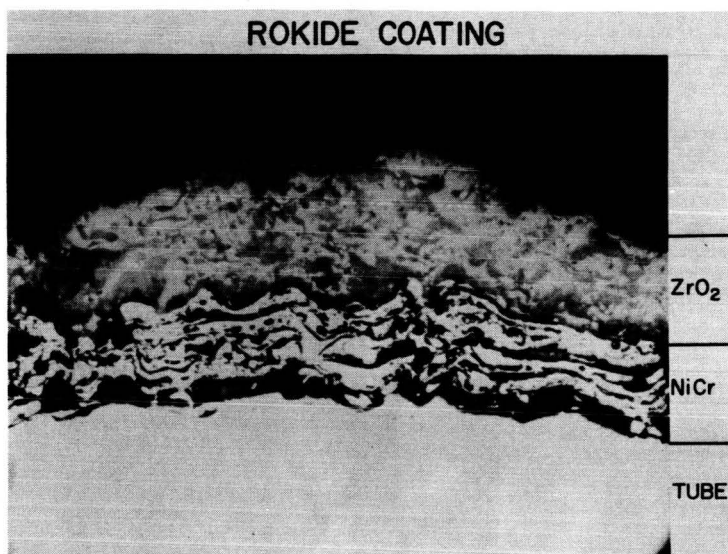


Figure 20

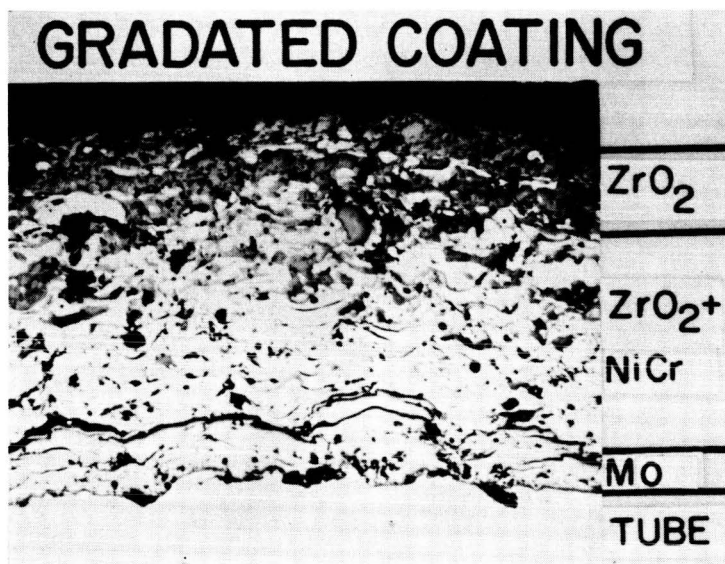


Figure 21

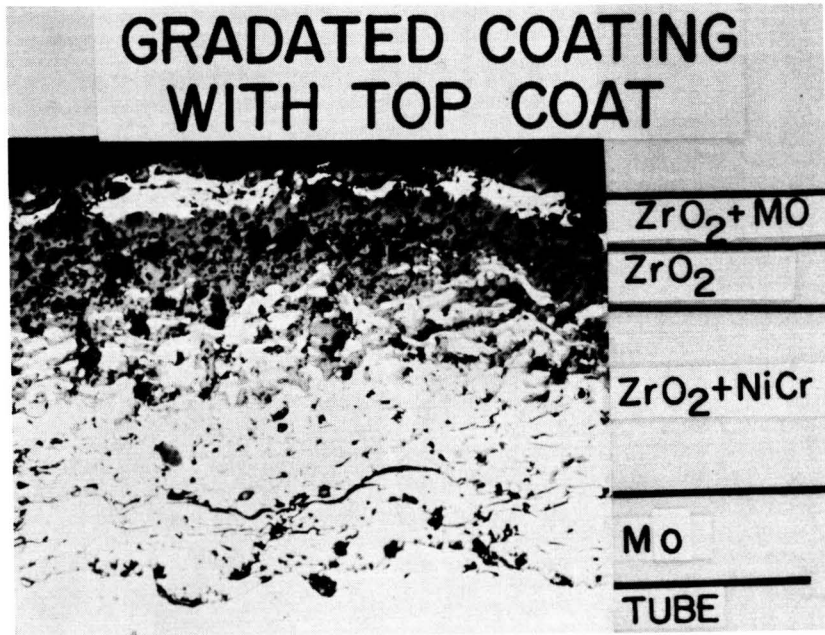


Figure 22

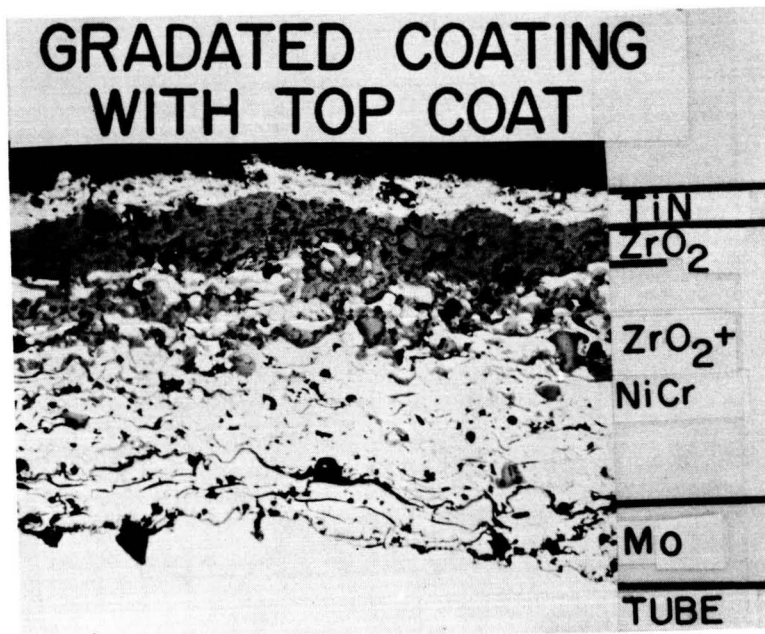


Figure 23

FUTURE OF COATING DEVELOPMENT

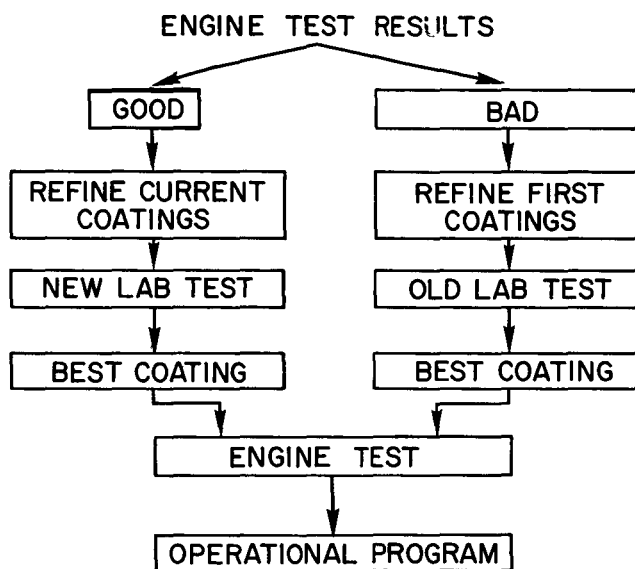


Figure 24

18. BIOASTRONAUTICS SUPPORT OF THE X-15 PROGRAM (U)

By Burt Rowen, Ralph N. Richardson
Air Force Flight Test Center

and Garrison P. Layton, Jr.
NASA Flight Research Center

The techniques of air-to-ground telemetry have been used in research aircraft testing since the start of the X-1 program in 1946. It became apparent during the development of the X-type research aircraft that personnel responsible for aerospace medical support of the pilot were not taking full advantage of the progress in telemetry systems to monitor for medical purposes the pilot and his environment during flight. One of the research objectives of the X-15 program is to obtain the pilot's physiological response to flight at increased speed and altitude. This objective is accomplished with the pilot wearing a full pressure suit; therefore, this garment and biomedical data acquisition equipment, techniques, and results are discussed in this presentation.

From March 10, 1959, through November 9, 1961, 85 hours of full pressure suit time have been accumulated by pilots who have flown the X-15. Sixty-two missions were flown with the original MC-2 garment which was characterized by a neck seal separating the breathing oxygen in the helmet above the seal from the nitrogen cooling and pressurizing gas below the seal. On March 21, 1961, a new-model protective garment was used for the first time in the X-15 program. This newer equipment is designated the A/P 22S-2 Full Pressure Suit. As of November 9, 1961, this garment has been used during 18 X-15 operations. These full pressure suits were evaluated in other aircraft flown at the Air Force Flight Test Center for a total flight time of 171 hours and a total ground time of 554 hours. This brings the total full pressure suit experience in support of the X-15 program to 725 hours. The new A/P 22S-2 garment (fig. 1) has several major improvements over the original MC-2 Full Pressure Suit (fig. 2) in the following areas:

(a) Increased visual area - The double curvature face plate in the A/P 22S-2 Full Pressure Suit, together with the use of a helmet face seal in place of the old neck seal, allows the face to move forward in the helmet so that the pilot has a lateral visual field of approximately 200°. This is an increase of approximately 40° over the single contoured lens of the MC-2 helmet, with an additional increase of 20 percent in the vertical visual field.

(b) Ease of donning - The older MC-2 Full Pressure Suit was put on in two sections: the lower rubberized garment and the restraining

Preceding page blank *

coverall, the upper rubberized garment and its restraining coverall. This was a rather tedious process and depended on folding the rubber top and bottom sections of the suit for retaining pressure. The new A/P 22S-2 Full Pressure Suit combines five components of the original suit into a one-piece garment with a pressure-proof zipper that runs around the back portion of the suit and is zippered closed in one operation. It took approximately 30 minutes for the pilot to be properly fitted into the older garment. Because of garment integration, the ease and rapidity of donning the new full pressure suit has improved to the point where a pilot can be dressed in a matter of 5 minutes.

(c) Removable gloves - In the original MC-2 garment, gloves were a fixed portion of the upper rubberized garment. The new full pressure suit has removable gloves which contribute to pilot comfort and ease of suit donning. This also prevents a buildup of excessive moisture from the hands during suit checkout and X-15 cockpit checkout prior to take-off. The removable-gloves feature facilitates dressing and makes it simpler for the pilot to get out of the full pressure suit himself, should this prove necessary. One other advantage is that, in the event of a last minute puncture of a glove, it is now possible simply to change gloves rather than to change the entire suit (fig. 3).

Following postflight oscillograph-data analysis, pilot body temperatures are plotted with aircraft cockpit wall temperatures, maximum aircraft structural temperatures, and ventilating nitrogen gas temperatures. To date, the ventilation and cockpit cooling system are adequately protecting the pilot so that his skin temperature remains at or below 100° F in spite of maximum aircraft temperature of over 1,200° F and cockpit outer wall temperature of 750° F. (See fig. 4.) The cockpit ventilating nitrogen gas temperatures range from 36° F to 81° F.

These suits have a new system of electrical connections installed through a pressure seal in the suit. This system facilitates data acquisition and avoids the older snap-pad arrangement used in the MC-2 suit. The previously used snap pad proved unsatisfactory for continual use. After several operations, the snaps either separated or failed to make good contact because of metal fatigue which resulted in a loss of data. To eliminate this loss of data, a continuous electrical lead from the pilot to the aircraft seat connection was sought. The approach was to find a lead that would not be bulky while penetrating the suit and would still maintain a satisfactory pressure seal. This continuous electrical lead from the pilot's body through the suit to the seat connection is now in use and has resulted in greatly increased reliability of data acquisition. The new A/P 22S-2 Full Pressure Suit has partially inflated on six flights during periods of partial cockpit pressurization loss and has proven to be a superior garment in terms of reliability and pilot acceptance. On these occasions, when the suit has inflated during flight, loss of cabin pressure

and suit inflation have been immediately observable on the real-time telemetry recorders at both Beatty, Nev., and Edwards Air Force Base, Calif. A schematic diagram of the physiological instrumentation as installed in the X-15 is shown in figure 5 and the onboard biological recording instrumentation is shown in figure 6.

Since May 5, 1960, in-flight physiological and environmental data have been recorded on 33 occasions. These data are both telemetered in real time and recorded by an oscillograph onboard the aircraft. The onboard data consist of electrocardiograph, respiratory, and pilot-skin and suit temperature information. The telemetered real-time data consist of respiratory rate, suit pressure, helmet pressure, cockpit pressure, normal (A_z) and longitudinal (A_x) acceleration data.

Initially, a signal conditioning package was installed on the instrumentation elevator that amplified the millivoltages of the EKG system, suit pressure transducers, and pilot body temperature thermistors. This resulted in a rather poorly recorded EKG signal on the aircraft oscillograph. Prior to the flight of September 12, 1961, a Tabor amplifier was installed on the ejection seat. This signal amplification close to the pilot resulted in a very much improved clinical-type EKG. Two mid-axillary leads and a common ground are used in obtaining the EKG data. The three electrodes are fabricated locally and are 3/4 inch in diameter. A silicone potting compound ring surrounds the metal mesh electrode, and a conductive paste is used to assure good contact between the skin and the electrode. A plastic cap is placed over each lead, and pressure-sensitive adhesive holds it in place. Respiratory rate data are obtained by a transducer in the oxygen-supply line. A sample of this onboard record showing EKG and respiratory rate from a flight of October 17, 1961, is presented as figure 7. Successive refinements within the EKG data collection process have led to obtaining a preflight and postflight record in the van used for pilot flight preparation. This can then be compared with in-flight data. To date, heart rates during flight have usually increased from the normal 70 to 80 per minute to 140 to 150 per minute, about double the pilot's resting preflight heart rate. No conductive cardiac abnormalities in the onboard EKG tracings have been detected. These rates represent the normal response pattern of the pilots who have flown the X-15.

Figure 8 shows the heart rate and respiration rate data obtained on a recent speed mission. These data are typical of most flights, both in magnitude and time variance. Since the heart has a better dynamic response to changing conditions, this discussion is concerned principally with the variation of heart rate with respect to the flight plan. Near launch, a peak in cardiac rate occurs and is apparent in all flights. This is a result of the physiological buildup prior to launch and engine start. On this particular flight of November 9, 1961, a speed of 6,005 fps, or Mach 6.04, was attained. From 314 seconds to 403 seconds, and from 438 seconds to 458 seconds, the pilot attempted to control the aircraft with the Stability Augmentation System (SAS)

turned off in the lateral directional mode. During these intervals, the heart rate increased and reached a peak shortly after the SAS-off interval. These peaks in heart rate are typical of such maneuvers. The windshield shattering between 438 seconds and 458 seconds also added to the increased heart rate. Throughout the rest of the flight, the heart rate decreased until just prior to landing where it again peaks. After landing, the heart rate rapidly decreases to typical resting values. Figure 9 is a plot of the heart rate and respiratory rate of a flight on March 30, 1961, when an altitude of 169,600 feet was attained. It is of interest to note the reduced heart rate during the 2-minute interval of 0.5g or less following rocket engine shutdown. This reduced heart rate, coincident with reduced normal acceleration, has been verified in the Mercury program and in the zero g profiles flown in F-100F aircraft. The increased heart rate at 520 seconds is the result of a normal acceleration at reentry of 4g and the simultaneous onset of aircraft vibration. The lack of data between 600 seconds and 800 seconds is the result of the oscillograph being intentionally turned off to conserve film for landing data.

The respiration rate also follows similar trends, increasing to three or four times the resting rate, but is less meaningful because the respiratory system has a poorer dynamic response and is influenced by talking. The large peak during the powered portion of the flight is the result of the physiological response during acceleration where pilots tend to breathe rapidly and shallowly.

To date, the data have been useful primarily from the standpoint of establishing physiological baselines for pilots of high-performance vehicles. These levels have also been confirmed in operational fighter aircraft where heart rates of 150 per minute have been observed during landings.

Since the high heart and respiratory rates recorded appear to be a normal response, these data will be useful in connection with future manned programs. Work is presently underway to determine more adequately the pilot's response to changing dynamic flight conditions. For this purpose, a blood pressure device, supplied by the School of Aerospace Medicine (SAM), and a linear pneumotachometer, supplied under Air Force contract to measure O₂ flow, are being installed. The major problem in determining the pilot's physiological condition is that of determining what parameters best show a realistic response and are still compatible with the pilot-aircraft combination. The School of Aerospace Medicine is presently doing much work in this area with two instrumented F-100F aircraft, and NASA has plans for obtaining additional physiological baseline information in their F-100C variable-stability aircraft.

On August 3, 1961, the Air Force Special Weapons Center, Kirtland AFB, delivered an ionizing radiation-detection device, designed and constructed specifically for the X-15. The package contains an ion chamber, two scintillators, a Geiger tube, and a multiple-channel tape recorder. The ion chamber and two scintillators are encased in different thicknesses of human-tissue-equivalent plastic. With the Geiger tube acting as a count rate monitor, the other detectors record radiation dose rate on the surface and at one-quarter-inch and one-inch depth in tissues. As changes occur in the radiation intensity, the change in ratio between count rate and dose rate gives some indication of the spectral characteristics of the change. This package, capable of recording dose rates from 1 or 2 millirad/hour to 100 millirad/hour has been installed in aircraft No. 670, and was first flown on September 29, 1961. The taped data from each flight are then sent to the Air Force Special Weapons Center, Kirtland AFB, for analysis. Appropriate to the altitudes attained to date, all radiation levels encountered have been as expected, or approximately 0.5 millirad per hour, which is equivalent to normal background radiation scatter. This package weighs approximately 10 pounds and is located on the left side console of the cockpit outboard of the ejection seat. It used 28 volts of aircraft power and is actuated by the pilot when the main instrumentation data switch is turned on during flight.

In summary, a method of providing pilot protection with a full pressure suit has been demonstrated during 80 X-15 operations from March 10, 1959, through November 9, 1961. The equipment, techniques, and results of obtaining real-time life-support data, including ionizing radiation, have been described and are receiving increased attention in all scheduled operations. The bioastronautics information and experience accumulated during the X-15 program have increased our understanding of personal equipment and physiological response to rocket flight and will be directly applicable to current and future United States manned space programs.

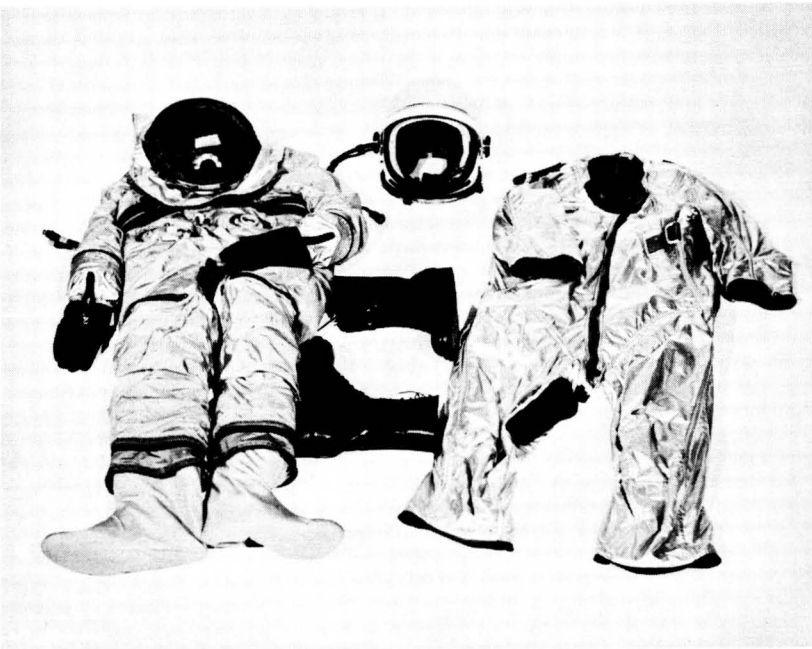


Figure 1



Figure 2

ORIGINAL PAUC
BLACK AND WHITE PHOTOGRAPH



Figure 3

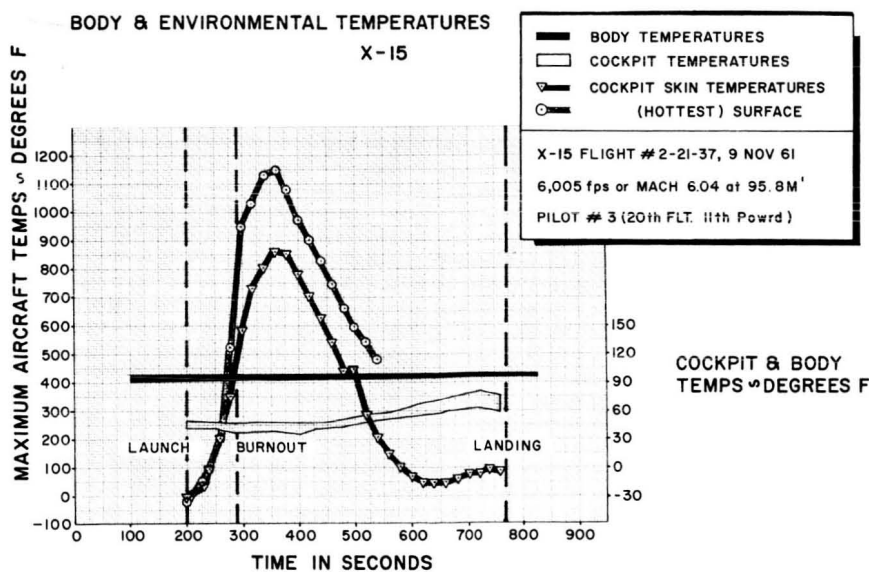


Figure 4

ORIGINALLY PRINTED IN
BLACK AND WHITE PHOTOGRAPH

X-15

**PHYSIOLOGICAL
INSTRUMENTATION**

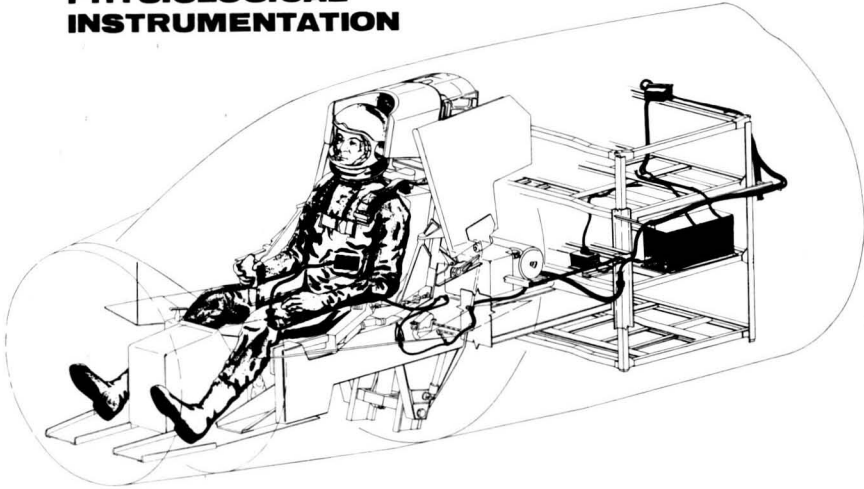


Figure 5

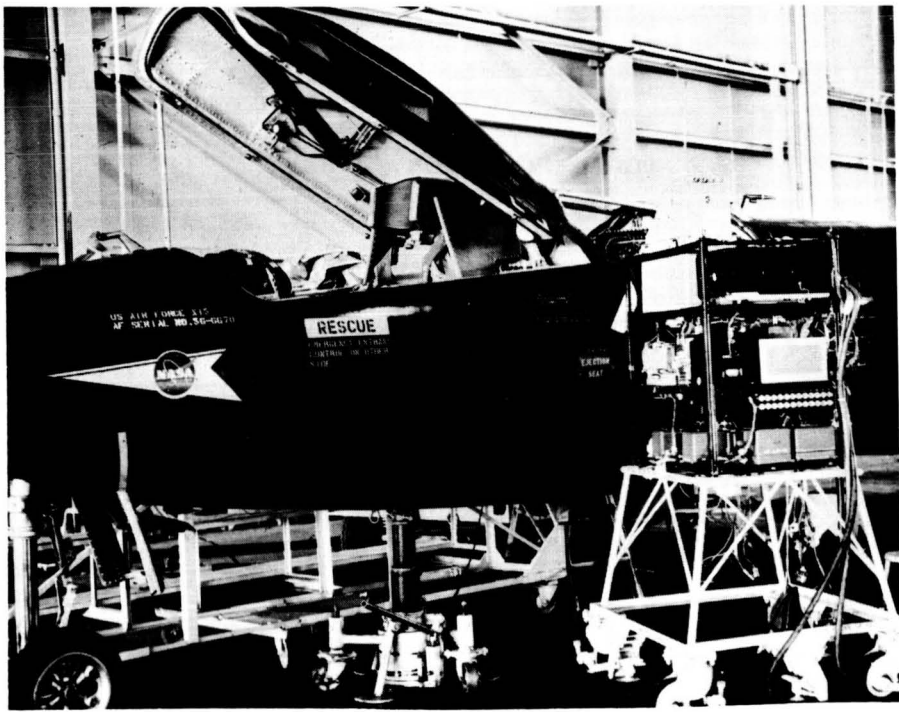


Figure 6

TYPICAL EKG AND PNEUMOTACHOMETER RECORD
BURNOUT + 10 SECONDS - FLIGHT 2-18-34

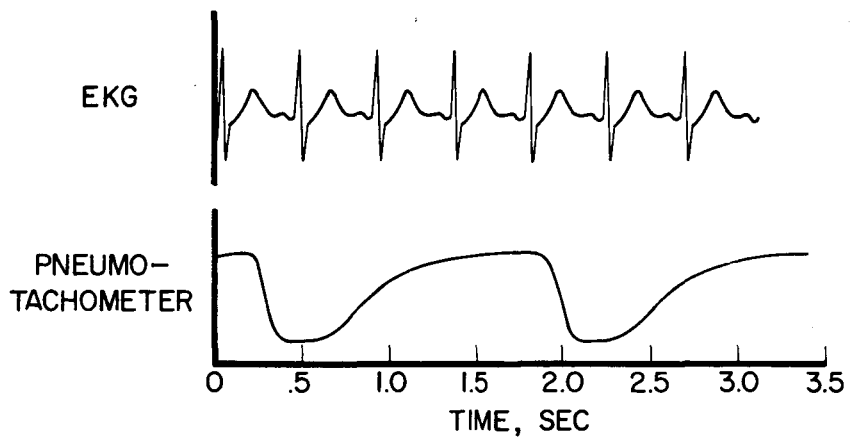


Figure 7

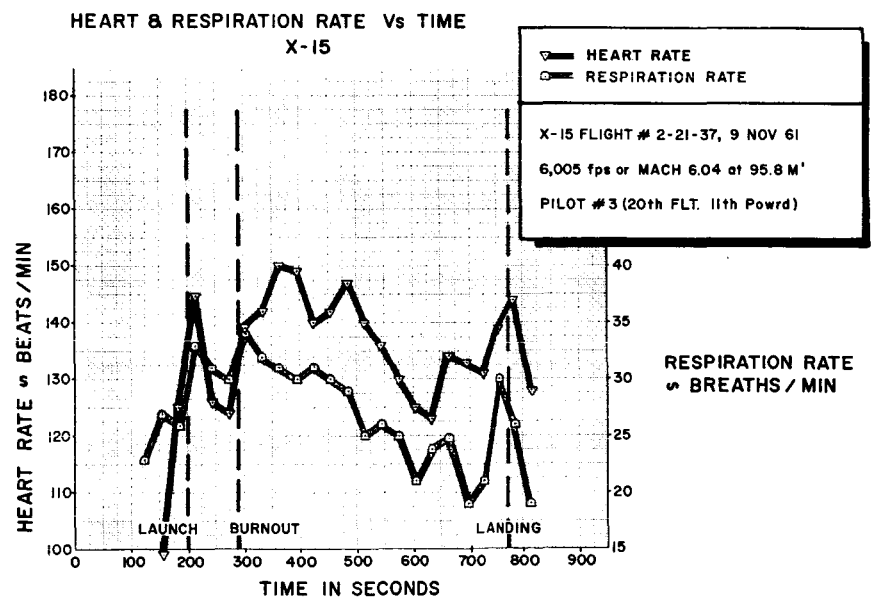
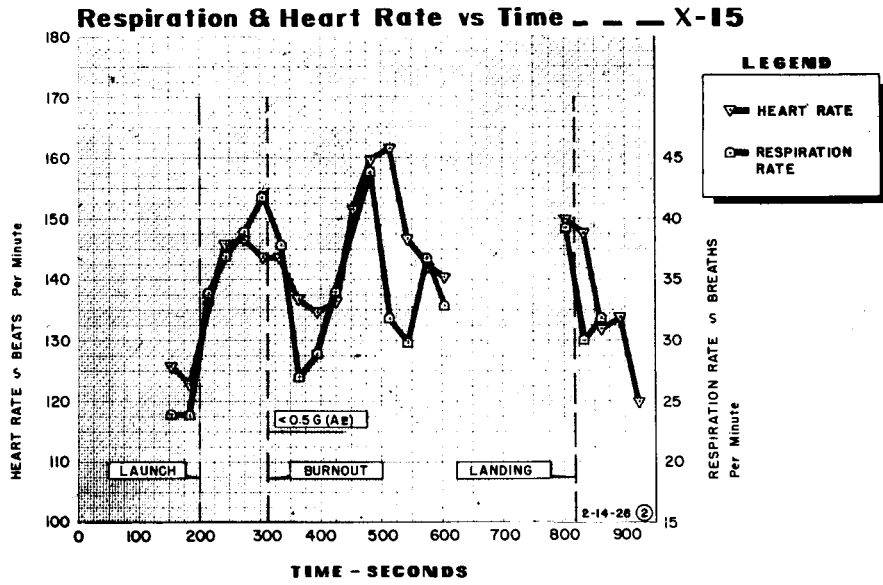


Figure 8



2-14-28 (2)

Figure 9

c-4



N71-75462

19. X-15 PROPULSION SUBSYSTEM COMPONENT DEVELOPMENT (✓)

By Robert L. Wiswell, Phillip Olekszyk
Air Force Flight Test Center

and John W. Gibb
North American Aviation, Inc.

SUMMARY


The X-15 rocket-powered research aircraft was developed by the integrated effort of various areas such as aerodynamics, thermodynamics, and structures. The propulsion subsystem development at the onset of the program was handicapped for varied causes. As a result, early in the flight testing phase, many time-consuming and costly delays were encountered as a result of individual component failures. A review of the X-15 propulsion subsystem components is presented, with a discussion of some of the development problems, how they were alleviated, and how they may be reduced or avoided in future programs. In order to avoid these problems in the future, a program is recommended in the hope that it will increase component reliability commensurate with vehicle objectives.

INTRODUCTION

The X-15 research aircraft is a rocket-powered aircraft utilizing a liquid oxygen-anhydrous ammonia rocket engine. Several major subsystems comprise the X-15 airplane. Among these are the propulsion system, auxiliary power units, and ballistic control rockets.

With the airplane being powered by a liquid rocket engine, it inherently involves numerous components. The propulsion system is manrated, and because of its safety requirements, it included redundant components. Because of these increased safety requirements and the ability of the system to be reused, the components are required to function with exacting reliability and accuracy. The safety, complexity, and the extreme combinations of environments of liquid rocket propulsion systems require that each component undergo a rigorous development program to establish the highest possible level of confidence prior to actual usage.

This paper explains the development of the X-15 propulsion subsystem components. The detailed review of the component development phase includes some of the development problems which confronted the program, how they were alleviated, and how these problems may be reduced or avoided in future programs.



The X-15 airplane was developed by the integrated efforts of various areas, such as aerodynamics, thermodynamics, and structures. At the initiation of the program, propulsion subsystem hardware development was handicapped by a lack of previous experience, technology, and availability of basic hardware elements. These handicaps contributed to the fluid component problems resulting in costly delays, failures, and a significant expenditure of manpower and resources. In order to combat these delays and increase confidence in the X-15 subsystems, various methods were employed.

If future developments of liquid rocket engine vehicles are to attain timely reliability, more emphasis must be placed on the development of system components. A recommended program is presented in the hope that it will stimulate component development to meet future needs, reduce the burden of paying for a component many times over, and increase component reliability commensurate with vehicle objectives.

X-15 COMPONENT DEVELOPMENT HISTORY

The methods used and the steps taken in the development of the X-15 propellant system components were very similar to those used on any airborne vehicle. The major difference was not in the methods, but rather in that the X-15 systems were taking a much larger step than usual into areas where too little was known; therefore, the development task was proportionately more difficult. The block diagram shown in figure 1 outlines the development steps.

First, by preparation of the propulsion subsystem schematic diagrams, the hardware needed was determined. Next, the individual item requirements such as fluid size, environment, operating characteristics, and expected life were determined or estimated. These requirements were subject to continuing change as the airplane design and flight profile were determined. With the preliminary establishment of the component requirement, a chart listing the items and the requirements in very general form was prepared and submitted to component suppliers. It was hoped from this survey to determine that the equipment required could be essentially "off-the-shelf" or easily developed. The results of the survey were rather disappointing in that very few suppliers were interested. However, from the survey, a limited list of suppliers to whom requests for quotations would be made was prepared, and also more rapid procurement of substitute hardware for initial test stand operation was permitted. Equipment-procurement specifications were being prepared concurrently with the initial survey. The major problem was to write an equipment specification so that the equipment would be acceptable for the task and not too difficult to build or even propose on and still attempt to cover future required changes without having to start over.

It was necessary to determine which, if any, of the existing military specifications were applicable and to what degree. Here again, there were some disappointing results. The military specifications were adequate for the then current generation of military aircraft, but with few exceptions they were not acceptable for the requirements of the X-15 airplane.

In order to get operable equipment in the minimum time, an additional step was taken; separate relaxed specifications were prepared for the initial equipment to be used on the test stands. Generally, the basic requirements were similar to those for the airplane equipment. However, the required tests were greatly reduced, and the requirements for envelope, weight, and environment were much less stringent. The reduced requirements were two-fold in purpose: first, to get the test stands in operation early; and second, to make the components function properly as soon as possible. Eventually, the flight hardware was also to be tested on the stands.

As each specification became sufficiently definitive, it was released to prospective suppliers for bid. As previously noted, the list of possible suppliers was very short. Experience compatible with X-15 requirements was limited. Additionally, in reviewing the prospective suppliers, it was necessary to determine whether they had the organizational capability to complete the job; that is, enough management, engineering, manufacturing, testing, and financial depth to deliver the specified equipment.

When the quotations were submitted and reviewed, it became apparent that the situation was even worse than the original pessimistic estimates. For the simpler, more routine type of equipment, there was sufficient response from suppliers with adequate experience. More often, though, the quotations numbered only two or three, and sometimes one. The reasons are simple and understandable - the cryogenic state of the art was not sufficiently advanced, the low X-15 airplane production made bidding very risky, and the tight delivery schedule permitted little time for basic research or to begin again in case the first design did not prove to be satisfactory. It is important to note that there never will be a program with sufficient time to do adequate basic research after that program is contracted and scheduled.

It became apparent very early that in many cases equipment, even at the reduced test stand requirements, would not be available in time. The test stands had to be operable in order to proceed with the engine development program. In order to assure that the test stands would be in operation in time, it was necessary to reengineer and modify the stands so that "off-the-shelf" hardware could be used. For example, figure 2 illustrates a liquid oxygen (LO₂) tank vent and relief valve which was made by combining a pneumatically actuated butterfly valve,

a separate relief valve, necessary pneumatic control valves and plumbing, and a safety burst disc. It can be seen that this arrangement was somewhat more cumbersome than the final integrated single valve shown in figure 3. This same type of temporary design was used for the ammonia and hydrogen peroxide tank relief valves, for the propellant feed and jettison valves, and for pressure regulators.

Some of the equipment development programs were proceeding on schedule. There were areas in which it was obvious that additional measures would be necessary to avoid delays in the flight-test program. One possible solution was the establishment of additional sources for the critical items. Second, and sometimes, even third sources were selected and contracts let. This program was successful to varying degrees: from the extremes of the delivery of usable hardware from all sources to the failure to procure from any source. In those cases in which none of the sources appeared to be destined for success, design and development was undertaken by North American Aviation, Inc., first by furnishing engineering aid to the suppliers, and then, if required, by assuming the entire responsibility, including manufacturing and all necessary testing.

Once again substitute temporary conglomerations of equipment were put together to do the job that one piece was supposed to do. As a case in point, figure 4 shows a liquid oxygen tank vent and relief valve used for initial flights. This consisted of a butterfly valve (an adaptation of the qualified liquid oxygen jettison valve), two relief valves, a pressure switch, a solenoid valve, and a shuttle valve. It was heavy, but it functioned satisfactorily, and it allowed sufficient time to conclude the successful development and testing of the final configuration valves without flight delays.

As the test stands were put into use, their operations often disclosed the need for design modification, which in turn led to specification changes. Added information relative to the airplane environment and tasks dictated modifications. Whenever possible, the specification requirements were relaxed. However, in many instances, changes of the opposite nature were necessary. Test stand operation was also put to good use in the development of the flight hardware. This equipment was installed and tested in actual operational use at the earliest possible time. In effect, test stand operation was used for development testing. The knowledge thus gained was available earlier than if the complete laboratory type of development and qualification testing had preceded operational usage. Many equipment malfunctions will not show up except during actual system operation. Basic research, development tests, qualification tests, and acceptance tests are all important and mandatory to obtain usable, reliable hardware. In the final analysis, however, the integrity of any piece of equipment is never assured until it has been used in its ultimate installation.

It was discovered during the flight test program that equipment which had performed satisfactorily on the test stands would occasionally malfunction in flight. The malfunctions were traced to various causes. For example, the environment in the airplane was more severe than that on the stands. Inadvertent flooding with liquid oxygen created temperatures far below those the equipment had been designed to withstand. Another example of unforeseen trouble was the ground explosion of airplane number 3 under operating conditions which had been accomplished many times on the test stands. A small change in environment probably made the difference.

In addition to the previously mentioned malfunctions causing specification modification and updating, the specifications were also modified as they were reviewed by the responsible military agencies. The requirements of these agencies for specification changes must be incorporated by the contractor. In the case of the X-15 airplane, these requirements for change were often not known until rather late in the program. This delay was primarily a result of a breakdown in the formal correspondence chain.

Because of this lack in communication, and because certain components had created repeated delays in the flight test program, including several airborne aborts, in February 1960, by order of Headquarters, United States Air Force, a component reliability team was formed.

The component reliability team, consisting of representatives from the Air Force Ballistic Missile Division, Space Technology Laboratories, Air Force Flight Test Center, National Aeronautics and Space Administration, Aeronautical Systems Division (WADD), X-15 Weapons System Project Office, and North American Aviation, Inc., was established as a means of increasing the confidence and reliability levels of the X-15 subsystems. This goal was attained by a careful review of the components and their respective specifications. Changes were recommended in all cases where applicable. The recommendations included the updating of specifications and reviewing component designs to reflect more realistic requirements as determined by individual system and flight testing. The component reliability team also succeeded in unsnarling the correspondence problems and insuring expeditious review of specifications and equipment. Table I shows that at the time of the formation of the component reliability team, less than 40 percent of the specifications and components had been reviewed and approved. It was determined that many disapprovals were only the results of minor points requiring clarification. The desirability of close personal contact between the prime contractor and Air Force technical personnel was well demonstrated by the manner in which these points were handled. Formal correspondence was thus reduced and the approval process was greatly accelerated. A review of the present subsystem status shows that all the specifications have been submitted and approved, and that all verification testing is complete and the reports have been submitted.

CONCLUSIONS

The following conclusions can be made of the development of the X-15 propulsion subsystem components:

1. Specifications: A portion of the component development problem can be attributed to the procurement specifications. Because of the lack of rocket systems technology, there were no military specifications directly applicable for the contractor to use as a guide in preparing detailed component specifications. As a result, the individual component specifications were continually being modified as the state-of-the-art knowledge became available.

2. Hardware development: Because of the lack of cryogenic fluid technology and understanding of rocket systems environments, many problem areas were underestimated. Also, for the component suppliers to make a profit and to meet the delivery schedules, many of the proposed components were merely a modification or redesign of an available "shelf" component. This approach was satisfactory in some cases, but for the more complicated components, such as regulators and vent and relief valves, this method was inadequate. This is evidenced by the fact that the development time period for some of the components was approximately 4 years.

3. System testing: The major factor in the successful development of components was the extensive use of system testing. By actual use of the individual components in the simulated flight environment, state-of-the-art problems were discovered and solved.

4. Coordination: Coordination between contractor and Air Force technical agencies did not flow smoothly. The components reliability team helped resolve this problem by close personal contact.

RECOMMENDATIONS

If the developments of future liquid rocket engine vehicles are to attain a high confidence level and timely reliability, a program should be instituted to attack component problems. Such a program should stimulate component development to meet future needs, reduce the tremendous burden of paying for a component many times over, and increase component reliability. The program outlined in figure 5 shown in its proposed sequence with the normal component development program will result in a reduced development time cycle. A program to improve components on future systems should (1) provide basic specifications, (2) provide module development so the programs can take advantage of advancements

in the state of the art, and (3) make component design data available to industry.

1. Specifications: It is recommended that a study of future programs be conducted of both the advanced projects and those in contractual stage to determine component requirements, and that general military specifications be prepared on basic component types. Six general areas can describe the large majority of all fluid system component requirements. The general areas would cover: (1) shutoff valves, (2) regulation devices, (3) vent and relief valves, (4) flow control devices, (5) disconnect and coupling devices, and (6) actuators.

2. Design data: Materials information and application data should be developed and widely disseminated, in advance of component hardware requirements, as new propellant combinations or environmental conditions are forecast. Many times, fluid system devices and phenomena have been rediscovered and forgotten over and over again. It is, therefore, recommended that a handbook be prepared to assist the designer in keeping up with such areas as future propellants, module development techniques, and future environmental requirements. Such a handbook would help prevent overdesign and the attendant results of overweight and low reliability.

3. Hardware development: A fluid system component is a package of subcomponents or modules such as seats, poppets, orifices, springs, diaphragms, and bellows. Usually, in a vehicle development program, time is not available for basic module development. Generally, a "newly developed valve" consists of reshuffling old modules. It is recommended that applied research programs be instituted, by both industry and government agencies, to develop advanced state-of-the-art module designs so that they can be utilized in many specific future components.

By having advanced state-of-the-art modules developed at the time of the program initiation, the component designer will be able to shorten the development time by incorporating the modules to meet his specific requirements. This will eliminate the need for each contractor to enter into a large component development program.

4. Coordination: In the future, in order to provide a timely dissemination of information gained from previous Air Force programs, early and close coordination must be maintained between the contractor and Air Force technical personnel. This would permit a free exchange of technical information and expedite the review of specifications and test data. Also, coordination between the prime contractor and component supplier is of equal importance.

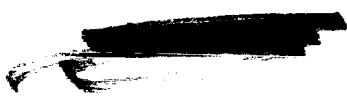
5. System testing: Implementation of the above recommendations will increase the chances of initial component success. System testing will

still be required and should be employed; however, the component changes resulting from such testing should be greatly reduced, and thus shorten the overall development time.



TABLE I
PROPULSION
SUBSYSTEM STATUS

	<u>FEB 9, 1960</u>	<u>OCT 15, 1961</u>
TOTAL FLIGHT-COMPONENT TYPES	72	72
COMPONENTS SUBMITTED	62	72
COMPONENTS APPROVED BY AIR FORCE	21	50
CRITICAL COMPONENTS	43	43
CRITICAL COMPONENTS APPROVED BY AIR FORCE	13	29
TOTAL COMPONENT SPECIFICATIONS	62	62
SPECIFICATIONS SUBMITTED FOR APPROVAL	52	62
SPECIFICATIONS APPROVED BY AIR FORCE	23	62
CRITICAL SPECIFICATIONS	34	34
CRITICAL SPECIFICATIONS APPROVED BY AIR FORCE	14	34



COMPONENT DEVELOPMENT

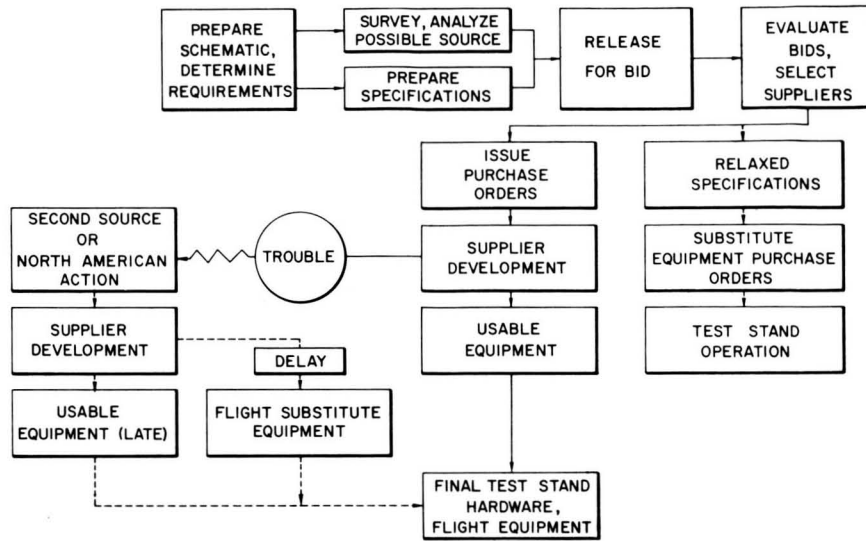


Figure 1

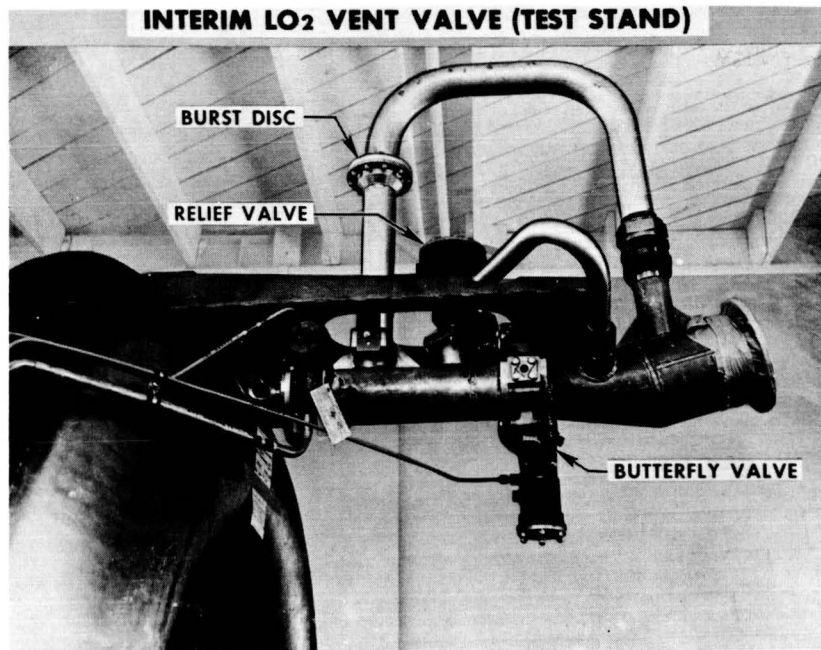


Figure 2



~~SECRET~~
DECLASSIFIED

LO₂ VENT AND RELIEF VALVE
FLIGHT CONFIGURATION

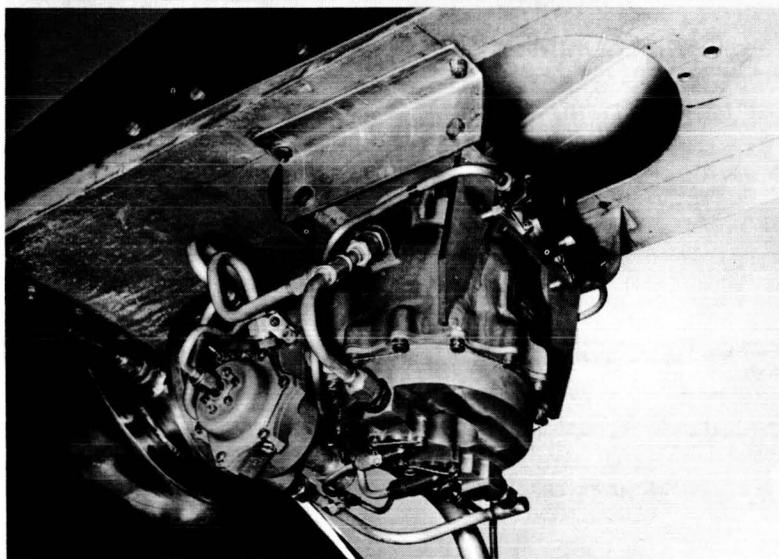


Figure 3

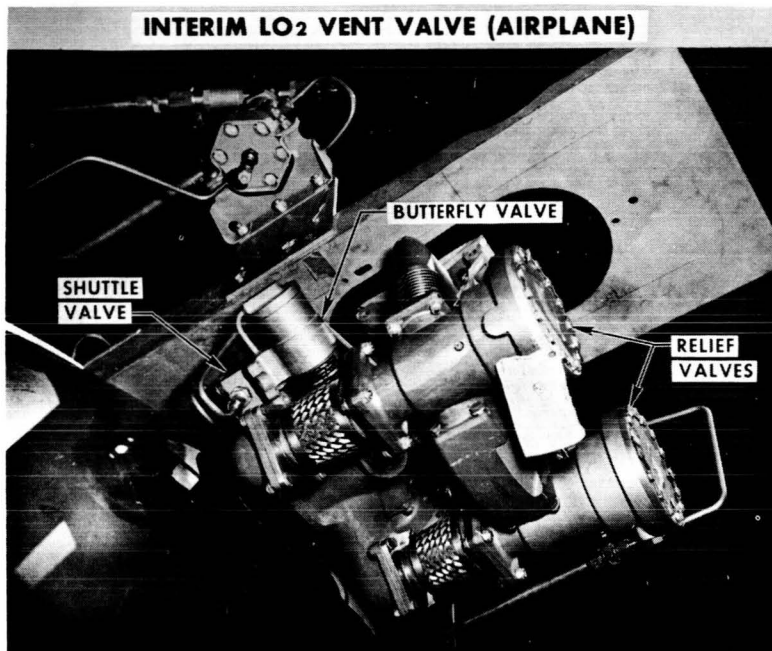


Figure 4

ORIGINAL PAGE
BLACK AND WHITE PHOTOGRAPH

~~SECRET~~

0371291030

RECOMMENDED DEVELOPMENT

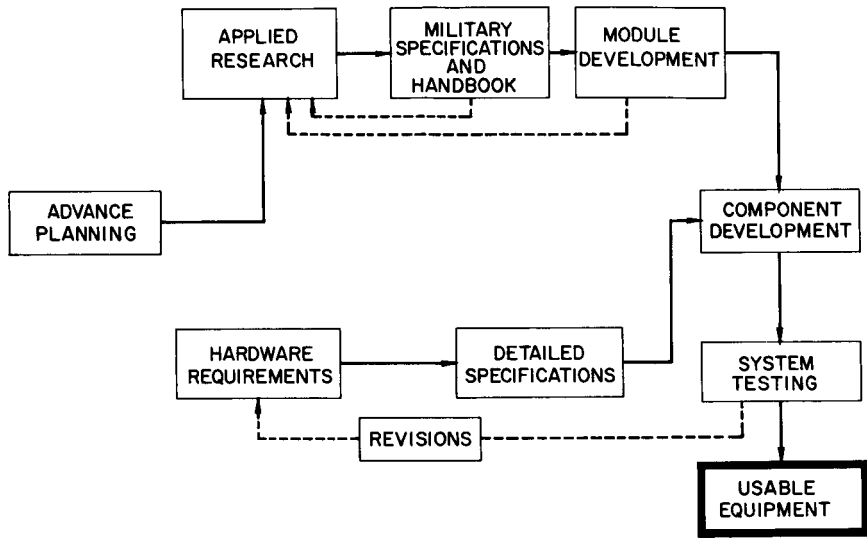


Figure 5

N71-75463

277



20. OPERATIONAL RELIABILITY EXPERIENCE

WITH THE X-15 AIRCRAFT (✓)

By James E. Love and John A. Palmer

NASA Flight Research Center

INTRODUCTION

It is the purpose of this paper to describe a comprehensive picture of X-15 operational reliability. The curves and text presented are based on actual parts failure records, flight logs, and the daily repair work sheets. It is therefore not only a picture of the reliability with regard to safety in flight, but also in view of ground preparation time and cost. Repeated system and component failures have resulted in many costly delays.

The X-15 airplane has an outstanding record of flight accomplishment and safety. In over 45 powered flights, the manned flight envelope has been enlarged beyond that of any other aircraft. This has been done without the loss of any aircraft and with no system failures after launch that were not readily managed by the pilot. However, due partly to the increased number and complexity of systems and partly to other problems which will be discussed subsequently, there have been many unsuccessful flight attempts and countless schedule delays. It is noteworthy that the wasted expenditure which occurs with an aborted airborne flight is over \$100,000.

GENERAL TRENDS

The in-flight reliability of the X-15 as a total vehicle has been excellent from the beginning. However, the reliability of major systems begins to drop noticeably when based on all airborne experience and quite drastically when based on all operational experience, both on the ground and in the air. An increasingly large amount of ground time has been spent and many cancellations have occurred because of parts failures or hard-to-analyze system malfunctions. As a result, the high mission success has been obtained at a disproportionately large cost in parts, materials, and technical and engineering man-hours. The same amount of preparation and testing is required for a cancelled flight as for a successful one.

The following items are discussed in this section in order to provide an understanding of some of the operational characteristics of the program: (1) number of scheduled flights as opposed to successful flights, (2) flight-preparation time, (3) system responsibility for schedule delays, and (4) system operational experience. Figure 1 shows a comparison of the number of successful, unsuccessful, and rescheduled flights plotted against calendar time. The lowest curve shows the progressively accumulated total of successful flights. The middle curve includes all successful flights and aborted air attempts, whereas the upper curve includes both lower curves plus all scheduled attempts. Note that the slope of each curve is greater than the one below it. Although the rate of successful flight accumulation has become approximately constant, the slopes of the other two curves are still increasing.

Flight-Preparation Time

Figure 2 depicts average time between successful flights. Increasing system complexity raises the amount of ground time required between flights and often increases the number of operations a system experiences prior to a flight. This increase is due to the fact that most ground checkouts are time limited and must be reaccomplished when failure of some other system causes delay beyond the period for which qualification is acceptable. Such a "snowballing" effect is partly responsible for the high rate of schedule cancellations.

A steady rise in average time between successful flights with program progression is evident, and a marked increase has followed XLR99 engine installation in both aircraft. This can be partially explained by the fact that during the interim engine program, ballistic control system and inertial system operations were not flight requirements and by the fact that the interim engine was more trouble-free. Major delays for XLR99 engine installation, the explosion of the X-15 number 3 airplane and other similar delays have been omitted for clarity. The curve should show a downward trend as all systems reach a greater state of maturity.

System Responsibility for Schedule Delays

The percentage of all flight schedule delays attributable to each major system since the beginning of flight testing is shown in figure 3. A great deal of time has been consumed in replacing components with repeat failures and in correcting conditions which caused an aborted flight. The percent allotted to a given system has been appropriately weighted for length of delay to give a truer comparison. Thus, the percent shown for bad weather is 10 percent as compared with an actual



20 percent of all delays. The APU and propulsion systems have obviously had the greatest growing pains.

Figure 4 presents the delays by systems for a period covering 13 recent flights of the XLR99 engine. As would be expected the engine problems far outweigh the others, and these have been discussed in previous papers. Next in importance are problems caused by the remainder of the propulsion system. Some new problems in this area were caused by the incompatibility of some plastic seal material with the anhydrous ammonia fuel, in addition to pressure regulation and relief difficulties that also appeared in the earlier program.

System Operational Experience

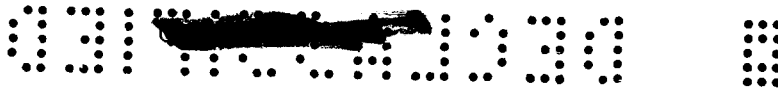
As the X-15 program has progressed, the failure rate of most major systems has decreased. The rates based on airborne experience only are currently fairly low. However, if failure rates are calculated by using all data for both ground and air, the current level for a given system is considerably higher. For example, figure 5 shows failure experience obtained by both methods for the auxiliary power unit (APU) and ballistic control rocket (BCR) system where the number of failures is plotted against airborne operations. In this figure and the figures that follow, a failure is defined as a system malfunction considered unsafe for flight. Since very few major failures have occurred in free flight, each point represents a malfunction which resulted in schedule delay, flight cancellation, or airborne abort. Note that most of these malfunctions occurred very early in the program.

Figure 6 is a similar plot for the engine and propulsion system and shows that malfunctions have been more prevalent for this system. The unevenness of the upper curve is indicative of the fact that propulsion problems seem to come in groups. The low frequency of airborne malfunctions as illustrated on the lower curve indicates a reasonably reliable system based upon airborne experience, but the figure shows more than five times the airborne failure frequency during ground checkouts.

Figure 7 shows calculations for the heating and ventilation system. Unlike the two previous systems, the most serious heat and ventilation failures have occurred after launch during the last 6 months, as shown by the upward trend at the end of each curve.

Similar data can be plotted for each of the remaining major systems. However, the three most troublesome systems have been discussed. These curves illustrate graphically the fact that high flight reliability is not a basic quality of the X-15 airplane. Rather, it has been obtained





at a high cost in parts, delays, and manpower and only by employing lengthy, complicated ground checkouts with the aid of equally complicated equipment.

CAUSES FOR SYSTEM PROBLEMS


Four of the causes of the systems problems discussed previously are as follows: (1) unexpected environmental conditions, (2) failure of qualification tests to duplicate true conditions, (3) contamination sensitivity, and (4) human factors. Each of these causes is discussed with examples.

Unexpected Environmental Conditions

The first cause of systems problems is unexpected environmental conditions which are as follows: (1) extreme cold due to ground holds, (2) extreme cold due to air holds, and (3) effects of new system installations. Since the beginning of actual flight operations a variety of last-minute problems, including poor weather conditions, has necessitated extended waiting periods prior to take-off. In the greatest proportion of these cases, the airplane has already been serviced with liquid nitrogen, oxygen, and chilled gases. As a result both structure and components have been cold soaked to extremely low temperatures. Since most parts and systems were designed for elevated temperatures, such cold-soak conditions have been one of the most aggravating sources of trouble encountered.

As an example, the heating and ventilation system is a heat-balanced, temperature-controlled design which provides a cryogenically cooled nitrogen atmosphere for pilot and equipment cooling. The liquid nitrogen injected to cool this atmosphere is enough to provide cockpit pressurization also. Recently, a change was made in the system in order to improve the cooling of certain components. As a result of this change, temperatures throughout the cabin area fell to unusually low levels, especially when long ground or air holds occurred. A series of six flights with cabin-pressurization failure followed. The cabin atmosphere had become so cold that additional cooling of liquid nitrogen was required to maintain pressure.

Even though all components of the system met rigid specifications, they were made to operate under conditions not considered in the original design. This environment was provided by a change made without full investigation of its effect on other systems.





Failure of Qualification Tests To Duplicate True Conditions

The second cause is failure of qualification tests to duplicate true operating conditions. Specifications covering procurement of a part always include a series of tests designed to assure that it will be able to withstand the conditions under which it must operate. It is impossible, however, to duplicate with such tests all circumstances that will occur in service.

For example, the auxiliary power unit and its fuel system were tested for many hours on an exact replica of the aircraft installation. Yet the APU system has been the cause of more schedule delays and cancellations than any other.

As an example of a component failure, a critical pressure switch in the APU system, although thoroughly qualified by the vendor, has been replaced by the dozen and even with improvements still constitutes a problem.

Contamination Sensitivity

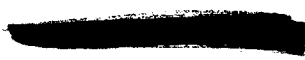
The major sources of contamination sensitivity are as follows:

- (1) residual or built-in debris, (2) oxidation, (3) wear, (4) corrosion, (5) deterioration, (6) decomposition, and (7) airborne particles (silica and dust).

Many parts and systems are made and tested under extremely clean conditions with exact tolerances. Qualification tests are conducted in a rapid series with special equipment to check the particular component or system.

In the actual aircraft, periods of activity for a system are followed by long quiet periods with stagnant fluid in lines. Systems are opened and closed many times and at many points. Actual aircraft configurations may contain dead ends or deposit points that did not exist in test setups. No matter what steps are taken to reduce it, there is bound to be more particle contamination in actual X-15 systems than in controlled test equipment.

That all this is true is borne out by the large number of repeat component failures due to contamination. If parts and systems were originally designed and tested with the idea in mind that they will be subjected to damaging particles, it would save considerable time and effort during actual use.





Human Factors

The last of these four causes is human factors, and some of the items which play a part are as follows: (1) misinterpretation of procedures, (2) faulty problem diagnosis, (3) use of standard but improper test methods on standard parts, (4) insufficient quality control, and (5) breakage or damage.

Although usually not due to poor design or service life, human error plays a large part in parts and system failures. Such occurrences would not appear to fall in the category covered by this report. However, the well-known existence of "Murphy's Law" dictates that human errors are a function of the design and procedures employed. Thus, if a system presents an opportunity for a mistake, a mistake will be made.

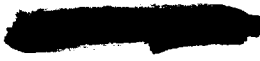
This is not to say that all such chances of errors can be eliminated through proper design. Actually, the only place where most of them can be detected is during actual field operations. However, many problems could be prevented by "idiot proofing" procedures and designing systems with the field mechanic in mind. A dramatic example occurred when shortly before launch a chase pilot reported peroxide flowing from the APU shutoff valve drain. Previous experiences indicated recycling of the valve would correct the problem and the APU was shut down. Restart produced what were described as "serious vibrations" and the flight was aborted.

Examination of the facts proved the drain was improperly identified and the leak was actually a small liquid oxygen leak not detrimental to flight. The APU restart had been attempted before proper sequencing occurred. The serious vibration could be explained only by a coincidental area of rough air. Thus, a series of human errors cost an entire flight without the occurrence of any failure.

CONCLUDING REMARKS

There have occurred many conditions, both physical and procedural, that could have been prevented had they been anticipated or more thoroughly accounted for in design and qualification testing. A greatly decreased program cost and increased flight frequency would then have been possible with attendant earlier attainment of research objectives.

This statement is understandably a broad one since it is impossible to provide for all contingencies. A research vehicle built in limited quantity with limited funds and incorporating untried systems is destined to experience many difficulties. Thorough realistic system and component



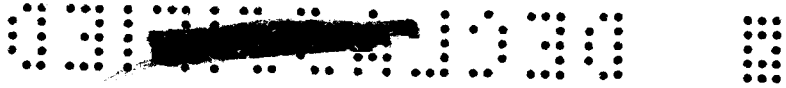
SECRET

testing should be completed as early in the program as possible. Neither component nor system testing can stand by itself.

It is hoped that many of the lessons learned with the X-15 can be applied to later research or operational vehicles so that its flight success and safety record can be duplicated or bettered without the expenditure of so much "ground time."

However, it should be pointed out that the reliability is increasing for nearly all of the systems, and the time between flights has begun to return to a reasonable figure. We are well into the research program and have every reason to believe that our future program should proceed at an acceptable rate.

SECRET



X-15 PROGRAM OPERATIONAL HISTORY

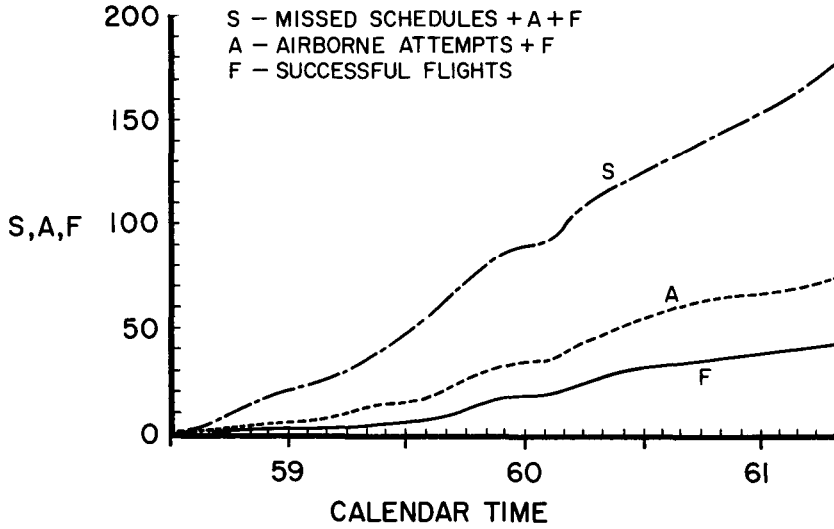


Figure 1

AVERAGE TURN-AROUND TIME (BASED ON AVERAGE OF SUCCESSIVE 5-FLIGHT GROUPS)

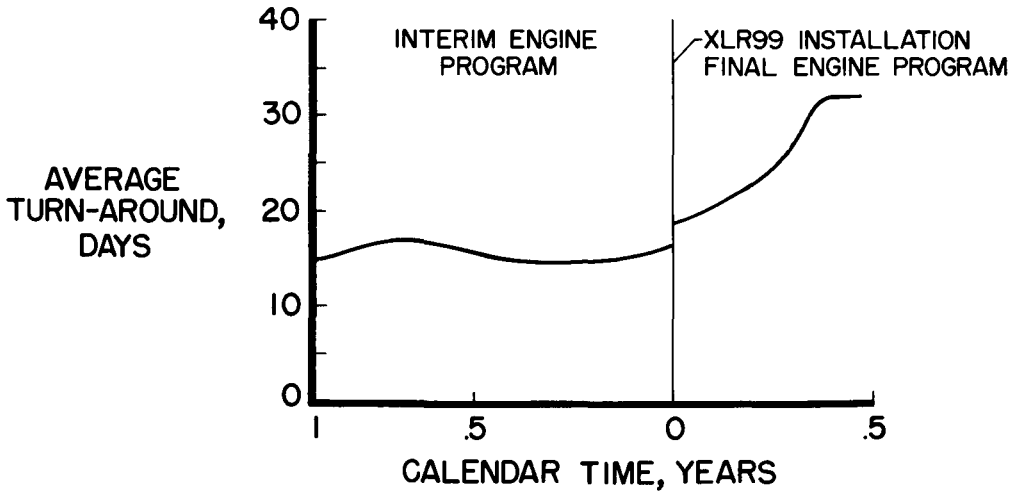
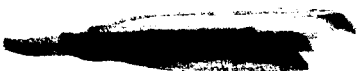


Figure 2



SOURCES OF SCHEDULING DELAYS
(TO OCT. 10, 1961)

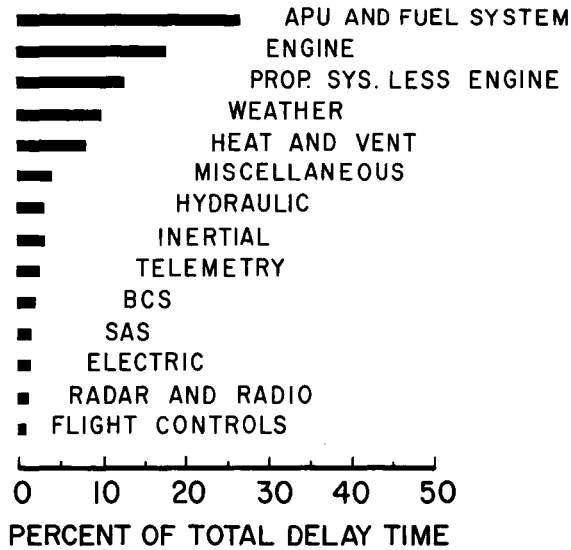


Figure 3

SOURCES OF SCHEDULING DELAYS
SINCE XLR99 INSTALLATION (13 FLIGHTS)
(TO OCT. 13, 1961)

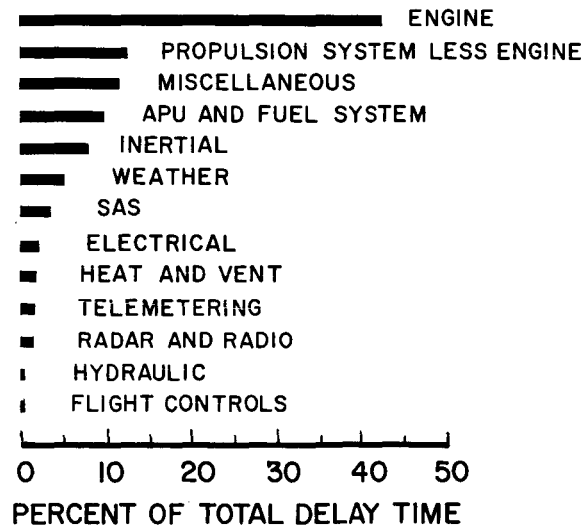


Figure 4



APU/BCR SYSTEM EXPERIENCE vs AIRBORNE OPERATIONS

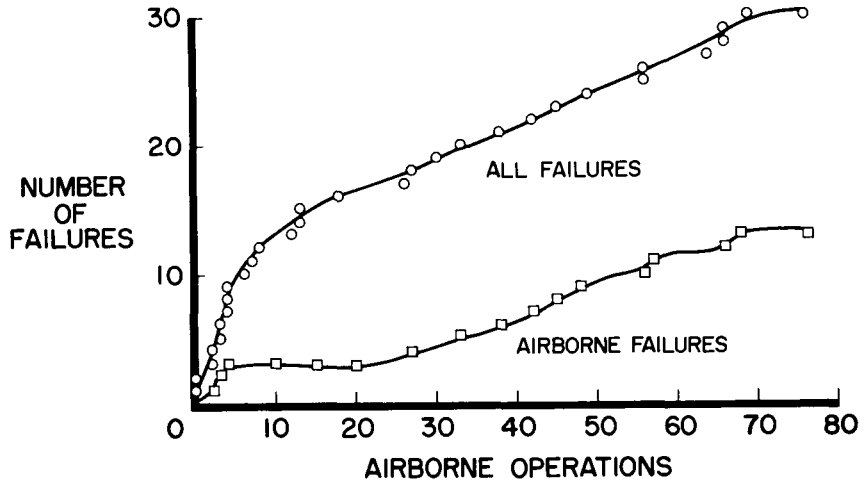


Figure 5

PROPULSION-SYSTEM EXPERIENCE vs AIRBORNE OPERATIONS

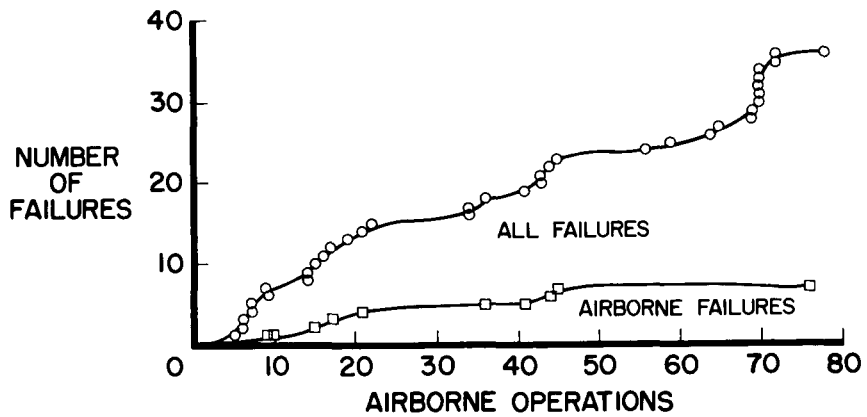


Figure 6





HEAT AND VENT SYSTEM EXPERIENCE VS AIRBORNE OPERATIONS

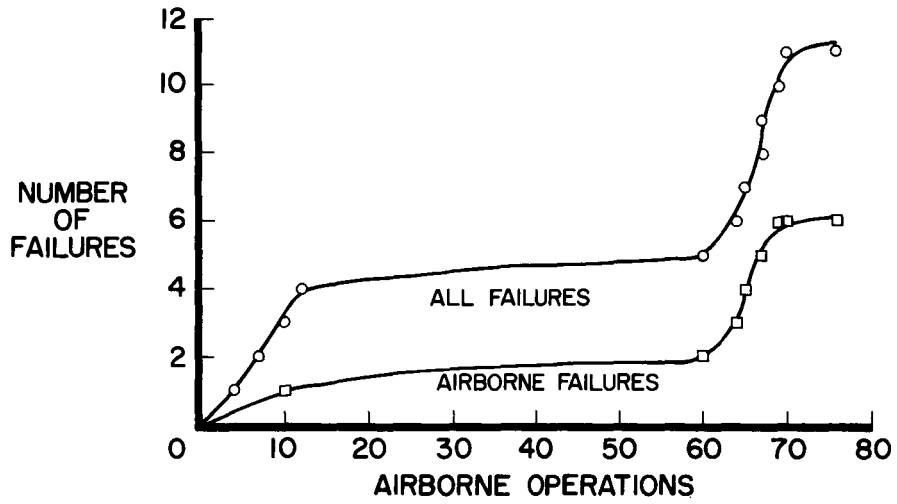


Figure 7

21. X-15 PILOT-IN-THE-LOOP AND REDUNDANCY EVALUATION (U)

By Robert G. Nagel

Air Force Flight Test Center
N71-75464

INTRODUCTION

The value of the human pilot and redundant systems is currently a matter of great controversy in the preliminary design of space vehicles. Unfortunately, quantitative results with previous aerospace systems have not been properly documented to assess directly either their pilot or redundancy aspects. Thus it is that much of the consideration in these regards is based upon intuitive projections and purely qualitative appraisals. The X-15 program, because of its currency and its many similarities to the next generation of aerospace craft, yields documented facts which lend realism and validity to the current considerations of piloted as opposed to unmanned vehicles and redundancy as opposed to nonredundancy in systems design, particularly for a vehicle developmental phase. (For the purposes of this evaluation "redundancy" is defined broadly to include dualized systems, emergency back-up provisions, and fail-safe devices.)

A comprehensive evaluation has concluded that the X-15 flights to date have greatly benefited from inclusion of a pilot in the control loops and from having redundant systems. These benefits have been accrued both in terms of mission success and safe recovery of the X-15 airplane. Figure 1 illustrates that all but one of the first 44 X-15 free flights actually resulted in mission success. However, the evaluation shows that with neither a pilot-in-the-loop nor redundant systems, less than one-half of those same 44 missions would have been at all successful. Similarly, there have been no losses of X-15 airplanes. But for a hypothetically unmanned, nonredundant "X-15," it was found that the airplane would have crashed on almost one-third of the flights.

DISCUSSION

The basic approach to the X-15 pilot-in-the-loop and redundancy evaluation was to perform a flight-by-flight detailed engineering analysis of each individual problem or failure which occurred for all X-15 launch and aborted flights. Each problem or failure was completely described and corrective action by the pilot or redundancy was analyzed. The effect and value of the pilot and redundancy were assessed with

Preceding page blank

PRECEDING PAGE BLANK NOT FILMED




regard to the impact on mission success and vehicle recovery. Then the hypothetical cases of an unmanned and/or nonredundant "X-15" were studied to confirm the previous assessment of the pilot and redundancy aspects of each in-flight problem or failure. Formalization of these procedures resulted in a "Detailed Flight History," which was then quantitatively summarized to serve as the basis for all further analysis. (This back-up documentation will be available in an AFFTC technical report on this subject to be published soon.)

For the purpose of compiling the Detailed Flight History, numerous sources of information were researched, no one of which was complete. This information was contributed by the NASA Flight Research Center, the Air Force Flight Test Center, and North American Aviation, Inc., and was extracted from periodic status reports, flight files, pilot's reports, flight failure records, and project engineers' notebooks.

Several important ground rules were strictly adhered to in the conduct of this evaluation, among which comprehensiveness and impartiality were basic. All problems or failures were initially documented, whether seemingly significant or not. The benefits of the pilot-in-the-loop and redundancy were assessed conservatively to avoid any glorification of either of these elements. Conjecture was minimized, especially for the hypothetical case of the unmanned, nonredundant X-15. Several incidents involving significant conjecture or uncertainties as to impact were properly de-emphasized by the introduction of fractional weighting factors. The pilot was not credited with detections nor corrective action which definitely would have been provided by some other element in his absence. Likewise, he was not assessed detrimental effects which would have been the same without a pilot. Redundancy was assessed similarly. Finally, in the hypothetically unmanned, nonredundant case, it was assumed that no system nor component changes were made other than removing all redundancy and substituting relatively simple and reliable present-day guidance and automatic control systems in place of the pilot.

A practical cut-off point for this evaluation was set at November 1, 1961. At that point 76 flights of the X-15 had been conducted, the first of which was flown on March 3, 1959. Figure 2 illustrates that 44 of these were actual free flights, 30 more resulted in launch abort after mated B-52/X-15 take-off, and the remaining two were intentional captive flights.

In evaluating the 44 free flights, the postlaunch phase was first analyzed. "Postlaunch" refers to that time period between physical launch separation of the X-15 from the B-52 carrier and contact with the ground upon X-15 landing. The postlaunch pilot and redundancy aspects as extracted from the Detailed Flight History are treated quantitatively in table I and figure 3. Table I lists the pilot and redundancy benefits in terms of mission success and safe airplane recovery.



RECAPITULATED

The first row of values show both the problematic flights and the hazardous individual incidents which required only pilot action to prevent loss of missions and aircraft. Next, are listed those situations safely handled by benefit of redundancy alone. The flights and incidents requiring both the pilot and redundancy acting in combination are then shown, and finally, these figures are added together on the bottom row to give the total pilot and redundancy benefits for the postlaunch phase. Examination of table I shows that on a flight basis, primary missions successfully completed as a result of pilot only were two; redundancy only, one; pilot and redundancy working in combination, 11; for a total of 14. On an individual incident basis the pilot and/or redundancy benefits are roughly twice as prevalent. Both the flight and individual incident bases show alternate missions accomplished as a result of pilot alone to be two; redundancy alone, none; pilot and redundancy acting together, four; for a total of six. And finally, the X-15 was safely recovered on five flights by virtue of pilot action only, one flight because of redundancy alone, and 13 flights requiring both pilot and redundancy combined, for a total of 19 aircraft saved. As can be seen, the pilot and redundancy benefits for aircraft recovery are also somewhat greater when appraised on an individual incident basis. The apparent dependence of the pilot upon redundancy to cope with in-flight problems and failures is in part due to the broad definition of redundancy as used in this evaluation. As stated earlier, "redundancy" is defined to consist of pure redundancy for improving reliability, such as dualized auxiliary power units plus emergency provisions for improving pilot and aircraft safety, examples of which are back-up flight data references and fail-safe propellant tank relief valves. The effect of this broad definition of redundancy will also be observed in the results being presented later for the prelaunch phase.

The postlaunch results are summarized in figure 3 to illustrate further the net pilot and redundancy effects on a flight basis. This diagram shows that total mission success after launch was 43 in 44 attempts for the actual X-15 as compared with 27 successful missions with pilot only, 24 with redundancy alone, and only 23 with neither pilot nor redundancy. The 23 mission successes of the unmanned, non-redundant X-15 would be comprised of 19 flights which were completely trouble-free plus four flights which were trouble-free after launch. Similarly, for safe aircraft recovery no X-15 airplanes have actually been lost, but this evaluation shows that with the pilot alone X-15 airplanes would have hypothetically been lost 14 times; with no pilot but with redundancy retained, 18 aircraft would have crashed; and with neither pilot nor redundancy 19 crashes would have resulted. The assessment of 14 crashes to a piloted but nonredundant "X-15" issues ominous implications in terms of pilot mortality rate, and all but the actual case figures would spell doom to such a research flight test program as the X-15 airplanes are engaged in. A further serious



implication of losing aircraft involves repeated failures because of the inability to thoroughly analyze initial failures and their causes following a crash.

Next, the prelaunch phase of each X-15 free flight was analyzed. "Prelaunch" refers to that time period between mated B-52/X-15 take-off and physical separation of the X-15 from the B-52 carrier at launch. The prelaunch pilot and redundancy aspects of all the free flights were extracted from the Detailed Flight History and are presented quantitatively in table II and figure 4. As illustrated in table II the pilot alone was able to avoid four aborted flights and coped with seven individual incidents of an abort nature. Redundancy alone avoided two aborts and successfully corrected four abort-type individual incidents. The pilot and redundancy acting in combination served to avoid six aborts and coped with five individual abortive incidents. These benefits were then tallied to give the total pilot and redundancy effects in terms of abort avoidance.

The prelaunch results are summarized by noting in figure 4 that of 74 total launch attempts there were 44 successful launches of the actual X-15 (that is, with a pilot-in-the-loop and redundancy). With the pilot only there would hypothetically have been 36 successful launches; with redundancy only, 34; and least of all, 32 launches, with neither pilot nor redundancy. Another interesting prelaunch ramification is that for the hypothetical unmanned, nonredundant "X-15," critical problems which occurred on four flights may not have been detected from the B-52, chase aircraft, or ground monitoring. If, in fact, these problems were not detected and corrected, launch would have occurred in each case and resulted in probable loss of the aircraft. Because of the conjecture involved, these possibilities are not included in the tally of hypothetical aircraft losses.

The results of the prelaunch and postlaunch analyses for the 44 free flights were combined to determine the overall pilot-in-the-loop and redundancy effects as previewed in figure 1. This consolidation compares the actual 43 successful missions in 44 launches with only 24 successful missions for pilot only, 20 with redundancy only, and 19 with neither pilot nor redundancy included. These are the 19 flights which were totally trouble-free. Comparison of results in figures 1 and 4 shows that safe aircraft recovery for the hypothetical cases appears to effectively increase from the overall flight standpoint as a result of abort preclusion of six hazardous free flights. In other words, in the absence of a pilot and redundancy six of the X-15 flights would have inadvertently aborted before launch with no knowledge of the impending postlaunch hazards thereby avoided. This leaves a net total of 13 flights of the unmanned, nonredundant "X-15" which would have definitely resulted in crashes with all effects taken into account.



There is an obvious trend in these results toward even greater interdependence between pilot and redundancy than was seen in either the prelaunch or postlaunch phases taken separately. This result is attributed to the multiplicity of individual incidents arising over the course of any one typical flight requiring pilot action or redundancy for safe solution. This is borne out from tables I and II by observing that in 25 flights which were not trouble-free, there occurred 47 individual incidents involving pilot-in-the-loop or redundant systems, and usually both, to avert mission failure. Since basic vehicle design can seldom directly account for greater than single-degree malfunctions, the pilot-in-the-loop plays a vital role in safely and flexibly handling such multiple failures and compounded problems. In this capacity the pilot must be supported by redundant systems, emergency provisions, and flexible control in order to be totally effective.

Of more than mere academic interest is an available comparison between the results just presented and those of a similar pilot-in-the-loop and redundancy evaluation performed independently by The Boeing Company for the first 60 flights of the Bomarc missile. The Bomarc is, of course, an unmanned and relatively nonredundant vehicle, and Boeing's evaluation consequently involved analytical extrapolation to a hypothetically piloted "Bomarc" having system redundancy comparable to that found in the X-15. Thus, the Bomarc results were arrived at by a reverse extrapolation to that utilized in the present X-15 study. And yet, as shown in figure 5, the results bear resounding similarities with regard to the percentage of total missions which were successful. For the actual X-15, total mission success was about 98 percent, which compares very closely with the 97 percent determined by Boeing for the hypothetically piloted "Bomarc" having redundant systems. Conversely, for both the actual Bomarc and the hypothetically unmanned, nonredundant "X-15," total mission success was found to be identically 43 percent. The pilot-only and redundancy-only mission success figures also compare quite closely. This comparison lends validity to the extension of such evaluations to other aerospace research and development vehicles. (Acknowledgement is made to Mr. Thomas K. Jones of The Boeing Company for the Bomarc data.)

After the X-15 free flights were thoroughly analyzed, the 30 aborted flights were evaluated. Generally speaking, the pilot-in-the-loop and redundancy aspects of the aborted flights are somewhat more elusive than was found in the free flights. However, some significant trends are still observed. Table III presents a summary of pilot and redundancy effects for the aborted flights on an individual incident basis. Pilot-in-the-loop and redundancy here consist not only of X-15 factors, but also the pilot and redundancy aspects of the B-52 and chase airplanes which are peculiar to the manned X-15 type of operation. It is seen that there were a total of 25 instances where pilot considerations and

redundancy either caused abort or provided an additional cause for abort. However, there were 14 cases preceding the actual first cause for abort where having the pilot and redundancy prevented hardware damage or avoided immediate abort. Furthermore, there were 24 instances of pilot and redundancy benefit in preventing damage or immediate abort of captive flight either during or after the actual first causes of aborts. Therefore, the pilot and redundancy were beneficial both in allowing the flights to progress normally as far as they did and in allowing informative and somewhat exploratory captive flights to proceed safely after the first call for abort. The byproduct in both cases was usually the gaining of invaluable systems knowledge and operational experience.

It is additionally observed from table III that the pilot and redundancy detected a total of 14 problems which otherwise would have gone undetected from the B-52, the chase airplanes, or the ground monitor stations. In all of these cases launch would have occurred and either the mission, the X-15, or both would probably have been lost.

In analyzing the 30 aborted flights on an overall flight basis it was determined as illustrated in table IV that pilot considerations and redundancy were at least partially the cause for abort on 16 of the 30 aborted flights. On the other hand, having a pilot-in-the-loop and systems redundancy prevented damage or immediate abort on 20 of the flights and on 8 flights provided the sole capability for detecting various problems which otherwise would have resulted in launch and probable loss of either the mission or the X-15, or both. A comparison of tables III and IV again illustrates the multiplicity of individual incidents arising over the course of any one typical flight, be it an aborted one or an actual free flight.

A comparison of the pilot and redundancy aspects of the X-15 aborted and free flights can be achieved on the basis of mission success. It has already been determined that 24 of the 44 free flights were dependent upon benefits of a pilot-in-the-loop and redundancy for completing successful missions. This number is compared with the 16 flights which were aborted either primarily or secondarily due to pilot and redundancy detriments; consequently, unsuccessful missions resulted. However, of these 16 aborted flights, 10 flights also involved one or more of the following type problems or failures in addition to the pilot-or-redundancy-caused abort incidents:

- (1) A problem requiring a pilot-in-the-loop or systems redundancy for correction in order to launch
- (2) A failure related neither to the pilot nor to redundancy

- (3) A problem or failure which could be detected solely by the X-15 pilot or by virtue of X-15 systems redundancy and which otherwise would have resulted in launch and a probable unsuccessful mission

In reality, then, having a pilot-in-the-loop and redundant systems cost only six unsuccessful X-15 missions through abort as opposed to 24 successful X-15 free-flight missions made possible only by virtue of pilot and redundancy.

Several qualifying remarks are appropriate at this point for a full appreciation of the quantitative results of this evaluation. Included in the Detailed Flight History were failures of X-15 subsystems under development and for which there were no operational requirements at the particular stage of the X-15 program when failure occurred. Examples of these are the inertial flight data system and the ballistic control system. However, these failures of developmental systems, owing to their very nature, were not reflected in assessing pilot and redundancy effects nor included in the quantitative results. The benefits of life-support redundancy (such as the pilot's pressure suit) were also purposely excluded by the rating process and do not reflect in the final results. It was believed that if it were not for the pilot's presence in the X-15, there would be no need for such life-support redundancy. This approach keeps the results conservative with regard to prohibiting any distortion of the virtues of redundant systems in general. Conservatism in rating the pilot-in-the-loop benefits was achieved by disregarding the inherent "unreliability" of the automatic guidance and control systems hypothetically substituted for the pilot in the cases of unmanned vehicles. Furthermore, the advantages of the human pilot in sensing, evaluating, and reporting qualitative flight test results were not included. And finally, it should be noted that no attempt has been made to cover the numerous ground aborts which have occurred in the course of the X-15 program.

There are two interesting peripheral aspects of this study which it is hoped will be developed in more detail in the forthcoming technical report mentioned previously. The first of these is systems maturity, and the other involves the effects of the B-52 carrier aircraft as a recoverable, recallable, slow "booster" having maneuver and loiter capabilities. In 16 of the aborted X-15 flights the B-52 in its booster capacity rendered 35 significant benefits which would not be realized with a conventional, nonrecoverable, fast booster.



CONCLUSIONS

In conclusion, it can be restated and emphasized that the X-15 flights to date have demonstrated resounding net benefits of the pilot-in-the-loop and redundant systems in terms of mission success, safe aircraft recovery, and the very continuance of the X-15 program. Even though the assessment was kept conservative, 24 of the first 44 X-15 free flights were found to require pilot-in-the-loop and redundant systems in order to culminate in successful missions. Only six of the first 76 flights of the X-15 were aborted because of overall pilot and redundancy detriments. The majority of the 24 other aborted flights were benefited by both the pilot and redundancy in deferring abort, allowing safe continuance of a captive flight after call for abort, or preventing launch in the presence of an otherwise undetected and unsafe condition. The pilot and redundancy were instrumental in safely handling most of the multiple failures and compounded problems which have been prevalent in the X-15 flight program to date. The most important pilot and redundancy benefit to the X-15 program is graphically demonstrated in figure 6. The upper curve is a time plot of the first 44 X-15 free flights. The lower curve plots hypothetical aircraft recovery for the unmanned, nonredundant vehicle. The shaded area between the two curves represents 13 losses of aircraft in the absence of a human pilot and systems redundancy. Decisions on preliminary design of future space vehicles should find considerable bases in these quantitative results and results similarly derived from other current aerospace programs with regard to the pilot-in-the-loop and redundancy functions.





TABLE I

PILOT AND REDUNDANCY BENEFITS FOR X-15 FREE FLIGHTS
POST-LAUNCH PHASE

BENEFITS AS RESULT OF	PRIMARY MISSION COMPLETED		ALTERNATE MISSION ACCOMPLISHED		SAFE AIRCRAFT RECOVERY	
	FLIGHT BASIS	INDIVIDUAL INCIDENT BASIS	FLIGHT BASIS	INDIVIDUAL INCIDENT BASIS	FLIGHT BASIS	INDIVIDUAL INCIDENT BASIS
PILOT ONLY	+2	+7	+2	+2	+5	+8
REDUNDANCY ONLY	+1	+1	0	0	+1	+2
BOTH PILOT AND REDUNDANCY	+11	+17	+4	+4	+13	+15
TOTAL (PILOT AND REDUNDANCY)	+14	+25	+6	+6	+19	+25

TABLE II

PILOT AND REDUNDANCY BENEFITS FOR
X-15 FREE FLIGHTS
PRE-LAUNCH PHASE

ABORTS AVOIDED BY:	FLIGHT BASIS	INDIVIDUAL INCIDENT BASIS
PILOT ONLY	+4	+7
REDUNDANCY ONLY	+2	+4
PILOT AND REDUNDANCY	+6	+5
TOTAL (PILOT AND/OR REDUNDANCY)	+12	+16



03712091030

TABLE III

**PILOT AND REDUNDANCY EFFECTS FOR X-15 ABORTED FLIGHTS
INDIVIDUAL INCIDENT BASIS**

EFFECT OF -	DETRIMENTS		BENEFITS			
	RESPONSIBLE FOR -		PREVENTED DAMAGE AND/OR IMMEDIATE ABORT		PROVIDED SOLE DETECTION OF PROBLEM RESULTING OTHERWISE IN LOSS OF MISSION AND/OR AIRCRAFT	
	PRIMARY CAUSE FOR ABORT	ADDITIONAL CAUSE FOR ABORT AFTER PRIMARY ABORT CAUSE	BEFORE ACTUAL ABORT CAUSE	DURING OR AFTER ACTUAL ABORT CAUSE	BEFORE ACTUAL ABORT CAUSE	DURING OR AFTER ACTUAL ABORT CAUSE
PILOT-IN-THE-LOOP ONLY	4	2	1	9	0	11
REDUNDANCY ONLY	9	8	8	8	0	2
BOTH PILOT AND REDUNDANCY IN COMBINATION	2	0	5	7	0	1
TOTAL FOR PILOT AND/OR REDUNDANCY	15	10	14	24	0	14
	25		38		14	

TABLE IV

**PILOT AND REDUNDANCY EFFECTS
FOR X-15 ABORTED FLIGHTS
OVERALL FLIGHT BASIS**

EFFECT OF -	DETRIMENTS	BENEFITS	
	PROVIDED A CAUSE FOR ABORT	PREVENTED DAMAGE AND/OR IMMEDIATE ABORT	PROVIDED SOLE DETECTION OF PROBLEM RESULTING OTHERWISE IN LOSS OF MISSION AND/OR AIRCRAFT
PILOT-IN-THE-LOOP ONLY	3	6	1
REDUNDANCY ONLY	11	3	5
BOTH PILOT AND REDUNDANCY IN COMBINATION	2	11	2
TOTAL FOR PILOT AND/OR REDUNDANCY	16	20	8

OVERALL PILOT-IN-THE-LOOP AND REDUNDANCY BENEFITS

PRE-LAUNCH + POST-LAUNCH
(THROUGH NOV. 1, 1961)

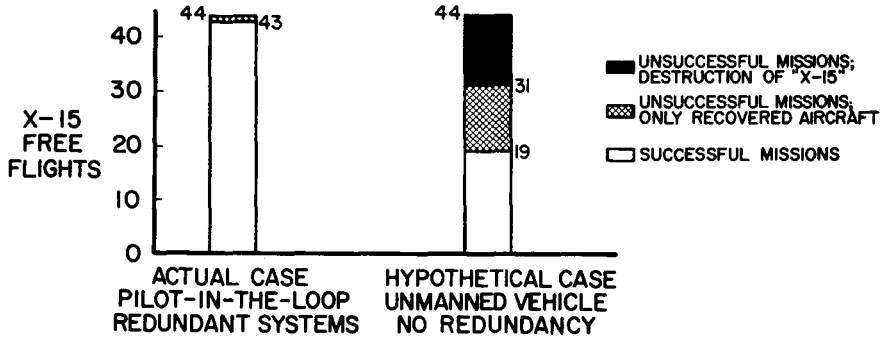


Figure 1

X-15 FLIGHT RECORD

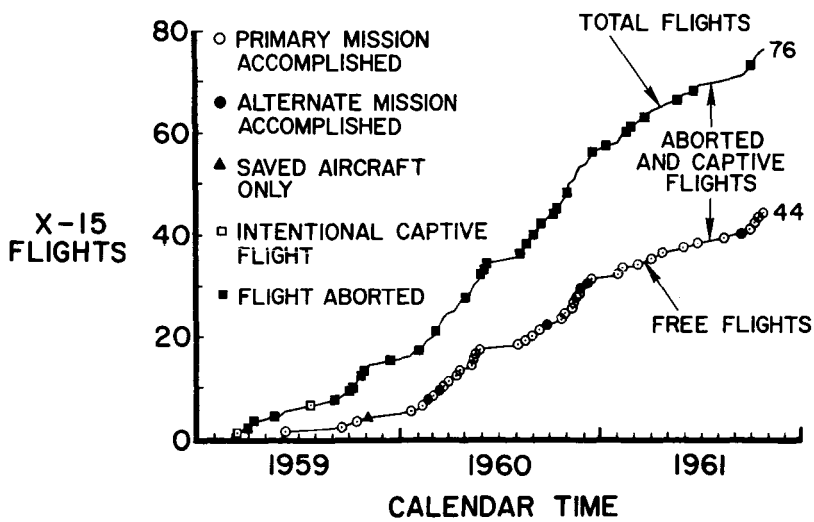


Figure 2

QUANTITATIVE SUMMARY OF X-15 FREE FLIGHTS
POST-LAUNCH PHASE

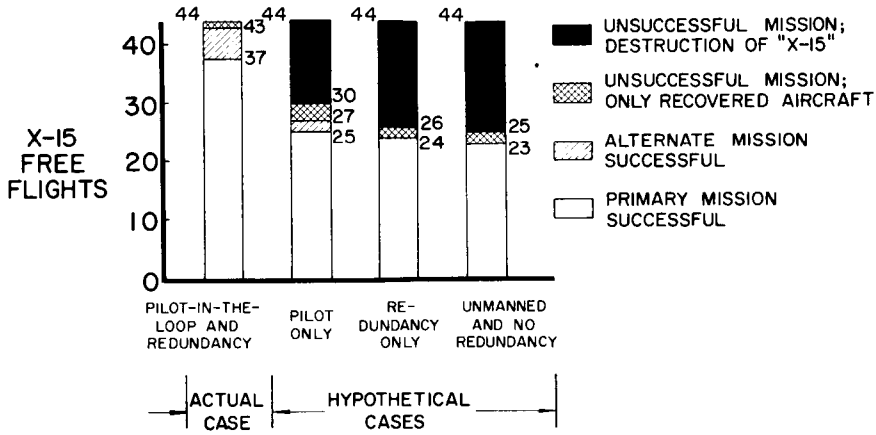


Figure 3

QUANTITATIVE SUMMARY OF X-15 FREE FLIGHTS
PRE-LAUNCH PHASE

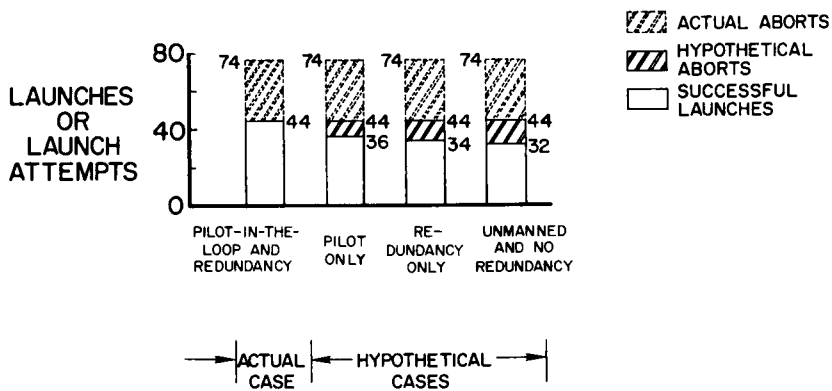


Figure 4



SECRET

COMPARISON OF X-15 AND BOMARC PILOT AND REDUNDANCY ASPECTS

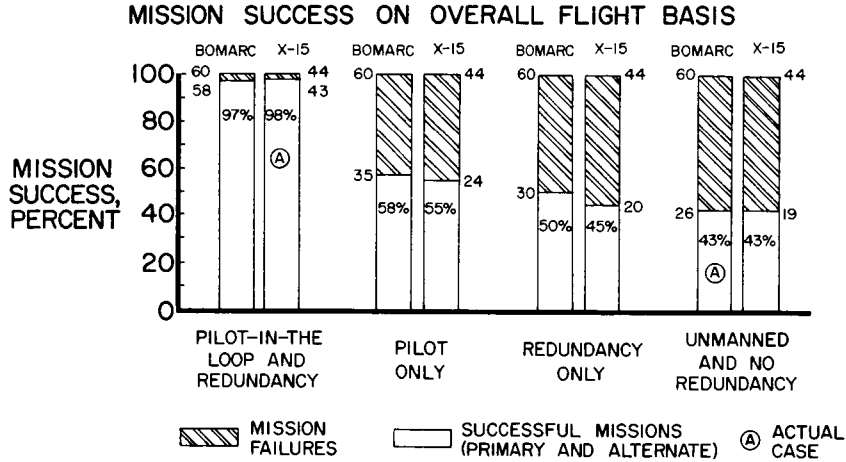


Figure 5

X-15 FREE-FLIGHT RECORD OF SAFE AIRCRAFT RECOVERY (PRE-LAUNCH + POST-LAUNCH)

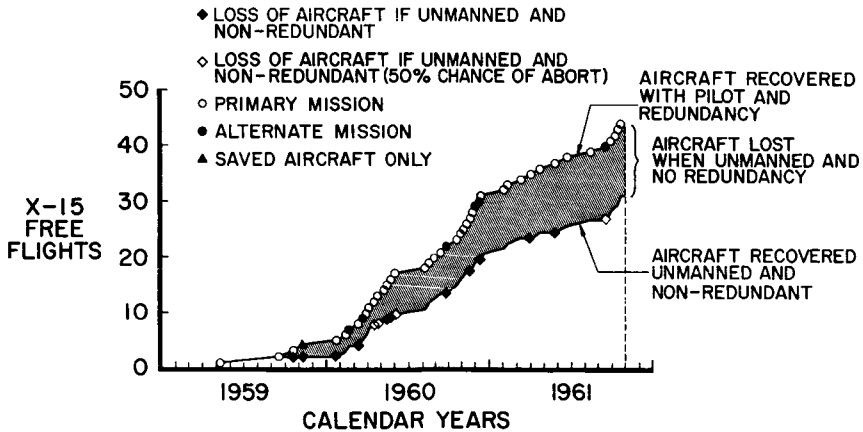


Figure 6

22. A PILOT'S IMPRESSION OF THE X-15 PROGRAM (U)

By Joseph A. Walker

NASA Flight Research Center

N71-75465

Although the X-15 is an advanced high-performance aerospace craft, capable of maneuvering in the atmosphere and of being controlled outside of the atmosphere, its stage of development, compared with vehicles of the future, is still fairly primitive. On the other hand, even if the X-15 were to accomplish no other purpose than that it was built and flown, the knowledge gained and technological advancement achieved has indeed been worthwhile. It is not the intent of this paper to be critical of the X-15 because of its deficiencies or problems. It should rather be kept in mind that many compromises had to be accepted in the design of the X-15 to get on with the job, and rightly so, because there are some questions which still have not been resolved. Inasmuch as the pilot flies the X-15 from launch to landing, much has been learned about his capabilities. It is consequently important to consider the program from the standpoint of the utilization of the pilot and see what has been verified or learned that can be carried forward to more advanced vehicles. The use of the word "pilot" in this discussion refers to all pilot input.

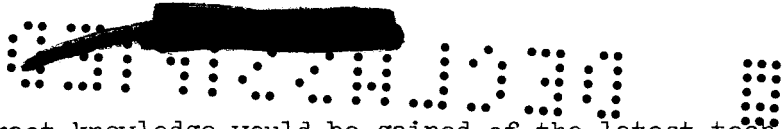
As a framework for this discussion, utilization of the pilot is considered to include four main categories, as follows:

- (1) Planning
- (2) Supporting research and development
- (3) Operations
- (4) Analysis and interpretation of results

How closely these categories are interlocked can be discovered if an attempt is made to establish a starting point. Logically this point would be the experience the pilot has gained from a recent project. This was the basis for initial X-15 pilot selection and participation in evaluation and planning.

The experience gained by pilots should be brought to bear early in planning an advanced project. Planning should include:

Basic design requirements
Simulation
Supporting research and development
Feasibility of design proposals
Operational concepts



From such plans, direct knowledge would be gained of the latest techniques, feasibility of human control, and operational concepts. From combinations of experience and extensive electronic simulation, better visualization of the operational problem would result and would aid in design specification and determination of required supporting research. The combination of knowledge of available equipment and the chance of availability for new equipment specified for the job will aid in evaluating feasibility of new design proposals. The pilot should be able to inject some practical approaches in the program, to avoid the influence of hobbyists who would unnecessarily complicate or overengineer a vehicle, and should draw on his experience to insure that adequate functional crew facilities and capabilities are provided. The pilot is able to aid materially in determination of necessary crew size and the distribution of crew responsibilities as well as in the development of operational concepts.

The real complexity of the problem of equipment for guiding and flying the X-15 was not brought out until actual simulations of design flight profiles were flown. Several variations of simulation were participated in by the pilots in order to get acquainted with the problems involved with attempting to fly anticipated maximum performance X-15 flight profiles. By this means, also, some appreciation of the control requirements and the pilot presentation requirements was developed. Also, dynamic simulation programs allowed a look at the control task accomplishment capability and any effects of accelerations expected from the X-15.

Supporting research and development requires the pilot to contribute to just about any portion of the job relating to his ability to fly and operate the vehicle. Items pertinent to the task include:

- Control systems
- Guidance
- Cockpit presentation
- Propulsion
- Environment
- Simulation

The items noted are not complete but are suggestive of the magnitude of the task. The point to be made here is that an accomplishment of supporting research and development has become an area of acute shortage, especially in point of timeliness. There is a need to begin at once to consider these items for future projects. Most important, hardware, now known to be required, needs to be developed, evaluated on simulators, installed in existing aircraft, and flight evaluated. The pilot should be active in evaluating progress and results. Items which are now extremely deficient are measurement and presentation of altitude or



distance from objects, velocity, and thrust. Even when desired information can be measured and presented, accuracy is in doubt or can only be expected for short periods.

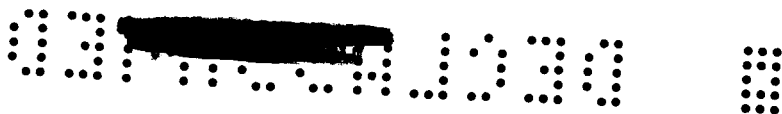
At the present time with the X-15, mission planning is done on the basis of pitch attitude and engine shutdown time assuming that thrust is nominally correct for a given throttle setting, and a stopwatch which starts with main thrust chamber ignition is utilized for timing flight path events and burning time. This stopwatch thus assumes importance of first magnitude.

Figure 1 illustrates the effects of pitch angle θ , thrust time t , and shutdown velocity upon the resultant altitude. To reach the intended altitude of 250,000 feet, 81 seconds of full thrust burning are utilized at a pitch attitude of 37° and shutdown velocity of 5,350 ft/sec. Indicated is the altitude resulting from an error of ± 2 seconds burning time as well as gross errors in θ of as much as $\pm 4^\circ$. The shaded area indicates the greatest error in θ which may be expected from flying the presentation. Observe that the pilot can run the engine longer to make up for low flight profile. Clearly, accuracy is essential to hitting objective altitude. Also, shown on the right-hand side of figure 1 are the resulting dynamic pressures during reentry as functions of pull-out angle of attack α and peak altitude. It can be seen that accuracy in the lower angle-of-attack ranges is critical, and these angles must be considered for roll-yaw SAS-off reentry. These curves represent holding the pull-out angle of attack to a load factor of 5g and then holding 5g to level flight.

The following examples from the X-15 program illustrate the active and productive part that the pilot can take in the supporting research and development preparatory to a flight project. The three-axis attitude presentation was brought into use after dynamic centrifuge simulation pointed out the need for presentation improvement. The approach and landing technique now utilized was developed by experiments with F-104 airplanes. Presentation sensing, control stick operation, and thrust requirements were developed for reaction controls by ground simulation and flight experiments.

One area where pilots considered the X-15 to be deficient was the stability augmentation system (SAS). The problem is, as has been discussed in the paper by Petersen, Rediess, and Weil (paper no. 10), that without roll and yaw damping, control of the X-15 at high angles of attack is extremely difficult. Although pilots requested that SAS be dualized, the final design had single-axis stabilization, and flight planning is restricted to flight profiles from which recovery can be made with SAS failed. This results in decreased flight planning flexibility and particularly limits peak altitudes.






As regards operations, the X-15 program has been successful enough so that the pilot would be expected to participate as an active and integral part of any advanced flight operation. Crews should still be selected from the best qualified experienced test pilots. No improvement in the selection process has been apparent by use of special aeromedical and psychological testing over the experience approach other than the expected medical aspects. However, thinking on the method of control has per force been modified. Not that the basic approach that the vehicle should be capable of manual operation has changed, but it is appreciated that a direct mechanical link to the control system actuator is impossible for the whole mission and electrical signals must be substituted. Also, it is recognized that quite a lot of electronic equipment, accomplishing automatic functions, is necessary. It still appears that the simplest arrangement of the pilot-control system-guidance presentation loop that can accomplish the job is the best assurance of successful operation. Also, pilots agree that the primary source of information required for the operation should be on board the vehicle to preclude loss in event of radio or data link failure or interruption.

Training would be accomplished by active participation in all phases as the project develops, as well as specific training required for the program. Some of this specific training would be in orbital and space mechanics, astronomy, celestial and space navigation, systems maintenance, and guidance computer operation. It would be much easier to develop sufficient knowledge and experience for these skills in the experienced pilot than to train specialized scientific personnel as capable aircrew members.

A very important part of pilot training would be simulator and flight evaluation of items included under supporting research and development. The desirability of flight simulation in the early project phases cannot be overemphasized. An effort should also be made to utilize existing aircraft for any possible portion of the flight profile demonstration. An example of successful use of existing aircraft is the experience of utilizing F-104 aircraft to develop the technique and provide practice for landing the X-15. An excellent benefit is derived from this flight work in maintaining pilot proficiency, alertness, response to flight stimuli, and morale.

The problem of obtaining high-performance aircraft flights at a reasonable frequency is becoming so acute as to represent an area where the entire space effort could begin to suffer; that is, no amount of simulation can completely replace flight experience. If the vehicle itself does not fly very often, the next best flight experience performance-wise is better than none; in fact, is essential.

At this point, it is appropriate to amplify a pressing need in the national research effort. If the United States expects to send a





vehicle to the moon or to any other planet, it would be best to start now to do more than develop boosters and vehicles to do the job. We are beginning to try to develop the operation of vehicles so they can be handled by the crew which is expected to fly them. Visualize a three man crew on the moon attempting to preflight the X-15, or any other manned rocket available today, for a return flight. It certainly will not be practical to have a lot of test and ground support equipment available there or at an orbiting space station. It is now time to start, with a selected crew, setting up operational procedures, test procedures, repair and replacement requirements, prelaunch procedures, and actually attempting the job with the objective that we develop here the knowledge and techniques which can be used anywhere. There is too much tendency to wear out equipment in making sure it will work and little earnest effort to simplify the check and maintenance procedures. One lesson that has been learned from the X-15 is that the best way to accomplish a job is to go out and do it.

The pilot's contribution to the analysis and interpretation of results includes the following:

- Report flight observations of results
- Specify required improvements
- Establish meaning of recorded results
- Carry over to planning future flights
- Apply knowledge gained to new vehicle designs

The followup on required improvements has been extremely difficult in the past because the pressure of the problems associated with accomplishing the operation left little time for reflection, recommendations, and design participation. The basic planning for the project should establish the means for rapid assimilation of information and implementation of improvements. We will never start a job if we attempt to answer every question before starting!

Pilots participating in the X-15 program were convinced at the beginning that it could be flown. As results have indicated, their confidence has been justified in most areas. They were sometimes wrong, and came up short in some areas. Other pilots have presented recorded results and have discussed their meaning and impact on future flight planning. (See papers no. 9 and 10.) Figure 2 is a tabulation of the X-15 mission successes. It includes the number of launches actually made, of those launched how many achieved desired performance, and how many achieved the prime mission objective. The smaller numbers in the latter two categories result from powerplant and propellant system problems and pilot presentation deficiencies from consideration of performance, stability augmentation, and cabin-pressure—pressure-suit-systems problems in the case of prime objectives. Alternative modes of operation were available to obtain increased probability of mission



success. For instance, if the attitude-sensor ball nose failed after launch the pilot could do a 2g pullup until specified pitch angle was achieved. Reentry could be accomplished by reference to pitch on the attitude indicator, setting predetermined stabilizer angle, or reference to the horizon. However, all these resulted in comparatively inaccurate flight profiles. Generous tolerances were allowed in performance when achievement of prime objectives were considered. Even on several flights which were successful there were problems similar to those mentioned. The significant point in this figure is that the pilot has been able to accomplish the task, if not prevented by factors beyond his control, and to recover the airplane in all cases. Of course, the flights were planned for pilot operation, but the tasks were challenging even so. The planning and execution of flights was generally successful and indicates that the initial concepts were correct. On this basis it can be recommended that utilization of the pilot in advanced vehicles be accomplished similarly to the way it was done for the X-15 but that pilots' participation be increased and extended.

However high the success rate subsequent to launch of the X-15, one of the less clearcut aspects of piloting is how to determine the workload. Comments such as "busy," "piece of cake," "no strain," or "hardly hacked it" are very descriptive but offer not even a good qualitative comparison. There is physical loading as a result of maneuvers, thrust and drag, temperature, restraint (straps, pressure suit, reaching), and control operation. There is mental loading resulting from observing, interpreting, and decision making. There is emotional loading from being keyed up, eager to do a good job, and from unknown or unexplained occurrences during the flight (limit cycle residual oscillations) or known criticality of some emergency conditions. Although pilots are not doctors, they do participate in the medical aspects of the program, and it therefore seems worthwhile for pilots to determine whether their efforts could be measured.

Figures 3 and 4 are presented to illustrate some of these points and to arrive at an approximate workload, relative to maximum capacity, being demanded by an X-15 flight. Figure 3 presents flight time histories of altitude h , velocity V , normal (a_n) and longitudinal (a_x) acceleration, breathing rate, and heart rate as measured during an X-15 flight. Figure 4 shows two quantities, heart rate in beats per minute, and work load measured in meter kilograms per minute plotted against time in minutes. These data were obtained from a dynamic ground test of the same pilot's physical condition. The work consisted of pedaling a bicycle equipped with a Prony brake device which could be tightened as indicated by the step increases in the work load while the subject was pedaling in rhythm with a metronome. The termination of the work load is determined in this case by the heart rate reaching 180 beats per minute, which is taken to be the maximum normal output rate. Also the



recovery heart rate is shown for 5 minutes while the subject was resting after the 19 minutes of work output. This information was furnished through the courtesy of Dr. Ulrich Luft of the Lovelace Foundation for Medical Education and Research. Two of the same variables are present, the desire to do as well as possible and the work load. In figure 3 can be seen the general parallel response of breathing and heart rate to greater or reduced physical loading caused by maneuvering and thrust and drag. The heart rate appears to be the more accurate indicator of work load, since breathing can be varied somewhat (holding one's breath at high g, for instance). Note that the last 4 minutes (time 400-630 sec) have the highest continuous heart rate, coincident with a steep descending turn with speed brakes extended, followed by pull-out and landing pattern maneuvering. One can also observe the anticipatory "spinup" surges before launch and before descent, followed by decrease to required load. Recall the previous discussion about the different kinds of loading; the heart rate curve here represents the sum of them all. When selected points are transferred, using heart rate as the base, it can be seen that the workload spread indicated is between 45 percent and 78 percent of indicated capacity and more often at 50 percent to 60 percent. Although the X-15 pilots are not willing to say "even your grandmother could fly it," these indications are consistent with the comments by the pilots that they do not feel they are getting behind the aircraft. No adverse impact of increase of g loading has yet been noted.

Still hidden, however, is the tendency for the pilot to delete portions of the panel scan when other portions become critical or trouble develops in one area. Although this may not be too much, still it is one way of reducing the workload. The same results could be brought about by better and more centralized information. Also, here is an indication that use of another crew member will be advisable for longer duration missions.

Another clue that, although not loaded to physical capacity, the pilot is loaded to duty capacity is the often heard remark that "he didn't have time to look out." It should be kept in mind that the manner in which pilots are operating probably parallels that for an emergency operation of a more advanced vehicle. A large part of the envelope expansion tests involve testing the aircraft to develop limit conditions of controllability in regions from which it can be recovered before the aircraft and pilot are committed to a profile where limiting conditions may be required. Hence, measurements are being obtained of the pilot's physical exertion at the same time as information on just what a pilot can accomplish and still get the aircraft through the speed-altitude profile. It is admitted that this is a preliminary run at the problem, but even so, it does not appear to be insurmountable.

0311200 10311 [REDACTED]

It can be concluded that there is a great wealth of experience and practical knowledge available in the persons of experienced pilots to which more will be added. In order to realize the greatest return from our project, this store of pilots' information should be utilized to aid in the development of future designs and the planning of future operations. In addition, pilots can make direct contributions through participation in the operational phase.

[REDACTED]

EFFECTS OF PRESENTATION ERRORS DESIGN ALTITUDE MISSION

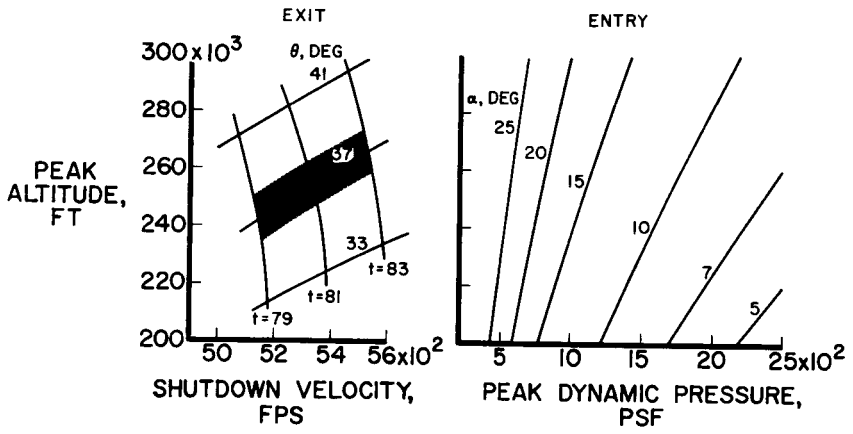


Figure 1

X-15 FLIGHT SUMMARY AS OF NOVEMBER 1, 1961

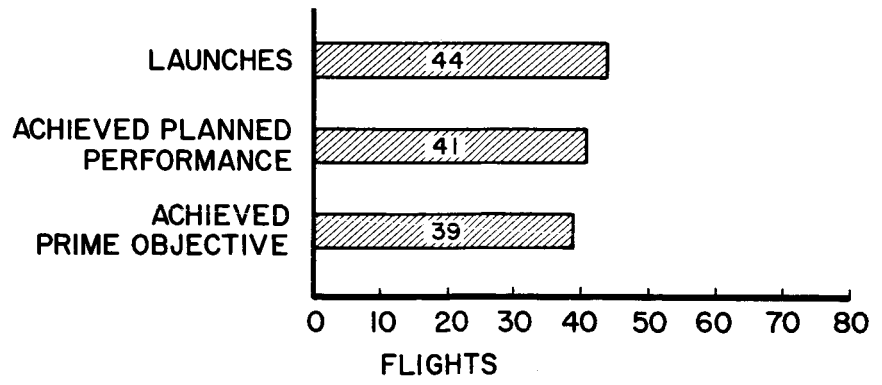


Figure 2

03 710 20 1973

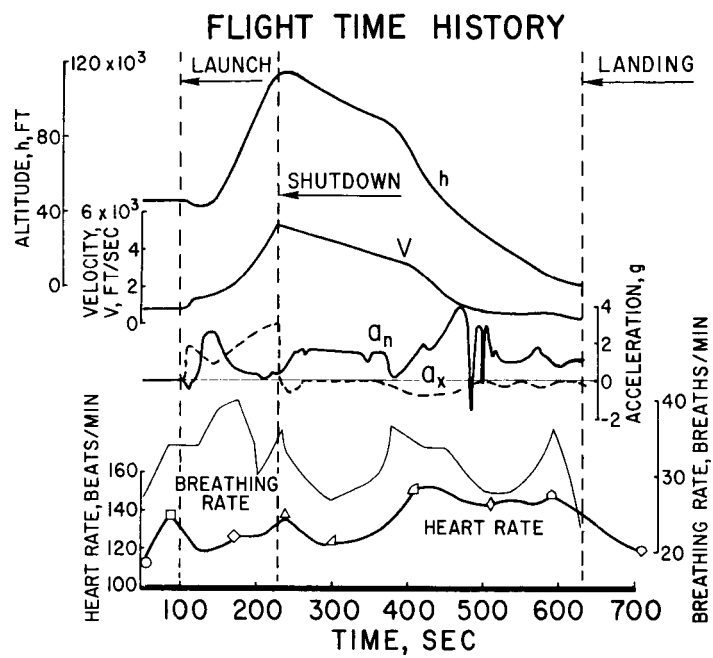


Figure 3

DYNAMIC GROUND TEST

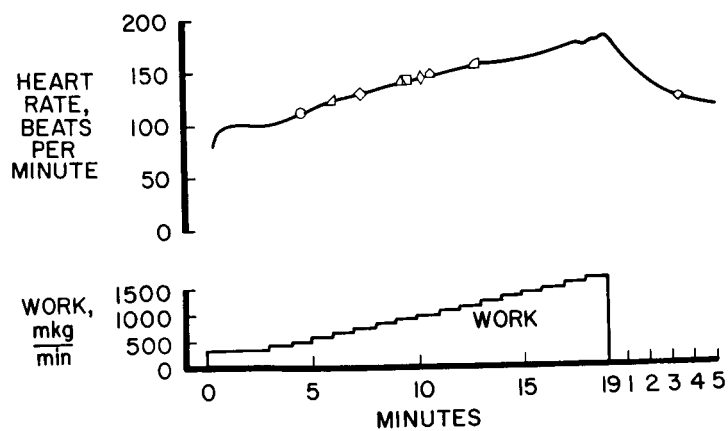


Figure 4

[REDACTED]

23. X-15 EXPERIENCE FROM THE DESIGNER'S VIEWPOINT (U)

By L. P. Greene and R. L. Benner
North American Aviation, Inc.

N71-75466

INTRODUCTION

23

In the introductory remarks at the October 1956 conference on the X-15 airplane, Dr. Hugh L. Dryden made the following statement: "First, in line with the urgency expressed in the memorandum of understanding, the project is proceeding on an expedited basis with the intent of realizing flights of a man-carrying aircraft at hypersonic speeds and high altitudes as soon as possible for explorations to separate the real from the imagined problems and to make known the overlooked and unexpected problems."

The purpose of this paper is to present with due candor some explanation of the differentiation of real and imagined problems, as well as the overlooked or unexpected problems.

In the original direction provided the contractor, the X-15 airplane was not to be an optimized configuration but was to be as simple as possible, and wherever possible conventional designs and methods were to be utilized.

This statement certainly belies the fact. Anyone who has come much closer than 1,000 feet to the X-15 airplane will recognize that the only thing conventional about the airplane is that it has a wing and tail surfaces and generally looks like an airplane.

LANDING EXPERIENCE

One of the most unique aspects of the X-15 airplane is recognized when consideration is given to the airplane landing characteristics and the associated landing-gear configuration. Initially, it was decided that with a maximum lift-drag ratio L/D of approximately 4 in the landing approach, acceptable landing characteristics could be provided. Figure 1 shows a comparison of the landing-approach lift-drag ratios as plotted against lift coefficient C_L for several earlier rocket-powered aircraft and the originally predicted L/D for the X-15 airplane. As the first flight was approached and the "adrenalin factor" increased, a reevaluation was made. In addition to the analytic studies of these flight characteristics, a flight program was conducted by both



North American Aviation, Inc., and the U.S. Government utilizing both an F-100C airplane and an F-104 airplane with specific drag configurations employed to simulate the X-15 approach L/D in order to permit actual in-flight assessment of the low L/D landing-approach phase. As reported upon in the July 1958 conference on the X-15 airplane by Finch, Matranga, Walker, and Armstrong, it was decided that the X-15 airplane was to fly the landing approach in the clean configuration to take advantage of the higher lift-drag ratio, and the flap and gear extension was to be delayed until about 15 seconds before touchdown. This plan was to allow for greater pilot freedom in approach from high key points. Even so, it was recognized that a certain degree of proficiency would be required in executing the approach and landing maneuver and, for this reason, much effort was expended in assuring the validity of the handling characteristics associated with these flight conditions.

Serious consideration was also given the landing dynamics (described in a previous paper by McKay and Kordes (paper no. 5)) associated with the X-15 landing-gear configuration which locates the main skid-type gear far aft on the fuselage. This specific gear configuration was selected in the interest of maintaining minimum compromise to the basic requirements of the airplane. Once again, analyses indicated that acceptable landing characteristics would be provided. Touchdowns were expected to be made at high landing speeds and at angles of attack of the order of 6° and at sinking speeds of 9 feet per second or less.

These landing-gear design requirements provided gear strength for landing an 11,900-pound airplane within a sinking-speed-angle-of-attack envelope, as shown in figure 2, encompassing an angle of attack of 8° at a sinking speed of 9 feet per second and an angle of attack of 9.5° at zero sinking speed. Because of airplane growth and the difficulty encountered during early flights to land consistently within the design envelope, it appeared that this original landing envelope was not adequate.

Subsequent to the first flight, when the main-gear cylinder bottomed and the gear was damaged, additional energy-absorption capacity was added to the main gear. Later, a still greater capacity was provided by increasing the cylinder stroke and allowing even higher peak loads by adding some beef-up to the gear and backup structure.

The nose-gear loads were known to be extremely responsive to airplane angle of attack as well as to airplane weight. The nose-gear energy-absorption capacity was thought to be adequate, even though the landing weights and touchdown angles during the first three landings were exceeding design values. However, during the fourth landing, a

hard emergency landing on Rosamond Dry Lake following an in-flight engine explosion, the nose-gear wheels were bent and the fuselage was broken aft of the cockpit area.

The investigation that followed the accident revealed that the principal problem existed in the nose-gear arresting system. In order to conserve space when the nose gear was retracted, the gear was stowed in a nearly compressed position. Upon rapid gear extension, the nitrogen gas which had been entrapped by the oil under high pressure was released and produced a gas-oil foam within the cylinder. Approximately the first one-third of the cylinder stroke was rendered ineffective by this foam, and consequently the loads built up to excessive values during the remainder of the stroke. A permanent solution was achieved by redesigning the internal mechanism of the strut to incorporate a floating piston which keeps the gas and oil separated at all times.

With the additional energy-absorption capacity provided in the main and nose gears, the operational sinking-speed—angle-of-attack envelope was enlarged as shown in figure 2 to encompass an angle of attack of 10° at a sinking speed of 9 feet per second and an angle of attack of 13° at zero sinking speed. Landing weights of 14,500 pounds are now permissible within the original envelope and a weight of 13,500 pounds may be landed within the larger envelope.

Since the first few flights, the landing techniques have been modified and these modifications have resulted in landing characteristics that are quite acceptable. The lift-drag ratio realized during actual approaches is slightly higher than that predicted and the angle of attack at touchdown has been reduced so that the landings are well within the allowable envelope. The procedure of extending the gear shortly before touchdown has proven to be satisfactory and the landings have become routine as indicated in a previous paper by White, Robinson, and Matranga (paper no. 9).

SYSTEM TESTING

The problems associated with obtaining reliable components have been discussed in a previous paper by Wiswell, Olekszyk, and Gibb (paper no. 19). The advantages of system testing have been pointed out both in the previous paper by Wiswell, Olekszyk, and Gibb (paper no. 19) and in a previous paper by Love and Palmer (paper no. 20) and were forcibly demonstrated on June 8, 1960, when the third X-15 airplane was severely damaged by an explosion. Figure 3 gives some idea of the extent of explosion damages. Investigation disclosed the initiating cause to be overpressurization of the ammonia tank, the result of a



combination relief valve and pressurizing gas regulator malfunction while operating on the ground with the ammonia tank vented through the vapor disposal system as shown in figure 4. Because of the toxic nature of ammonia fumes, the vapor disposal system had been incorporated into the facility at Edwards Air Force Base to dispose of ammonia fumes from the airplane tankage. At the time of the explosion, the ammonia tank pressurizing gas regulator probably froze or stuck in an open position while the vent valve was operating erratically or modulating only partially open. This condition had been considered as a failure possibility in the airplane; however, these malfunctions in conjunction with the back pressure associated with the vapor disposal system combined to cause ammonia tank pressures high enough to fail the tank. Redesign of the pressurizing gas regulator to reduce maximum flow through an inoperable regulator, redesign of the regulator to provide additional closing forces in the event of freezing, relocation of the regulator to minimize possibility of the moisture entrance and subsequent freezing, and redesign of the relief valve and relief system plumbing, all were results of the explosion.

This was a costly lesson, but it pointed out the need for more complete system analyses and/or testing under not only design conditions, but also under operational and test conditions since analytical evaluation of such involved systems is extremely difficult and not completely reliable. Real-time monitoring of system and component performance during testing is also indicated.

The optimum approach then would include not only conventional test-stand testing of the various systems and the ground testing of the completed airplane, but specific "fail safe" tests including the utilization of any ground support equipment and/or facility equipment which become integral with the airplane system at any time. "Fail safe" tests are those in which critical components are intentionally failed to insure that no single failure can cause damage to the airplane.

AERO HEATING AND STRUCTURAL TEMPERATURES

A primary design objective of the X-15 airplane was to achieve skin temperatures of 1,200° F over significant areas of the airplane. Involved in this objective is structural temperature prediction. As indicated in previous papers by Banner, Kuhl, and Quinn (paper no. 2) and Kordes, Reed, and Dawdy (paper no. 3), sufficient data have been gathered to make it evident that modifications to standard thermodynamic techniques are required for the successful prediction of hypersonic-flight structural temperatures. In the initial design, the predicted surface temperatures were calculated by assuming full turbulent flow except for the wing and empennage surfaces where a transition

Reynolds number of 100,000 was assumed. It was always recognized that these assumptions might contain some conservatism for the specific design-type missions, but the structural design resulting from these criteria might therefore provide greater latitude in airplane flight missions for other investigations. No one had real confidence in the basic heat-transfer theory so an extensive wind-tunnel test was made with pressure and heat-transfer instrumentation. The model was tested in a manner to produce the maximum confidence in results with maximum available temperature gradients and turbulent flow. In figure 5, the introduction of the resulting wind-tunnel factors caused further conservatism in predicted peak temperatures as compared with actual flight data. The result of the basic assumptions and the modified heat-transfer coefficients has been that average skin temperatures of primary structural areas of the fuselage, main wing box, and vertical tail are running several hundred degrees below predicted values at the peak Mach number by using the temperature-prediction methods used for design of the X-15. This is a conservatism in structural temperature prediction. This does not necessarily imply a structural integrity conservatism since thermal gradients may be adversely affected by this fact. Also, as mentioned earlier, there are some specific areas, such as the wing leading edge and speed brakes, which are experiencing local temperatures essentially equivalent to those which were predicted. This experience should serve as a reminder that extrapolation of heat-transfer model testing to actual airplane conditions may give results which are inaccurate. This is not to say that the wind tunnels are at fault; it is believed that either they were used incorrectly or that their results were interpreted incorrectly. The continued flight program that will be conducted by the U.S. Government should help to improve this situation. Additional understanding of boundary-layer conditions and these highly transient conditions will greatly assist the designer in interpretation of wind-tunnel results.

Although surface temperatures in general have been somewhat lower than predicted, there have been those specific locations where the reverse is true as indicated in a previous paper by Kordes, Reed, and Dawdy (paper no. 3). As shown in figure 6, the wing leading edge is fabricated from an Inconel X bar which serves as a heat sink to absorb heat generated at the stagnation point. Principal loads are carried by the main wing box immediately aft of the secondary structure leading-edge box. In order to minimize attachment stresses between the bar and the wing skin, as a result of unequal thermal expansion, the bar was segmented into five pieces with an expansion joint or slot about 0.080 inch wide between the segments. As indicated by previous papers, temperature-sensitive paint on the wing defined the temperature patterns resulting from the turbulence generated by these leading-edge slots. Although this localized turbulence had been anticipated, the magnitude or profile of the resulting temperatures and the stresses induced locally on the



CONFIDENTIAL

wing skin could not be adequately predicted. This condition contributed to the local permanent buckling. One obvious solution to this problem would be to replace this leading-edge structure with one which did not have high thermal expansion characteristics and which, therefore, did not require these expansion slots. This approach has some areas of concern, however, on mechanical attachment of the leading edge and the heat transfer within the structure. These problems will be aggravated, of course, by heat flux and transients occurring on higher performance vehicles.

Aerodynamic heating of the outer panel of the double paneled windshield provides another area of interest. The arrangement of the double panels is shown in figure 7. The original analysis for selection of outer windshield glass was based on theoretical heat-transfer data and the then known thermal properties of the glass selected. That analysis indicated that soda-lime glass would be adequate for conditions imposed by the X-15 flight program. Temperature data obtained during early flight testing of the airplane began to point toward a higher surface temperature and greater temperature gradient through the glass than had been originally predicted. A subsequent reevaluation of the wind-tunnel data showed that these data actually correlated well with the flight temperatures. A sample of the outer windshield soda-lime glass was then subjected to the surface temperature and temperature gradient extrapolated for a high-temperature flight and the glass failed. Meanwhile, alumino-silicate glass, developed under contract to the U.S. Air Force, had been qualified for aircraft glazing. This material, which has a greater heat capacity, higher thermal conductivity, lower coefficient of expansion, and greater strength at high temperatures than the soda-lime glass, was subjected to the same thermal test and did not fail. The alumino-silicate sample was then subjected to a surface temperature of 1,050° F with a temperature gradient from outer to inner surface of 790° F without failure. These temperatures are more than 150 percent of the maximum predicted. These thermal conditions are regarded to be considerably more severe than the X-15 mission will require; thus, the soda-lime outer windshields were replaced with alumino-silicate glass on all three airplanes.

However, there have been two recent flights where failures of the outer panel have been encountered. As indicated in a previous paper by Kordes, Reed, and Dawdy, the first failure was primarily caused by the inadvertent installation of one of the original lower temperature tolerant soda-lime panels when the left-hand panel was replaced a few months prior to the failure. The second failure obtained during the speed flight on November 9, 1961, however, did involve the alumino-silicate panel, but one thing common to both failures was the similar location of the initial point of failure even though the second failure involved the right-hand outer panel. In both cases, the failure

[REDACTED]

originated at a point approximately 1/2 inch down from the upper edge of the glass, nearly coincident with the trim line of the retainer, and at approximately the midpoint fore and aft. Since in both cases this location was approximately at the aft edge of a buckle in the retainer, it is deduced that the failure occurred as a result of thermal stresses produced by excessive local temperature gradients caused by the retainer buckle. It is noteworthy that the buckle was much more severe in the latter flight and would contribute to the higher local temperatures. Remedial action has been to convert the material for the retainer from Inconel X to titanium since the reduced coefficient of expansion of titanium compensates better for the differential expansion associated with the cooler Inconel X substructure frame.

On the basis of what can really be considered as only preliminary data at this time, experience to date relative to aerodynamic heating and structural temperature prediction can be summarized as follows:

(1) The assumption of turbulent airflow for hypersonic aerospace vehicles remains a good design criterion but it could be conservative in idealized areas.

(2) No flight correlations have been obtained on the variation of transition Reynolds number with Mach number that has been indicated in some wind-tunnel tests.

(3) Laminar-airflow tendencies can be made turbulent by local airflow disturbances such as leading-edge slots, production joints, and protuberances. These conditions should be evaluated in great detail in design stages, particularly when deformed structures due to aerothermodynamic stresses are being investigated.

STABILITY AND CONTROL DERIVATIVES AND HANDLING QUALITIES

The handling characteristics of the X-15 airplane have been the subject of many studies prior to and during the airplane flight testing. These studies, which are currently being verified by flight tests, indicated that the X-15 airplane would display satisfactory handling characteristics throughout its intended design envelope when all systems are operating normally; however, a control problem area, as described in a previous paper by Petersen, Redies, and Weil (paper no. 10) and as shown in figure 8, does exist should the pilot experience a critical stability augmentation system damper failure while he is operating in this area. Control problems are caused at the high angles of attack associated with reentry primarily by an aerodynamic derivative, adverse roll due to yaw, and these problems cause the pilot much difficulty in controlling the airplane in the lateral directional mode.

03713291000

At the July 1958 conference on the X-15 airplane a paper by George B. Merrick and C. H. Woodling described the effects of angle of attack on controllability. Figure 9 is essentially a reproduction of the data from that paper. For the simulator evaluation for the condition of all dampers off, flight characteristics for reentry maneuvers were satisfactory for angles of attack from 0° to 6° , acceptable for emergency for angles of attack from 6° to 17° , and unacceptable beyond 17° .

Flight evaluations reflected in many papers of this conference indicate grossly different results. These more current analyses show acceptable characteristics at angles of attack below 7° to 8° and definitely unacceptable characteristics at angles of attack above 10° . There is little or no angle-of-attack range considered acceptable for emergency.

There are at least two reasons which could contribute to this gross change in evaluation. The first is that the simulator mechanization used in the early phases of the program and in the centrifuge-simulator pilot-training phase did not include the secondary incremental effects of trimming the airplane with the horizontal tail. The position of the tail changes the roll-due-to-yaw parameter $C_{l\beta}$.

The second reason is much harder to describe. It would appear that the centrifuge and these early simulator evaluations received a much coarser evaluation. Reentries were considered successful even where significant vehicle dynamic motions were experienced. Later, in the pilot training and especially in the actual flight evaluation, a much finer analysis was made and a more restrictive envelope was defined. No matter how realistic a simulation becomes, a pilot feels safer in a simulator than he does in an airplane.

To the designer of aerospace vehicles, these evaluation trends should be remembered and final aerodynamic parameters should be incorporated into simulator studies as soon as possible.

Wind-tunnel tests have shown that this aerodynamic derivative $C_{l\beta}$ generally becomes favorable with the removal of the lower vertical stabilizer; thus, the control problem is minimized. In retrospect, let us briefly review the design philosophy associated with the configuration of the X-15 vertical tail.

At the July 1958 conference on the X-15 airplane a paper by Jim A. Penland and David E. Fetterman, Jr., was presented on the high-speed static stability characteristics of the X-15 airplane. In that paper, it was indicated that for reasons of stability and control near zero lift, the vertical tail was changed from the original design configuration of a large upper vertical tail and a short span lower vertical

4

tail to a vertical-tail arrangement which was more nearly symmetrical above and below the fuselage - the current configuration.

It will be recalled that the X-15 airplane was designed specifically for an altitude and a speed mission. A representative altitude mission is shown in figure 10. These missions specified that an angle of attack of 0° be established as soon after launch and engine light-off as practicable, approximately 15 seconds, and be maintained during both the exit-powered phase and the ensuing free-fall ballistic trajectory. This specification placed a heavy emphasis on the aerodynamic characteristics for zero angle of attack. The flight testing to date has not placed such an emphasis on operation at low angles of attack.

In a paper by Windsor L. Sherman, Stanley Faber, and James B. Whitten in the October 1956 conference on the X-15 airplane, the original design configuration with the large upper vertical tail was shown to be unsatisfactory from a piloting standpoint for the altitude design mission when a random-direction 1-inch thrust misalignment was considered. This was one of the several primary factors involved in changing the vertical-tail configuration and led also to the requirement for determination of the specific location of the thrust vector on each of the XLR99 engines delivered for flight use. Thus far, the thrust-vector information has been used to align properly each of the engines when they were installed for flight. All flights to date have indicated no discernible thrust misalignment. However, since spare engine chambers presently under procurement for future support of the program will not be indexed for thrust-vector location and, hence, may not be properly aligned when installed, a directional control problem may yet be encountered. The consequence of this condition would be to add somewhat to the pilot's workload with the ballistic control system in decreasing any airplane oscillations which may have been encountered.

Now, to reiterate, the unacceptable handling characteristics encountered at angles of attack of approximately 10° and above due to adverse $C_{L\beta}$ are experienced only after loss of a critical stability augmentation system damper. Although the reliability of the stability augmentation system is generally good, in order to enhance the accomplishment of flight missions to altitudes beyond 250,000 feet, for which the X-15 airplane is capable from all other aspects, and which dictate reentry angles of attack well beyond the present unaugmented critical angle-of-attack range, a standby or backup damper is currently being developed. This system will provide the necessary redundancy for the critical damper to assure adequate handling qualities. The redundant system should be ready for flight usage within the next 2 or 3 months, and this system should eliminate much of the uncontrollability considerations for flight operations in the future.

037132A J030

CONCLUDING REMARKS

In reviewing the broad aspects of the design analyses and developments which have been accomplished in the X-15 program, the following conclusions can be drawn:

1. The exploratory flight studies conducted have indicated that hypersonic aerodynamic heating effects can be predicted with sufficient accuracy to support the design of a hot structure vehicle such as the X-15 airplane. The high-temperature structural design approach utilized for this configuration has been successful; no major design deficiencies were encountered nor major modifications required. The local thermal problems encountered have, with but few exceptions, not affected primary structural areas.

2. In general, the aerodynamic derivatives extracted from flight-test data have confirmed the estimated derivatives obtained from wind-tunnel tests and thereby provided increased confidence in wind-tunnel evaluations at hypersonic speeds.

3. The aerodynamic flight control system and the simple stability augmentation system of the X-15 airplane have proven to be good technical designs. The airplane can be flown with satisfactory handling qualities through the range of dynamic pressures from above 1,500 pounds per square foot to below 100 pounds per square foot through the range of Mach numbers from about 6.0 to subsonic landing conditions.

4. Although only limited flight experience has been gained with the reaction-control system, its basic design appears to be completely adequate and this type of system apparently provides an adequate means of attitude control for future space vehicles. Pilot transition from aerodynamic controls to reaction controls has been accomplished without problems.

5. Reports from the pilots, Robert M. White, Forrest S. Petersen, and Joseph A. Walker, indicate there are no piloting problems peculiar to the X-15 flight regime other than conventional pilot workload tasks.

On the basis of this recapitulation, it can be said that the X-15 airplane has essentially achieved the intended goals with satisfaction. Proof of the technical feasibility of the X-15 design and fabrication has been demonstrated since exploration of the flight envelope has not been hampered by major design deficiencies.

COMPARISON OF L/D OF X-15 WITH PREVIOUS ROCKET AIRPLANES

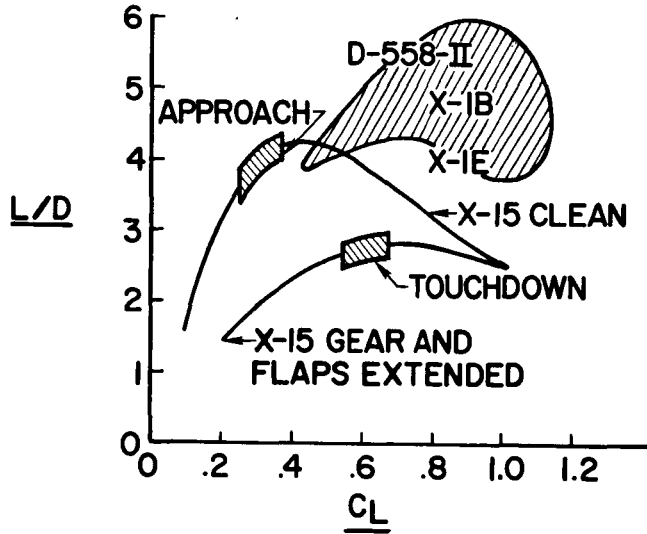


Figure 1

X-15 GEAR DESIGN ENVELOPE

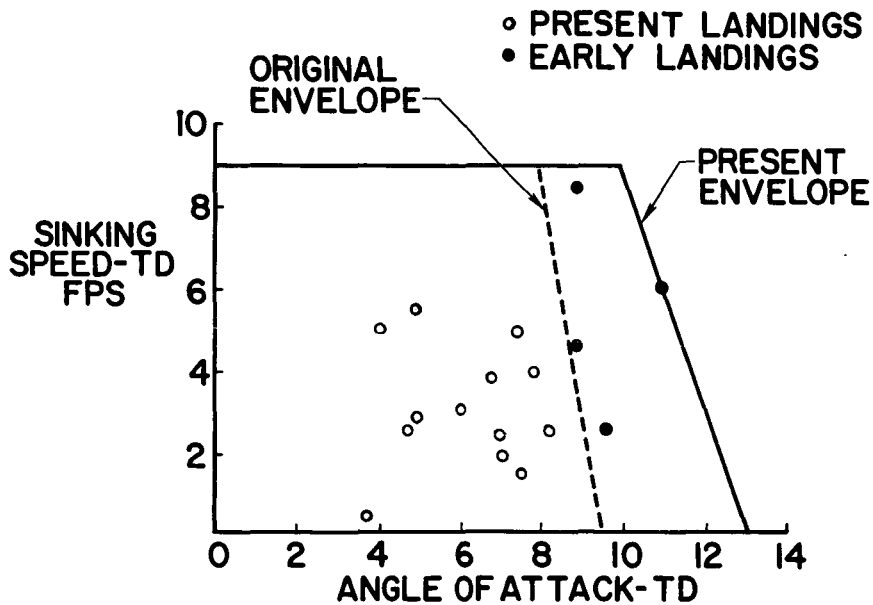
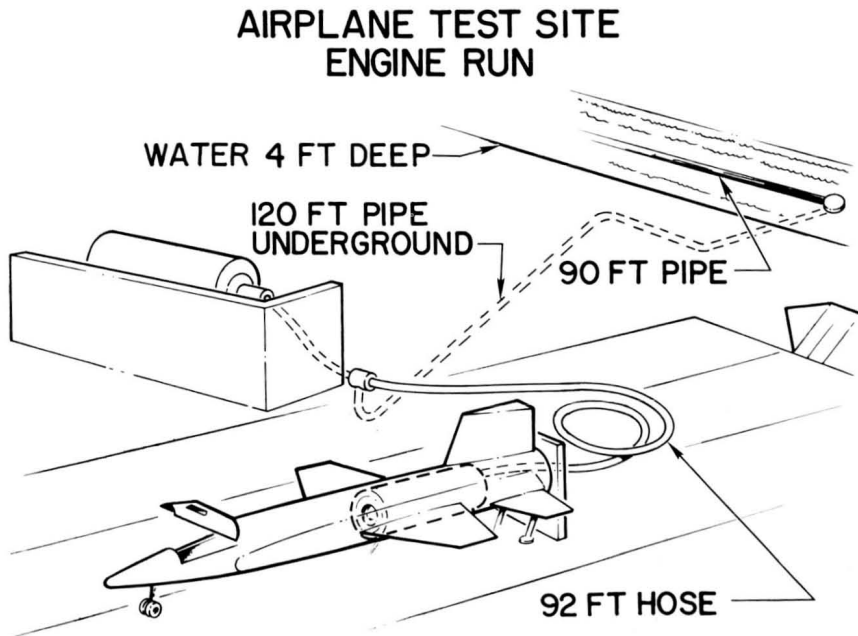


Figure 2



X-15 EXPLOSION SCENE

Figure 3



AIRPLANE TEST SITE
ENGINE RUN

Figure 4

TEMP VS TIME AFTER LAUNCH
TYPICAL FUSELAGE SURFACE TEMP
STA 26 BOTTOM ζ

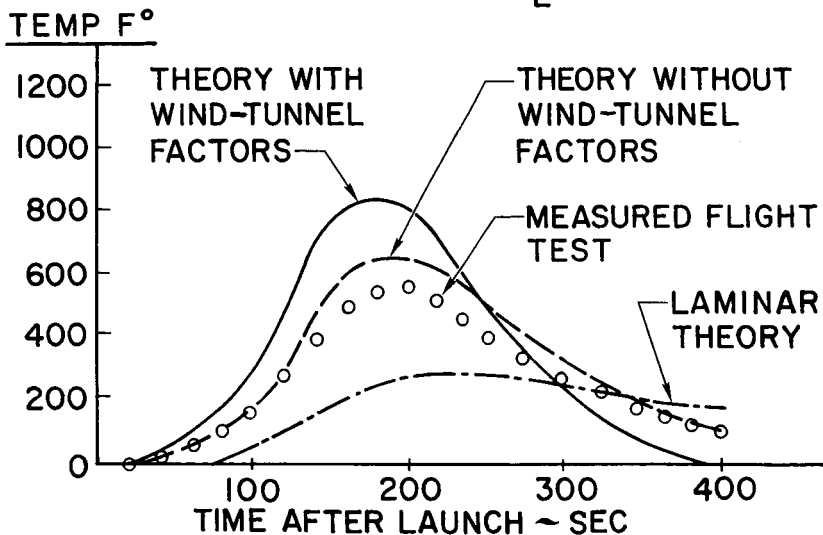


Figure 5

TYPICAL WING STRUCTURE

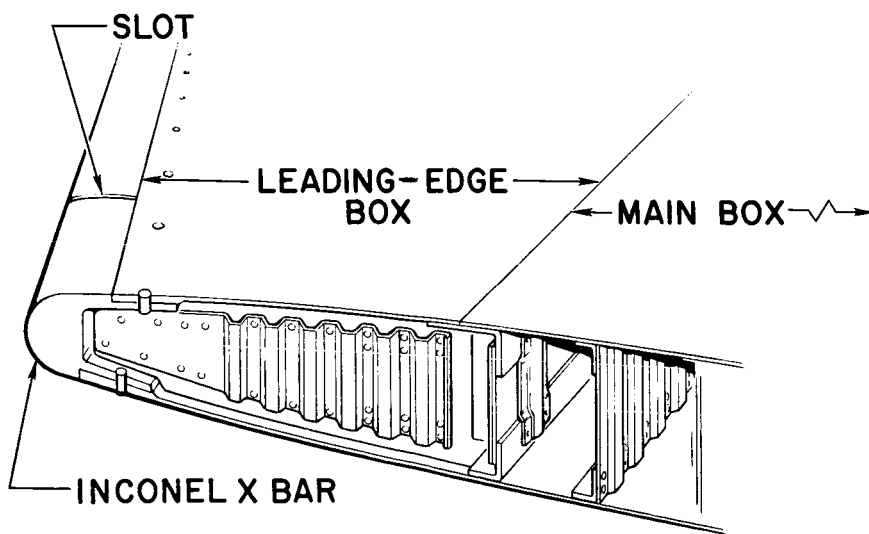


Figure 6

WINDSHIELD CONFIGURATION

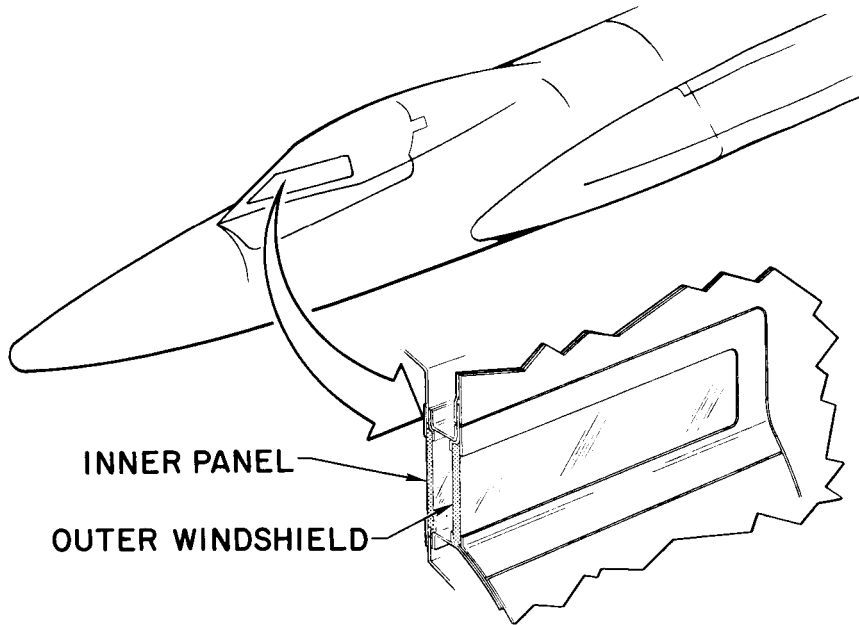


Figure 7

REDUCED AREAS OF ACCEPTABLE HANDLING CHARACTERISTICS FOLLOWING THE LOSS OF A CRITICAL SAS DAMPER

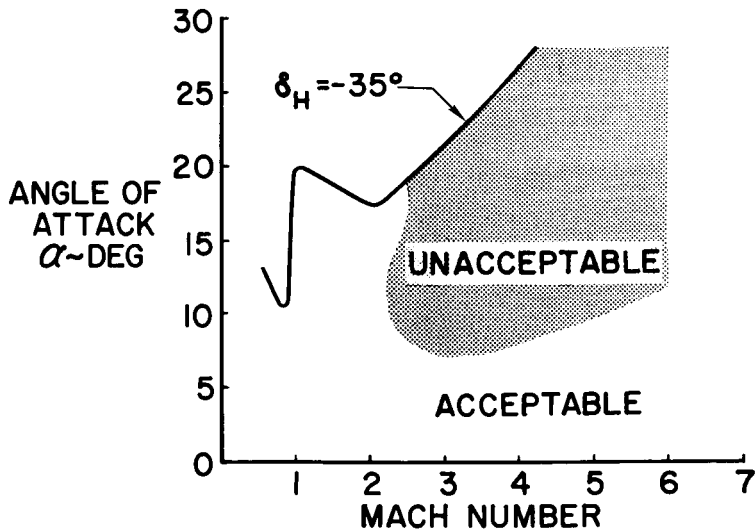


Figure 8

EFFECT OF ANGLE OF ATTACK ON CONTROLLABILITY

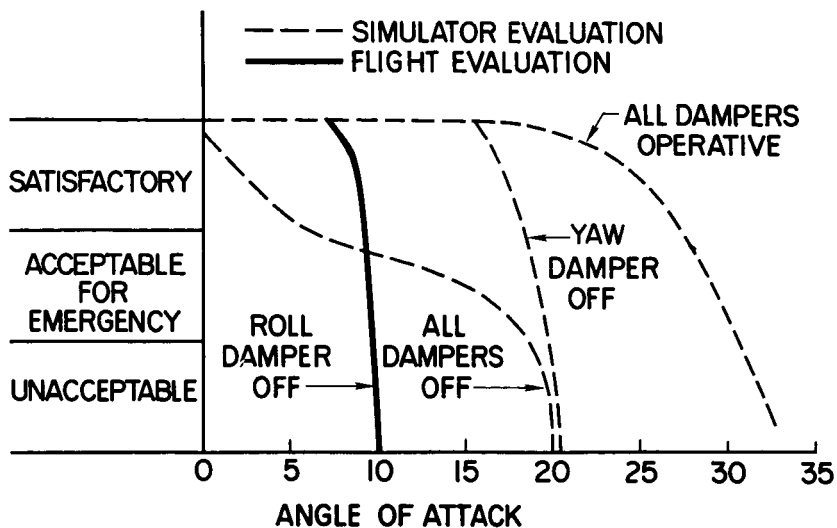


Figure 9

X-15 DESIGN MISSION PROFILE

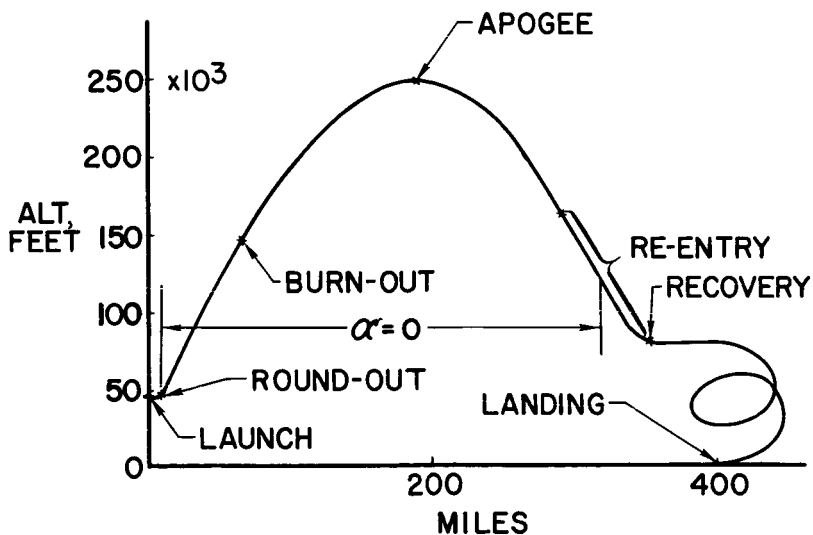


Figure 10

N71-75467

24. FUTURE PLANS FOR THE X-15 (✓)

By Paul F. Bikle
NASA Flight Research Center

and Edwin F. Pezda
Aeronautical Systems Division, U.S. Air Force

This third X-15 conference has given us an opportunity to review and evaluate, in considerable detail, the progress that has been achieved in the flight research program to date. Figures 1 and 2 have been selected as a summary of the areas thus far explored. Similar results have been discussed in detail in the papers presented. Although it is not possible, in any one or two figures, to show the desired information for all the varied areas of interest in the program, these plots of altitude and angle of attack against velocity do represent two of the many parameters of interest, and the shaded areas demonstrate roughly the progress that has been made. It appears that most of the work originally planned is nearly completed, with perhaps 50 percent of the aerodynamics, structures, heating, and bioastronautics information already obtained.

24

The X-15 program for the immediate future will be oriented toward continuing the research investigations in the following primary areas:

- Flight characteristics at high angle of attack
- Aerodynamic heating
- Reaction controls including rate damping
- Adaptive control system
- Performance
- Displays and energy management

Determination of the flight characteristics at high angles of attack, in the range from 15° to 25°, is required before attempting flights above the 250,000-foot design altitude. Aerodynamic-heating information has been of great interest thus far in the program, and a number of future flights will be pointed in this direction. Reaction control research data are just now becoming available from the flight program; future flights at high altitude and low dynamic pressure should be of great interest in this area. An important feature of flights to come will be the incorporation of rate damping in the reaction control system. The flight behavior with both the stability augmentation system and the reaction rate augmentation system will be compared with the flight behavior with the adaptive control system described in paper no. 13 of the conference by Johannes, Armstrong, and Hays. During these flights, data will also be obtained to more completely define the lift and drag characteristics of the X-15 configuration. Work on

Preceding page blank

displays and energy management, an example of which was given in paper no. 11 by Hoey and Day, will be continued. In this particular case, the goal is to provide a working onboard display for the use of the pilot in selecting his landing site.

A flight to the 250,000-foot design altitude will be attempted as soon as a satisfactory modification to the windshield has been designed. Altitude exploration flights above 250,000 feet will be initiated after the installation of a backup stability augmentation system, sometime after March 1962. Figure 3 shows the performance available in the aircraft from an energy standpoint and also the probable limits dictated by high dynamic pressure, high acceleration, stability and control, and aerodynamic heating during the recovery. Although it appears that flights in the area to the left of the vertical dashed line could be safely executed, this area does not seem to be of sufficient interest to warrant special flights for this purpose. The future altitude exploration flights are planned to acquire information between 200,000 and possibly 400,000 feet at speeds from 2,000 to 5,500 feet per second. Of major interest in this phase of the program will be such piloting aspects as display, guidance, precision of control, and bioastronautics.

As these programs are completed, follow-on programs will explore, with new instrumentation, areas already partially investigated, such as display, boundary-layer noise, skin friction at high Reynolds numbers, and structural panel tests. A large number of space experiments have been proposed which make use of the X-15 as a test bed to obtain information at altitudes from 150,000 feet to possibly 350,000 feet; heights greater than those obtained by balloons but lower than satellite altitudes. These experiments capitalize on the ability of the X-15 to provide on-the-spot pilot input in the conduct of the experiment and the return of the experiment to the ground for detailed evaluation and adjustment or correction of deficiencies if required. A few of the many interesting experiments being considered for the follow-on program are:

- Ultraviolet stellar photography
- Infrared exhaust signature
- Landing computer
- Detachable high-temperature leading edges
- Horizon definition
- Hypersonic propulsion

Many proposals that have been made are now in the process of evaluation. Some of the experiments will ride free in piggy-back fashion. Others may be grouped together to share the cost of operation. Some proposals require extensive modifications and are expensive in both time and money. For example, figure 4 shows a stellar photographic

experiment which would involve a stabilized platform extended through clam shell doors from a modified instrument bay.

It appears that the completion of the present research program will require about 30 flights in the next 18 to 24 months. The extent to which the addition of worthwhile follow-on experiments will extend the program is to be decided by the Research Airplane Committee: Vice Admiral J. T. Hayward, Major General M. C. Demler, and Dr. H. L. Dryden. A recommended follow-on program is now being prepared for consideration of this Committee.

At this time, some comment should be made concerning the degree of reliance, or degree of certainty, in any future plans involved with a research program. A future plan can only be as good as are the estimates on what the problem areas are going to be - not only problem areas in the X-15 program but problem areas in other programs which may require information from the X-15. For example, when the X-15 was first approved, the objectives were clearly stated in terms of aerodynamic heating, speed, altitude, reaction control research, and bioastronautics. As the program has progressed, it appears that, while these worthwhile objectives have been or will shortly be achieved, many important benefits have been of a different sort. The X-15 program has kept in proper perspective the role of the pilot in future programs of this nature. It has pointed the way to simplified operational concepts which should provide a high degree of redundancy and increased chance of success in future space missions. And, perhaps most important, is the fact that all of those in industry and in the government who have had to face up to the problems of design, building the hardware, and making it work have gained experience of great value to the future aeronautical and space endeavors of this country.

The same type of seemingly intangible consideration will influence our future X-15 program. The future program will be kept flexible and will be modified, extended, or terminated on the basis of timely reviews by the Research Airplane Committee.





X-15 PERFORMANCE ENVELOPE

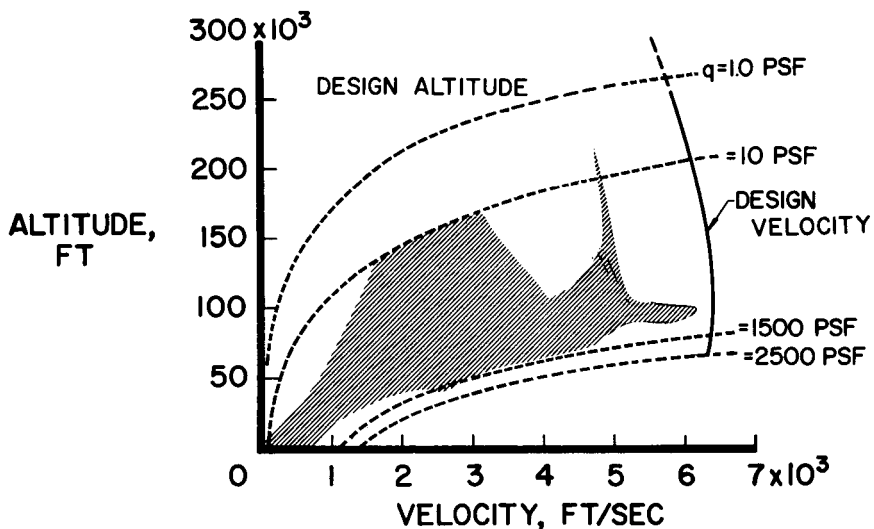


Figure 1

ANGLE OF ATTACK-VELOCITY ENVELOPE

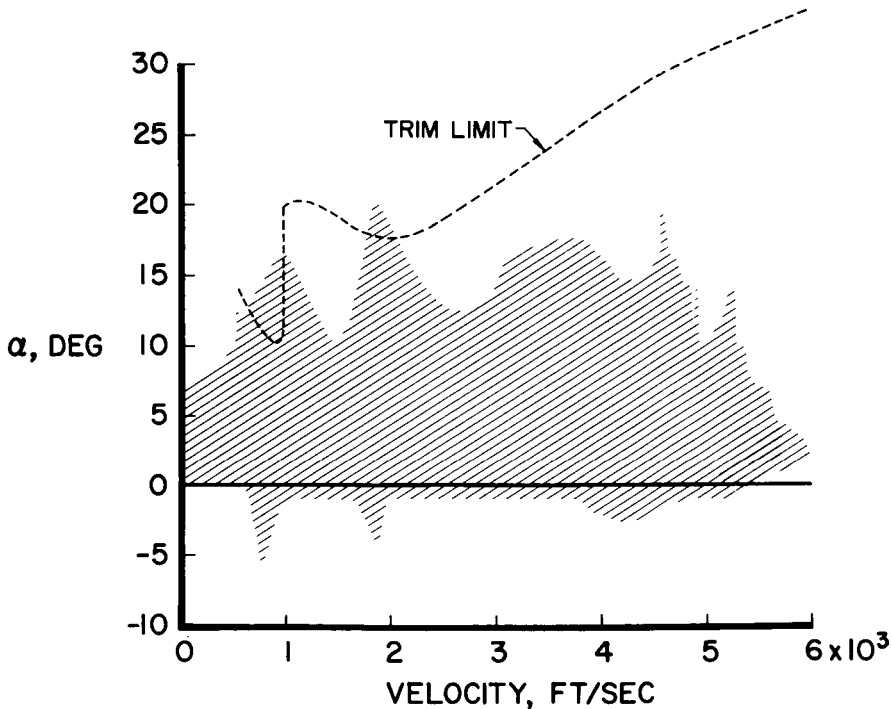


Figure 2



AREA OF FUTURE INTEREST

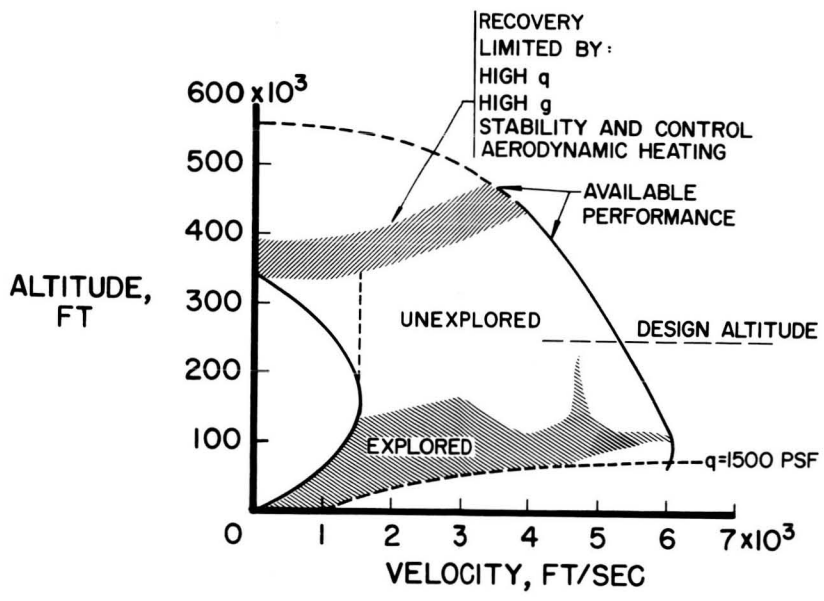


Figure 3

X-15 INSTRUMENT-COMPARTMENT MODIFICATION ("SKYLIGHT")

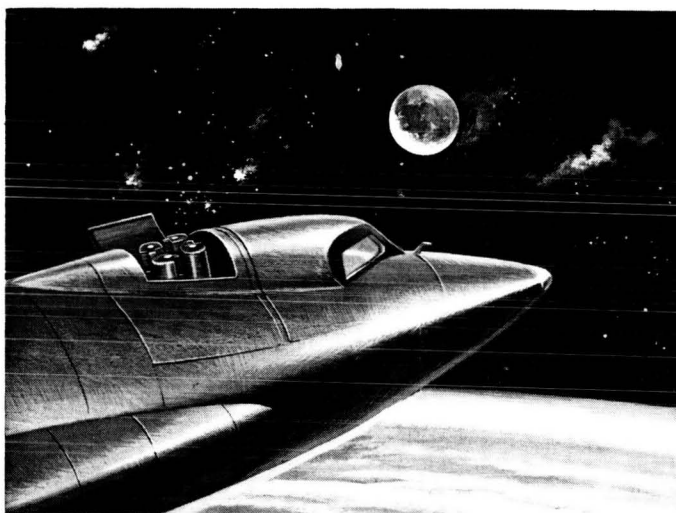


Figure 4

CONFIDENTIAL

CONFIDENTIAL